FINAL REPORT

INVESTIGATION OF LAND-USE SPECTRAL SIGNATURES

National Aeronautics and Space Administration
Marshall Space Flight Center

NASA Research Contract
NAS8-30620

Dupree Maples
John F. Hagewood
Department of Mechanical, Aerospace & Industrial Engineering
College of Engineering
Louisiana State University
Baton Rouge, Louisiana 70803

March 1975

ACKNOWLEDGMENT

The author would like to express his appreciation and gratitude to the following individuals who provided much needed help during his doctoral program.

Dr. Dupree Maples, who served as major advisor and committee chairman. His advice and guidance were invaluable during my graduate program.

Dr. Herbert Pillar for his advice in the area of optics.

Dr. Robert Courter for his help and encouragement in designing and launching the balloon system.

Mr. Ron Foster for his help in the initial study of the design of the balloon system.

My wife, Grace, for her help in organizing and typing the rough draft and in providing the encouragement needed to continue the program.

Diane Marabella for typing and preparing the final manuscript.

The LSU Dairy Farm personnel for the use of their land on which the balloon system tests were made.

In addition, I would like to thank the National Aeronautics and Space Administration for their financial support during this investigation.

TABLE OF CONTENTS

LIST OF TABLES

LIST OF ILLUSTRATIONS

LIST OF ILLUSTRATIONS - Continued

LIST OF ILLUSTRATIONS - Continued

LIST OF ILLUSTRATIONS - Continued

LIST OF ILLUSTRATIONS - Continued

LIST OF ILLUSTRATIONS - Continued

LIST OF ILLUSTRATIONS - Continued

LIST OF ILLUSTRATIONS - Continued

ABSTRACT

A technique was developed to obtain bidirectional reflectance data from natural surfaces by using a folding mirror to transfer the reflected energy from the test surface to a spectroradiometer. The folding mirror was a first surface reflector made by stretching Mylar vacuum coated with aluminum over a light weight frame. The optically folding mirror was positioned over the test surfaces with a moveable platform for both laboratory and field tests. Field tests were also conducted using a tethered balloon system to position the folding mirror. A spectroradiometer was designed and built specifically for this investigation. The spectroradiometer had an angular field of view of twenty-four minutes in one axis and ten minutes in the other axis. The radiometer was capable of detecting energies in small bandwidths throughout the electromagnetic spectrum from 0.3 microns to 3.0 microns. Bidirectional reflectance data and variations in the data with source angles were obtained for Saint Augustine grass, Bermuda grass and a black alluvium soil from the Mississippi River delta.

CHAPTER I

INTRODUCTION

> Remote sensing of agricultural and other earth resources involves the detection of electromagnetic energy that is reflected or emitted from the complex assemblage of biological, geological, and hydrological features at the earth's surface. The data obtained can be meaningfully interpreted and processed only if we have a fundamental understanding of the energy-matter interactions at the earth's surface that account for variations in the quantity and quality of radiation recorded by the air- and space-borne sensors. This knowledge also is necessary for us to derive new applications of existing remote sensing systems and to design new systems capable of sensing and recording potential and predictable differences in data. [1]*

There are a number of basic problems which face the researcher involved in remote sensing. One of the most troublesome of these problems is how to automate the process of data interpretation. This is an especially challenging problem when the remote sensing data is to be used as a tool in identifying objects such as plants or soil types from a natural scene. Fundamentally, this problem arises because of the large number of variables which affect multispectral data received by remote sensing. These variables may be divided into several groups based on their origin. They are effects of the environment, changes in the surface characteristics of the objects sensed, and variations in the instrumentation and methods used to do the sensing. Any information or technique which would help to eliminate

---

* Numbers in brackets designate references listed in the Bibliography.

or better understand these variables would be of great value to many remote sensing projects by helping to speed up the data interpretation process or by helping improve the accuracy of object identification.

Presently, two techniques are generally used to overcome the problems arising from the many variables affecting the data. One technique is to find a unique characteristic in the reflectance data for each plant or object type which is to be identified by remote sensing. The uniqueness of this characteristic must be such that it is always present in the data regardless of the changes in the environment, the object, or the sensing system. Obviously, this is rarely possible; however, a unique characteristic in the reflectance data which is always present with reasonable variations of many of the variables can often be found for certain objects.

Another technique which is almost always used involves the taking of ground truth measurements. In this case spot checks are made, and plant and soil types are identified by investigators on the ground within the area covered by each scan. This data is then correlated with the data received by the remote sensing detectors.

In general, both techniques mentioned are used simultaneously in order to get good results in interpreting multispectral remote sensing data. However, this method is limited both in the accuracy of the results obtained for many applications, and in the amount of time and money required when making ground truth measurements.

Another approach which could be used to interpret multispectral remote sensing data is to identify the many variables and the effects they have on the data. By computerizing this information and having available standard spectral curves for normal values of the variables

for each item to be identified, either ground truth measurements could be eliminated or minimized and/or greater accuracy in data interpretation could be made. The identification process could theoretically be completely automated using this type of approach provided enough information were known and one had a large enough computer capacity. Regardless of whether one automates the process or not, any information which can be generated that will identify the effects of variables on the data obtained by remote sensing techniques will help in the data identification process.

In order to help collect this type of information, this research deals with a method for taking reflectance and emittance data from natural objects under natural conditions in a manner which will allow the effects of many of the variables to be determined. There were several objectives of the research as described below.

The first objective was to formulate a method of taking reflectance data from natural surfaces in the natural environment in a manner that simulated data taken from aircraft while reading from a constant and consistant surface. The second objective of the study was to design, build, and test the equipment needed. The third objective of the study was the taking of data and determining the effects of at least one variable on the data. In particular, the data taken concentrated on the effects of the solar or source zenith angle on reflectance data in the wavelengths range of 0.3 to 3.0 microns.

CHAPTER II

LITERATURE SURVEY

A literature survey was taken of past investigations made to determine reflectance and emittance properties of natural surfaces. The survey revealed that most of the work done prior to 1950 was generated in an attempt to determine the albedo characteristics of the earth in order to better understand the energy exchange between the earth and the sun and in particular its effect on the field of meteorology. Because of this as well as the nature of the sensors used, these early studies generally concentrated on total reflectance of broad formations on the earth such as land, water, snow, or clouds.

With the rapid advances made in electronics and sensors after World War II, investigations of the reflectance and emittance properties of natural surfaces increased exponentially. These later studies were made for various reasons and applications; however in general, they tend to be more discriminatory in separating the properties of the many different types of natural surfaces. Because of the massive number of studies made in the past few years, no attempt was made to review all of the investigations made after 1950. However, selected studies were reviewed thoroughly in two areas. One area reviewed was attempts made to understand the effects of the many variables involved in making reflectance and emittance readings of natural surfaces from aircraft (remote sensing). A second area reviewed was experimental approaches used to obtain this type of information. A survey which details the

techniques presently available for use in taking remote sensing data from aircraft and satellites is given in Appendix A.

Historical Survey 1900-1950

Coblentz [2, 3] near the turn of the century appears to have made the first pioneering studies on the reflectance of natural surfaces. His studies were made of the reflectance and emittance of mineral and inorganic surfaces in the infrared region from 1 to 8 microns. His studies were made under laboratory conditions using a pyranometer which he helped develop and which was used by Aldrich [4] and Angstrom [5] as well as others in later studies. The pyranometer is basically a radiation measuring device. It consists of two sets of metal strips on the back side of which thermoelectric junctions of copper-constantan are fastened. One set of strips is painted black, and the other set is painted white. The thermojunctions are connected to a galvanometer. The deflection on the galvonometer which is recorded is assumed to be proportional to the radiation intensity received on the metal strips. The strips were usually covered with a glass case for protection and to eliminate radiation in the far infrared.

Aldrich [4] in 1919 with the help of the U. S. Army Air Corps carried a pyranometer aloft in a balloon to make reflectance measurements of clouds. The balloon was manned, and the pyranometer was first held to point towards the sun and then down towards the clouds. Interestingly, wires were run from a galvonometer on the ground to the pyranometer held by the occupant in the balloon.

O'Neil [6] in 1923 tried to assess the effect of soil moisture content on the color or reflectance characteristics of soils. His method consisted of taking a series of black and white photographs of

soils under different moisture conditions and comparing them visually with standard tone shades of gray from white to black.

Angstrom [5] in 1925 used a pyranometer to measure the reflectance of bare ground, grasses, trees, snow and water. In his studies he also showed some of the effects of solar angle and water moisture content on the reflectance readings. He used a filter over the pyranometer to obtain some spectral effects. His measurements were made in natural light with the pyranometer mounted on a tripod approximately one meter high. He also used photography and tone comparisons in his studies.

Richardson [7] in England in 1929 used a device he called a photometer while flying in an open aircraft to measure the albedo of clouds, woods, and pasture lands. The photometer was a visual device as shown in Figure II-1 [7]. With this device the albedo or reflectance was measured by the ratio of the area of the iris openings required to get the same brightness at the screen. Spectral effects were obtained by using red, green, or blue filters at the screen. Richardson also suggested using such a device from a tower to monitor seasonal changes of the albedo.

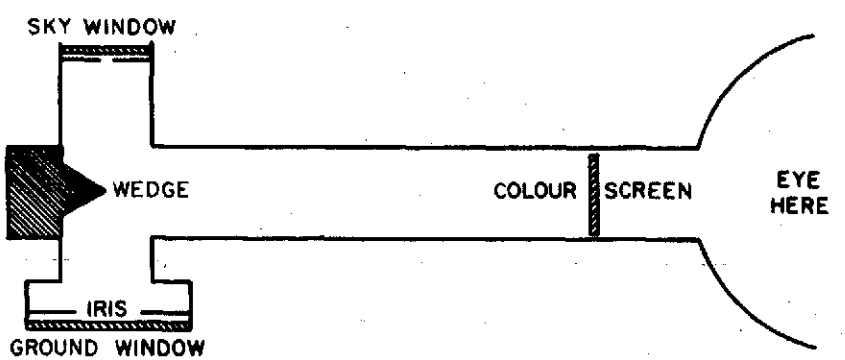

FIGURE II-1. SCHEMATIC OF PHOTOMETER

A classical investigation of the reflectance of natural surfaces was made by Krinov [8] in Russia beginning in 1932. His studies apparently continued until World War II but were not published until 1947. The first English publication was not made until 1953. Krinov took some 10,316 spectrograms during his study and reported on the spectral reflectance of 370 natural objects. His investigations covered the wavelength region from 0.4 to 0.9 microns. He took his spectral data every 100 Angstroms. His data included the effects of both solar and viewing zenith angles on the reflectances.

Krinov's technique of obtaining data was based on taking, what he called, a spectrogram of the natural object and then taking a spectrogram of a standard surface of magnesium oxide. The two spectrograms were then compared to get the reflectance. His spectrophotometer was mounted on a tripod above or to the side of the object. A spectrogram as made by Krinov was basically a photographic strip taken on black and white film of the radiation intensity of the surface being investigated. The strip was obtained by making intensity readings at different wavelengths.

An instrument called a pyrheliometer was used in the late forties and fifties by English and American investigators. This instrument was in essence simply a refinement of the pyranometer used earlier. Fritz [9] in 1947 used two of these devices to measure albedo over the United States. One instrument was mounted in a B-29 pointing upward, the other pointing downward. A flight across the country was then made at 10,000 feet. Neiburger [10] in 1948 made the same type of measurements using a blimp. However, he also investigated the effect

of solar zenith angle on the albedo of the sea. The pyrheliometers used in these investigations measured total intensity in the wavelength range of 0.3 to 2.5 microns.

Survey of Techniques

The following is a survey of many of the experimental techniques which have been used in the past twenty years to collect data under natural conditions. They show the effects of the many natural variables on the radiation intensity received from a natural object when viewed with a remote sensing device. Colwell [11] in a study suggested that the following types of platforms could be used for sensors in such investigations:

1. Tripods and platforms used for taking photographs;
2. Earth surfaces such as buttes, cliffs, and bluffs;
3. Towers, ladders, boom suspensions, cranes, etc.;
4. Dirigibles, balloons, helicopters;
5. Fixed wing aircraft.

All of these have been used as platforms for remote sensing of natural objects in recent years.

Ashburn and Weldon [12] in 1955 made reflectance measurements of dessert terrain in the 0.4 to 0.65 micron region using what they called an albedometer. The albedometer was mounted on a platform two meters above the terrain for most measurements. However, some tests were made with the albedometer supported by a helicopter 300 meters above the terrain. Some effects of the solar zenith angle on the data were noted. The albedometer consisted of a photomultiplier tube mounted in the side of a integrating sphere with an entrance aperature. The

exact field of view of the device was not given, but from the description of the equipment it was probably 30° or greater.

Graham and King [13] used a Eppley pyrheliometer and a Kipp solarimeter to take reflectance readings from a field of maize over a period of 17 days. The pyrheliometer was mounted on a building 900 meters from the corn field and was used to measure the incident radiation. The solarimeter was mounted two meters above the corn plants and used to measure the reflected radiation. Natural variables noted in the study included plant maturity, solar zenith angle, and soil moisture content.

Boileau and Gordon [14], and Gordon and Church [15] in 1960 presented data on the directional reflectance of snow and water for various viewing and solar zenith angles. Their data was made with a telephotometer carried on board an aircraft while flying over large areas of the earth covered with snow or water.

Winkler [16] made a study to determine the variables affecting soil color by taking photographs of test samples in natural light from a height of three feet. His film response was from 0.4 to 0.9 microns. He concluded that soil color is determined by original soil color of the glacial drift, moisture content, and the amount of organic matter in the soil. Light soil tends to be well drained with coarse grains; whereas dark soils tend to be finely grained with a higher water content.

Carneggie [17] used a Barnes Engineering Thermal Infrared camera to make studies of the emissivity of objects in the 8-14 micron region. This device has a photographic type of output; however, the image is produced by the use of electronic infrared sensors. For these studies Carneggie mounted his instruments atop Glacier Point and made readings

of the valley 4000 feet below. He also made readings from the platform area of a 150 foot water tower. His recordings were made over twenty-four hour spans and used to show the diurnal temperature effects of various natural and manmade objects. The intensity readings made were of the total energy emitted in the 8-14 micron region.

McClellan, Meiners and Orr [18] made 250 reflectance curves of plants in the field and in a greenhouse. These measurements were made in the 0.4-2.0 micron region in a spectral manner. The equipment used was a spectrophotometer to record the data and a tungsten lamp as a source rather than the sun. All the equipment was housed in a light tight box which was fitted over the test plot to be studied. The field of view of the equipment was a six inch diameter circle.

Watson [19] and Howard, Watson and Hessin [20] looked at the reflectance of rocks and tree leaves in a spectral manner through the wavelength range of 0.4 to 1.5 microns. They took data both in the laboratory using a spectrometer and in the field. Data taken in the field was taken with an ISCO spectroradiometer with a fiber optic head. Measurements were taken with the probe held at a height of 2-3 feet above the rock surface or leaves to be studied. Reflectance was obtained by comparing these readings with readings taken from a standard surface of Fiberfrax. The field of view of the instrument was 30^{o}. Measurements made of the rock surfaces were made at different observation angles but due to the large field of view of the fiber optic head the results obtained showed only generalized trends.

Chia [21] made measurements of the total reflectance of soils and crops in a tropical region by using two Kipp solarimeters mounted on top of a 20 foot irrigation pipe held vertically. One solarimeter was

pointed down and the other pointed up. The effects of moisture content, crop height, solar zenith angle and clouds were noted.

In the late 1960's and extending to the present time, a number of unique and interesting techniques have been used to try to look at consistent areas of natural surfaces under varying natural conditions in order to document the effects of natural variables on the reflectance data which it is now possible to take with airborne sensing devices (see Appendix A). Several of these studies are those undertaken by Salomonson [22], and Salomonson and Marlett [23, 24]. Their studies involved the use of an airborne scanning radiometer which recorded total reflection readings in two bands. The radiometer used was a slightly modified version of the Nimbus F-3 radiometer. The bands used were 0.2-4.0 microns and 0.55-0.85 microns. The field of view was 50 milliradians. A silicon cell pyranometer was used to record incident solar intensity. Sites and natural surfaces chosen for study were such that the area flown over by the aircraft was constant in composition. Surfaces studied included clouds, snow, white gypsum sand, a dry lake bed, prairie grass, a swamp area covered with consistently dense vegetation, and the ocean. Based on the data taken, bidirectional reflectance (see Figure A-5) versus solar zenith angle, radiometer viewing angle and relative azimuth angle between the solar and radiometer plane was plotted for several of the surfaces. It was noted that the bidirectional reflectance of natural surfaces under natural conditions is anisotropic.

Suits and Safir [25] at the University of Michigan have recently completed a study of the effects of canopy structure on reflectance measurements. They used a ISCO spectrophotometer in their field tests

which were made in a corn patch. The spectrophotometer was mounted on a cherry picker approximately ten meters above the field. The field of view of the instrument was twenty degrees. Reflectance was obtained by first reading from the corn field and then reading from a standard reference gray Lambertain panel mounted on the cherry picker. Spectral data was obtained for a wavelength range of 0.4 to 1.1 microns.

Lyon [26] and Lyon and Patterson [27] in studies to try to identify rock types by their spectral emissivities in the 8-13 micron range built a mobile field laboratory carried on a three-fourths ton pickup truck. The laboratory was powered by a gasoline engine driven generator. The optical heads of their radiometer and spectrometer were mounted on a tripod which could be moved up to one hundred feet from the vehicle which contained all the electronics in a controlled environment. The tripod held the optical heads approximately three feet above the rock surfaces to be studied. The field of view of the optics was not given. Emissivities were obtained by comparing the readings made to the irradiance expected if the rocks were black bodies at the temperature measured. It was noted from the study that the emissivity of all rock surfaces approached unity as the surface became rougher.

Yost [28] in making field studies of the effect on the spectral signatures of trees by the mineral content of the soil used a portable spectroradiometer mounted on a cherry picker. Due to the height limitations of this device much of his data was taken by looking at the side of the trees. Later he mounted a 40 foot periscope tower with a mirror at the top of the back of a truck. The radiometer was then

mounted at the base of the tower and readings were made from the mirror surface.

Miller and Pearson [29] made a spectral reflectance study of grasses, geologic material and road materials under natural conditions. Their techniques of gathering data consisted of using an EG&G 580-585 spectroradiometer. This instrument is comprised of a reflective telescope with a variable field of view from 7.5 minutes to two degrees, a monochromator housing which accepts one of three gratings to cover the spectral region from 0.18 to 1.6 microns, two photomultiplier detectors with S-1 and S-10 sensitivities, a readout unit which contains a six decade low level current amplifier and a readout meter. A one meter fiber optics probe is also available to replace the telescope. The spectroradiometer was mounted inside a small laboratory trailer which could be connected to a truck or jeep and moved on location for field measurements. The trailer had a small opening in the side through which the instrument could be sighted to read data from a folding mirror mounted on a tripod. Although the radiometer had a variable field of view in discrete steps between 7.5 minutes and 2 degrees, the useful field of view in this study was limited by the size of the folding mirror which was 15 cm. and by the distance between the radiometer and the mirror.

In recent years much work has been done at the University of Michigan and Purdue University in developing a multispectral scanner and technique whereby plants and soils can be identified from low flying aircraft with all variables present. The operation of the multispectral scanner is given in some detail in Appendix A. The technique used for identifications is based on comparing the intensity

levels recorded in each channel or bands of the electromagnetic spectrum to find a unique combination for each item to be identified. Ground truth data is collected or standard spectral signature curves are used to determine what items correspond to what intensity levels. The identification process is done by computer and has given results with eighty percent accuracy.

Marshall, Thomson, Thomson and Kriegler [30] used the University of Michigan multispectral scanner and ground truth measurements to distinguish and map winter wheat in an agricultural area near Lafayette, Indiana in 1969. A study by Earing and Ginsberg [31] was made at the same time to predict using a library of standard multispectral signatures the probability of wheat detection. Maturity of plants, time of year, altitude and background effects were studied to determine their influence on wheat recognition. Tanguay, Hoffer and Miles [32] made a similar study at about the same time using a multispectral scanner for mapping of engineering soils. This study indicated the need for additional research to quantify and predict the spectral and thermal properties of soil types and textures under various conditions of moisture and irradiance. Another study to map true islands, sawgrass, grasslands, spikerush grasslands and water using a multispectral scanner was made in a portion of Everglades National Park by Kolipinski, Hizer, Thomson and Thomson [33].

Studies on the Effects of Variables

There have been a number of other studies made with the expressed intent of studying the effects of variables on the reflectance readings or the emissivity of natural objects. These studies were surveyed

and are listed not so much for the techniques with which they collected data but for the data they present on the variables.

Block [34] obtained the emissivity of several soil surfaces versus wavelength and grain size. His studies covered a wavelength range of 2.0 - 5.0 microns. Brettner, Kern and Cronin [35] used a Barnes IT-2 IR Thermometer to take emissivity values of mineral surfaces versus wavelength for various temperatures. Most of their data was taken in the 8 - 12 micron region and was taken in a direction normal to the mineral surfaces which had been polished.

Lyons [26] in 1965 presented data which contained 330 normal emittance, reflectance and transmittance spectra of roughened rock and mineral surfaces. His data was taken from 8 - 25 microns with a Perkin-Elmer Model 112 single beam spectrometer. He heated his samples in a furnance, then directed the irradiance from the test surface to his instrument with mirrors. He showed the effects of temperature, surface roughness, and particle size on the spectral emittances of the samples.

Gates and Tantraporn [36] studied the spectral reflectance of deciduous trees and shrubs in the infrared region of 1.0 - 25 microns. The study was done in a laboratory by reflecting the irradiance from a Globar source from picked leaves to an infrared spectrometer. Several different angles were used between the source and the samples. The reading angle used was not given in the report.

Other variables studied were the effect of leaf maturity on the reflectance spectra of cotton plants in the 0.5 - 2.5 micron region by Gausman, Allen, Cardenas and Richardson [37], and also the effects of

water vapor in the air on data taken in the infrared region, 8 to 14 microns, by Oshiver, Stone, Clark and Besberian [38].

Several investigators have made computer models of the atmosphere to calculate the effects of atmospheric variables. Rose, Anding, and Walker [39] made a model to calculate the effects of the atmosphere on radiation transfer in the infrared region from 1 to 30 microns. Turner, Malila and Nalepha [40] also have made an atmospheric model to show the effects on radiant energy transfer in the 0.4 to 3 micron region. Their model was used to compute irradiance, path radiance, sky radiance, transmittance, contrast transmittance in a cloudless sky for various solar angles, viewing angles, altitudes, surface reflectances and haze conditions.

Hisim [41] in his study at LSU showed the effects of various trace gases and pollutants on the transmissivity of the atmosphere for different particle counts of the trace gases. His data was taken spectrally from 0.3 to 15 microns.

There have been many studies on the effects of angular variations on the data received by remote sensing. Hapke and Van Horn [42] in 1962 made measurements in the laboratory on many types of powered rocks and mineral surfaces at different viewing angles. They used a lamp with a S-6 spectral output as a source and made total directional reflectance measurements in the visible region. A surface coated with magnesium oxide was used as a standard. The source and viewing instrument were kept coplanar but the angles of both with respect to the test surfaces were varied.

Shockley, Knight and Lipscomb [43] made laboratory tests using a Perkin-Elmer Model 221 Spectrophotometer to get the effects of grain

size, moisture content, density, soil type and angle of incidence on reflectance and emissivity properties. A carbon arc light source was used. Measurements were made at 1.4, 1.75, 1.94, 2.15, 4.0 and 4.5 microns.

Chen and Rao [44] made a study using a similar technique on desert sand, white sand, soil and water. They took data at 3975, 5000 and 6050 Angstrons. The bandwidth of the radiation sensed was 150 Angstrons. Their study included polarization and reflectance effects resulting from various combinations of angle of illumination, angle of observation and relative azimuth between the source and the viewing instrument. Stockhoff and Frost [45] made a similar study showing the influence of viewing angles, solar angle, percent moisture content, soil type and particle size on the reflectance and polarization effect of soils.

Coulson [46, 47], and Coulson, Bouricius and Gray [48] made hemispherical maps showing the directional reflectance of soil as a function of viewing and illumination angle. They used various soils and sand as their test surfaces. Measurements were made at wavelengths of 0.49, 0.64 and 0.80 microns in a laboratory. An incandescant light source was used. A standard surface was made from an aluminum plate covered with antimony oxide paint and then coated with a 2mm layer of magnesium oxide smoke. The size of the viewing area on the samples was 10 cm. This study outlines very well the dependence of reflected radiation on angle of incidence, azimuth and elevation angle as well as wavelength and the physical state of the surface.

A Russian paper published in 1971 by Hodarev, Dunaev, Rodionov, Serebryakyan, Tchesnokov and Etkin [49] presents reflectance data for many natural objects for various sun angles, time of year, wavelength and vegetative phases. The techniques used to collect this data are unknown.

CHAPTER III

TEST PROCEDURE

A generalized test procedure was developed in order to meet the objectives outlined in Chapter I. The first step in this procedure was to decide upon a practical and inexpensive technique which could easily be used for taking reflectance and emittance data in the natural environment. A consideration in designing the technique to be used was that it simulate airborne techniques with the major exception being that the same test plot could be viewed over a long period of time. Since the use of this technique was such that the sensing system and the surface viewed were constant, the only variables affecting the data taken were the variables of the natural environment such as solar zenith angle, soil moisture content and atmospheric conditions. By taking enough data over a period of time, the effects of these variables on the reflectance and emittance characteristics of natural surfaces in a natural environment can be determined with the technique. Since the time, money, and effort required in order to take enough data to completely separate and identify the effects of all the possible variables in the natural environment on reflectance and emittance data was prohibitive, this research concentrated on developing and testing the technique and equipment which was designed.

The method developed for taking data is shown in Figure III-1 (also see Reference 50). The sun is used as the source. The test plot can be any large area of consistent vegetation or soil. The balloon is helium filled and must contain at least 1000 cubic feet

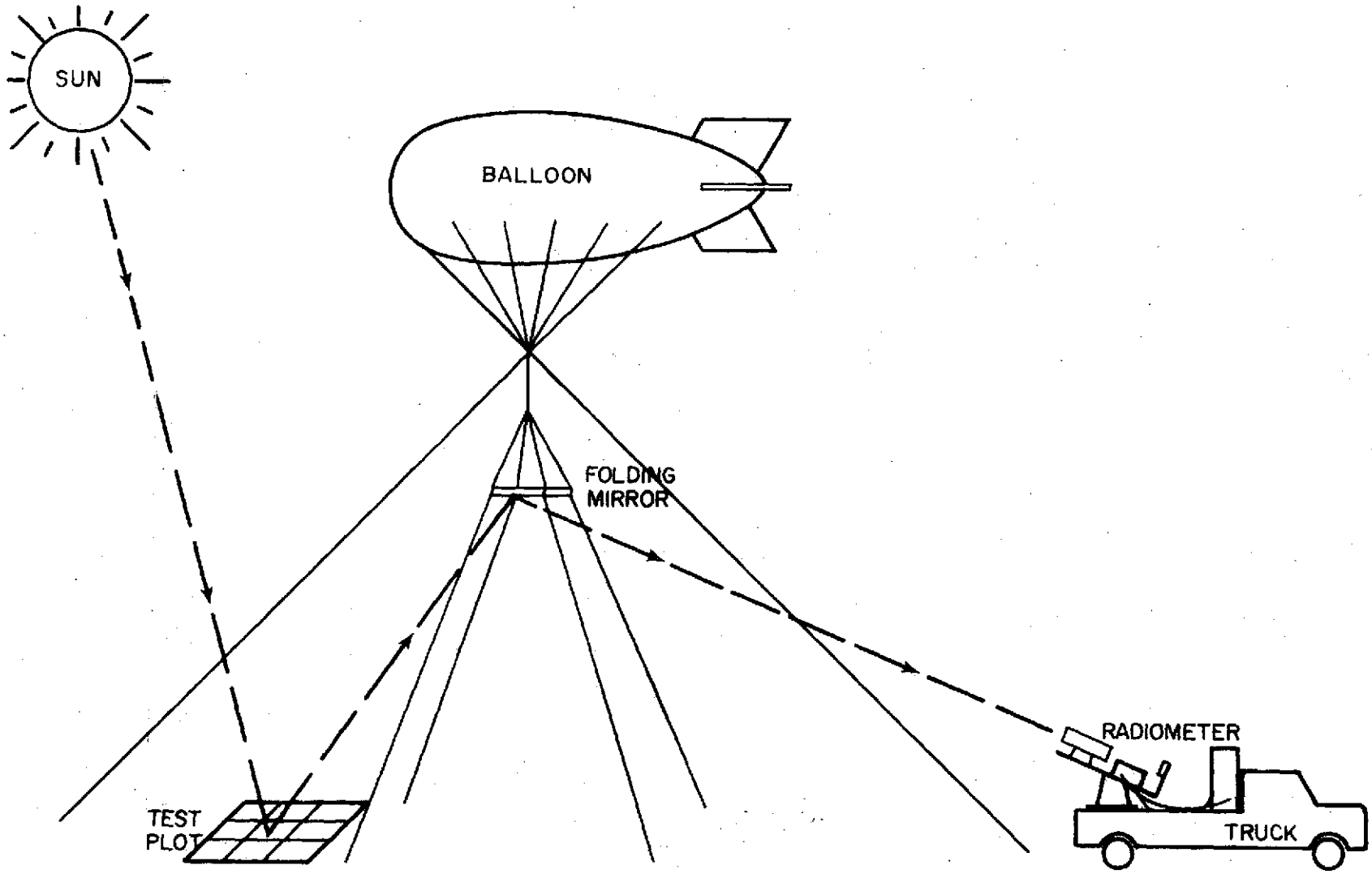

FIGURE III-1. SCHEMATIC OF SENSING TECHNIQUE

of gas in order to produce enough lift to be stable and to carry the folding mirror aloft. The balloon was held stationary by three steel cables. The folding mirror+ was also held stationary by three lighter weight steel cables and was the surface from which the spectroradiometer recorded the intensity of the energy being reflected or emitted from the test surface. The spectroradiometer was mounted on the back of a truck and was used to collect and record the data. The spectroradiometer could also be mounted in a small mobile trailer or covered van for a more protected environment.

There are several advantages to using this type of method to collect information on the effects of parameters in the natural environment on the reflectance and emittance of natural surfaces. When compared to laboratory techniques used to determine the effects of natural variables, the method as shown in Figure III-1 allows all the variables to be studied as they really are and not simulated. The balloon/mirror technique also allows a constant plot to be viewed over a long period of time. Another advantage is that a large surface area is viewed while still maintaining a small angular field of view. Therefore, individual surface irregularities are prevented from having a significant effect on the reflectance readings made, but angular characteristics of the data are still maintained. The technique described also simulates very closely the taking of data from an aircraft. This is an advantage since the data obtained with this technique can easily be correlated with the information received from airborne remote sensing techniques. The balloon/mirror method has the advantage of being able to vary many of the parameters involved in

+ The mirror itself does not fold but instead folds the optical path of the radiation.

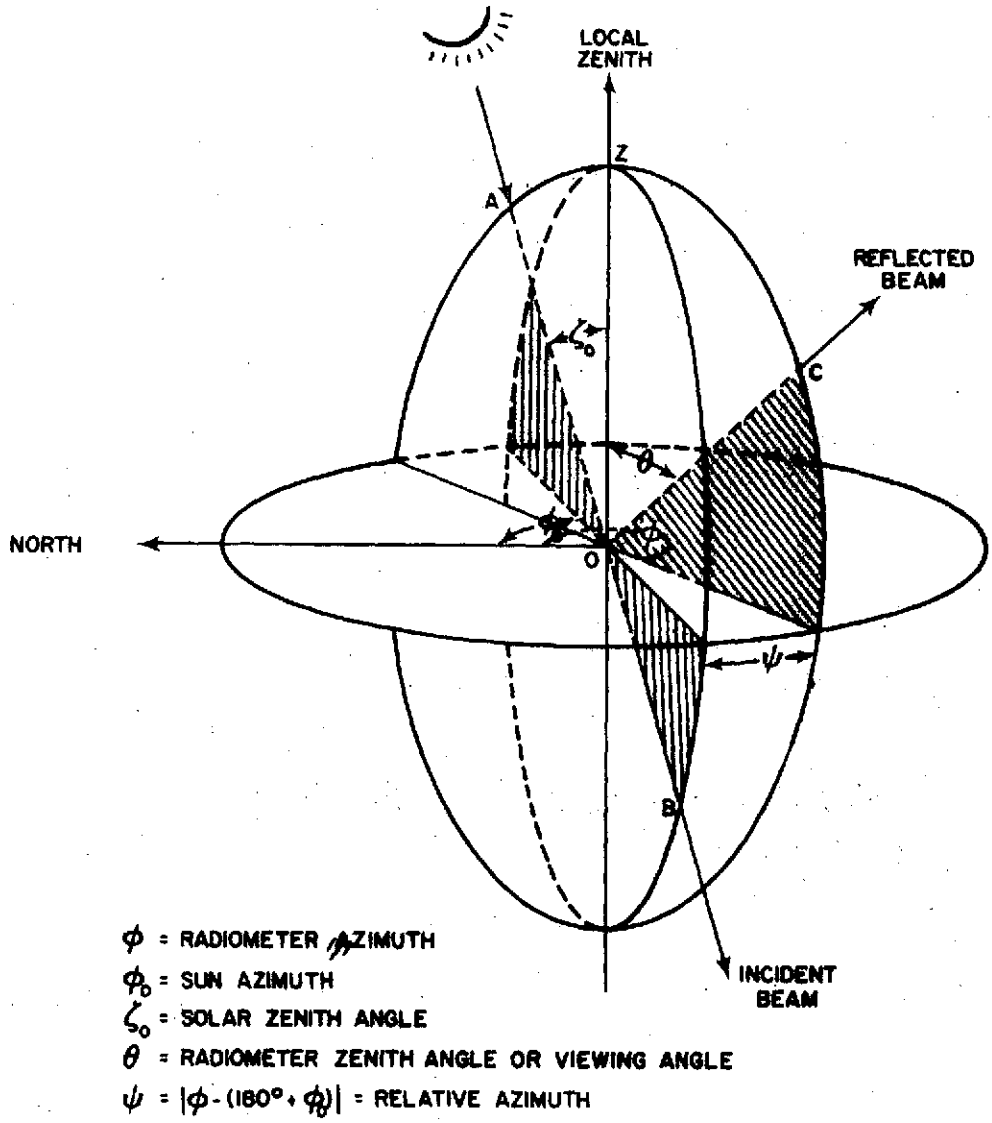

FIGURE III-2. RADIATION GEOMETRY

taking remote sensing data such as solar zenith angle*, viewing angle*, relative azimuth angle*, resolution and air column length without major difficulty. Finally, the overall costs involved with this technique are minimal.

The balloon/mirror technique for taking reflectance data has several disadvantages. First of all, a large first surface reflector approximately one-half the size of the plot to be viewed is required since the mirror is positioned approximately half way between the spectroradiometer and the test plot. The spectroradiometer must be portable and either be protected or must operate satisfactorily in the natural elements. The problems associated with field spectroradiometers are well outlined in Reference 51. The mirror must also be stabilized. The balloon/mirror system as such is rather difficult to launch and operate. The mirror height is limited since the cable weight and land size required for launching the system increases as the mirror height is increased.

The second major step undertaken to meet the stated objectives was to build and test the equipment involved in the balloon/mirror technique. The first item developed was the spectroradiometer. This item is described in Chapter IV. Since the effects of the parameters in the natural environment on the irradiation from natural surfaces is a function of the wavelength of the energy, the spectroradiometer was designed to collect data as a function of wavelength. Coincidental with the development of the spectroradiometer, the balloon/mirror system was designed, built, and tested. A discussion of the results

---

* See Figure III-2 [24] for definition of these terms.

of this work is given in Chapter V. Other components involved in the technique were then built and tested as outlined in the first part of Chapter VI.

The third step in the study was the taking of data. This was accomplished by three different methods. The first two methods were derivatives of the balloon/mirror technique and were used for a comparison to the balloon/mirror technique. The first set of reflectance data was taken in the laboratory. The spectroradiometer and a folding mirror mounted on a portable platform were used. A plot of grass contained in a shallow pan and a soil sample were tested. Readings from a standard surface were used to compare with readings from the test surface in order to obtain reflectance. Variations in the reflectance data with different source angles was obtained by accurately positioning the source at various zenith angles to the test plot and making readings. Data was taken in the spectral region from 0.3 to 3.0 microns. A 150 watt light bulb and a 500 watt photolamp were used as energy sources. In order to narrow the study, the only parameter varied was the source zenith or incident angle. The viewing or radiometer zenith angle was 15 degrees. The relative azimuth angle between the source zenith plane and the viewing plane was zero. The results of these tests are given in Chapter VI.

A second set of data was then taken in the field with the spectroradiometer and the folding mirror on the portable platform. This data was taken in a manner as close as possible to that used in the laboratory tests. The major differences were that the sun was used as the source and the data was taken in the natural environment. A test plot of grass and the same standard surface as used in the

laboratory tests were utilized in the field tests. The relative azimuth angle between the solar zenith plane and the viewing plane was kept as small as possible.

A third set of data was obtained with the balloon/mirror system. For this data the standard surface was not used. Data was taken from the same grass surface as used in the previous tests. The results of all the field testing are presented in Chapter VII.

The results of each series of tests were analyzed before the next tests were made and in this way the limitations of each method were found as well as the best procedure to be used for each of the three methods. Chapter VIII contains a brief summary of the work accomplished for the investigation and the conclusions that were made.

CHAPTER IV

SPECTRORADIOMETER DESIGN AND CHECKOUT

In order to collect the data required to meet the objectives of the research as outlined in Chapter I, a spectroradiometer was designed and built. The equipment available for building the spectroradiometer included a Celestron 8 telescope to be used as an energy-collecting device and a Perkin-Elmer Model 99 monochromator to be used as a wavelength and bandwidth selecting device. A guideline used throughout the design of the spectroradiometer was that the system be responsive to radiation within the wavelength range of 0.3 to 15 microns. However, a cooled thermocouple detector which would be responsive to energy in the 3.0 to 15 micron region was not available for the study. Therefore, the data taken was limited to the 0.3 to 3.0 micron region.

The spectroradiometer design can be divided into three main systems. These are the optical, electrical, and mechanical elements of the device. A description of each of these elements is given in the following discussion. The calibration and checkout procedure used to determine the capabilities of the spectroradiometer are also discussed.

Radiometer Optical Design

A basic block diagram of a radiometer is given in Figure IV-1 below. The focusing device and the wavelength selector contain the

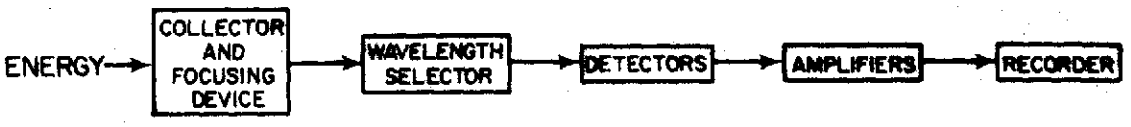

Figure IV-1: Radiometer Block Diagram

optics used in the radiometer. A schematic of the optics used for collecting and focusing the radiation is shown in Figure IV-2.

An eight inch telescope made by Celestron-Pacific was modified and used for collecting the energy being reflected or emitted from a test or standard surface. The telescope had a Schmidt-Cassegrain lens system. The primary mirror is concave, eight inches in diameter, and movable with respect to the secondary mirror which is fixed. Movement of the primary mirror is the technique used to focus the system. The secondary mirror is two inches in diameter and is convex. The image formed by these two mirrors is focused near the exit to the telescope as shown in Figure IV-2. The affective Cassegrain focal length of these two mirrors as positioned in the telescope is two meters. The near focus of the telescope is 25 feet. The field of view is 15.2 inches at 100 feet when the image is focused slightly outside the drawtube.

The telescope was modified in several respects. First of all the ocular or eyepiece was removed. Also, the Schmidt lens in which the secondary mirror was mounted was removed to allow measurements to be made in the infrared region. Therefore, a new holding device for the secondary mirror was designed and built. A photograph of the holder is shown in Figure IV-3. The final modification to the telescope was an iris or restrictor placed inside the drawtube. This iris had an inside diameter of one-half inch. The energy received by the telescope was focused at the iris. The iris helped to reduce slightly the diameter of the beam of light received by the third reflecting surface of the optical system and also made the size of the image formed at the entrance to the monochromator more compatable with the size of the entrance slit.

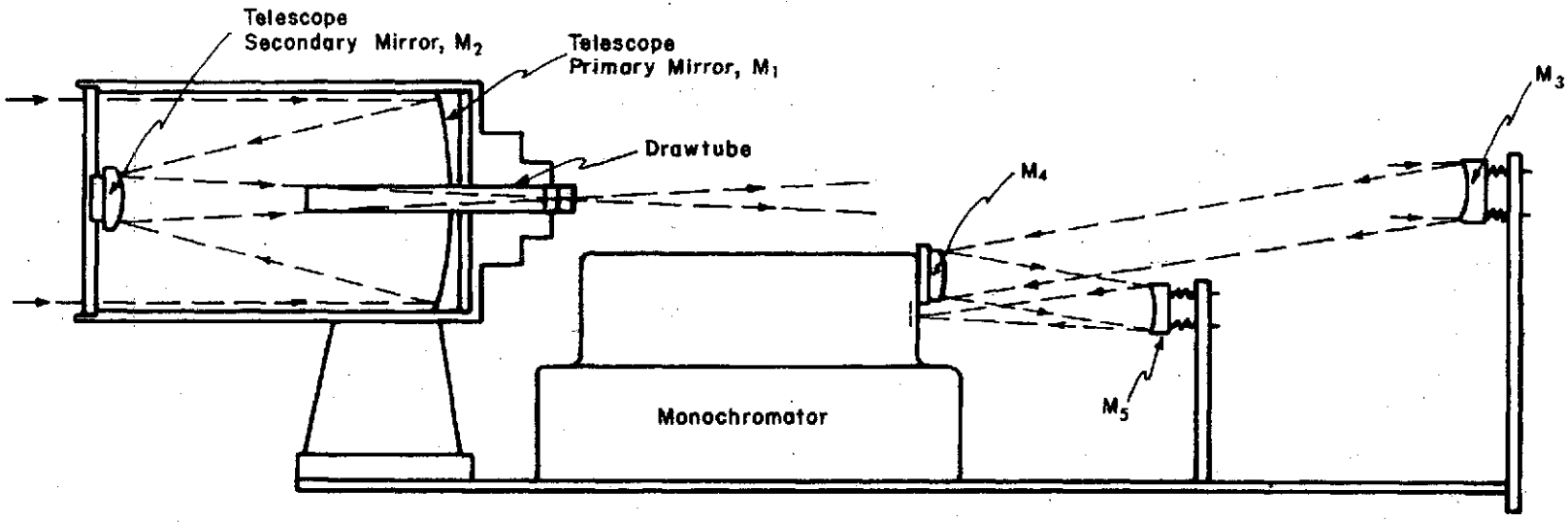

FIGURE IV-2. SCHEMATIC OF COLLECTING AND FOCUSING OPTICS

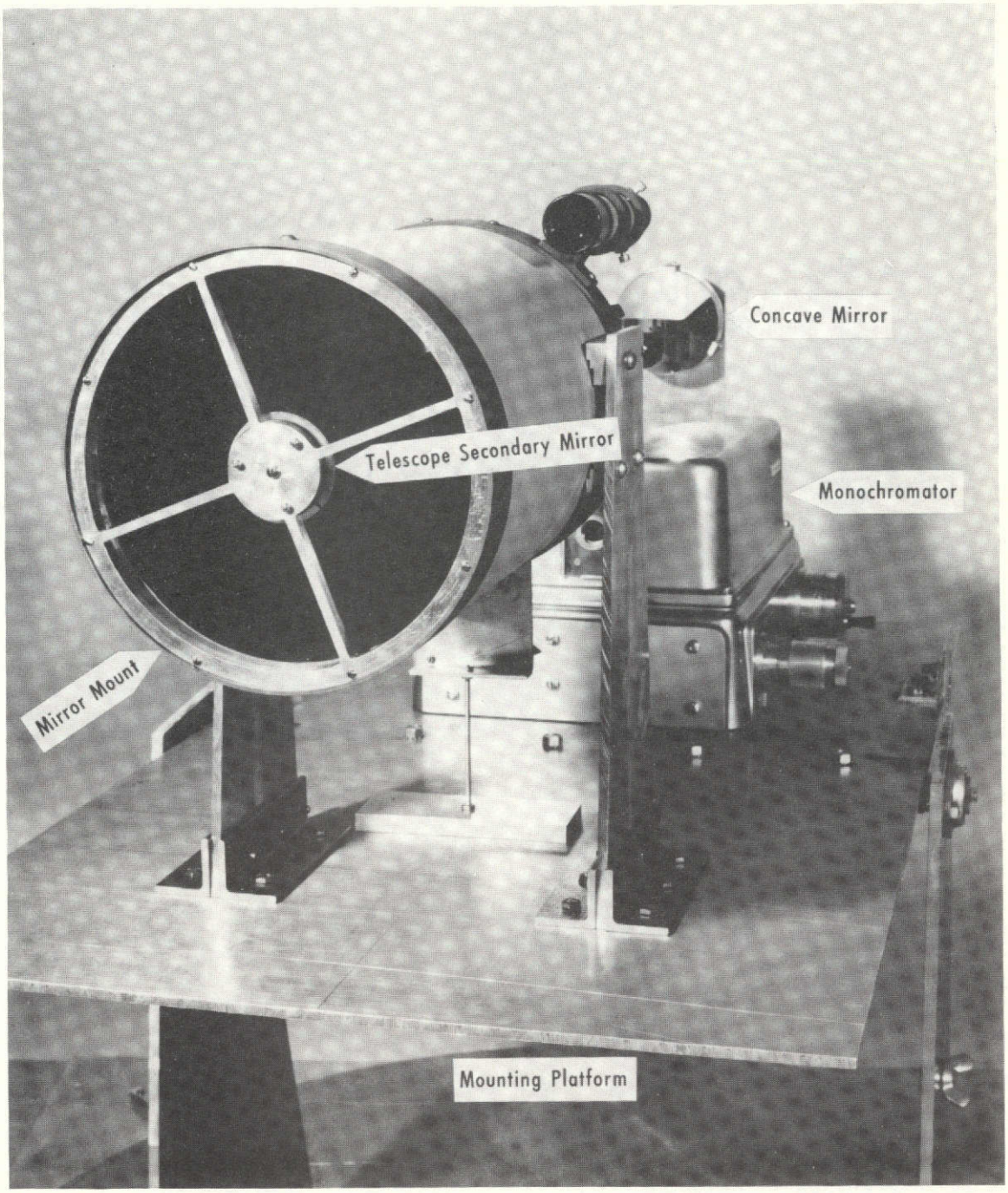

FIGURE IV-3. Photograph of Secondary Mirror Mount

The most difficult task in the optical system was designing the mirrors used to take the energy received from the telescope and focus it on the slit opening of the monochromator with as little loss in intensity as possible. The slit opening to the monochromator is 12 millimeters in height with a maximum opening width of 2 millimeters. The internal optics of the monochromator requires that the extreme aperture be f/3.5 and the effective aperture be f/4.5 of the incoming electromagnetic energy beam. Of the many design possibilities the optical arrangement shown in Figure IV-2 was chosen as the one which could be used to best match the monochromator optics with a minimum loss of beam intensity and which had the smallest off-axis angles.

A four inch diameter concave mirror, M_3, with a focal length of 0.55 meters is located 34 inches from the focused image formed by the telescope. This mirror was built by the Oriel Optics Corporation and consists of pyrex glass, vacuum deposited with aluminum, with an overcoat of silicon monoxide. The surface is spherical to an accuracy of one-fourth wavelength of visible blue over 80 percent of the diameter.

M_4 is a 2.6 inch diameter flat mirror. It is located (surface to surface) 18.75 inches from M_3. It is built of the same materials and to the same accuracy as M_3. It has a thickness of one-fourth inch. It was built by the Dudley LeRay Clausing Company.

A 2.0 inch diameter concave mirror, M_5, with a focal lenth of 0.25 meters is located 7.5 inches from the slit opening to the monochromator. It was also built by the Dudley LeRay Clausing Company of the same materials and to the same accuracy at M_3 and M_4.

The image formed by the telescope at the iris is demagnified by the focusing optics by a factor of 0.384. Therefore, the image formed

at the monochromator entrance has a diameter of 4.87 millimeters. The aperature of the beam entering the monochromator is 4.9. The projection of the image focused on the slit entrance is as shown in Figure IV-4. Therefore, the energy looked at by the monochromator from a test plot 200 feet away is that received from a strip 11.7 inches wide. This roughly corresponds to looking at a plot or strip of ground 50 feet wide from an altitude of 10,000 feet.

A Perkin-Elmer Model 99 double pass monochromator was used as the wavelength selector. The optical path of the monochromator is given in Figure IV-5. Light or electromagnetic energy entering the entrance slit, S1, is collimated by the 21 degree off-axis paraboloid, M1, on the prism, PR. After one refraction the beam is reflected by the Littrow mirror, M2, for a second refraction by PR. The returning beam is brought to a focus by M1 between the two halves of M4 after reflection from the small diagonal mirror, M3. M4 reflects the beam back through the system, slightly displaced so that, after a second traversal through the parabola-prism-Littrow system, it is brought to a focus on the exit slit, S2, after reflection from M5.

The monochromator is designed to operate in a range extending from the ultraviolet to 15 microns in the infrared region. However, it is necessary to interchange prisms when operating over this entire range. For that reason a fused silica prism with an apex angle of 50 degrees was used through the wavelength range of 0.2 to 3.0 microns. A NaCl prism with an apex angle of 60 degrees must be used throughout the infrared region from 3.0 to 15 microns.

Wavelength control is obtained with a wavelength micrometer drum which controls the movement of the Littrow mirror. The drum is graduated

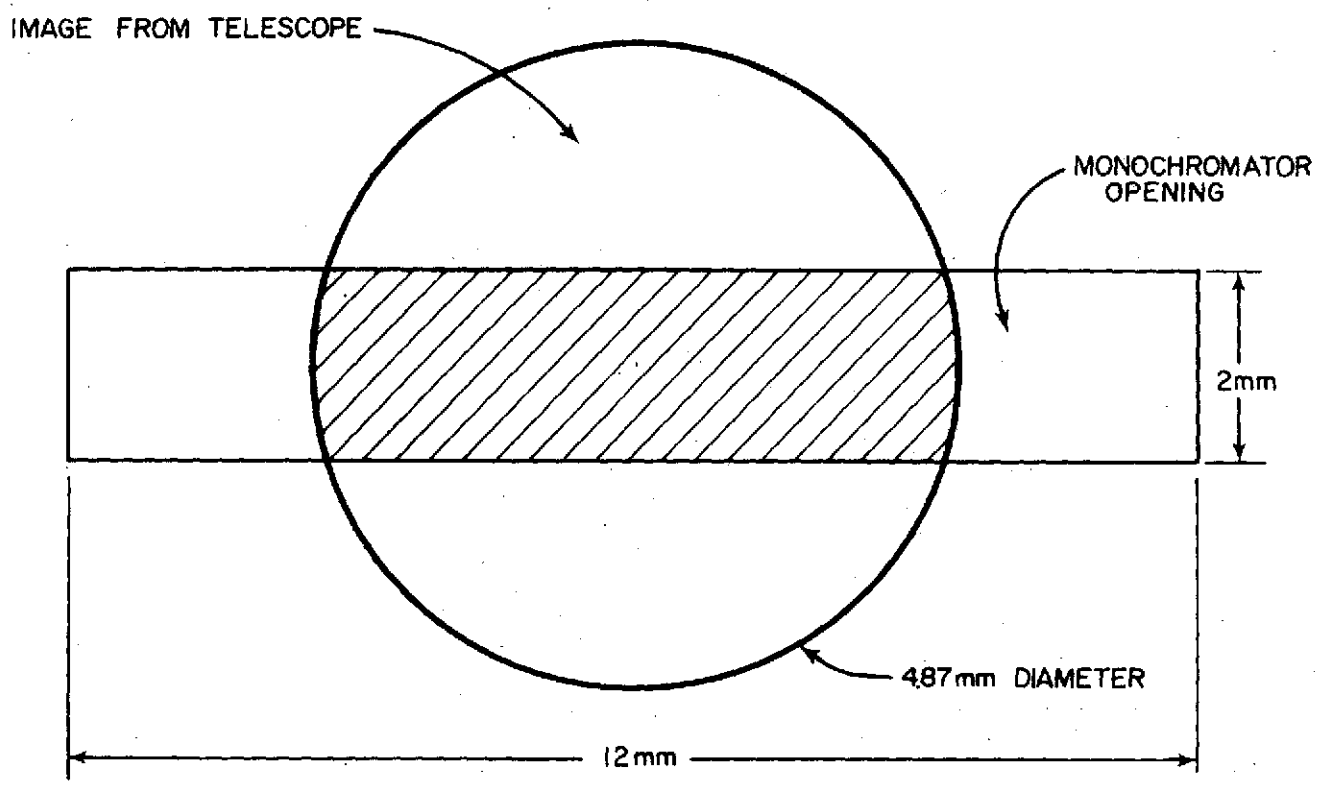

FIGURE IV-4. PROJECTION OF IMAGE ON MONOCHROMATOR ENTRANCE

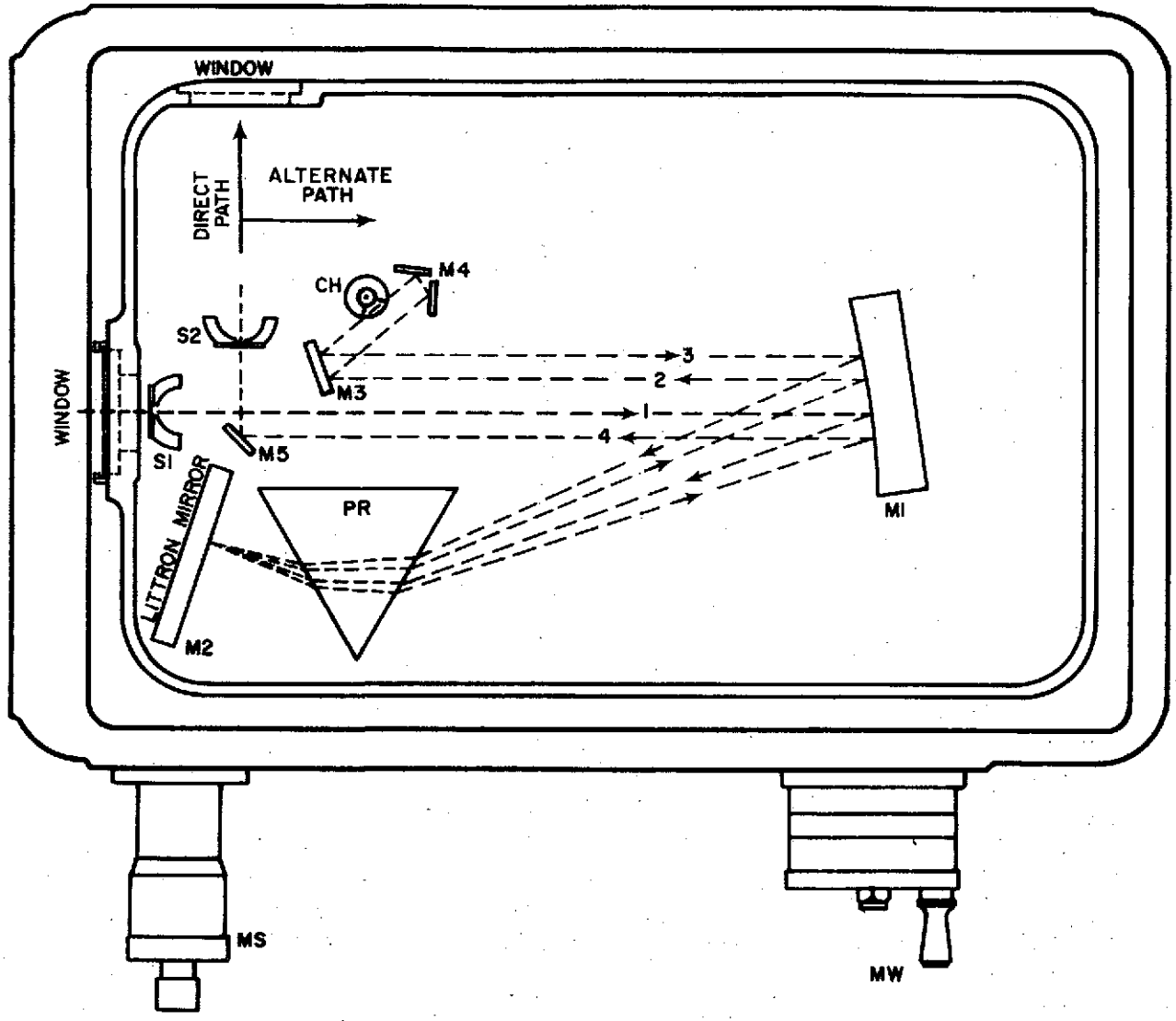

FIGURE IV-5. SCHEMATIC OPTICAL PATH OF THE MODEL 99 DOUBLE PASS MONOCHROMATOR

in 2400 divisions. Each division represents 16.1 seconds of Littrow rotation arc. Total arc movement is 10.7 degrees. In addition, there is a fine screw on the Littron mirror mount which permits 18 degrees of motion from any arbitrary initial setting of the mirror. The shaft of the wavelength micrometer extends through the back of the monochromator to permit motor coupling for automatic scanning of the spectrum.

Electrical/Electronic Design

An overall schematic of the electrical/electronic components of the radiometer is given in Figure IV-6. Each component shown in the schematic is described in the following paragraphs. The numbers shown in the schematic refer to the cable numbers which connect the components. These cables were purchased from the Perkin-Elmer Company.

The energy exiting from the monochromator is focused onto detectors which convert the electromagnetic energy into an electrical signal. Two detectors were required to cover the wavelength range in which measurements were made.

A RCA 1P28 photomultiplier tube was available for measurements in the wavelength range of 0.2 to 0.68 microns. The tube is a nine-stage side-on type with an S-5 spectral response. Power was supplied to the photomultiplier tube at a regulated voltage of 900 volts D.C. from a Perkin-Elmer photomultiplier power supply, Model number 112-0038. The tube was mounted in an external mounting assembly in the side of the monochromator. The external assembly (Perkin-Elmer Model 012-0180) contained a quartz condensing lens with a focal length of 59 millimeters, for focusing the energy on the tube.

A lead sulfide detector (Perkin-Elmer Model 012-0353) was used in the spectral range of 0.69 microns to 3.0 microns. The unit was housed

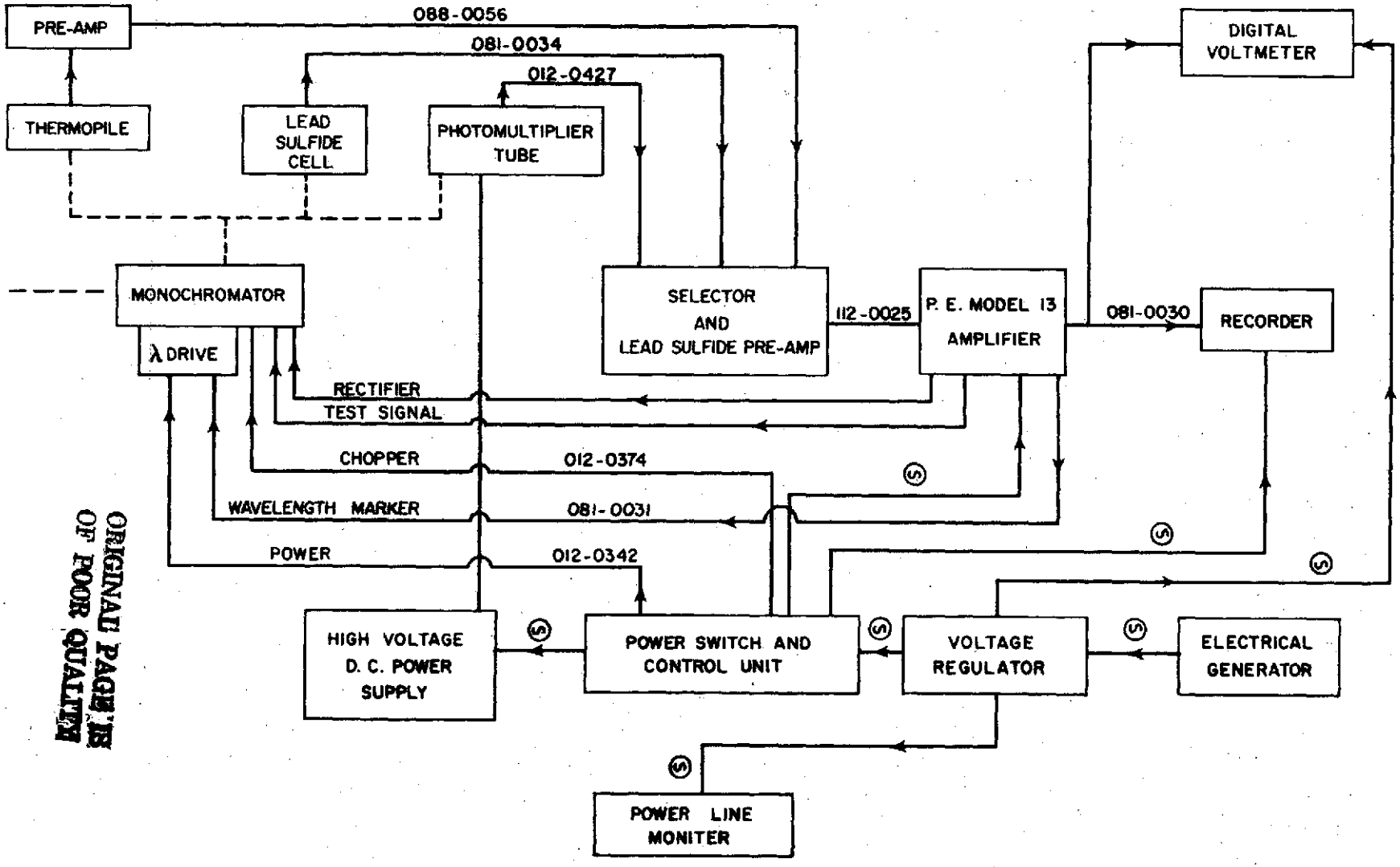

FIGURE IV-6. ELECTRICAL BLOCK SCHEMATIC

in an assembly (Perkin-Elmer Model 099-0019) mounted at the exit slit of the monochromator. The housing assembly included an ellipsoidal mount for focusing the energy on the cell unit. The cell was simply connected to a preamplifier and switching unit (Perkin-Elmer Model 112-0028). The preamplifier operates on a 13 cps input and has a gain of 100.

If it is desired to make emittance measurements in the far infrared region, it is necessary to use a cooled thermopile detector and a NaCl prism in the monochromator. The manner in which the thermopile would be connected electrically into the system is also shown in Figure IV-6.

The Perkin-Elmer amplifier consists of standard resistance-capacitance amplifier circuits using dual triodes to provide amplification and a suitable output stage to match the rectifiers, filters and loads. It is a three-stage, 13 cycle per second carrier amplifier. A panel mounted resistor controls the gain of the amplifier in 4 decibel steps.

The model 13 amplifier was originally intended for use in a Perkin-Elmer Model 13 Ratio Recording Infrared Spectrophotometer. Since in its original capacity the amplifier was used to compare and amplify two inputs, several modifications were required so that the amplifier would work satisfactorily in this application. The first modification consisted of taking the test output from the amplifier circuit and connecting it directly to the recorder, therefore bypassing the comparison circuits. Secondly, a switch was installed so that the filter circuit could be switched back into the system between the output of the amplifier and the recorder to control the response. Another modification which was required because of the first modification was to put a variable resistor into the standard cell circuit of the amplifier which controlled the

range and calibration of the recorder. This control was then used to calibrate the recorder. The digital multimeter was used as the standard in this calibration.

The amplified signal was recorded by a modified Leeds and Northrup Speedomax type G recorder. The modification included removing the standard cell circuit from the recorder and placing it in the amplifier and providing internal connections to the recorder slidewire. A standard 450 ohm resistance slidewire was used and the original amplifier and damping circuits were retained. A Fluke digital multimeter (Model 8000A) was also connected parallel with the recorder so that a digital readout was available.

Power was supplied to the system by a Sears 5000 watt portable alternator during field use. The alternator is powered by a 12 horsepower gasoline engine. The alternator will produce up to 43.5 amps at a voltage level of 115 volts, 60 cycles. The power produced by the alternator is regulated by a Sorenson A. C. Voltage Regulator, Model No. 1000S. The regulator requires an input voltage range of 95-130 volts and has an adjustable output range of 110-120 volts. The regulation accuracy against both line and load changes is $\pm$0.1 percent at nominal frequency. The input current at full load is 13.5 amps at 115 volt input. An RCA WV-120A power line monitor is used to check the regulator output.

A Perkin-Elmer Model 012-0455 control unit is used to control the power distribution to the various units of the radiometer. The wavelength output of the monochromator is controlled by a wavelength micrometer drum coupled to the Littrow mirror and to a wavelength drive mechanism. The wavelength drive is controlled by the control unit and can be operated manually or at any one of three fixed speeds.

The control unit also controls a mechanical rectifier and chopper assembly housed in the monochromator.

Most of the electronics equipment was mounted in a 19 inch rack so that it could be easily moved and mounted on a truck. A photograph of the mounted equipment is shown in Figure IV-7.

Mechanical Design

There were a number of mechanical items which were designed and built for the experiment. The largest of these items was the mounting platform for the optical train of the radiometor. The platform was required to have three degrees of freedom. A photograph of the resulting design is shown in Figure IV-8. The majority of the weight of the platform is in the base which is made of two one-half inch aluminum plates. The two plates are attached by a center pin and bearing. Teflon rings attached to each plate allow the top plate to be rotated. The platform itself was mounted on a 1 inch by 1 inch steel bar which was mounted on bearings. The platform zenith position was fixed by use of a sliding arm and wing nut arrangement. The entire assembly was designed to be easily broken down into three parts which could be carried by two men and reassembled on a truck bed. This design allowed the entire optical train to be assembled, aligned and checked out in the laboratory while attached to the platform. Then the mounting platform could be disassembled while still leaving the optical train intact.

The mounting platform included locking devices for holding the telescope and optical train in any position desired. The design also included a method for obtaining fine adjustments.

Other mechanical holders and devices were also built for the

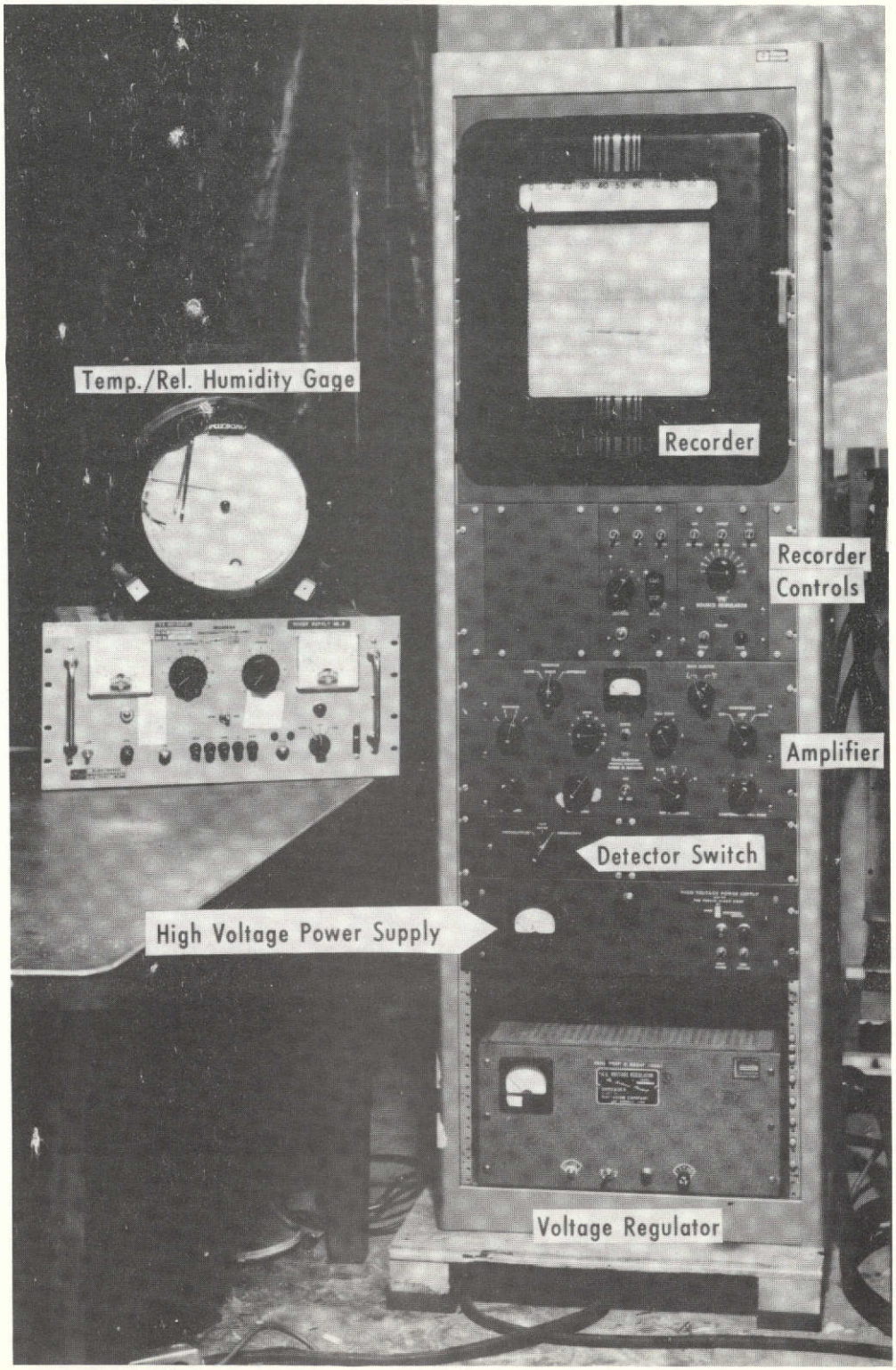

FIGURE IV-7. Photograph of Mounted Electronics Equipment

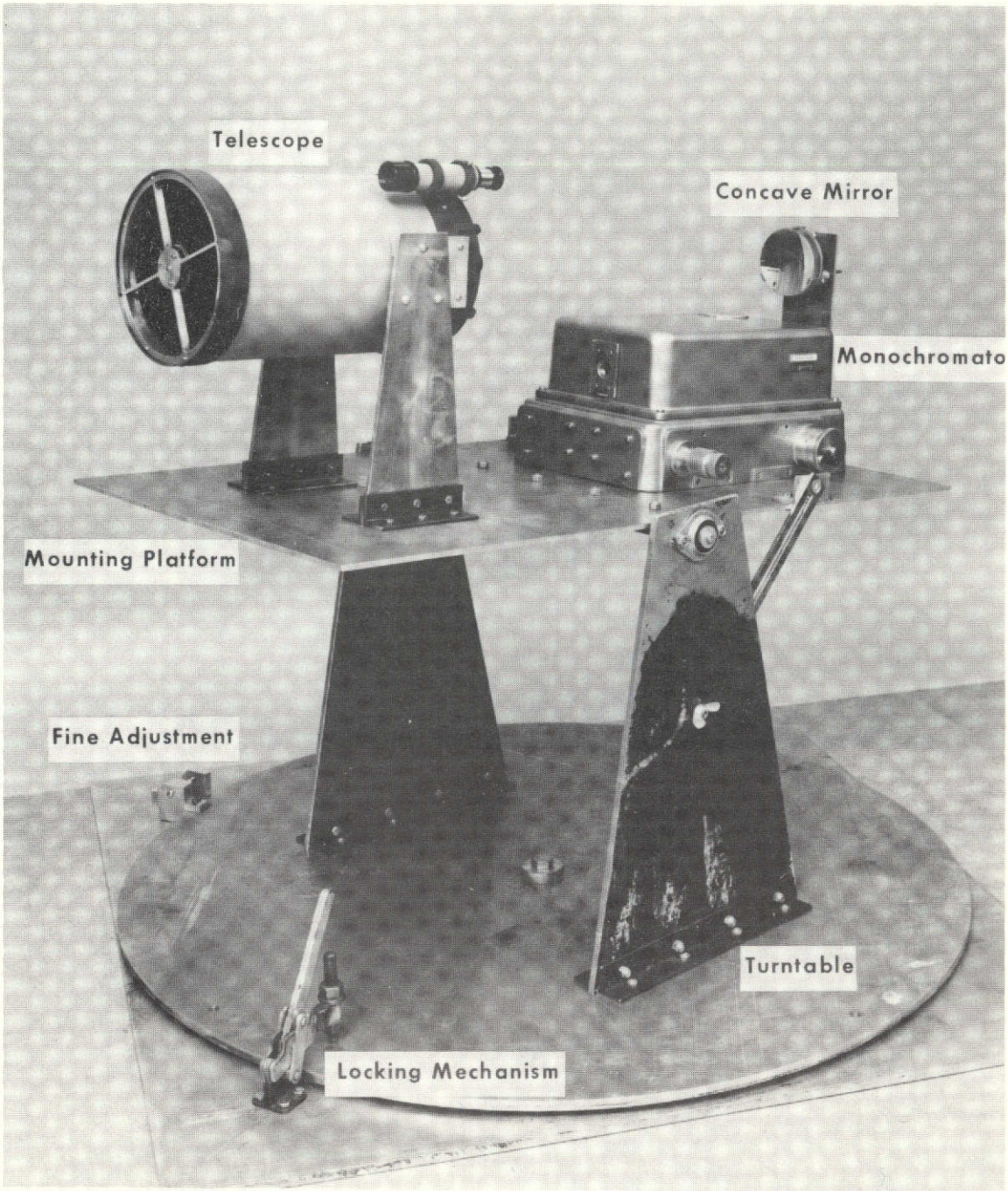

FIGURE IV-8. Photograph of Optical Mounting Platform

radiometer. These included the mounting arms for the telescope and covers made of aluminum sheet used to make a light tight area between the telescope and the monochromator. Holders and braces were also designed and built for the mirrors used to reflect and focus the energy between the telescope and the monochromator. A photograph showing the holders and part of the cover, is given in Figure IV-9.

Another item which was designed and built exclusively for this experiment was the secondary mirror mount for the Celestron 8 telescope. Ordinarily, the secondary mirror is held in place by a corrector lens that is made of crown glass. In order to make measurements in the infrared region, the corrector lens had to be removed. Therefore the new mounting system shown in Figure IV-3 was build and installed. Slightly, better light gathering ability could have been achieved had three arms been used in the design instead of four as seen. The secondary mirror is attached by a single screw in the middle of the mount. The three additional screws seen are not connected to the mirror but are used to position the mirror and thus collimate the telescope optics.

Calibration of Monochromator

The monochromator had to be calibrated in order to obtain the wavelength of energy being transmitted versus the position of the micrometer drum which controlled the angle of the Littrow mirror. Since two different prisms were available to be used in the system, two calibration curves were determined. The final results are given in Figure IV-10.

The first calibration was made for the NaCl prism. The NaCl prism

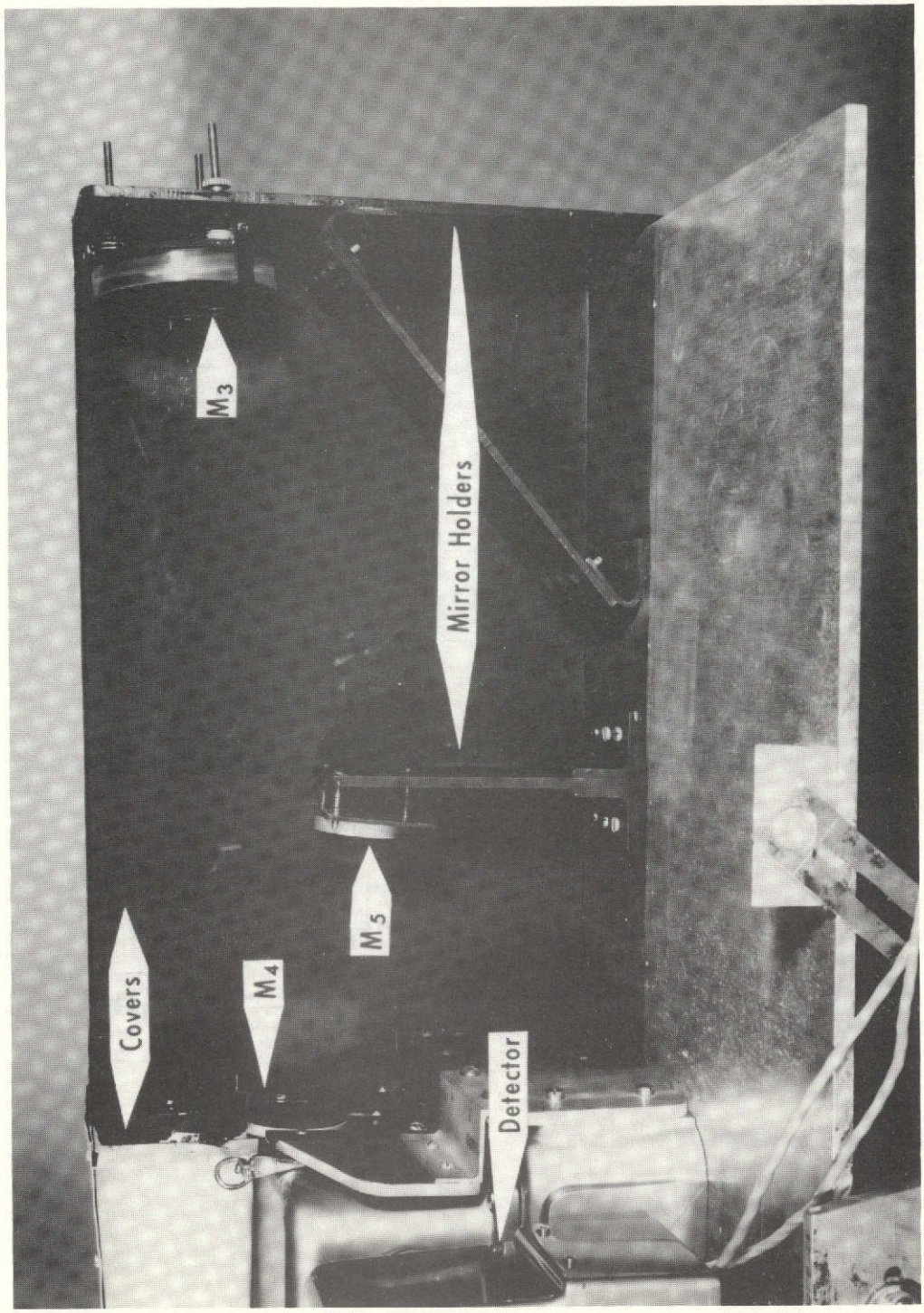

FIGURE IV-9. Photograph of Mirror Holders and Covers

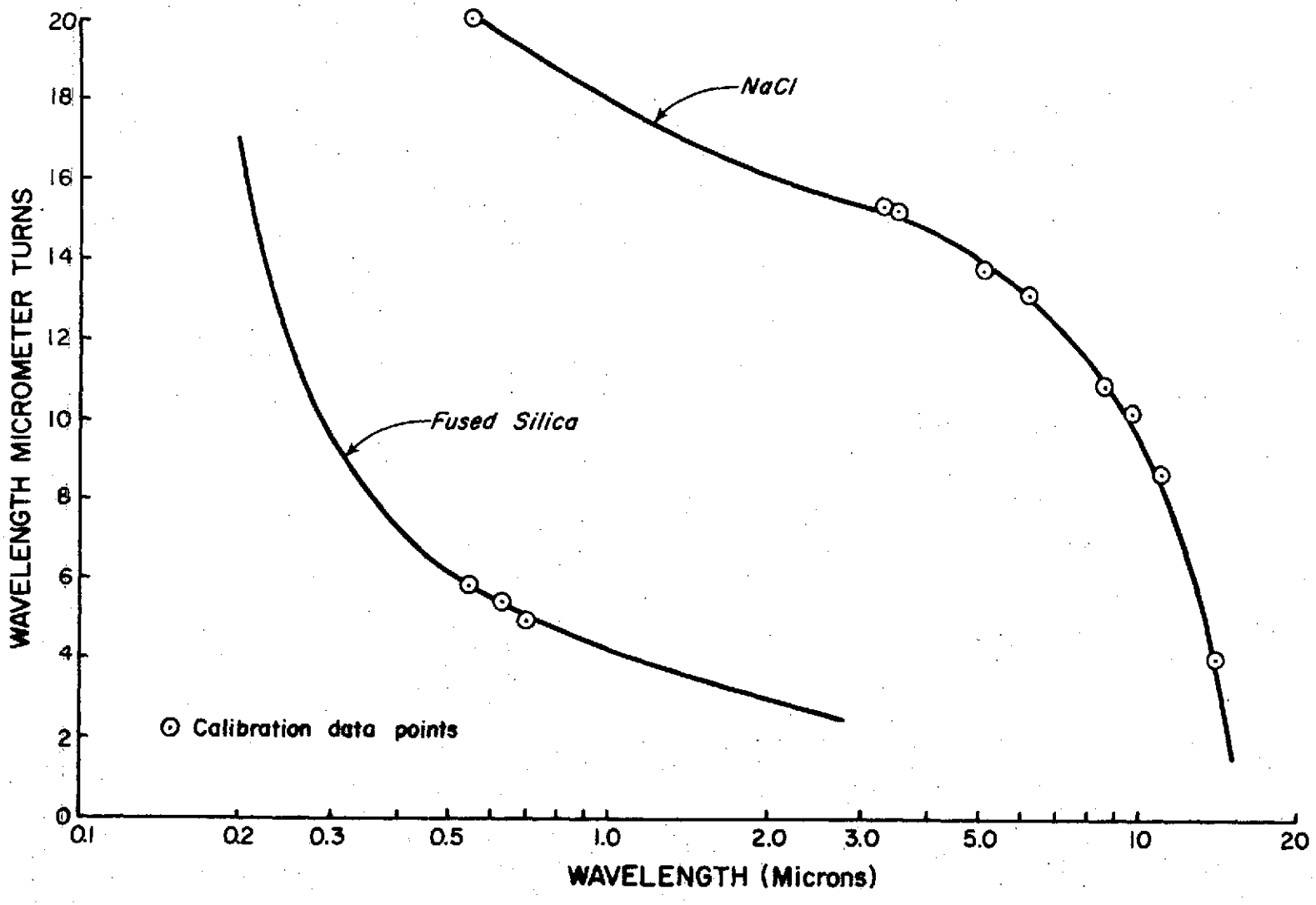

FIGURE IV-10. CALIBRATION CURVE FOR NaCl AND FUSED SILICA PRISMS

was mounted in the monochromator and a mercury calibration lamp was set up so that its output was focused on the entrance slit to the monochromator. An approximate calibration curve was available from the monochromator manufacturer. This curve indicated the mercury lamp spectra of 5461Å should be obtained at the monochromator output when the drum micrometer reading was 20.0. An adjustment screw on the Littrow mirror was adjusted so that this condition was obtained. The Littrow mirror adjustment screw was then marked so that the mirror could be returned to this condition at any time without re-calibration.

A glowbar lamp was then set up in place of the mercury vapor lamp and an uncooled thermocouple detector was placed at the output of the monochromator and connected up to the amplifier and digital voltmeter. A wavelength filter calibrator was then placed at the entrance to the monochromator. The filter was originally made for use with a Beckman infrared spectrophotometer for calibration purposes. Eight points were available in the infrared region with the filter where the transmissivity of the filter had definite known values that were easy to distinguish. These points were then found with the system as described and the drum setting at each point recorded. These points were then plotted as shown in Figure IV-10. The approximate calibration curve obtained from the monochromator operator's manual was then fitted to the calibration data points to obtain the curve shown.

Calibration of the fused silica prism was made in a similar manner. The mercury lamp was set up, and the Littrow mirror was adjusted so that the micrometer drum reading matched the approximate calibration curve at 5461Å. Only one other calibration point was then obtained by using a helium neon laser which produced light at 6328Å. Another

point was plotted by using a tungsten lamp as a source and a 1P28 photomultiplier tube with a S-5 response as a detector at the output of the monochromator. The S-5 curve has a cutoff point at approximately 6800A. The drum was then rotated until this point was found and the reading recorded and plotted as shown in Figure IV-10. This third point can only be considered as approximate and therefore was not considered to be a reliable calibration point. The approximate calibration curve from the operator's manual was then fitted to the data as shown.

In order to complete the calibration, the bandwidths of the energy exiting from the monochromator versus the median wavelength were calculated. The results of these calculations based on manufacturer's data are given in Tables IV-1 and IV-2 for the two prisms. The bandwidths shown are based on an exit slit width of 2 millimeters. Unfortunately with the Model 99 monochromator used, the entrance and exit slits were connected to the same adjustment. Therefore, since it was required to keep the entrance slit at a maximum value of 2 millimeters in order to have as large a field of view with the radiometer as possible, the exit slit was also required to be at 2 millimeters. The internal design of the monochromator then resulted in the variations in the bandwidths for different wavelengths. The manufacturer's bandwidth curve for the NaCl prism had to be extrapolated into the far infrared region in order to get the data shown in Table IV-2. This data is shown plotted in Figure IV-11.

Checkout of Spectroradiometer

After the monochromator calibration was completed, the spectroradiometer system was assembled in the laboratory as shown in Figure

TABLE IV-1

BANDWIDTH TABULATION FOR FUSED SILICA PRISM

Median Wavelength (Å)	Drum Setting	Δλ (Å)	Band Limits (Å)
3000	9.50	40	2980-3020
3500	8.20	70	3465-3535
4000	7.30	100	3950-4050
4500	6.60	150	4425-4575
5000	6.20	200	4900-5100
5500	5.80	260	5370-5630
6000	5.50	340	5830-6170
6500	5.30	440	6280-6720
7000	5.10	530	6735-7265
8000	4.70	650	7675-8325
9000	4.40	720	8640-9360
10000	4.20	780	9610-10390
12000	3.80	840	11580-12420
14000	3.60	860	13570-14430
16000	3.30	850	15575-16425
18000	3.10	800	17600-18400
20000	3.00	700	19650-20350
22000	2.80	600	21700-22300
24000	2.70	460	23770-24230
26000	2.60	360	25820-26180

TABLE IV-2

BANDWIDTH TABULATIONS FOR NaCl PRISM

Median Wavelength (μ)	Drum Setting	Δλ(μ)	Band Limits (μ)
2.0	16.05	0.36	1.82- 2.18
2.5	15.60	0.48	2.26- 2.74
3.0	15.30	0.60	2.70- 3.30
3.5	15.00	0.80	3.15- 3.85
4.0	14.65	0.78	3.61- 4.39
5.0	13.95	0.88	4.56- 5.44
6.0	13.20	0.96	5.52- 6.48
7.0	12.40	1.02	6.49- 7.51
8.0	11.60	1.06	7.47- 8.53
9.0	10.80	1.10	8.45- 9.55
10.0	9.50	1.12	9.44-10.56
12.0	7.00	1.14	11.43-12.57
14.0	4.00	1.16	13.42-14.58
16.0	-----	1.18	15.41-16.59

Note: Bandwidths and limits above 8μ are only approximate.

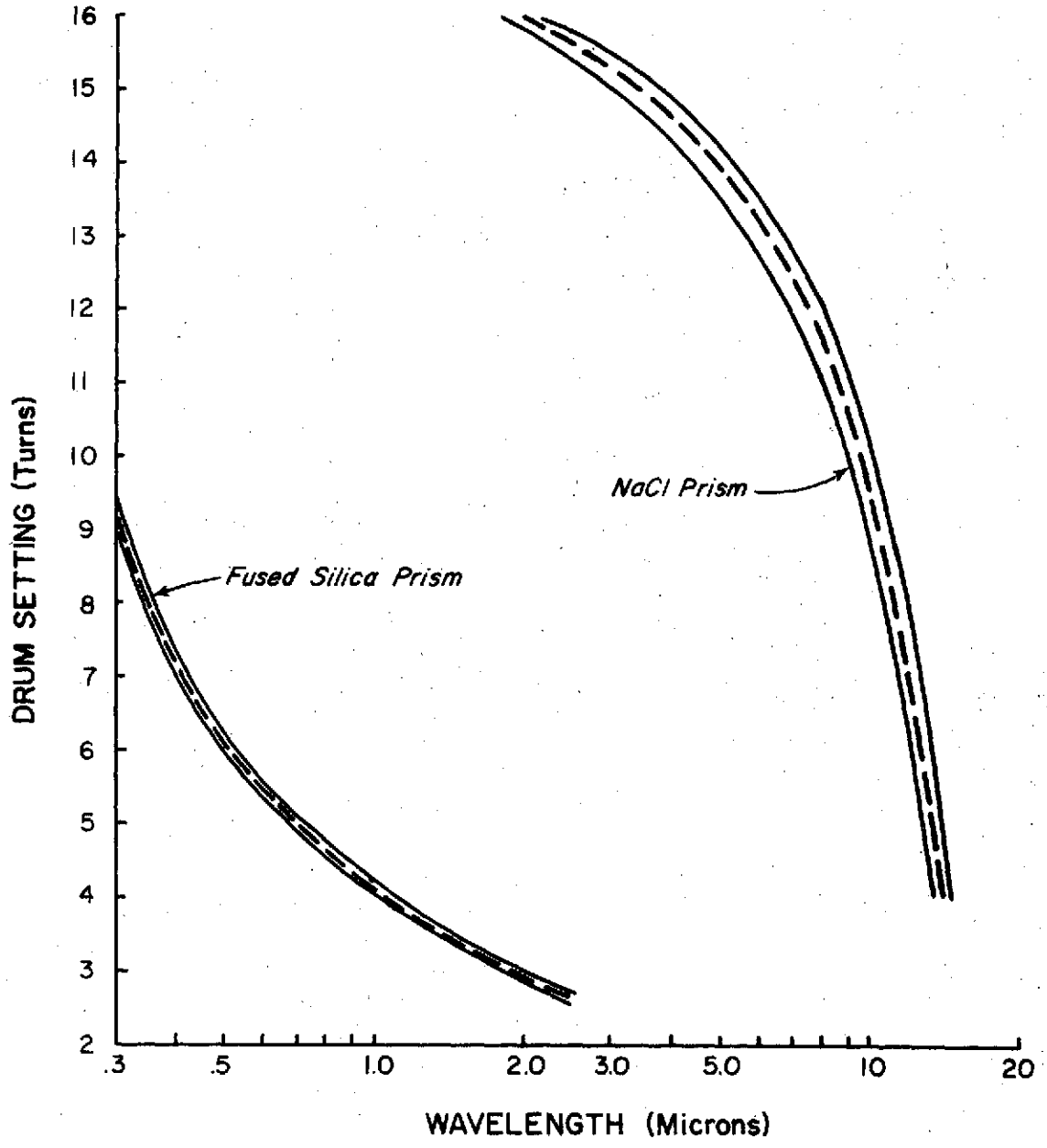

FIGURE IV-11. BANDWIDTHS OF ENERGY VERSUS DRUM SETTING FOR PERKIN-ELMER MODEL 99 MONOCHROMATOR

IV-12. A white cardboard target was mounted on a wall at the far side of the laboratory. A 150 watt spotlight was then shown on the target and readings were made with the radiometer which was located 56 feet from the target. The photomultiplier detector was used throughout the checkout of the system.

The first item checked was the responsiveness of the spectroradiometer. The 150 watt spotlight was first located only six to eight feet from the target; however, a quick scan through the detectable energy spectrum (0.3-0.68 microns) of the photomultiplier detector showed that the photomultiplier tube was flooding out through much of the region. It was then found that the spotlight had to be at least twelve feet from the target if the detector was to operate properly. The input voltage to the photomultiplier tube was 900 volts D.C. By lowering the input voltage, the sensitivity of the system could be lowered so that higher energy could be detected accurately. However, in the visible region the responsiveness was such that a flash light shining on the target from ten feet away could be easily detected. Therefore, the only problem with the sensitivity of the system in the visible region was flooding the detector so that the output was not linear.

The alignment of the radiometer optical system was then checked. This was done by setting the system up and then adjusting the focusing mirrors until the highest value for intensity at a particular wavelength was obtained. The results of these tests showed that the alignment of the system was not critical. That is, the system could be aligned by eyesight and the highest reading for the intensity obtained. Also some error in the alignment could be tolerated without affecting the readings. The capability of the system to withstand vibration without

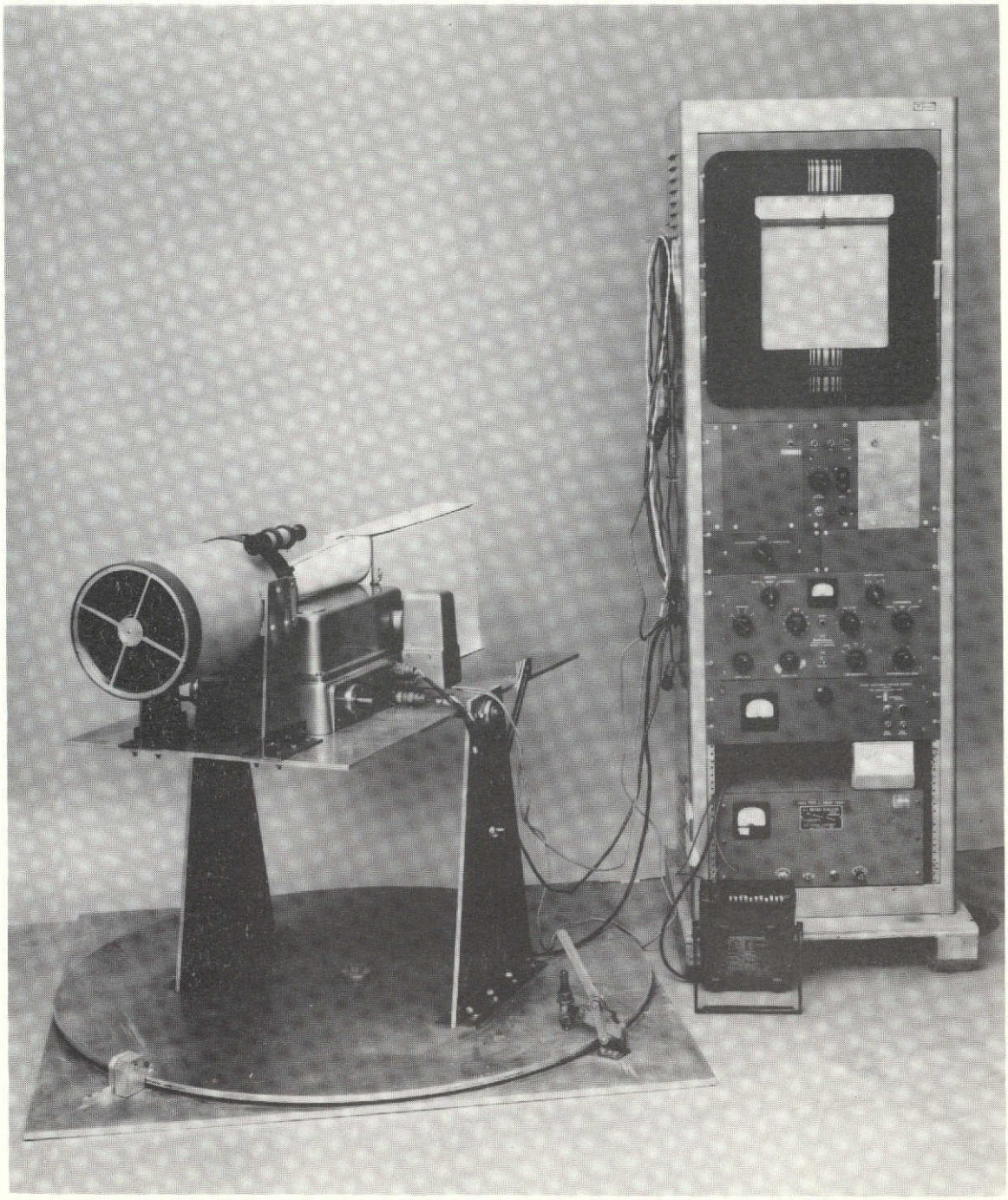

FIGURE IV-12. Photograph of Assembled Spectroradiometer

changing alignment was also checked. This was accomplished by shaking the mounting platform and mirror mounts while reading from the target. No variation in the intensity read or change in the optical alignment of the system was noted during these tests.

The optical portions of the radiometer had originally been focused visually. This focus was checked after the system was completed by changing the focus while reading the intensity from the target at selected wavelengths. It was found that the focus obtained visually gave the brightest reading; however, considerable changes in the focus knob on the telescope from the original setting had little or no effect on the intensity readings.

The field of view of the radiometer was determined by moving a piece of black cardboard across a white target and marking the points where the intensity reading decreased by 2 percent. The results of these tests showed the shape of the field of view of the instrument to be as shown in Figure IV-13. At 56 feet, the field of view had a width of 1.98 inches and a height of 4.86 inches. The angular field of view is therefore 0.40 degrees or 24 minutes in the vertical direction and 10 minutes in the horizontal direction. Table IV-3 gives the size of the spot viewed by the radiometer at various distances if the area viewed is perpendicular to the line of sight of the radiometer.

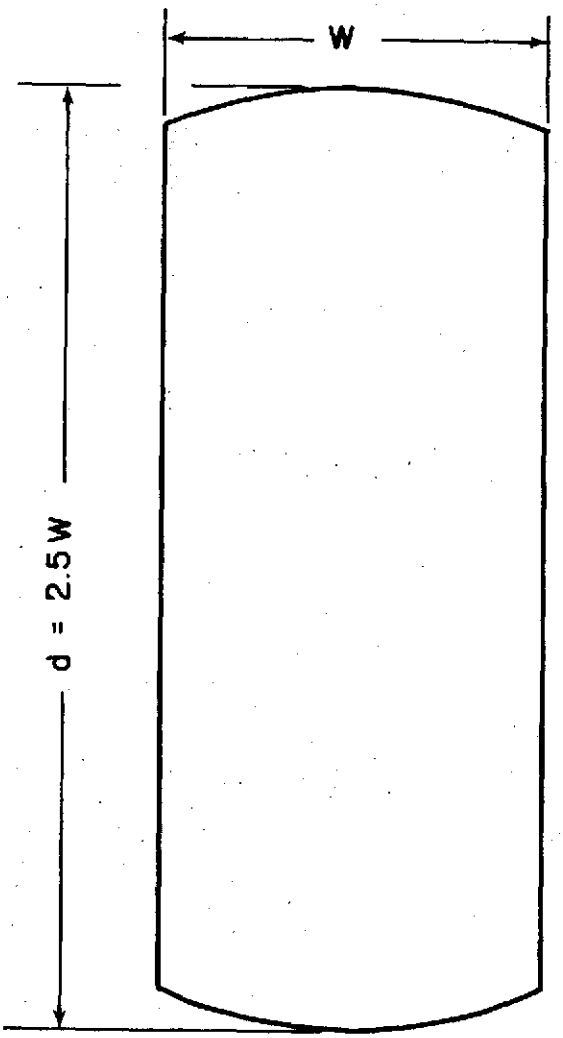

FIGURE IV-13. SHAPE OF RADIOMETER FIELD OF VIEW

TABLE IV-3

FIELD OF VIEW OF SPECTRORADIMETER

Distance* (Feet)	Width of Spot Viewed (Inch)	Height of Spot Viewed (Inches)
50	1.75	4.2
100	3.50	8.4
150	5.25	12.6
200	7.00	16.8
250	8.75	21.0
300	10.50	25.2
350	12.25	29.4
400	14.00	33.6
450	15.75	37.8
500	17.50	42.0

* Distance is obtained by adding 1 foot to the length measured between the focal plane of the telescope and the target.

CHAPTER V

BALLOON SYSTEM DESIGN AND TESTS

The design and analysis of the tethered balloon/reflecting surface system consisted of three parts. The first part was an initial design study made primarily to determine the feasibility of the concept. The second part consisted of experimental tests using helium filled balloons to gain operational experience of the system and to collect data on the stability of the reflecting surface under actual flight conditions. The third phase was the final system design which was made for the balloon/reflecting surface system used for the taking of reflectance readings.

Part I. Initial Design Study

The objective of the initial study was to design and determine the feasibility of a method to be used in stablizing a mirror or reflecting surface suspended by a tethered balloon. The mirror if properly stabilized could then be used to make remote sensing readings of the energy reflected and emitted from a fixed point on the earth's surface. The initial design specifications were as follows:

(1) The reflecting surface was to be suspended at altitudes ranging from 100 feet to 200 feet.

(2) Vertical, lateral and angular excursions were to be minimized.

(3) The system would operate normally in wind speeds up to 20 knots.

(4) The balloon system could not become unanchored during severe thunderstorms.

The design study was made with the initial idea that the entire system including the balloons would be built at Louisiana State University. However, it was quickly found that this would be too expensive and time consuming therefore, the balloons used were obtained from the Robert Fulton Company. A balloon with a volume of 1000 cubic feet was used as a reference throughout the initial study.

Gas for Filling Balloon

The two primary gases used for lift in balloon systems are hydrogen and helium. Hydrogen is much less expensive than helium although the cost difference is not a major design factor when the lifting force and thus the balloon volume is relatively small. Hydrogen gas is lighter than helium and thus provides more lift in the same volume. However, hydrogen in mixtures from 41 percent to 82 percent by volume of air is extremely flammable. The safety factor of helium was considered to be more important than the lift advantage of hydrogen, therefore, helium was the only gas considered for filling the balloon.

Balloon Skin Material

One of the most recent developments in the materials used for tethered balloons has been nylon/Mylar laminate. This structure has both strength and low permeability. The exterior nylon cloth provides the needed strength while the Mylar inter film provides an effective gas barrier. The weight of this laminated material varies from 3.53 to 4.09 ounces per square yard.

Balloon Shape

Traditionally, balloon shapes can be categorized into three classifications: (1) spherical, (2) natural or teardrop shape and, (3) aerodynamic shape. Tethered balloons have often been a spherical shape. This shape gives the highest gas volume per unit of surface area but also has a large drag due to a high frontal area which would make a system using this type of balloon difficult to stabilize.

The teardrop shape is more efficient from a structural point of view when the payload is to be a finite, concentrated load supported by the balloon. Also there is a cost advantage in construction of a spherical or teardrop shaped balloon as compared to one with an aerodynamic shape.

The primary advantage of an aerodynamically shaped balloon is that it has better flow characteristics. This is of major importance for a stable balloon system. Also, with a streamlined shape, additional lift and added stability is possible in the presence of straight winds. These advantages alone eliminated the further considerations of the other general types of balloon shapes.

Many options are still available under the general heading of an aerodynamic shape. Rather than an elliptical shape as used traditionally, an airfoil shape was chosen for more streamline flow and less drag. A cambered shape was considered since more dynamic lift would be available; however, the increase in drag and complexity of construction were disadvantages which outweighed the added lift advantage.

Since an airfoil shape was decided upon, the fineness ratio (ratio of maximum width to chord length) also had to be selected. The optimum fineness ratio for the hulls of submarines and airships is considered

to be 4.0 [53]. The NACA 0024 symmetrical airfoil (Figure V-1) with a circular cross section was chosen since it had a fineness ratio of 4.17. As shown by the dotted line in Figure V-1, the end of the balloon will be rounded which causes a decrease in length of approximately 10 percent. Thus the final fineness ratio was reduced to a value of 3.75. This aerodynamic shape for the balloon reduces the balloon drag and provides a large amount of dynamic lift at relatively low angles of pitch, and is therefore somewhat self-stabilizing as the wind speed is increased.

Angle of Pitch

As previously noted, the balloon must be flown at an angle of pitch so that additional lift is generated in the presence of a wind. In order to select the best angle of attack, the lift and drag at various pitch angles was compared. As shown in Figure V-2, at a given angle of pitch, the resultant of the lift and drag forces act at an angle θ to the horizontal. The tension, T, in the balloon cable is equal in value and directly opposite in direction to the forces generated by the balloon.

A major parameter of importance in the stabilization of the system is the slope of balloon cable #4 shown in Figure V-2. The greater the angle α, shown in Figure V-2, the greater the lift component of the resultant force due to winds and the more side forces required to make the system unstable. Conversely, as α is increased, the side forces also increases. Shown in Figure V-3 is a plot of pitch angle versus the cable slope (from Foster [52]). The curves show that at an angle of pitch of approximately 6 degrees, the slope of the cable is near its maximum value for the wind conditions considered. Since the highest possible value of θ is desired to stabilize the system, a

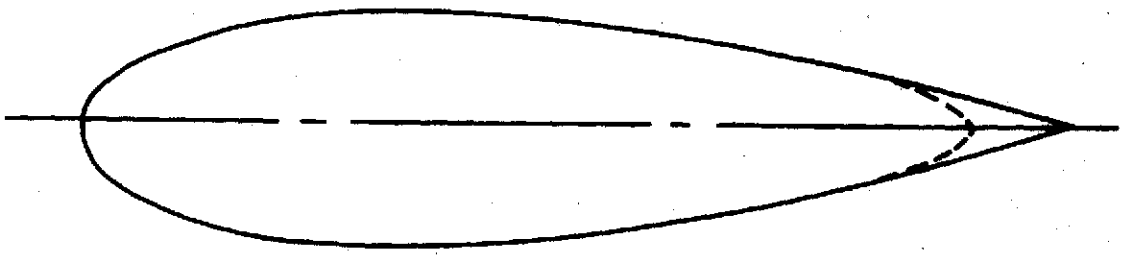

FIGURE V-1. NACA 0024 AIRFOIL

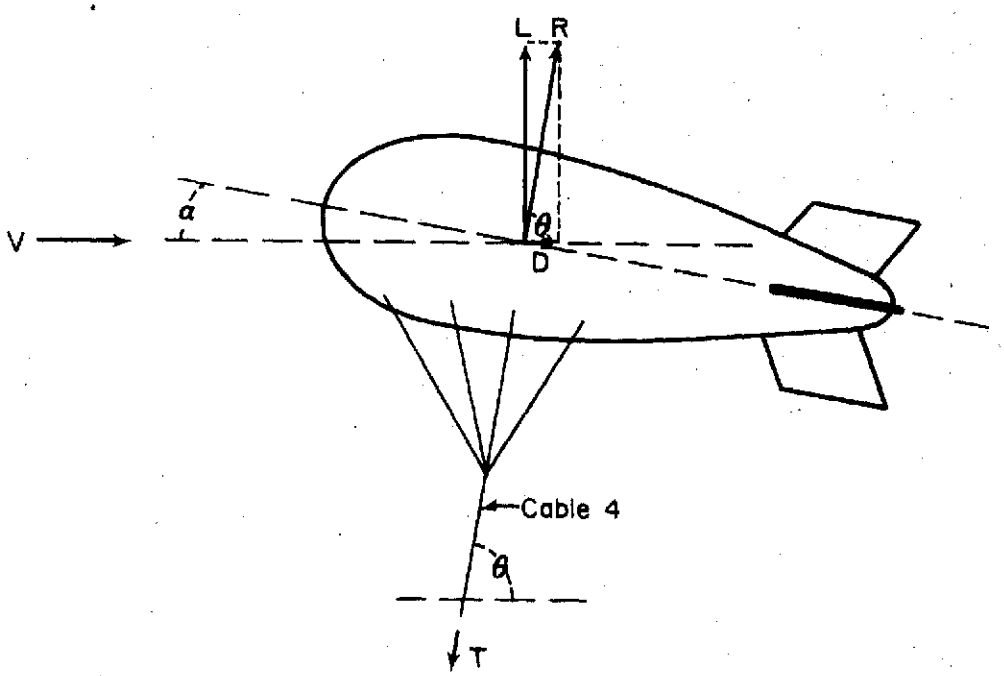

FIGURE V-2. BALLOON FORCES

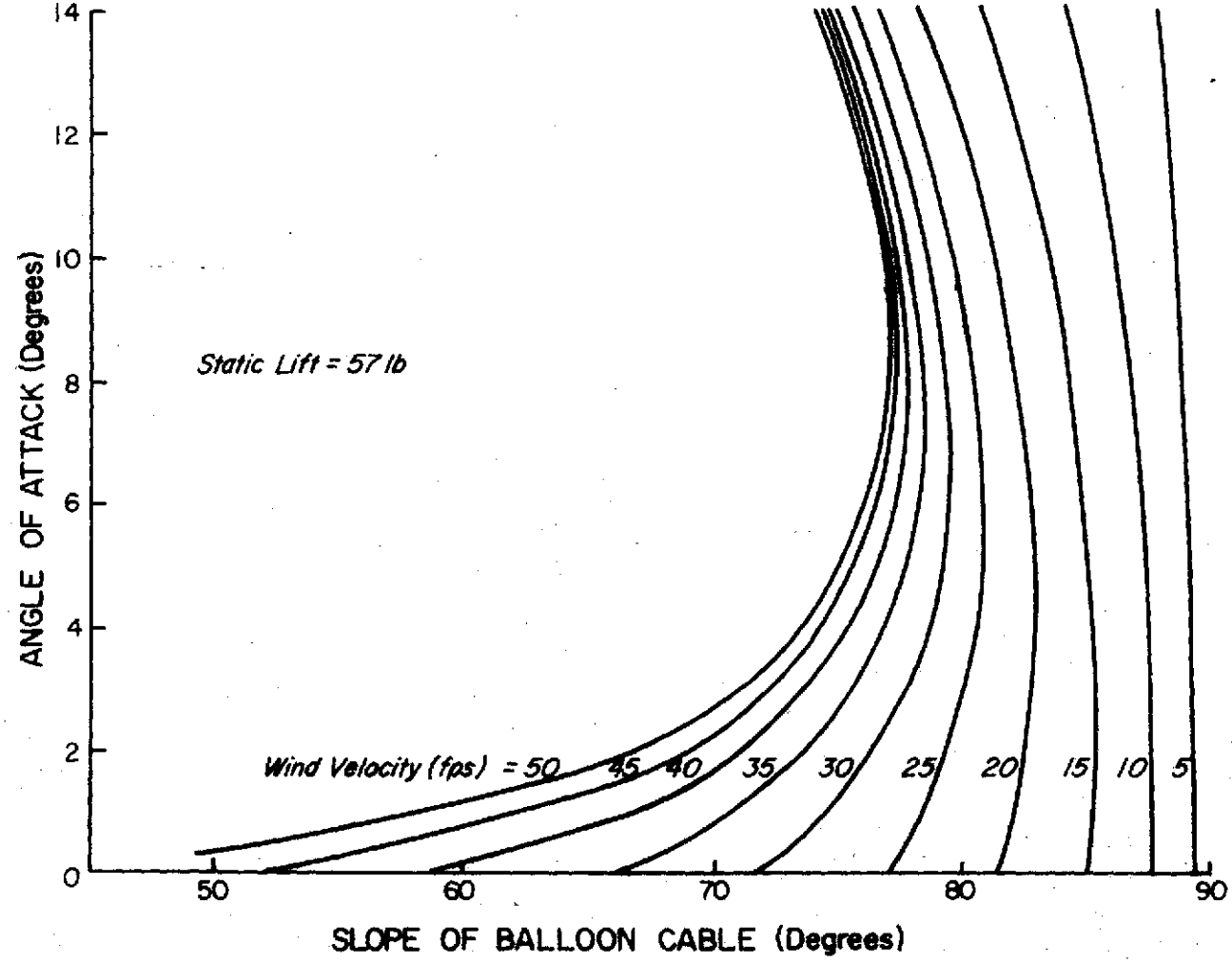

FIGURE V-3. ANGLE OF ATTACK VERSUS SLOPE OF BALLOON CABLE

pitch angle of 6 degrees was selected as the best at which to fly the balloon.

Horiztontal and Vertical Stabilizers

Horizontal and vertical stabilizers are necessary to keep the nose of the balloon into the wind and thus stabilize it. Various types of stabilizers have been used on balloons. However the most important factor in stabilizer design is the amount of stabilizer area used and the span of the tail surfaces. According to Hoerner [53], past airships have effectively employed stabilizers of an area equal to 8 percent of the total surface area of the body. For a balloon with a volume of 1000 cubic feet and the shape described earlier, the stabilizers should comprise a total surface area of 50 square feet (25 square feet for the horizontal and 25 square feet for the vertical stabilizers).

Using the NACA 0024 airfoil as the balloon shape and a volume of 1000 cubic feet, the maximum diameter of the balloon would be 8.25 feet. This results in a cross-sectional diameter of the wake following the balloon of 3.8 feet. Therefore in order to insure that the majority of the tail surface is outside the wake, a span of 9 feet is required for the stabilizers. This resulted in an aspect ratio of 3.24 for the stabilizers.

Balloon Tethering System

A three tether arrangement was selected for mooring the balloon. Three tethers is the minimum which can be used and still resist movement in any direction except downward. The objective of the balloon tethering system was to try to maintain the apex as shown in Figure V-4 at a fixed position. The mirror which is the payload is attached at the apex. By using this system, movements of the balloon itself will not

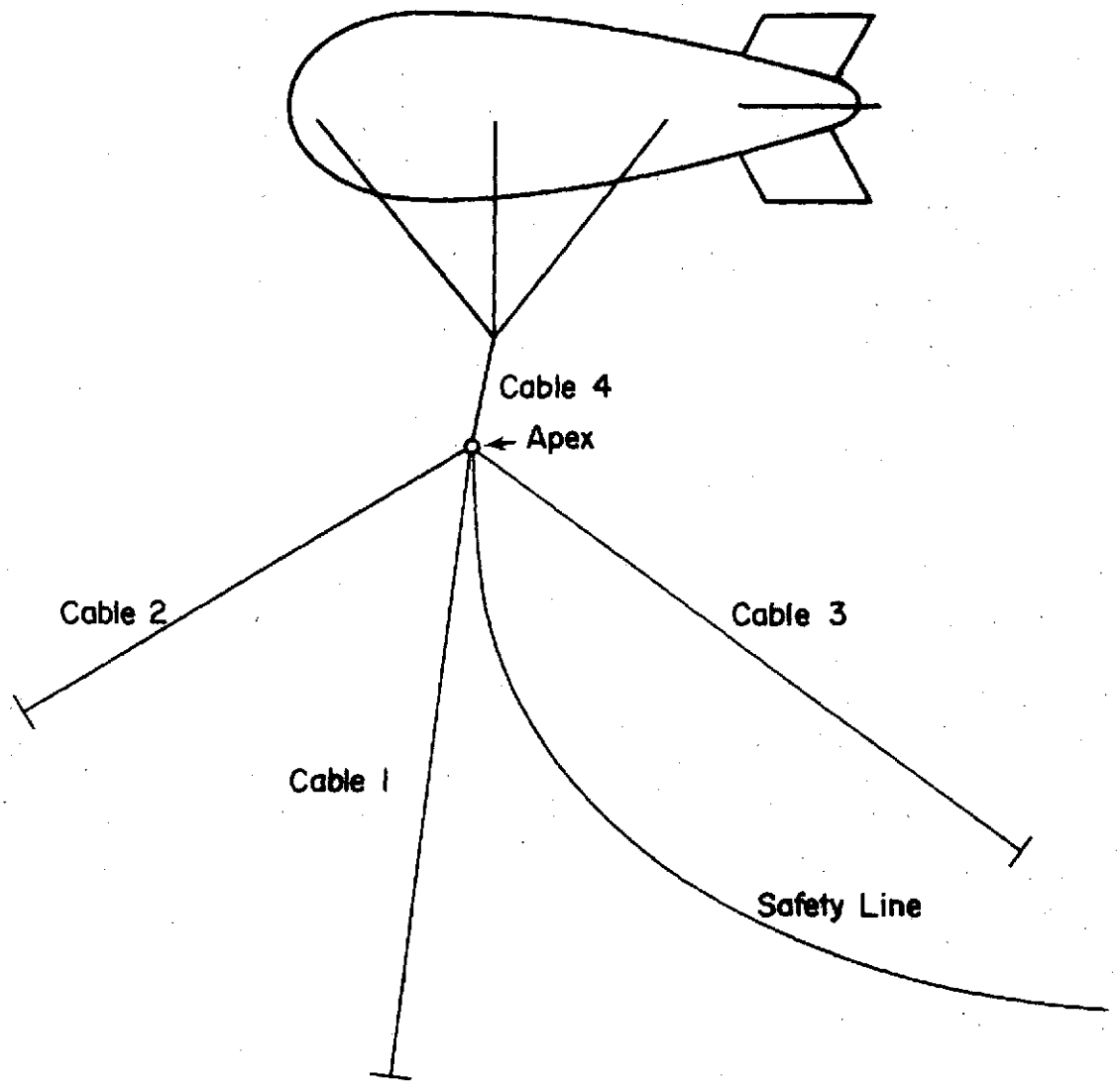

FIGURE V-4. BALLOON CABLING SYSTEM

effect the stability of the mirror system except through movement of the apex.

Since the cables cannot resist compression, it was desirable to have enough balloon lift so that there would always be tension in all the cables in sidewinds up to the design criteria of 30 feet/second. As long as the three cables are kept in tension, the apex will not move except as caused by sag and elasticity of the cables.

In order to reduce the weight of the cable system and still provide safety, the three main cables were designed to hold in winds of only 45 feet/second. Since the system in variable and gusty winds of 45 feet/second or greater would completely lose its stability and its usefulness destroyed, there seemed little reason to design the cables to hold more. However, since winds in thunderstorms and hurricanes, of which Louisiana is frequently visited, can become higher than 45 feet/second a fourth cable made of nylon was used in the design as a safety feature. This fourth line must be elastic to withstand jerks and with a high enough strength so that the balloon would be riped before the cable would break. Normally this cable carries no load but falls free to the ground where it is attached.

In order to optimize cable arrangement and cable angles with the ground, a complete dynamic force analysis of the entire system must be made using typical wind profiles. This was not done, however, a simplified analysis was made by Foster [52] under a National Science Foundation Grant. Foster found in his study that an equilateral tether system should be used with one cable oriented towards the prevailing wind direction. This lead cable should make an angle of approximately 33 degrees with respect to the ground. The back two cables should make

angles of approximately 47 degrees with respect to the ground. Foster concluded that with this type of arrangement the withstandable side force is increased substantially over an arrangement where all the cables make the same angle with the ground. Optimum cable angle with the ground will depend in actuality on the weight of the cables used, the height of the system, the lift produced by the balloon, and the downward pull of the mirror system.

Strength of the tether lines were designed based on balloon flight conditions consisting of a pitch angle of 90 degrees in winds of 45 feet/second. In order to be conservative, the value of the drag coefficient for a circular cylinder in turbulent cross flow was used. This drag coefficient was found from Hoerner [53] to be 0.50. The total drag was then calculated as follows:

$$\text{Drag} = C_D \, q \, s$$

where $C_D = 0.5$

q = dynamic pressure = $1/2 \, \rho v^2$

$= (.5)(.002365)(45)^2$

$= 2.4 \text{ lb/ft}^2$

S = projected profile area

$= 182 \text{ ft}^2$

$\text{Drag} = (0.5)\ 2.4)\ (182)$

$= 218.4$ lbs.

ρ = fluid density

v = fluid velocity

Adding the balloon lift of 57 lbs (from Figure V-5) and assuming both the drag and lift act colinearly and using a factor of safety of 1.5,

the maximum design load was found to be 410 lbs. Therefore, each cable was designed to carry this load.

Mirror System Design

The mirror system is connected to the apex of the balloon system. Both the balloon and the mirror systems should be attached to the apex with swivel type connections to eliminate any twisting due to rotation of the systems. In order to stabilize the mirror, which would otherwise hang free, it is necessary to use three cables attached to the ground. These cables eliminate the effects of any wind loads on the mirror and are used to position the mirror. These cables were oriented in the same manner as the balloon cables for the tests made. Only light tension is necessary in the mirror cables. Tests were made to determine the best relationship between tension in the mirror cables and the balloon cables for the most stable configuration. The mirror cables should be as light weight as possible. The maximum design loading of these cables was calculated to be 13 pounds. However, in designing the mirror system, it was found from the tests made that care must be taken to insure that if the balloon escapes, that the mirror system will break off. Therefore, it is suggested that the mirror cables be capable of holding at least 100 pounds of tension and that the connection between the mirror and the balloon break at 50 pounds of tension or less.

If cables which can bend are used between the balloon's apex and the reflecting surface system, then the mirror system can be analyzed in the same manner as the balloon system. That is the mirror is held in tension by three cables attached to the ground and by an upward force.

Side forces which can only come from movement of the balloon apex would have to be great enough to make one of the mirror cables go limp in order for the mirror to move. Angular excursions of the mirror can come only from varying wind loads on the mirror and movement of the apex. Again if the cables were totally inelastic, the mirror could be permanently fixed with no lateral or angular movement as long as there were tension in all three mirror cables.

Balloon Forces

Forces produced by a helium balloon on the apex result from the static lift of the balloon, dynamic lift and drag due to the wind blowing around the balloon, and the weight of the balloon skin and rigging. Static lift can be found by:

$$\text{Lift} = (\rho \text{ air} - \rho \text{ helium}) V_{gas}$$

where ρ = density

V = volume of lifting gas

Using the densities of AROC air at 1 atmosphere and 95 percent pure helium at 1 atmosphere, calculations of static lift were made for temperatures of 60 degrees and 100 degrees and are given in Figure V-5 [52].

The stability of a tethered balloon system is totally dependent on the aerodynamic characteristics of the balloon and how they affect the dynamic lift and drag. For a symmetrical shape like the NACA 0024 airfoil, the pressure distribution is also symmetrical when the balloon is flying at a zero angle of attack. However, when the balloon is flying nose up at an angle of attack to the wind direction, the distribution of pressure is uneven between the upper and lower surfaces and causes a net lift on the balloon in an upward direction. The

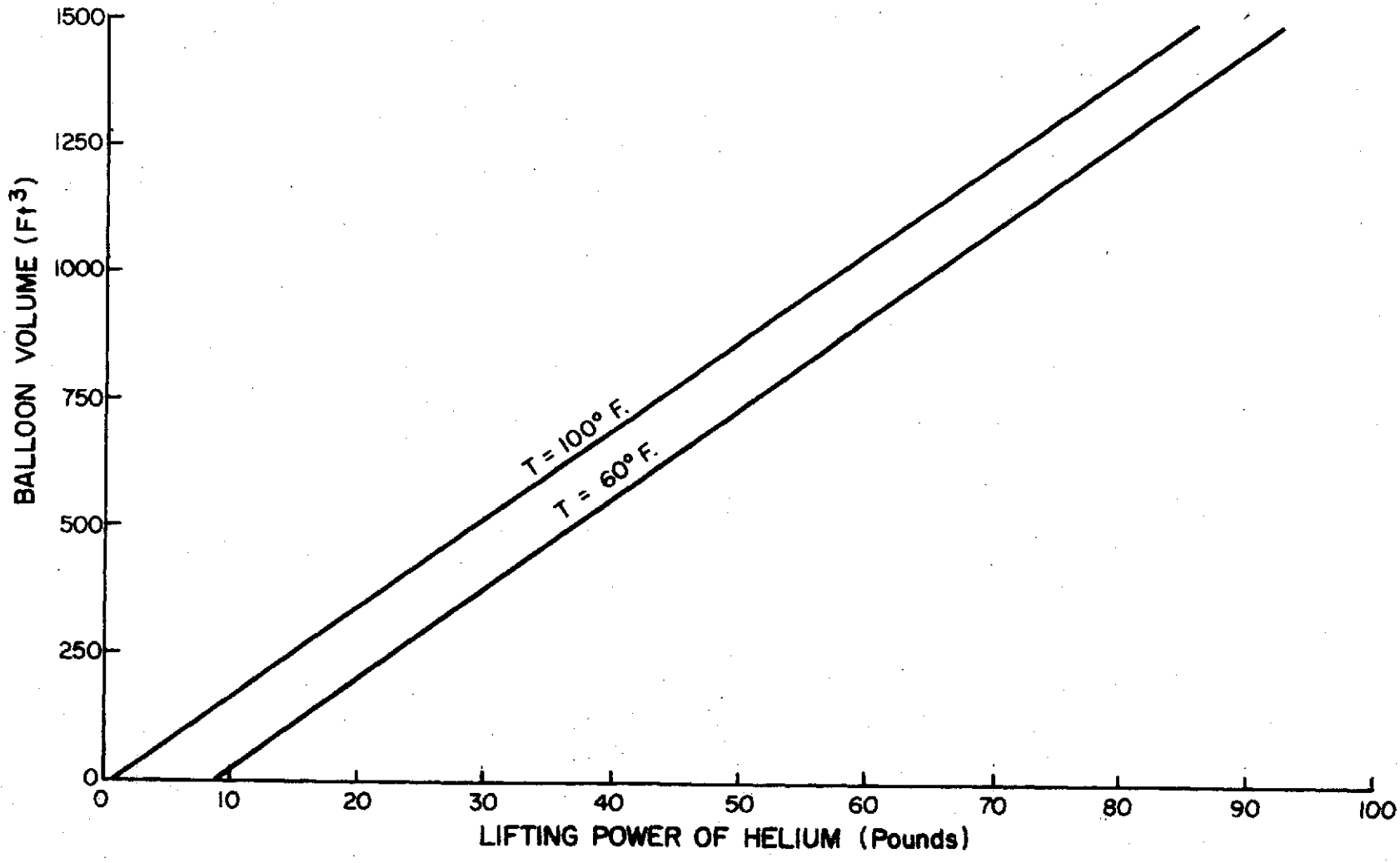

FIGURE V-5. STATIC LIFTING POWER VERSUS BALLOON VOLUME AT T = 100°F. AND T = 60°F.

lift is defined as the upward force on the airfoil surface or balloon perpendicular to the wind direction caused by the speed of the wind over the surface. Dynamic lift for a balloon based on the design described and a volume of 1000 cubic feet was calculated by Foster [52] and is given in Figure V-6.

Drag is defined as the force on an object in the direction of the wind due to the wind. The drag on the balloon was also taken from the study by Foster [52] and is shown in Figure V-7.

The weight of the balloon skin and rigging was estimated to be 28 pounds. This estimate is based on a surface area of 570 square feet with a skin weight of 4 ounces per yard. Therefore, the skin weight was 16 pounds. The tail weight was assumed to be 8 pounds. The additional 4 pounds was added to account for the rigging, filling valve and strengthening need at rigging and tail attachments. A 1200 cubic foot balloon later purchased had a total weight of 20 pounds. However, the stabilizers were pneumatic and were only one-half the 50 square feet area estimated as needed in this study.

Table V-1 contains a summation of the expected forces acting on a 1000 cubic foot balloon system. The final value listed of side force/vertical tension (SF/T_v) in the balloon cables is the critical item used to determine the feasibility of stabilizing the balloon/mirror system. These values can be compared to Figure V-8, which shows the SF/T_v needed to buckle any cable and thus make the system unstable. Figure V-8 was made from the results of a force balance made at the balloon apex for varying balloon flight conditions and the cable arrangements shown. The side force is always opposite in direction to the wind direction.

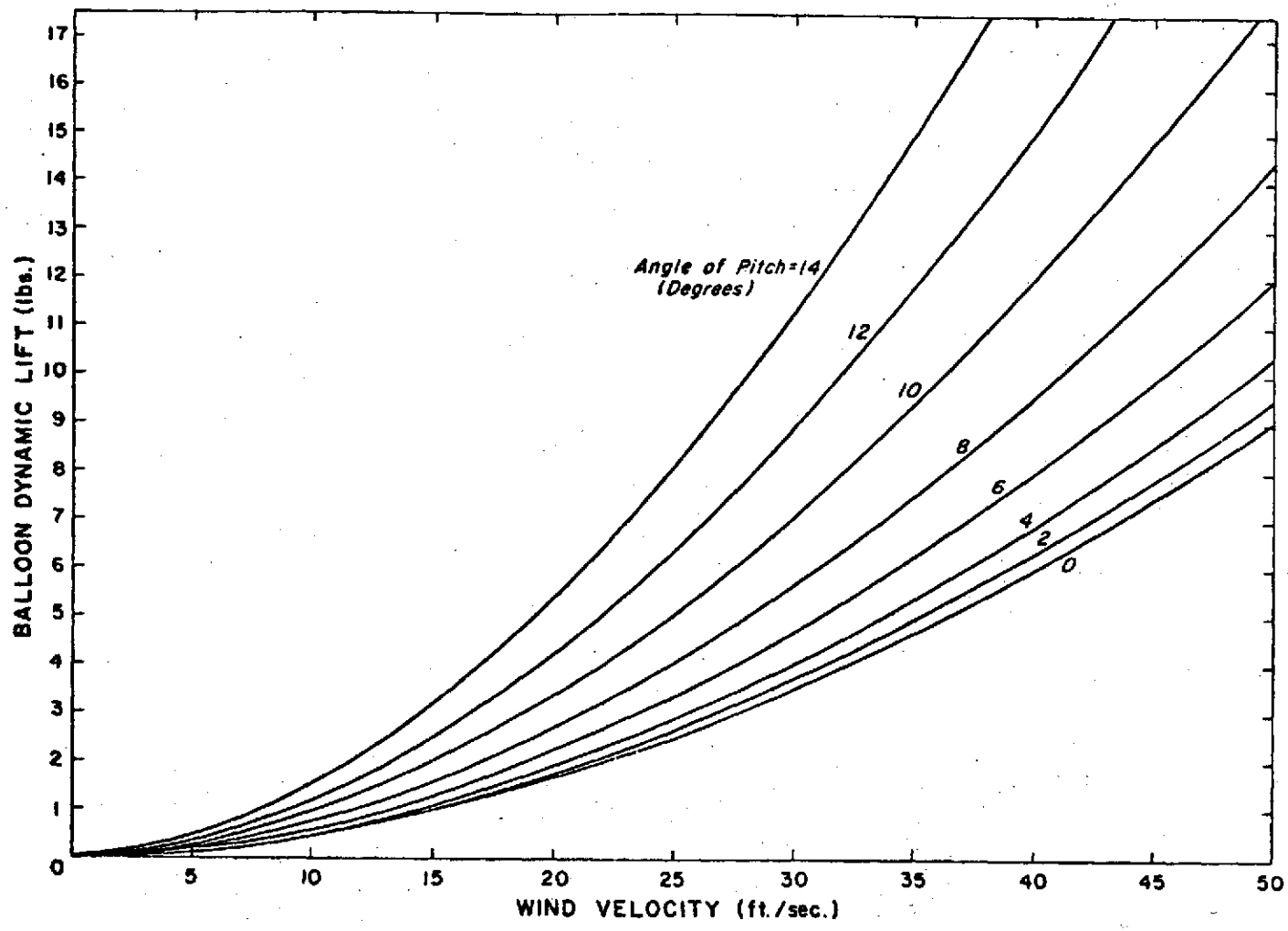

FIGURE V-6. BALLOON DYNAMIC LIFT VS. WIND VELOCITY

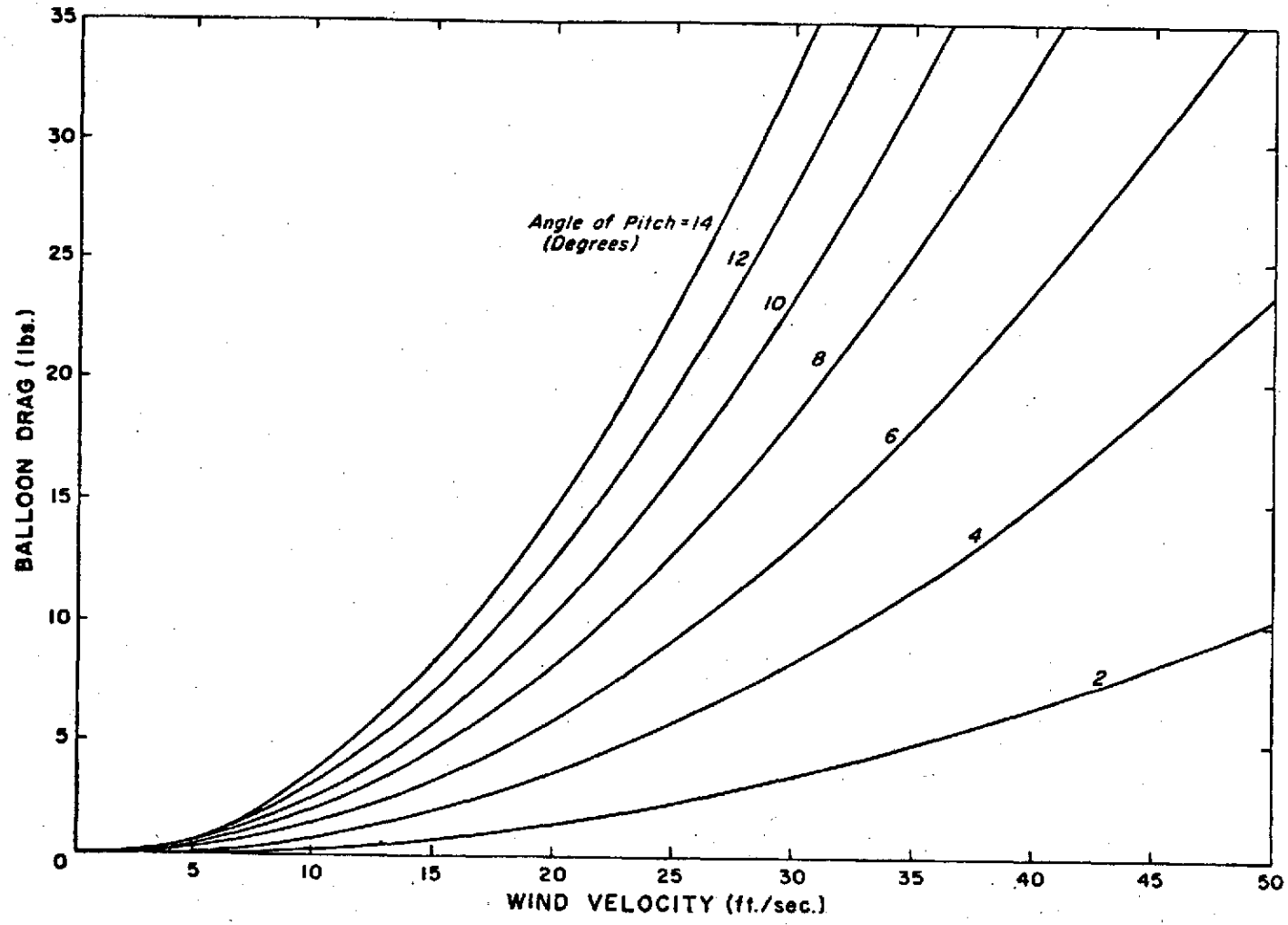

FIGURE V-7 BALLOON DRAG VS. WIND VELOCITY

TABLE V-1

FORCE TABLE FOR 1000 CUBIC FOOT BALLOON

Wind Velocity	0 ft/sec	15 ft/sec	31 ft/sec
Balloon Static Lift @ 80°F	60 lb	60 lb	60 lb
Balloon Dynamic Lift	0	3 lb	13 lb
Gross Lift	60 lb	63 lb	73 lb
Balloon Weight	28 lb	28 lb	28 lb
Lift at Apex	32 lb	35 lb	45 lb
Drag or Side Force	0	1.3 lb	4.8 lb
Side Force/Lift (SF/L)	0	.037	.107
Angle of Balloon Cable #4 at Apex With the Vertical	0°	2.1°	6.1°
Mirror System Weight	8 lb	8 lb	8 lb
Total Vertical Force in Mirror Cables	7 lb	7 lb	7 lb
Total Downward Pull at Apex Due to Payload	15 lb	15 lb	15 lb
Total Vertical Component of Tension in Balloon Cables - T_v	17 lb	20 lb	30 lb
Side Force/Vertical Tension (SF/T_v)	0	.065	.16

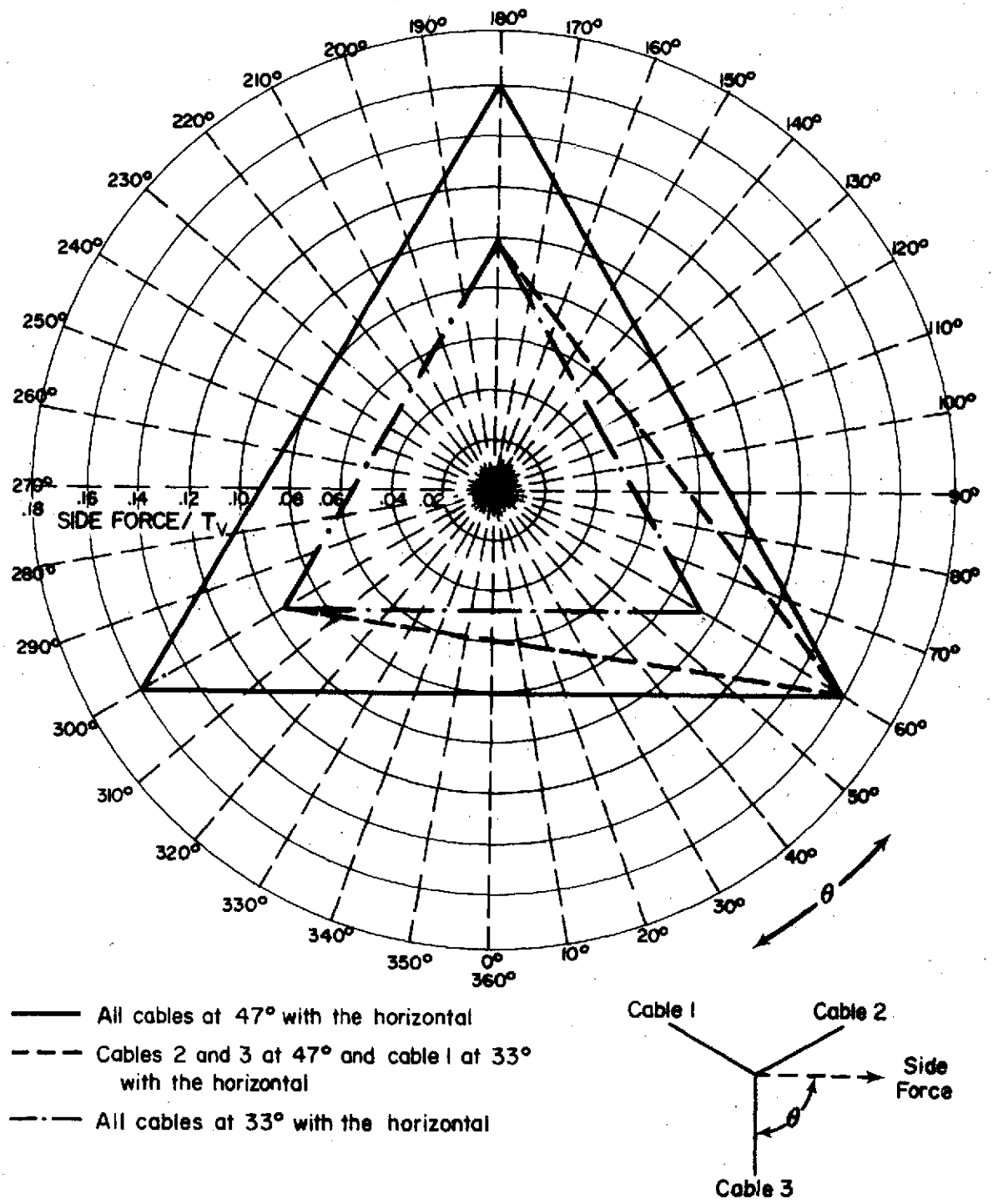

FIGURE V-8. SIDE FORCE / T_V REQUIRED FOR BUCKLING ANY CABLE VERSUS THE ANGLE OF SIDE FORCE IN THE X-Y PLANE

Conclusions

The major conclusion of the inital study was that the tethered balloon/reflecting surface system was feasible and that stability of the reflecting surface could be achieved. However, in order to assume stability in winds as high as 30 feet/second it is necessary that the cable leading into the wind be at an angle of 33 degrees or less with respect to the ground. It was also noted that the aerodynamic characteristics of the balloon are extremely important and that unless the balloon flies as designed that the system will not function as required.

One of the factors not considered in the study was sag and elasticity of the cables, however, with cables angles as low as 33 degrees with respect to the ground sag and elasticity of the cables cannot be ignored. As a result of these factors some oscillatory movement of the reflecting surface is expected to occur. One way to help this problem is to increase the balloon size so that the cable angles can be increased and the system still be stable in winds up to 30 ft/sec.

Another factor not considered in the initial study was wind turbulence. Since the system was designed only for low altitude flight, the winds will not be consistant in either direction or magnitude. Assuming that a strong gust acted at 30 degrees to the prevailing winds into which the balloon was headed, a drag force of 17 pounds or more could be easily achieved which would cause the system to become unstable. It is therefore necessary that the stabilizers be sufficient to readily direct the balloon into the wind.

Part II. Balloon System Tests

Since the initial design study had shown that stabilizing a reflecting surface attached to a tethered balloon appeared feasible, it was decided to purchase a balloon to test the concept. The balloon was purchased since the cost and time involved in building a balloon to the specifications determined earlier appeared prohibitive. The balloon was obtained from the Robert Fulton Company. It had a volume of 1200 cubic feet. The model number was DUED-12-1. At the same time five smaller balloons also built by the Robert Fulton Company were obtained as surplus from the U.S. Air Force. The smaller balloons had a volume of 800 cubic feet. An adapter and quick disconnect for filling the balloons was also purchased. Since the smaller balloons had been made available, it was decided that tests would first be made with the smaller balloons to obtain operational experience and to obtain data on the stability of the reflecting surface.

Unfortunately, the balloons obtained did not have the same characteristics as the balloon design used in the initial design study. The importance of these differences became very apparent as operational experience was gained with the balloon system. The balloons purchased differed in that they had a smaller fineness ratio than the balloon designed in the initial study. The stabilizers area was smaller, the stabilizer span was smaller, the stabilizers were pneumatic and not rigid and the balloons had a high leak rate, especially in gusty winds.

Design of Rigging for First Balloons Launched

Two of the smaller balloons (800 cubic feet) were used for the first tests of the balloon system. Design of the cables was based on the strength requirements calculated in the initial feasibility study.

For all the balloon and mirror cables a 1 x 7 stranded steel wire made by the American Chain and Cable Company for aircraft control cables was used. The strand diameter was 0.038/.040 and had a minimum breaking strength of 380 pounds. The weight of the cable was 3.85 pounds/1000 feet. The cable was very stiff and had a tendency to spread when bent or wrapped around a sharp object.

A figure eight hook was bent and welded and used at the apex to connect the balloon, cables and mirror system. The cables were looped at one end and attached to swivel snaps similar to those used for dog leases. The loops were made by looping and twisting the wire after which it was wrapped with smaller wire. The other ends of the cables used for the balloon were attached to hand operated winches. The winches were originally designed for boat trailers. In order to use them for this application, a drum 5 inches in diameter was made to fit over the center bar of the winch. A photograph of the winch is given in Figure V-9. The winches were then attached to one and one-half inch angle iron stakes 4 feet long which were driven into the ground.

For the mirror cables, angle iron stakes 2 1/2 to 3 feet long were used. Eye hooks were mounted on the stakes. The mirror cables were wound on wire spools and unwound as needed. The mirror cables were attached to the stakes with electrical wire clamps which could be moved up and down the cables. A spring measure was connected between the cable and the stake in order to determine and adjust the tension in the mirror cables.

Results of First Balloon Launchings

The first two balloons were launched in June, 1973. Both of these launches were unsuccessful since one ballon was destroyed and the other

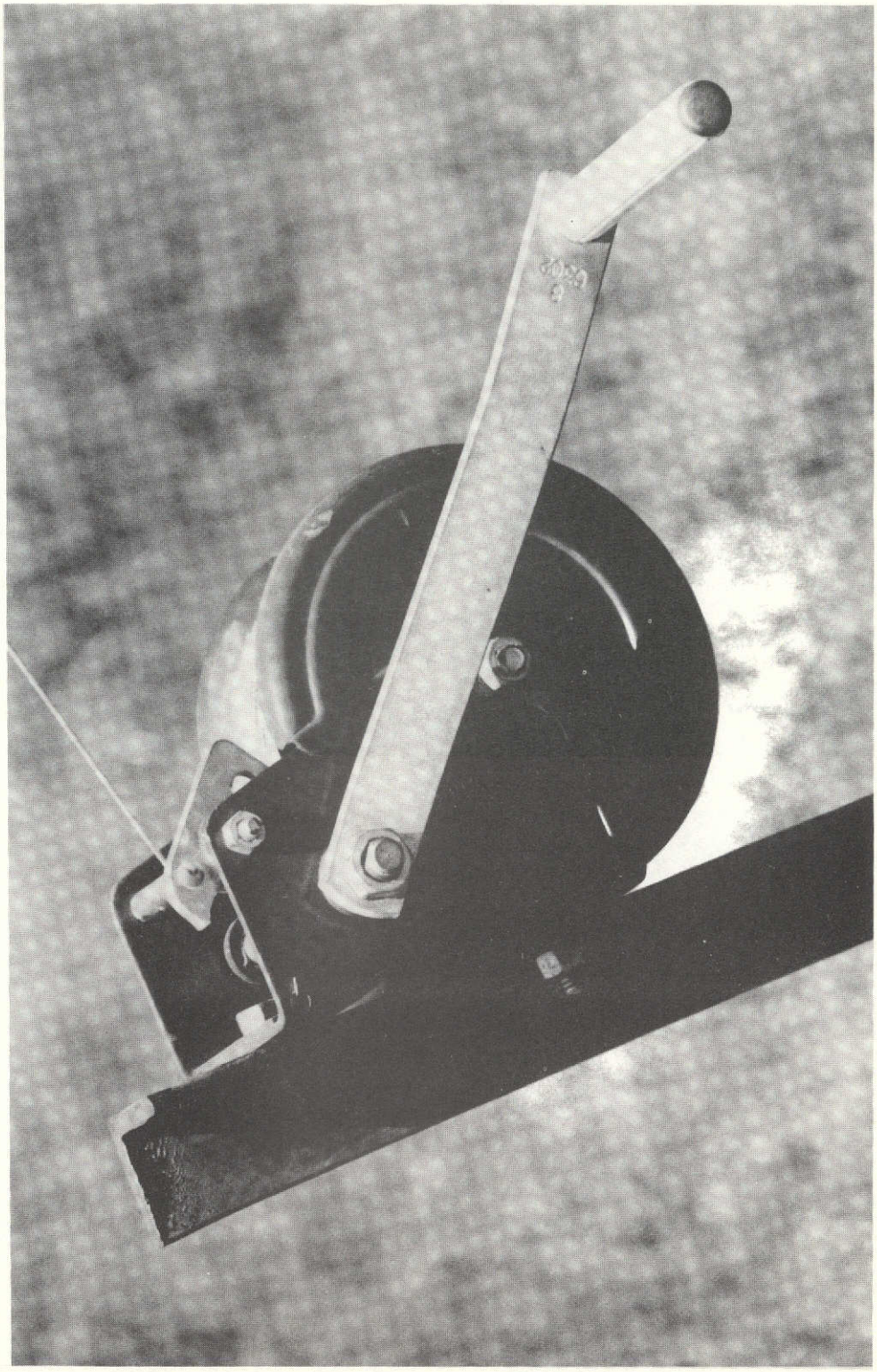

FIGURE V-9. Photograph of Balloon Cable Wrench

escaped and no data on the stability of the system was obtained. However, some operational experience was gained, and the conclusions made helped in the redesign of the system. An account of the balloon launchings is given in Appendix B.

A number of conclusions were made from the failure of the first two tests. It was found from the first test that taking a balloon down was difficult. From the second attempt it was seen that leaving the balloon up in a thunderstorm could be disasterous. It was therefore concluded from the tests that using a tethered balloon/reflecting surface system for taking remote sensing data over a long period of time would be unrealistic unless thunderstorms could be avoided or a way could be found to safely take the system down during periods of bad weather.

Another conclusion was that the mirror rigging should not be left free as done in the second test and that the mirror system should be designed to break off if the balloon gets free. Also the safety line should be stronger and should be attached to the apex of the balloon system and not the balloon nose since attaching the line to the nose forces the balloon down and sideward into the wind thus increasing the drag force when the other cables break or when the balloon is lowered by using the safety line. Also the balloon cabling system should be strengthened while the mirror cabling system could be lightened and weakened. The major item which appears to have caused the cables to fail was twisting and looping the cables to attach the snaps. This greatly reduced the cable breaking strength. Also a different type of wire should be used to make the cables.

Jerks or impact loading also need to be considered in determining the cable design strength. It was concluded that no attempt should be made to lower the balloon if a storm is coming unless the balloon can be completely taken down. Finally, if additional tests were to be made, wait until several days of good weather can be predicted and be ready to start taking stability data as soon as the balloon is launched.

Redesign of Balloon/Mirror System Rigging

There was not complete satisfaction with the cables used in the first tests. Since these cables were also badly tangled and twisted, it was decided to abandon their use. A roll of 1 x 7 stranded galvanized steel wire 1/16" in diameter was obtained and used to make the new balloon cables. The ends of the cables were looped and brazed to attach heavy swivels and snaps. This cable when tested in the laboratory after being twisted over a ½ inch bar was found to carry 410 pounds. The break point was at the bar as would be expected. The cable had an approximate weight of 0.7 pounds per 100 feet. These cables were used for all subsequent tests.

An 800 pound test nylon rope was purchased for use as the safety line. This size of rope was decided upon since it matched the lines used on the balloon itself. Also a ¼ inch diameter steel ring was used as the apex to which the balloon, the balloon cables, the safety lines, and the mirror system were connected.

For the mirror system a ¼ inch aluminum plate 14 inches by 18 inches was used as a holder. A 12 inch by 16 inch mirror made by a polyester film, vacuum-coated with aluminum, stretched over a lightweight frame was attached to the aluminum plate. Half of the mirror was then

covered with a ruled target for use in determining lateral movements. Six eyehooks were attached to the aluminum plate. Three hooks were on the top to attach the cables between the mirror and the apex. Three hooks were on the bottom and were where the mirror cables were attached. The cables between the apex and the mirror were connected to the apex ring by a snap and swivel. A diagram of the tethering arrangement is seen in Figure V-10.

Number eight music wire was used as the mirror cables. This wire was tested in the laboratory and found to have a breaking strength of 102 pounds. The weight of this wire was 1 pound for 1000 feet. Aluminum utility wire purchased at a local hardware store was used for the cables between the mirror and the apex.

Swivel snaps were attached to the mirror cable by looping the wire, twisting it slightly and then hand wrapping the loop with smaller wire. In order to connect the other end of the wire to stakes, two aluminum plates with four screws and a large hole were used. The two plates could be placed over the wire and screwed tightly together and then the plate attached to the stake by using an S hook. Tension in the cables could be adjusted by the position of the plate on the wire. A spring scale was used to measure the tension in the cables. With this arrangement the strength of the steel wire was not diminished by the connections.

Measuring Equipment

The equipment used for checking the stability and parameters of the balloon/mirror system after launching included binoculars, tape measure, compass, wind speed and direction indicator, laser, laser

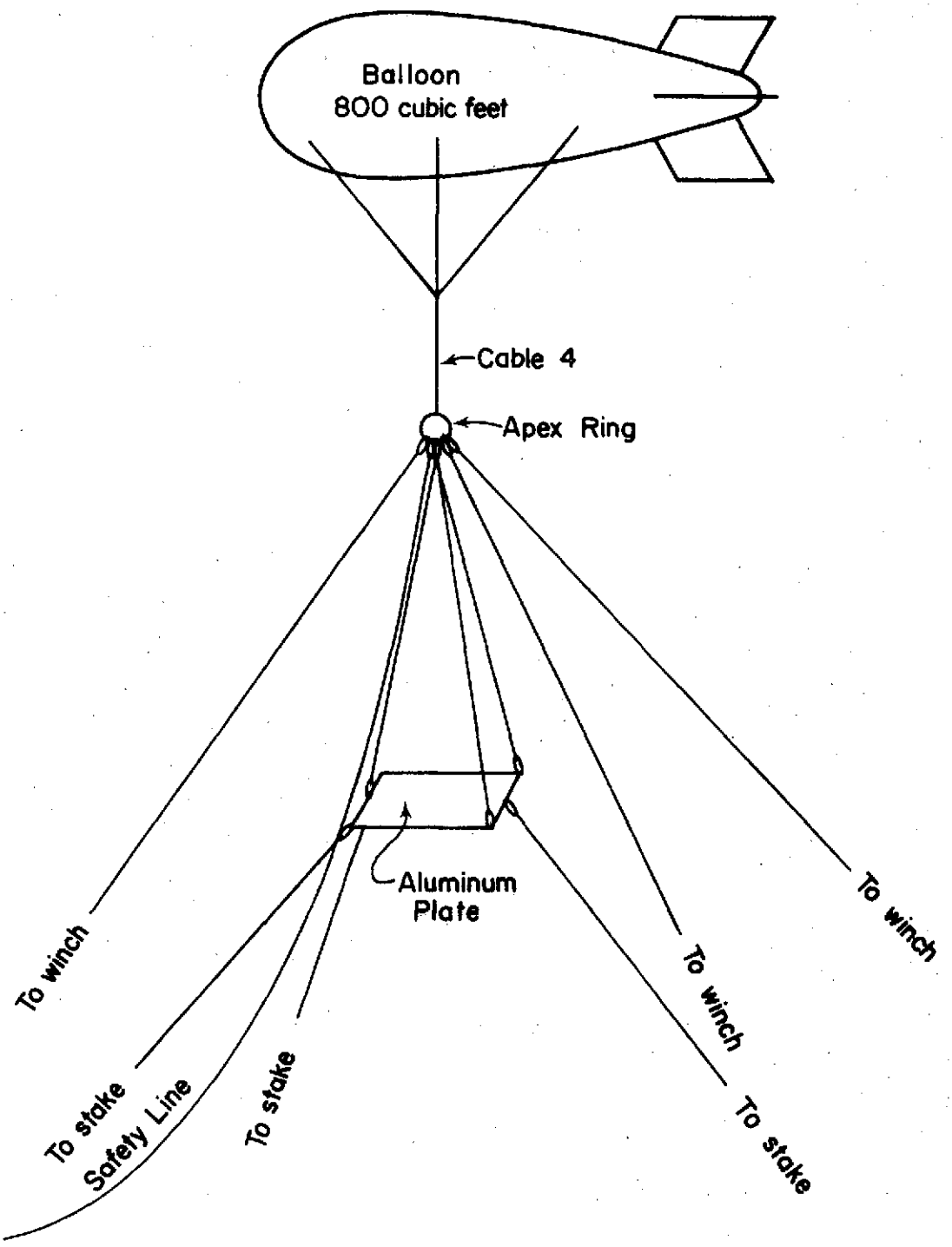

FIGURE V-10. TETHERING ARRANGEMENT

holder, electrical generator, scales, plumb-bob and line, level, camera, barometer, and a temperature/relative humidity gage.

The binoculars were used to view the lateral movements of the laser beam on the mirror target. The tape measure was used for laying off the stakes and measuring distances between the center marker and the reflected laser beam as well as the beam movement as it impinged the ground. A compass was used in setting the wind direction indicator and the cable orientation.

The wind speed and direction indicator was Model W121S as made by the Weather-Measure Corporation. It was read periodically during all tests to determine average wind speed and direction as well as variation in these parameters. Unfortunately the inertia in the wind speed indicator was such that it did not function well in determining wind gusts or light breezes.

A laser was used to measure the lateral and angular variations of the mirror. The laser was mounted vertically in a box used as a holder. A torpedo level was used to determine when the laser was vertical. The laser was powered by a Sears 5000 watt gasoline powered electrical generator which also provided the power for the wind speed and direction indicator.

In order to test lateral movement of the mirror, the laser was set up directly beneath the target attached to the mirror. The movement of the laser beam on the target could then be easily seen with binoculars. In order to test angular motions of the mirror, the laser was set up as before except that the laser was aimed at the mirror and the beam reflected back to the ground. Movement of the beam on the ground was then recorded and the angular variations calculated.

Spring fish scales (0-8 pounds force) were used to measure and adjust tension in the mirror cables. Mirror height was determined by using a plumb-bob and line attached to the mirror. The plumb-bob could be removed after the proper height was achieved. General atmospheric conditions were measured with a barometer and a continuously recording Foxboro temperature/relative humidity gauge. Photographs of the equipment used is shown in Figures V-11 and V-12.

Results of Third and Fourth Balloon Launches

Two additional 800 cubic feet balloons were launched in March and April, 1974 using the redesigned rigging. Both of these launches were fairly successful and resulted in the data given in Appendix C on the stability and operation of the system. The third balloon launched resulted in a stability check of the mirror in only one configuration; whereas, the tests made on the fourth balloon/mirror system launched resulted in stability data with several parameters varied. The procedure used for launching the balloons and a log of the flights is given in Appendix B. A photograph of the balloon in flight is given in Figure V-13.

Several conclusions were made based on the third balloon tested and the subsequent analysis. Most importantly it was found that as long as tension was maintained in the balloon cables there was little or no lateral movement of the mirror. Also the angular movements of the mirror were not severe but would require a test area of consistent composition large enough that the radiometer reading reflections from the mirror would see inside the test area at all times. Therefore, it appeared from this test that the stability of the system was such that the idea of taking reflectance readings from a reflecting surface held

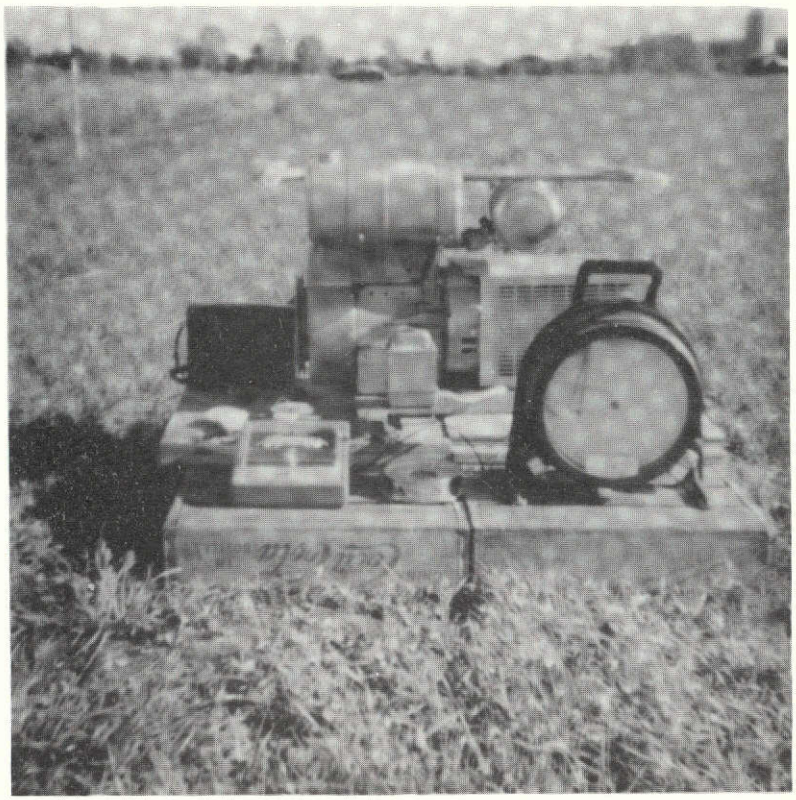

FIGURE V-11. Photograph of Gas Generator

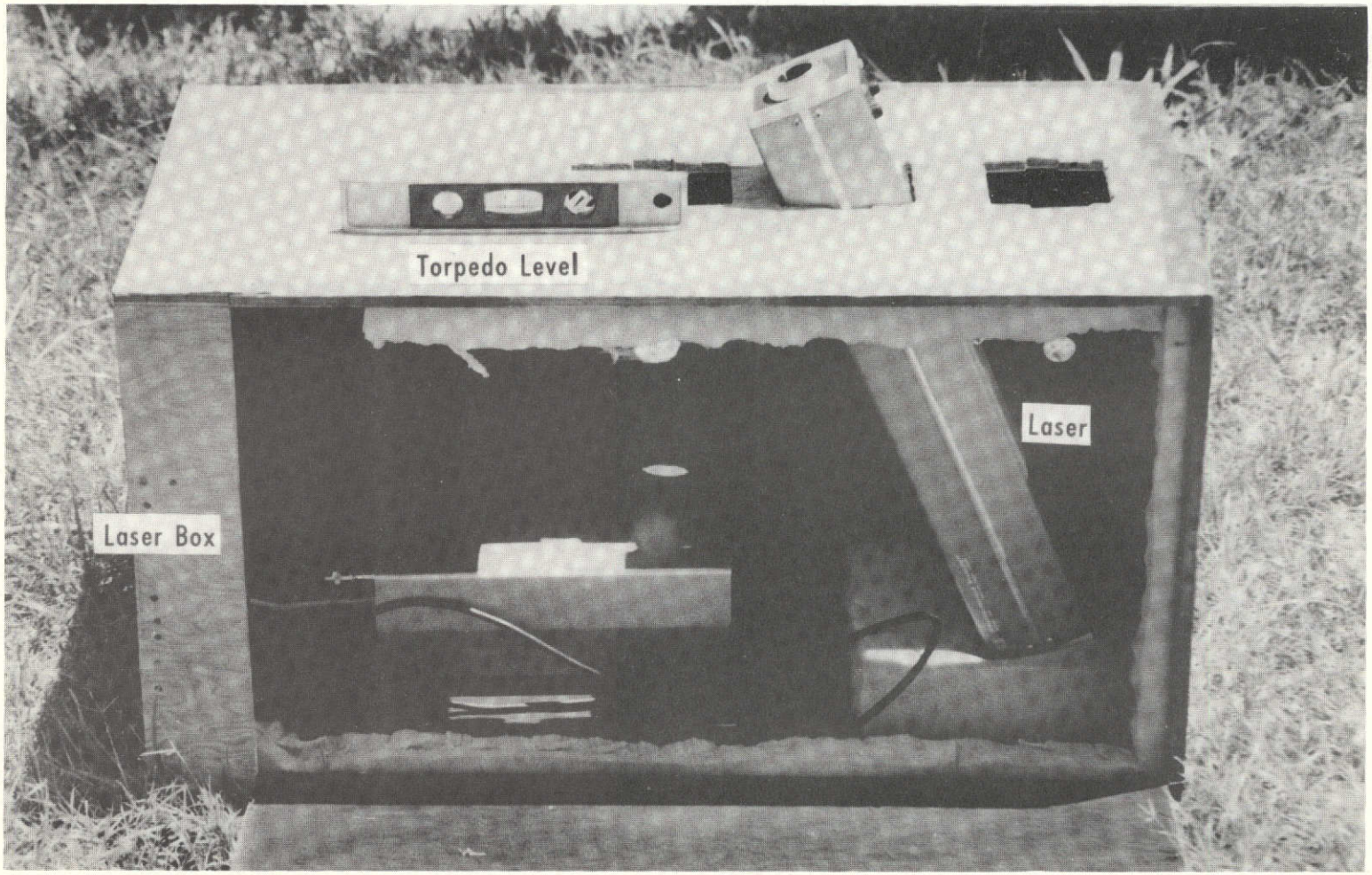

FIGURE V-12. Photograph of Laser

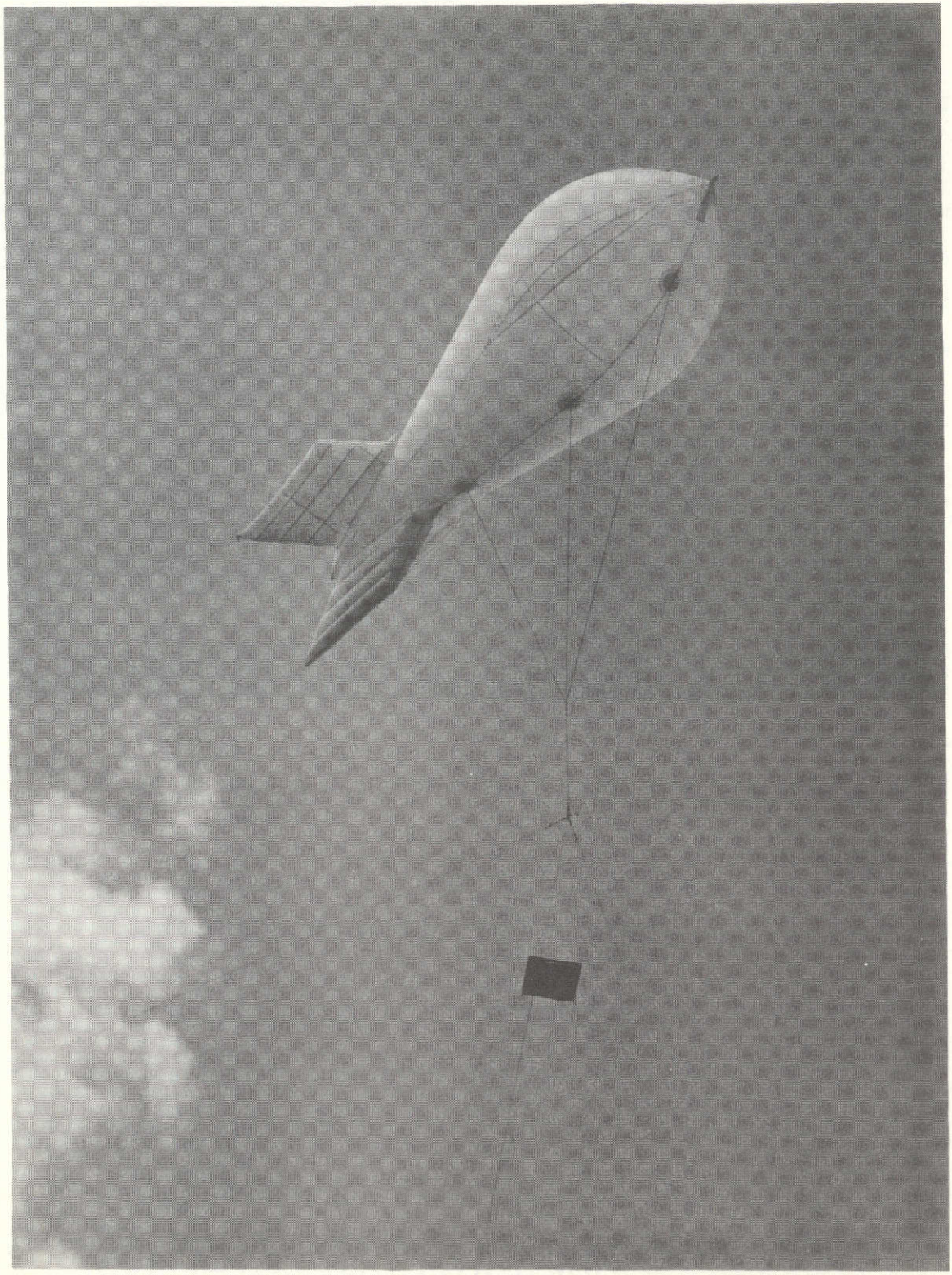

FIGURE V-13. Photograph of Balloon/Mirror in Flight

C-2

aloft by a balloon was feasible but difficult. It was particularly encouraging that the lateral movements were so small, since this meant that the mirror only had to be large enough to accommodate the field of view of the radiometer.

It was also concluded that the balloon could be easily taken down and put back up by using a safety line attached at the apex. Also the balloon could be taken down in thunderstorms or bad weather by pulling it down and expelling the helium. However, this is slow and costly. It took an hour to expell the remaining helium from the balloon after it had come down at the end of the third test which means that at least an hour warning before a storm hits would be required in order to take a balloon down and store it using this method.

The final conclusion reached from the test was the importance of the aerodynamic characteristics of the balloon. As long as the balloon acted as analyzed the system worked as theorized. However, if the balloon does not have the aerodynamic characteristics theorized either because of design or loss of gas, the system will not operate satisfactorily.

Redesign of the rigging for the fourth balloon system launched included putting a swivel between the balloon and the steel ring used as the apex and redesigning the mirror holder to make it as light as possible. Number four music wire with a lesser breaking strength was used to connect the mirror to the apex. The distance between the apex and the mirror was also increased from five to ten feet. In addition, a slip knot was used to release the plumb-bob line and let it drop to the ground as soon as the mirror was properly positioned.

The major design change made for the fourth launch was to position all the balloon cables at the same angle with respect to the ground. The angle used was 45 degrees since it gave sufficient resistance to sag forces from the balloon with a minimum of sag. The main reason for placing the cables at the same angle was that the wind direction was different each day and almost never in the direction of the expected prevailing winds. The mirror cable angles were also changed so that tests of mirror stability was obtained with mirror cable angle (β) of 60 and 70 degrees.

The data collected with the fourth balloon system launched were analyzed with the results shown in Figures V-14 through V-22. Figure V-14 shows the side forces/vertical tension required to buckle any one cable for a balloon system with all three cables at forty five degrees and oriented like the system used for the fourth balloon. The direction of the wind forces and subsequent side forces are also shown on this figure. From this figure it can be seen that if the ratio of side forces/vertical tension is greater than 0.05 that one cable will buckle and the system will become unstable.

Figure V-15 shows the downward force produced on the balloon system by the mirror system for the different valves of tension in the mirror cables and different cable angles. This figure is based on the mirror system weight of 2.3 pounds as used in the fourth test series. Figure V-16 gives the predicted wind speed which will cause a side force/vertical tension ratio of 0.05 and thus cause cable one (Figure V-14) to buckle. This data was calculated by making a series of force tables as given in Table V-1 and plotting the resulting data to find the wind speed at which a side force/vertical tension of 0.05 is obtained. Drag forces

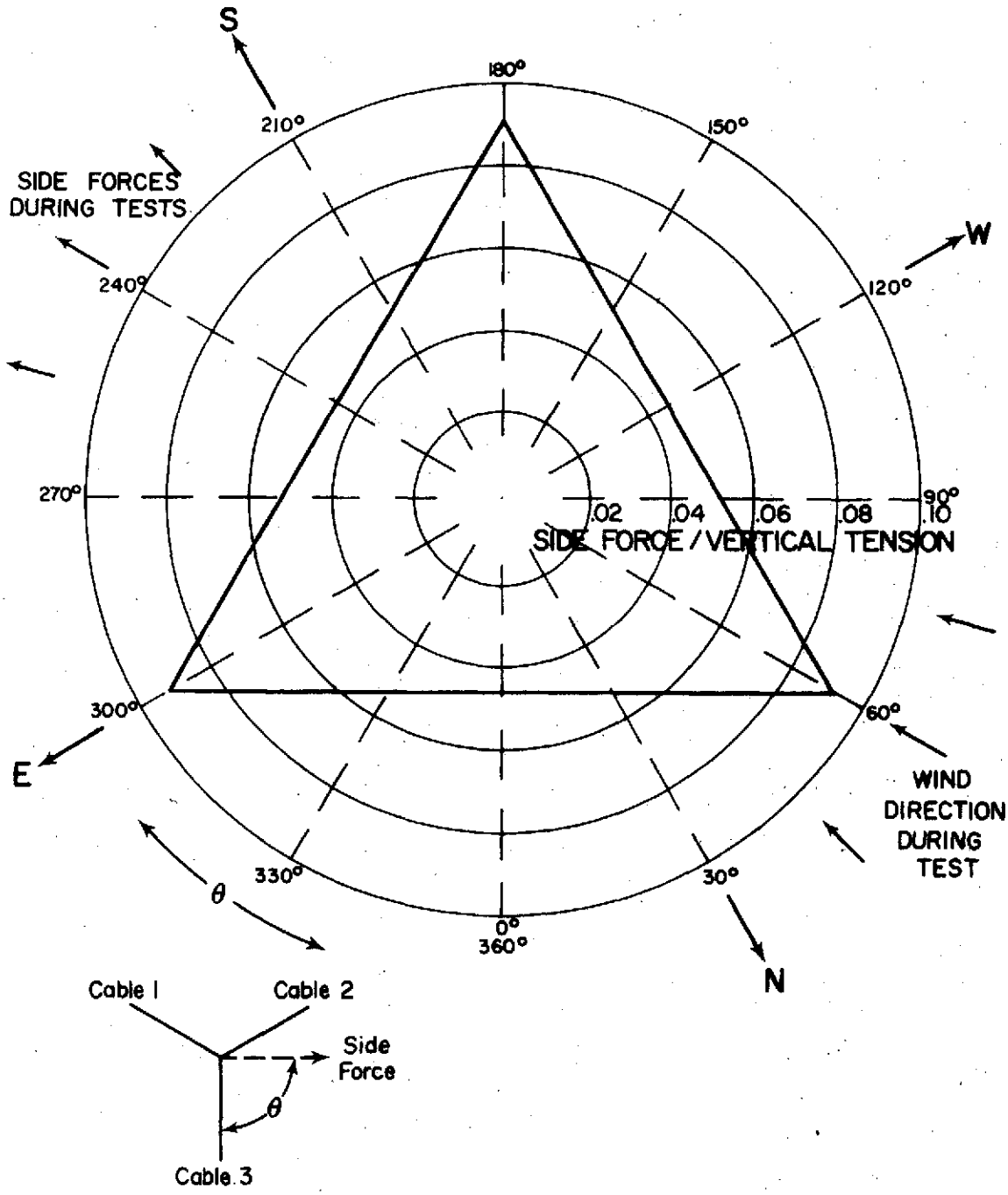

FIGURE V-14. SIDE FORCE/VERTICAL TENSION REQUIRED FOR BUCKLING ANY BALLOON CABLE FOR SYSTEM USED IN FOURTH TEST

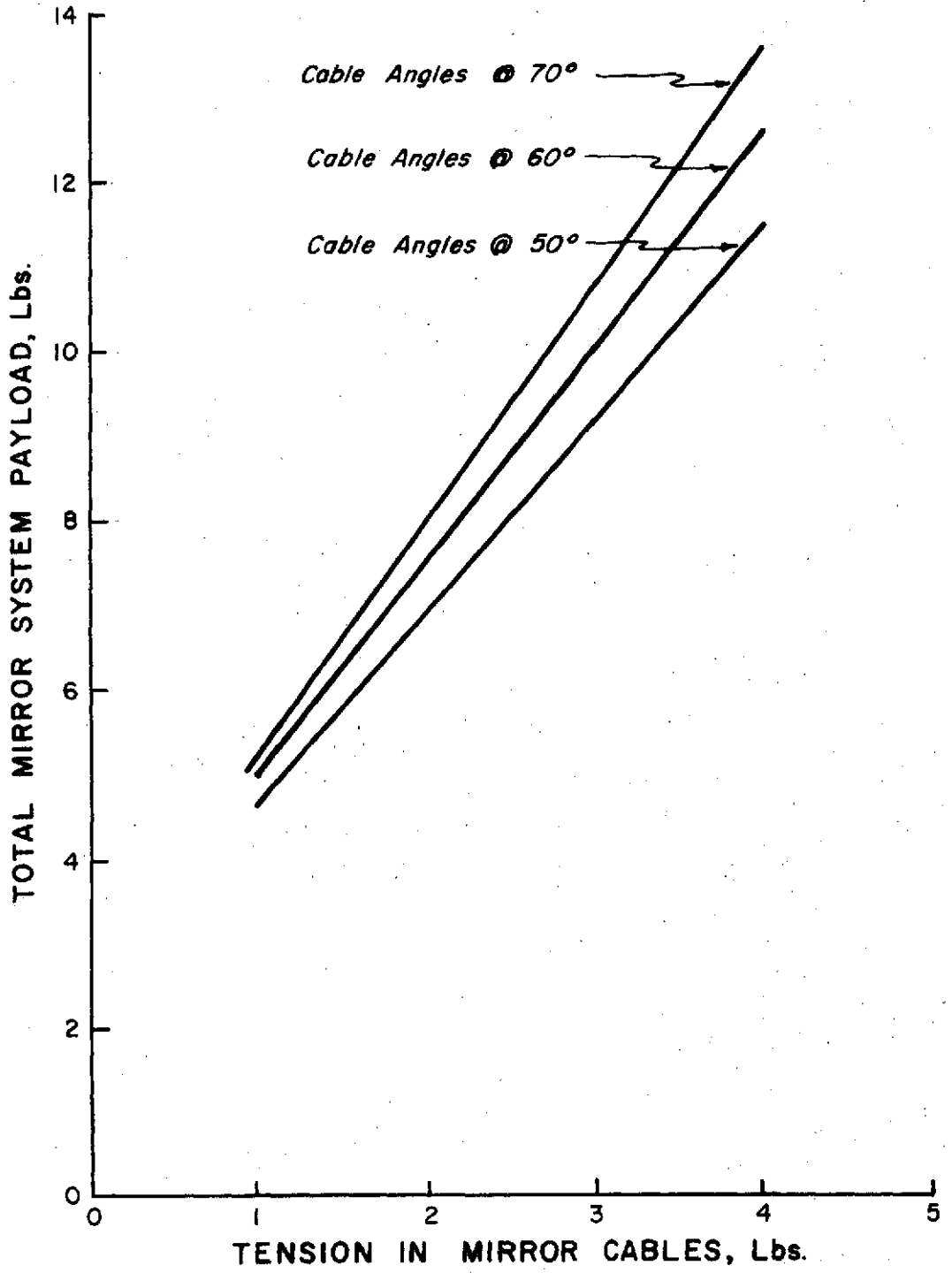

FIGURE V-15. PAYLOAD WEIGHT VS. MIRROR CABLE TENSION

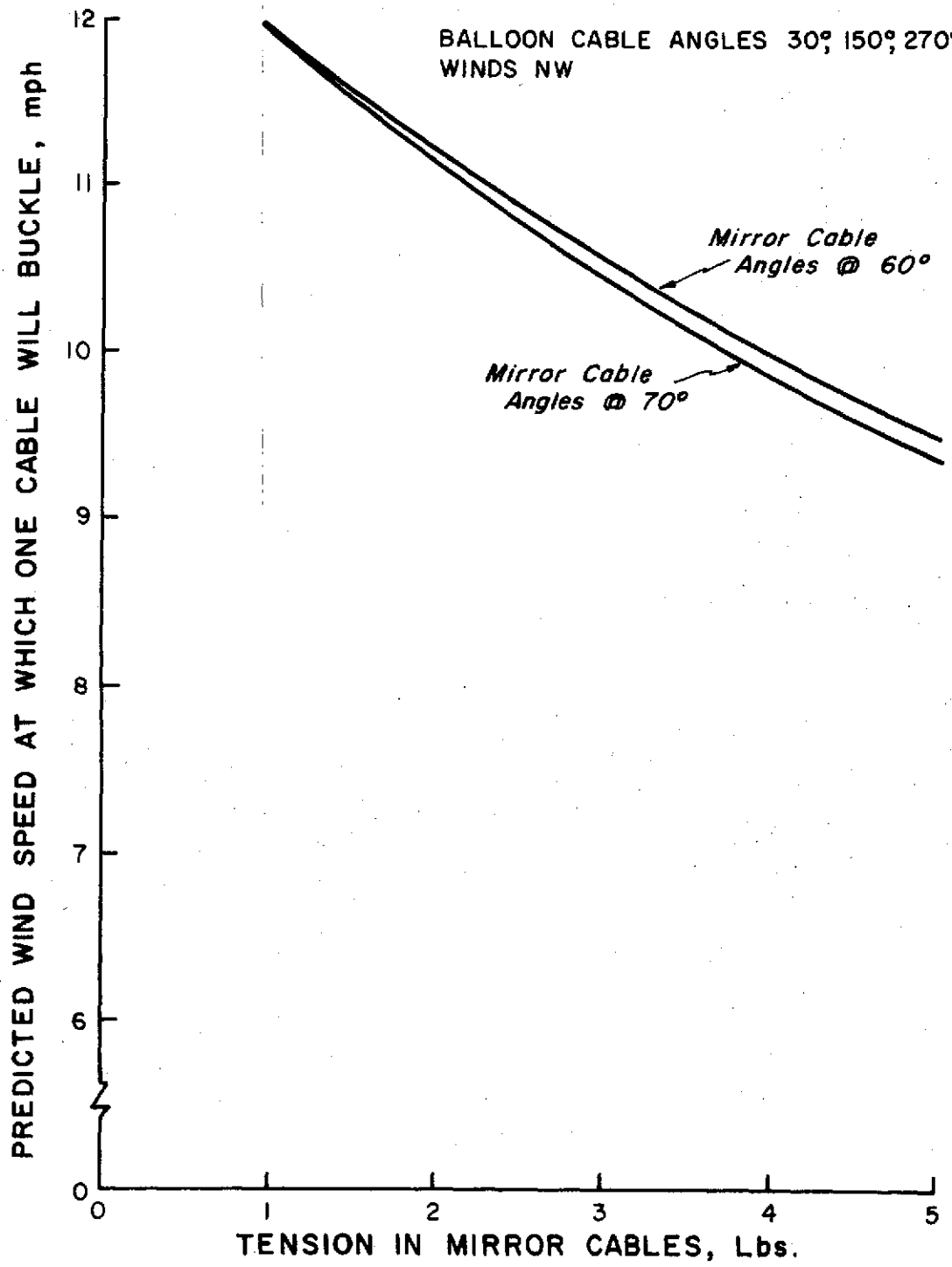

FIGURE V-16. WIND SPEED REQUIRED TO BUCKLE ONE BALLOON CABLE

were determined based on Figure V-7. Figure V-7 is for a larger balloon but also for one with better aerodynamic characteristics. The two effects are assumed to cancel one another. Again as seen in the third balloon test, the wind speed at which the balloon system was predicted to become unstable was reached and as predicted the system became unstable.

Figures V-17 through V-22 show the movement of the mirror during the tests. These curves indicate that tensions of two to three pounds of force in the mirror cables gave the least movement. Lateral movement was small and was least for the lower cable angle although the difference is insignificant if the mirror cable tension is two to three pounds of force. Maximum angular movement is seen to be $\pm$ 1 degree to $\pm$ 2 degrees for cable tensions of two to three pounds of force. Slightly less angular movement was seen at the higher mirror cable angle (β), however it was not enough to be considered as significant.

A recommendation which was concluded from the fourth balloon launched was that six stakes for the balloon cables be driven into the ground 60 degrees apart on a circle whose diameter is such that the calculated cable angles will be obtained when the balloon is launched. This will allow the winches to be mounted on the three stakes which will always place one cable within thirty degrees of the prevailing wind. With this arrangement the side force/vertical tension required to buckle any cable is as given in Figure V-23.

Part III - Final System Design and Conclusions

A 1200 cubic foot balloon of the same design as the smaller test balloons was available for use in making reflectance readings with the radiometer. Therefore, a system was designed based on using this balloon

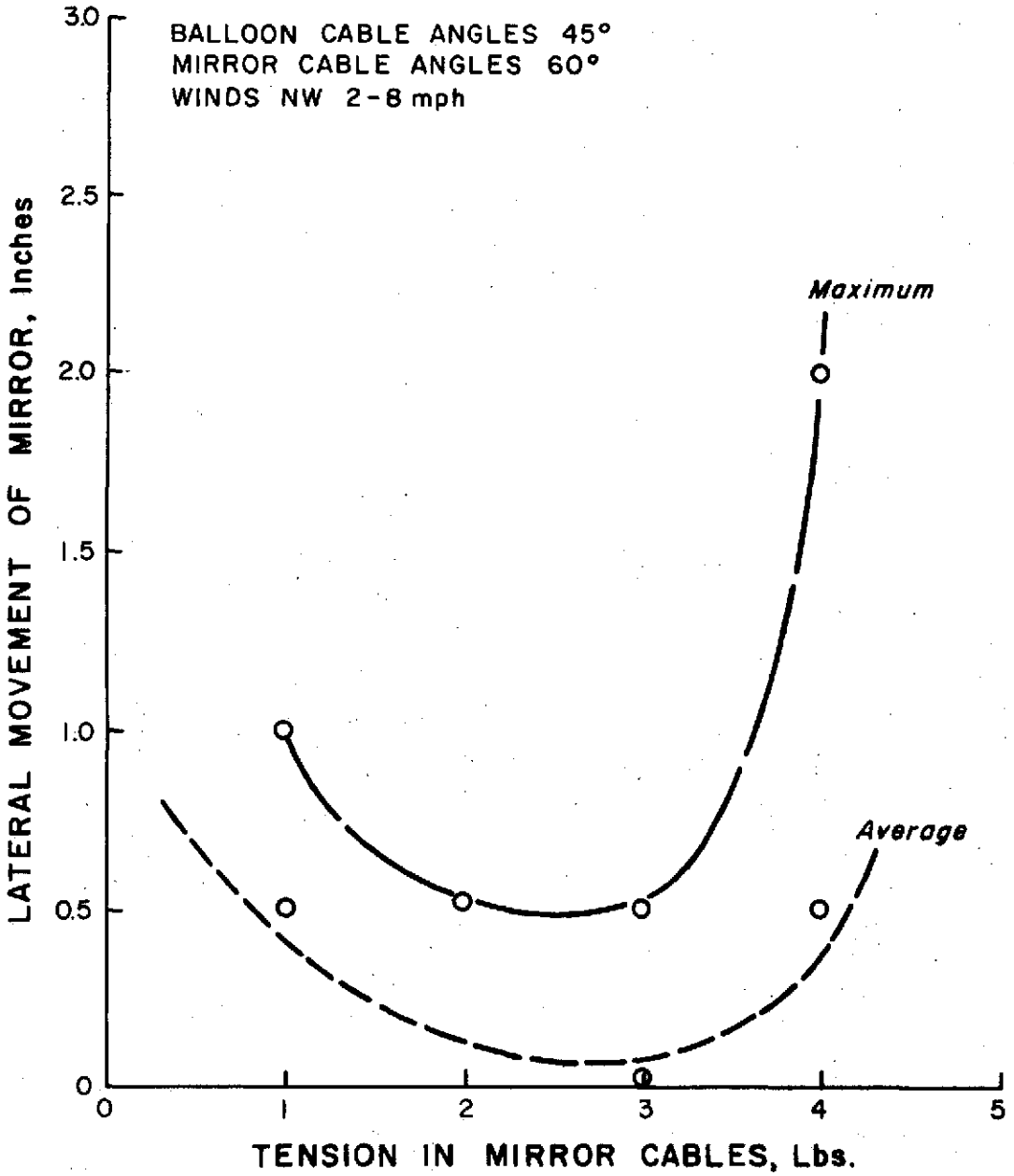

FIGURE V-17. LATERAL MOVEMENT VS. MIRROR CABLE TENSION, β=60°

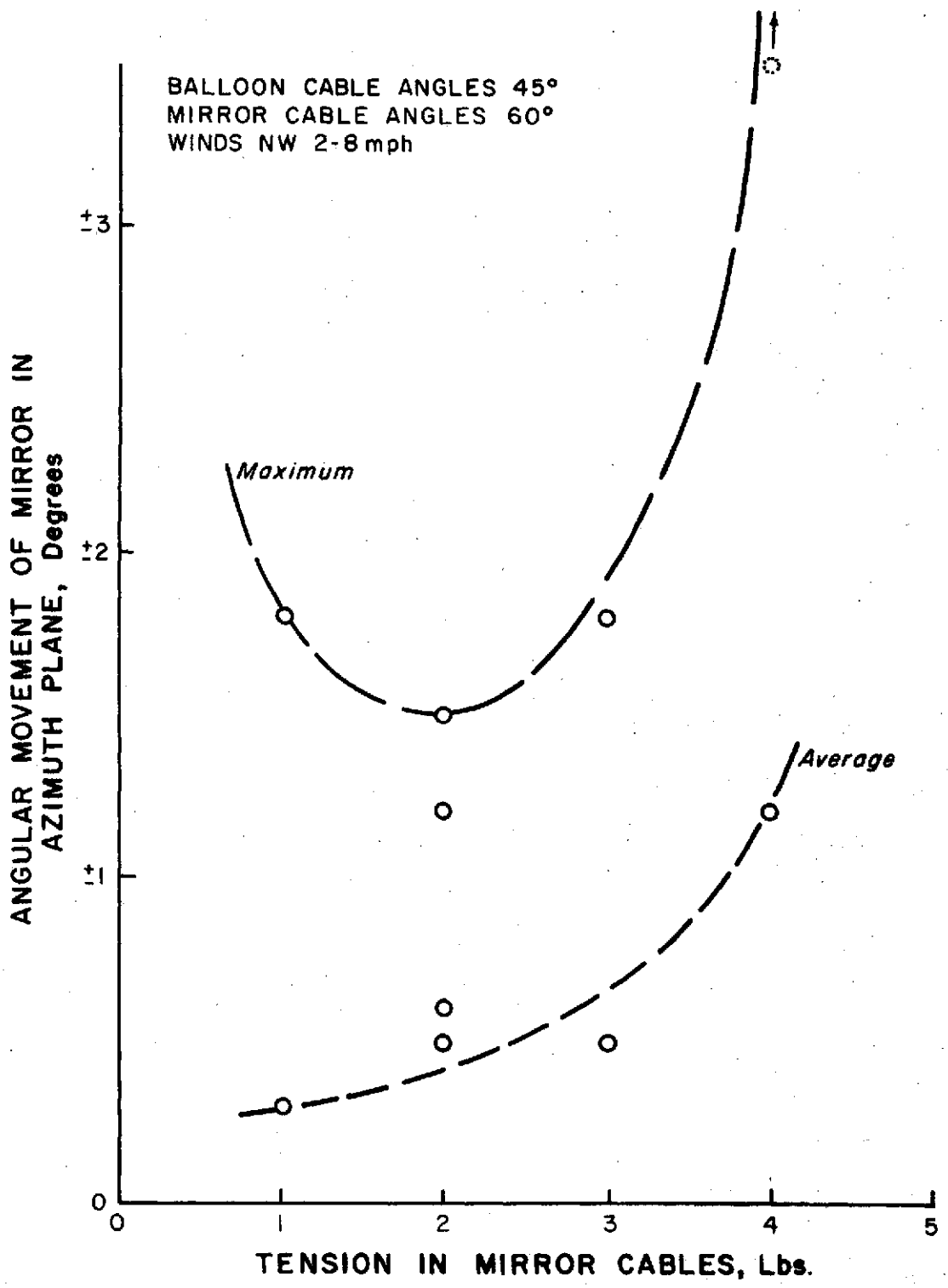

FIGURE V-18. PARALLEL ANGULAR MOVEMENT VS. MIRROR CABLE TENSION, $\beta = 60°$

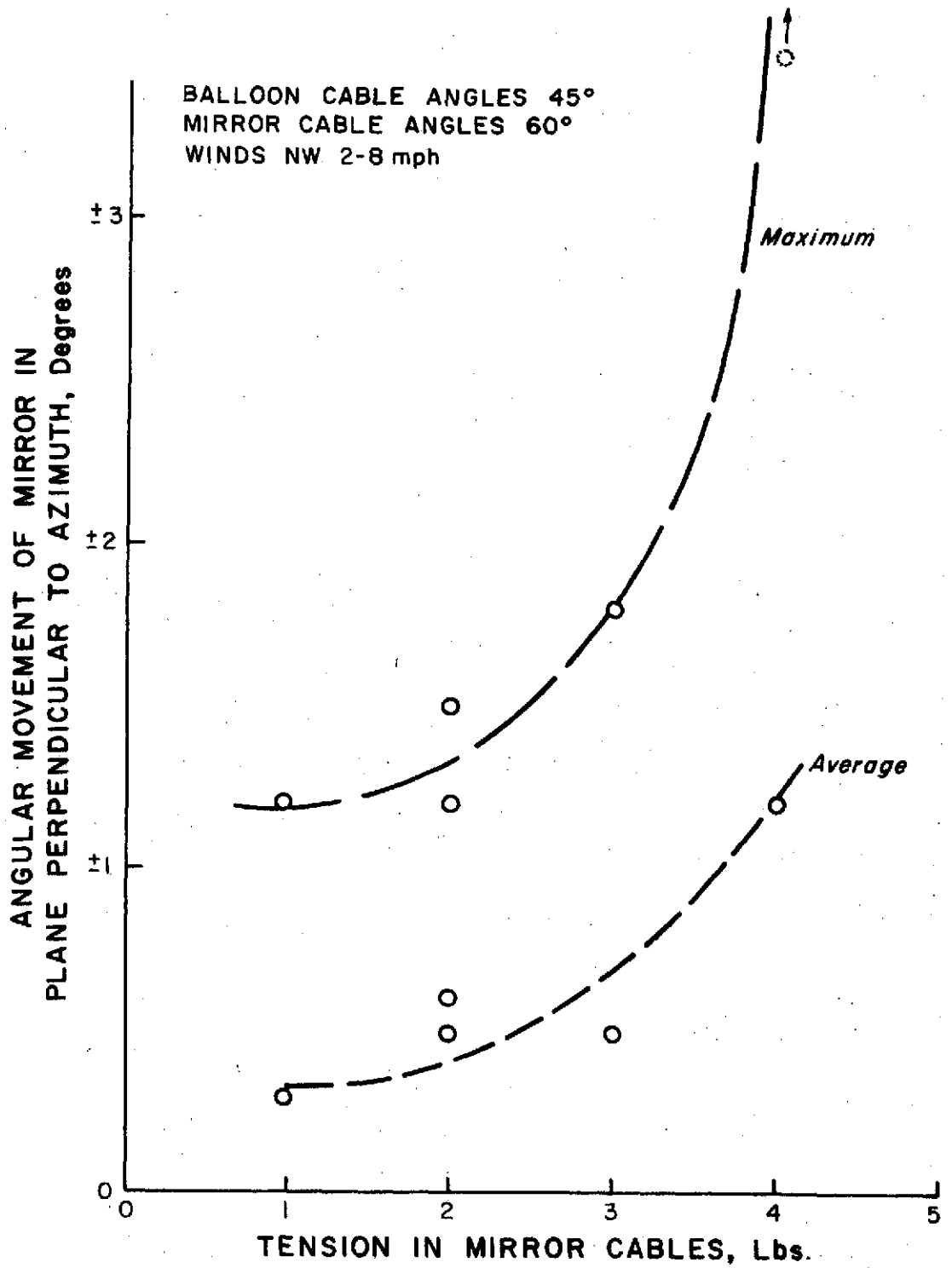

FIGURE V-19. PERPENDICULAR ANGULAR MOVEMENT VS. MIRROR CABLE TENSION, β=60°

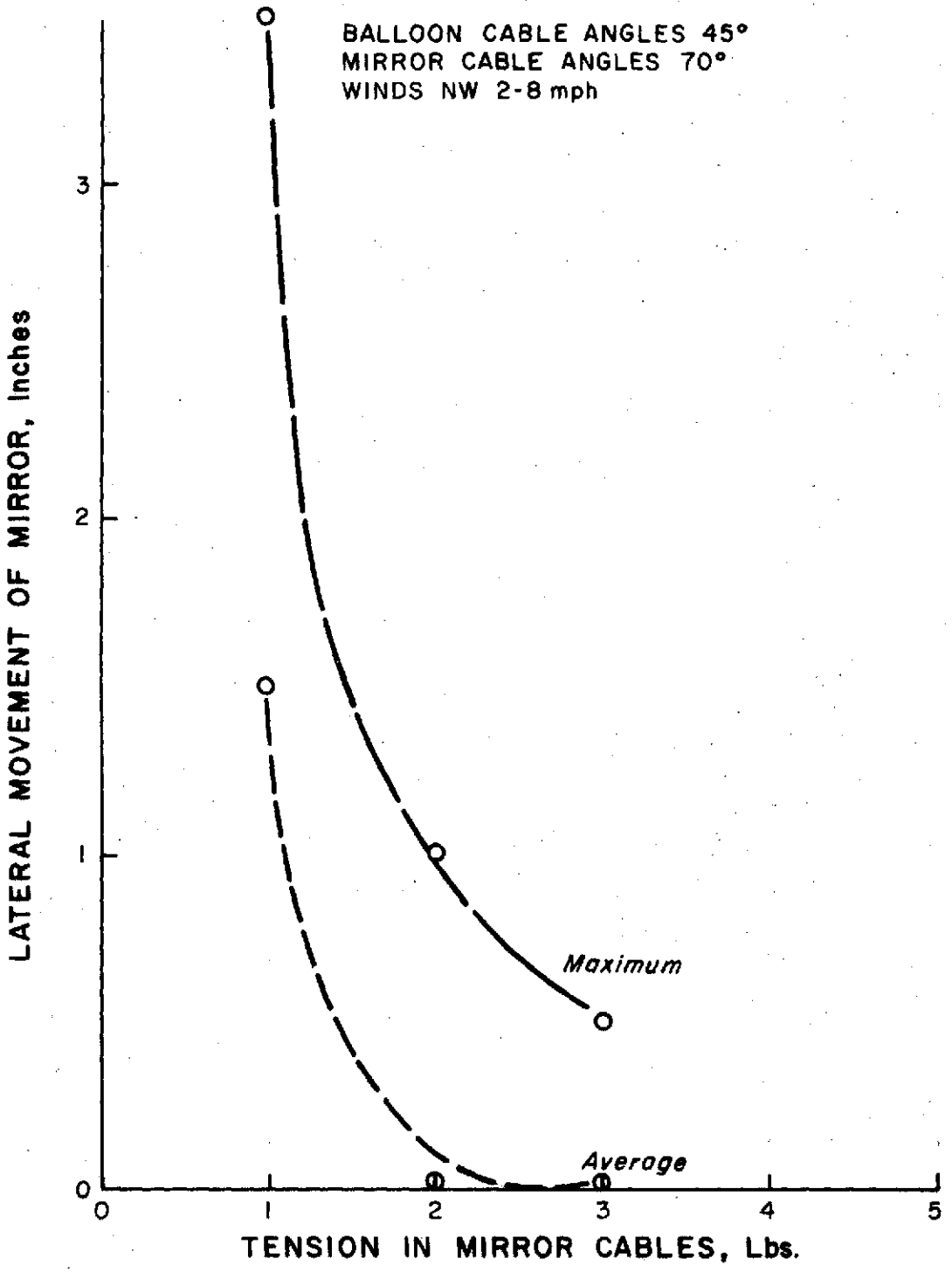

FIGURE V-20. LATERAL MOVEMENT VS. MIRROR CABLE TENSION, β=70°

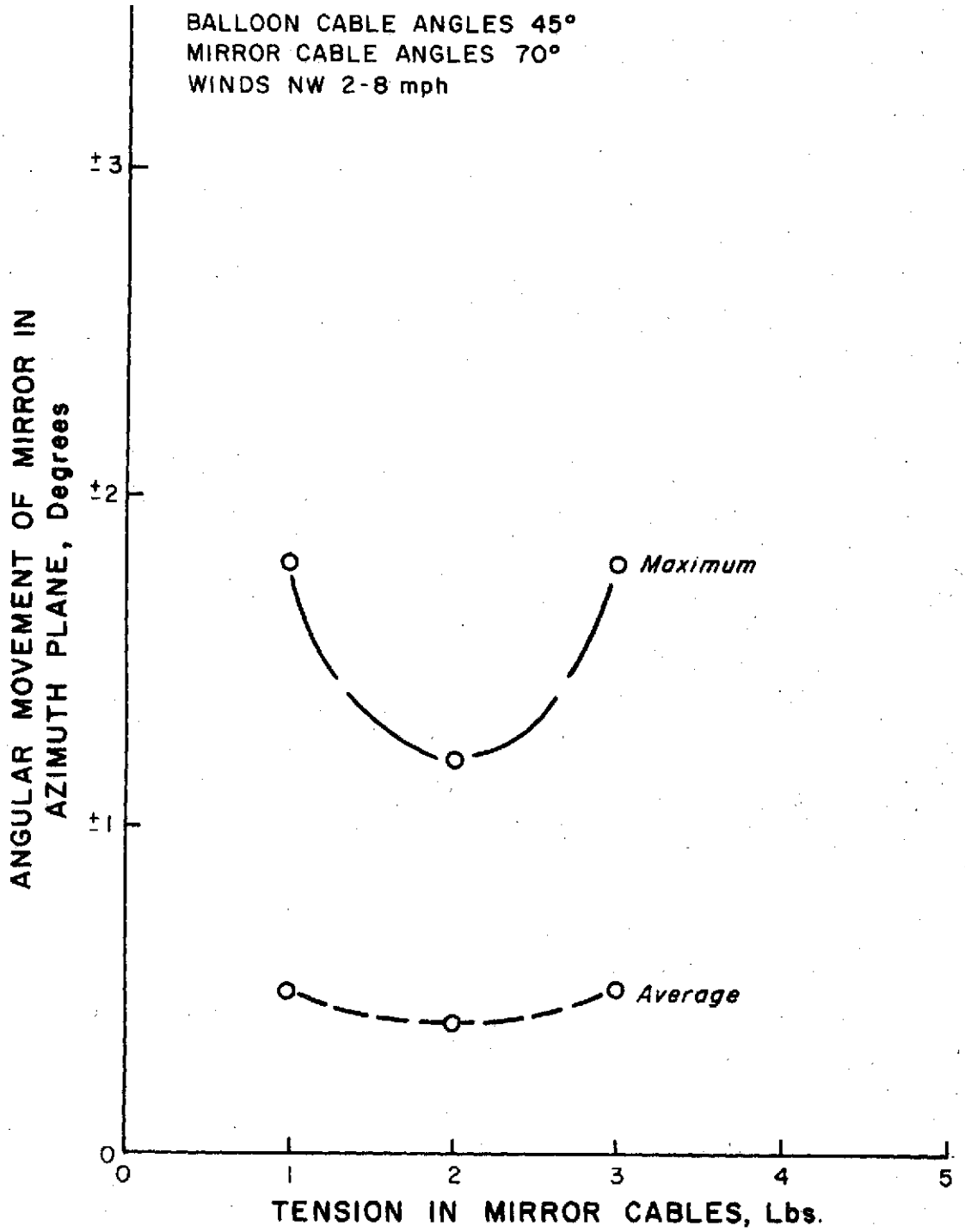

FIGURE V-21. PARALLEL ANGULAR MOVEMENT VS. MIRROR CABLE TENSION, β=70°

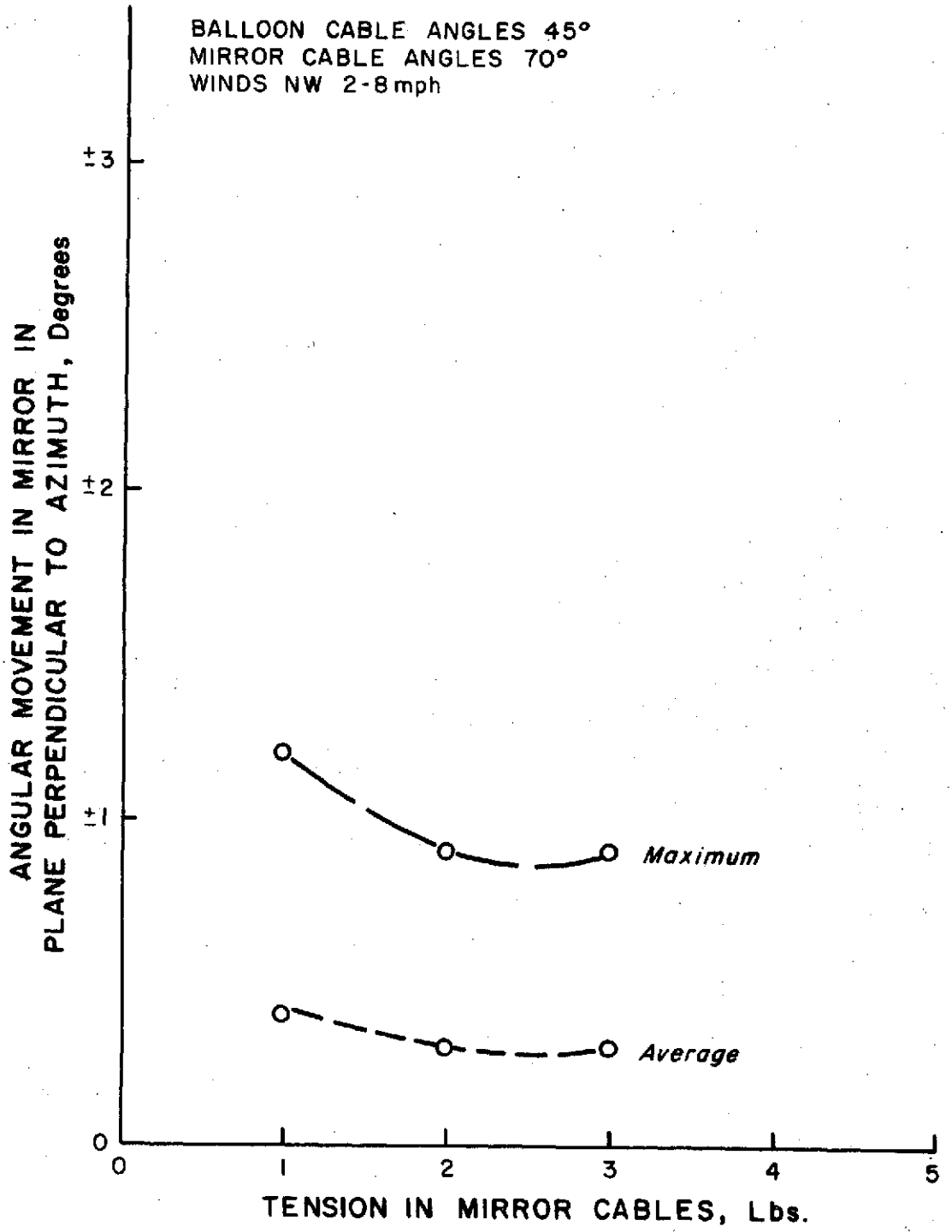

FIGURE V-22. PERPENDICULAR ANGULAR MOVEMENT VS. MIRROR CABLE TENSION, $\beta = 70°$

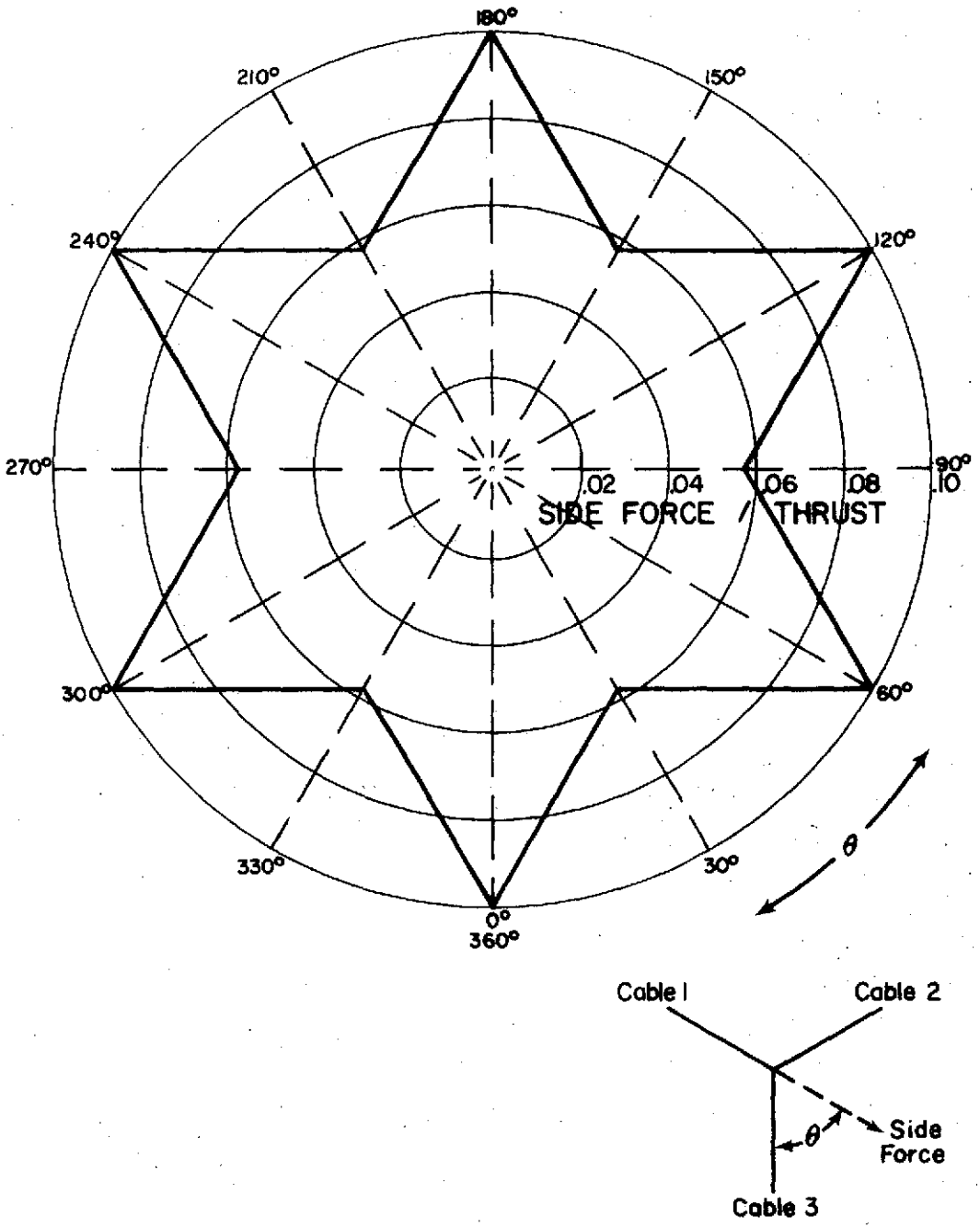

FIGURE V-23. SIDE FORCE/THRUST REQUIRED FOR BUCKLING ANY BALLOON CABLE FOR RECOMMENDED TETHERING ARRANGEMENT

to hold a reflecting surface aloft. The system was designed to remain stable in winds up to seventeen miles per hour (twenty five feet/second). This wind speed on which the design was based was picked since tests with the smaller balloons had shown that the balloon itself deteriorates rapidly at wind speeds much above ten miles per hour. By using seventeen miles per hour as the design wind speed, allowance is made for increased drag due to loss of helium and the resulting change in the balloon aerodynamic characteristics. Therefore, the cable system should remain stable as long as the balloon acts properly.

Table V-2 gives a force table for the 1200 cubic foot balloon. The vertical force in the mirror cables is based on mirror cable tensions of three pounds of force with the cables at an angle of sixty degrees. The drag force is taken from Figure V-7 with thirty per cent added to account for the size increase and the blunted aerodynamic shape. The design criteria for the cable arrangement was based on a side force/vertical tension ratio of 0.095. The mirror weight was estimated based on using a two foot by two foot aluminized polyester film stretched over a light weight frame as the first surface reflector.

In order to maintain the balloon in a stable configuration in winds up to twenty five feet/second, all the cables angles must be at thirty five degrees and a six stake arrangement must be used as discussed in the conclusions obtained from the third stability test. This results in a diagram of the side force/vertical tension required to buckle the system as seen in Figure V-24. The mirror cable angle suggested was sixty degrees with three pounds of tension pulled in each cable. By using this arrangement the system will survive the winds to be expected during most days of the year. The exception are days when thunderstorms

TABLE V-2

Force Table for 1200 ft^3 Balloon System

Wind Velocity	0 ft/sec	15 ft/sec	25 ft/sec
Balloon Static Lift @ 80^o	71 lb	71 lb	71 lb
Balloon Dynamic Lift	0	2.3 lb	9.3 lb
Gross Lift	71 lb	73.3 lb	80.3 lb
Balloon Weight	17.5 lb	17.5 lb	17.5 lb
Lift at Apex	53.5 lb	55.8 lb	62.8 lb
Drag on Side Force	0	1.7 lb	4.4 lb
SF/Lift	0	.030	.070
Mirror System Weight	6 lb	6 lb	6 lb
Total Vertical Force in Mirror Cable	10 lb	10 lb	10 lb
Total Downward Pull at Apex Due to Payload	16 lb	16 lb	16 lb
Total Vertical Component of Tension in Balloon Cables - T_v	37.5 lb	39.8 lb	46.8 lb
SF/T_v	0	.043	.095

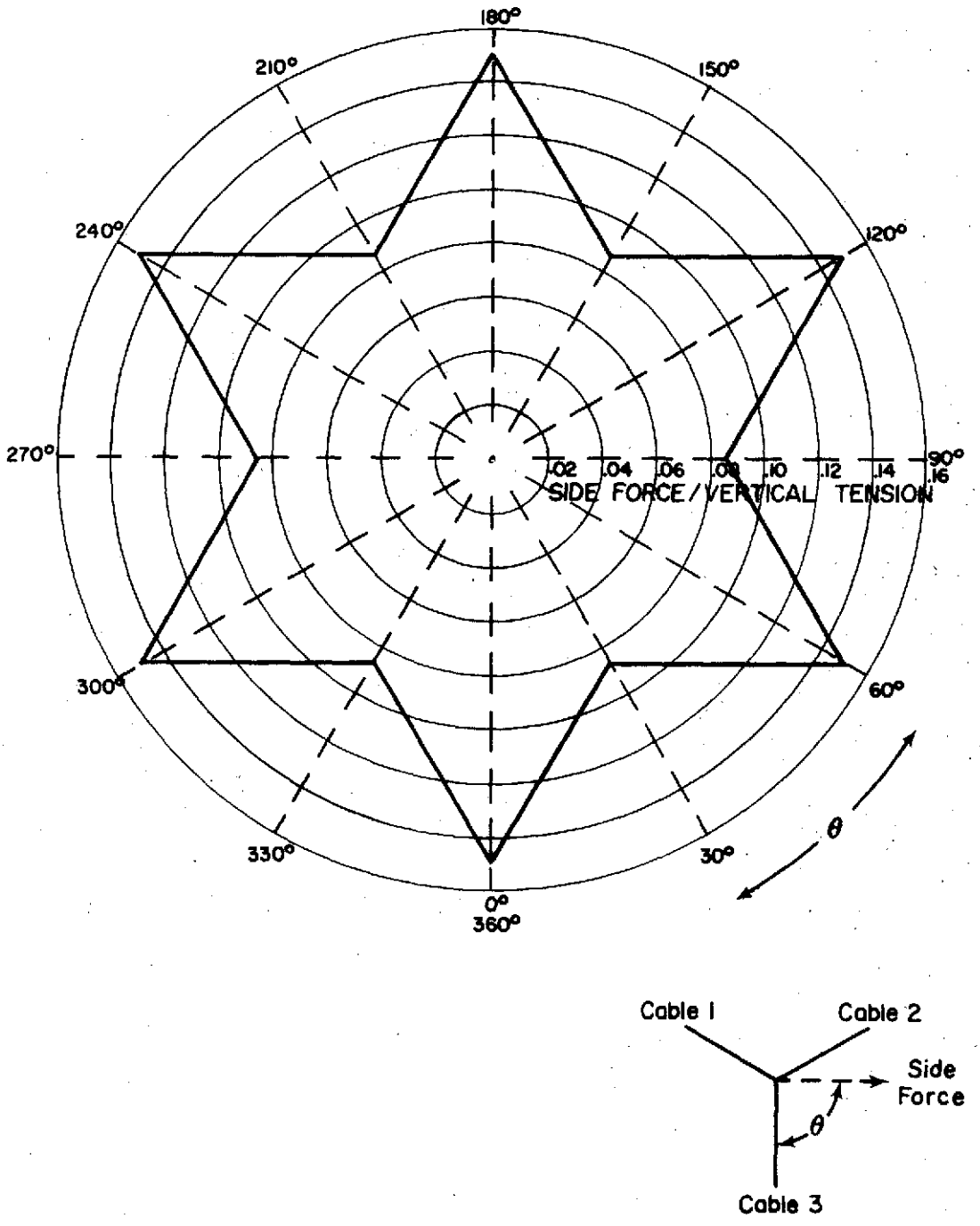

FIGURE V-24. SIDE FORCE/VERTICAL TENSION REQUIRED FOR BUCKLING BALLOON CABLE FOR 1200 FT^3 BALLOON SYSTEM

develop and/or a cold front is passing through the area causing winds to increase above seventeen miles per hour.

Using an altitude of one hundred feet for the mirror, lateral movements were expected to be almost negligible for the reflecting surface. Angular movements were expected between one to two degrees. Therefore, a consistent plot of ground three to four feet larger on each side than the field of view of the radiometer was used in making measurements.

The cables, winches, safety lines, stakes, etc. used in the smaller balloon tests were designed for the larger system so that these same elements were used in the final balloon system design.

Conclusions

Several conclusions about the use of a tethered balloon system to hold an object stationary above the ground in general were made as well as several conclusions about the system used in particular. In general, it appears that an object can be held aloft with little or no lateral movement by using a tethered balloon system as designed at altitudes as high as one hundred feet and possibly as high as five hundred feet. However, angular movements of the suspended object will be significant using the system as designed especially if the object is to be suspended at an altitude greater than one hundred feet.

For many applications the biggest limitations in the use of the system will be the inability to make long duration tests of several weeks with this system. As presently conceived the system's duration is limited to the time between balloon launch and the time that winds due to thunderstorms or otherwise become high enough to make one of the cables go slack. This problem is further complicated by helium losses

from the balloon. Also a watch needs to be kept on the system day and night when it is put up in order to adjust the system for wind changes, gas losses, and the presence of thunderstorms.

In particular for the system tested, lateral movements of the mirror were negligible and angular movements were reduced to $\pm$ 1 to 2 degrees for the mirror at one hundred feet. Similar results were obtained for all the tests conducted. It was also seen from the balloon tests that the type of balloon used was not very well suited for this type of application. The balloons had large losses of helium especially at winds above ten miles per hour. The balloon would have also worked better had it been cleaner aerodynamically and had larger and rigid stabilizers. The balloon should also have been able to withstand higher winds without losing its shape. Another conclusion made was that a larger balloon with more lift should have been used for the tests. This would have allowed the system to withstand higher winds.

A number of suggestions for further study or improvements of the system were made. It was concluded that if the system were to be studied further the first step should be to make a complete mathematical model of the system and to write a computer program. Data obtained from the tests already made can be used to check the program. Based on a typical wind profile and balloon characteristics, various elements of the system can be optimized. Once this is finished, a new system could be designed and tested if it is seen that significant improvements could be made in the performance of the system as compared to the balloon systems tested in this study.

It was also concluded from the tests made that some way is needed to take the balloon down quickly and to save the helium. One

possibility might be to use a pump to empty the balloon and to refill the helium storage bottles. Another possibility is to have a large storage van or hanger where the balloon can be placed fully inflated. Some way to quickly check the balloon for leaks and tears is also needed so that repairs can be made. Better winches are needed. The winches used in the tests had a small diameter and caused the wire to curl. Therefore when a line went slack the wire curled and then when pulled back tight would cause a kink in the line. This problem affected both the strength and elasticity of the cables.

Another possibility for improving the system might be to use hydrogen rather than helium as the lifting gas. Making this study would result in a trade off between the safety of helium and the cost, lift for same drag component, and containability of hydrogen.

A final suggestion for further study is the use of a spring and damper system as the connection between the balloon apex and the payload. The system should be swiveled on both ends. The design parameters of the system would have to be determined from the computer analysis.

In conclusion it should be stated that the design parameters found to be of most importance in stabilizing a mirror suspended underneath a tethered balloon are:

1. The balloon shape must be such that a minimum of drag is produced.
2. The balloon stabilizers must be such that the balloon reacts quickly to changes in wind direction,
3. The balloon must have a low leak rate while being held fairly stationary in varying winds.

4. The mirror must be as light weight as possible.

This last requirement indicates the importance of the use of an aluminum coated mylar film as the first surface reflector.

CHAPTER VI

LABORATORY TESTS AND RESULTS

The first tests made to determine the reflectance of natural surfaces were made with the spectroradiometer described in Chapter IV under laboratory conditions. Reflectance readings and variations in the reflectance with source angle were obtained for a plot of Saint Augustine grass, a plot of black alluvial soil taken from the Mississippi River flood plain and a plot of Bermuda grass. The method used to make reflectance readings in the laboratory was the same as that used later in field tests. The only exceptions were the controlled environment of the laboratory, the use of photolamps as a source instead of the sun and the use of a folding mirror mounted on a moveable platform instead of underneath a balloon.

Mathematical Analysis

Reflectance generally is defined as the ratio of reflected energy to the original irradiation where the irradiation is the total power incident or incoming to a surface per unit area of surface[55]. As mentioned in Appendix A, reflectance is a function of wavelength (λ). Bidirectional reflection, also defined in Appendix A, is the ratio of the energy reflected from a surface at a particular angle to the incoming energy to the surface at some other angle. In order to describe these angular quantities completely, three angles are required. They are the source zenith angle (ζ), the viewing or reading zenith angle (θ) and the relative azimuth angle (Ψ) between the planes defined by the source and the surface and the viewing element and the surface. Therefore, bidirectional reflectance ($\bar{\rho}$), is

a function of wavelength, source zenith angle, viewing zenith angle and relative azimuth angle and can be written $\bar{\rho}(\lambda, \zeta, \theta, \Psi)$.

In order to measure bidirectional reflectance directly in the laboratory, the detector system must be placed to read the energy reflecting from the test surface at a particular angle and to read in a similar manner the energy incoming to the test surface at some other desired angle (see Figure VI-1). If the incoming energy is designated as I_{in} and the reflected energy as I_{out}, and the angular and wavelength dependences are included, the definition for bidirectional reflectance can be written

$$\bar{\rho}(\lambda,\theta,\zeta,\Psi) = \frac{I_{out}(\lambda,\theta_{out},\zeta_{out},\Psi_{out})}{I_{in}(\lambda,\theta_{in},\zeta_{in},\Psi_{in})} \qquad \text{(VI-1)}$$

where Ψ_{out} and Ψ_{in} are measured from some reference plane and $\Psi = |\Psi_{out}-(180^{o} + \Psi_{in})|$.

There are several problems involved if this definition is to be used directly to measure the bidirectional reflectance of natural surfaces under natural conditions. One of these problems is that the spectroradiometer must be positioned so that it reads first the reflected energy and then reads the incoming energy in exactly the same way. The second problem is that in the natural environment the incoming energy to be measured is the direct sunlight which is several magnitudes greater than the outgoing energy for the same solid angle or detector area. It is therefore difficult to use the same system to measure both I_{in} and I_{out}.

Because of these problems, the reflectances measured and calculated in this investigation were relative bidirectional reflectances. That is, a signal, S_T, was first recorded from a test surface and then

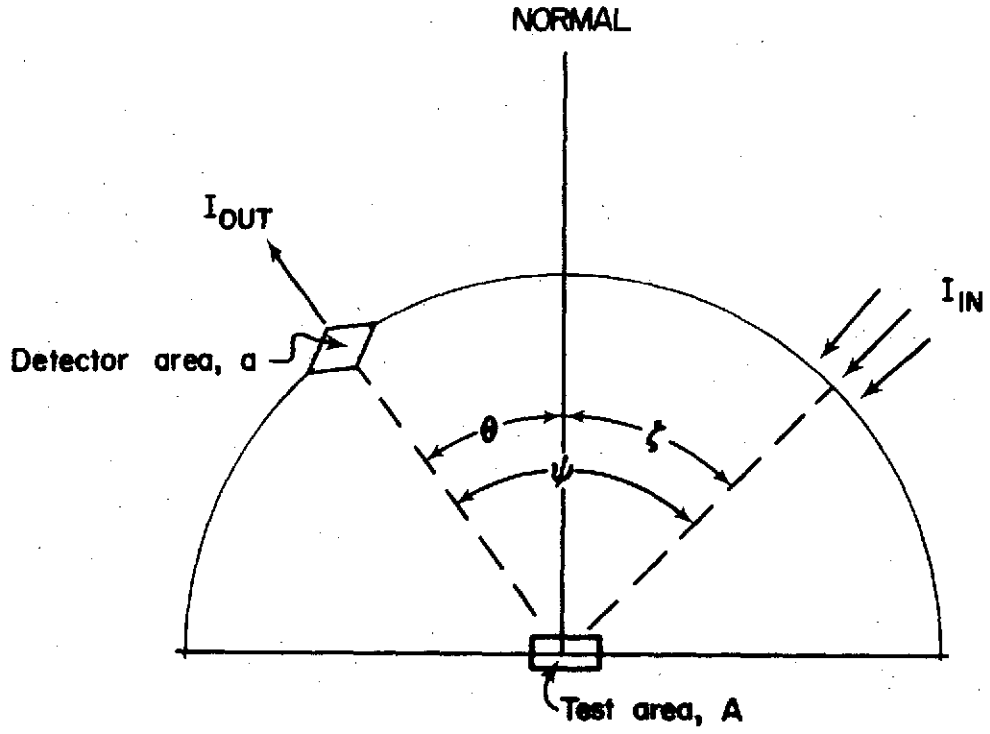

FIGURE VI-1. MEASURING SYSTEM FOR BIDIRECTIONAL REFLECTANCE

rationed to a standard signal S_s recorded from a standard surface of 101-A10 white paint (see Appendix D). Both signals are taken in the same manner with the same recording system, solid viewing angle, wavelength, bandwidth, irradiation, and angular conditions. If the detector and amplifier systems are linear, then the recorded signals S_T and S_s are porportional to the intensity of the energies coming from the sufaces under the prescribed conditions. Therefore,

$$S_T = k\, I_T\, (\lambda\ ,\ \theta_{out},\ \zeta_{out},\ \Psi_{out}) \tag{VI-2}$$

and

$$S_s = k\, I_S\, (\lambda\ ,\ \theta_{out},\ \zeta_{out},\ \Psi_{out}) \tag{VI-3}$$

If the incoming energy from the lamp source is kept constant while both measurements are being made, then mathematically the relative bidirectional reflectance, $\hat{\rho}$, is

$$\hat{\rho}(\lambda,\theta,\zeta,\Psi) = S_T/S_s = \frac{I_{T\ out}(\lambda,\theta_{out},\zeta_{out},\Psi_{out})}{I_{S\ out}(\lambda,\theta_{out},\zeta_{out},\Psi_{out})} \tag{VI-4}$$

from Equation (1)

$$I_{out}(\lambda\ ,\theta_{out},\ \zeta_{out},\ \Psi_{out}) = \bar{\rho}(\lambda,\theta,\zeta,\Psi) I_{in}(\lambda,\theta_{in},\zeta_{in},\Psi_{in}) \tag{VI-5}$$

Therefore,

$$\hat{\rho}(\lambda,\theta,\zeta,\Psi) = \frac{\bar{\rho}_T(\lambda,\theta\zeta,\Psi) I_{in}(\lambda,\theta_{in},\zeta_{in},\Psi_{in})}{\bar{\rho}_S(\lambda,\theta,\zeta,\Psi) I_{in}(\lambda,\theta_{in},\zeta_{in},\Psi_{in})} \tag{VI-6}$$

$$\hat{\rho}(\lambda,\theta,\zeta,\Psi) = \frac{\bar{\rho}_T(\lambda,\theta,\zeta,\Psi)}{\bar{\rho}_S(\lambda,\theta,\zeta,\Psi)} = S_T/S_s \tag{VI-7}$$

Since the standard surface used was neither perfectly diffuse or totally reflecting, it is necessary to correct the values of relative bidirectional reflectance as obtained in this study in order to compare them to similar studies made by other investigators. This is accomplished by multiplying $\hat{\rho}$ by the monochromatic hemispherical reflectance, $\rho(\lambda)$ of the standard panel from Figure D-1 and a term to correct for the lack of diffuseness of the standard surface. That is,

$$\hat{\rho}(\lambda,\theta,\zeta,\Psi) = C_D(\lambda,\theta,\zeta,\Psi)\rho_S(\lambda)\ \frac{\bar{\rho}_T(\lambda,\theta,\zeta,\Psi)}{\bar{\rho}_S(\lambda,\theta,\zeta,\Psi)} \qquad \text{(VI-8)}$$

where C_D, the diffuseness coefficient, is defined as the ratio of the actual energy outgoing from the standard surface at a particular angle to the amount of energy that would be outgoing at that angle if the surface were perfectly diffuse.

$$C_D(\lambda,\theta,\zeta,\Psi) = \frac{I_{\text{Actual out}}(\lambda,\theta,\zeta,\Psi)}{I_{\text{Diffuse out}}[I_{in}(\lambda)]} \qquad \text{(VI-9)}$$

By definition the amount of energy being reflected from a perfectly diffuse surface at any angle to a detector is a function only of the energy incoming to the surface as seen in Equation (VI-9).

An indication of the values of C_D for different source angles can be seen in Appendix D. From these data it was determined that C_D can be assumed equal to one for all the studies made in the visible region. However, this factor must be accounted for in taking data to determine information on angular variations of the reflectance in other regions of the electromagnetic spectrum.

Experimental Apparatus

The setup of the experimental apparatus used to make reflectance readings of natural surfaces is shown in Figure VI-2. The spectroradiometer was set up in one room and aimed through a door onto the folding mirror located approximately 60 feet away near a wall in another room. The folding mirror was mounted on a moveable platform and was made by stretching a polyester film which was vacuum coated with aluminum over a lightweight cardboard backing. The mirror was 24 inches by 24 inches and was obtained from the Edmund Scientific Company. The same type of first surface reflector was later used in the field tests.

The moveable platform used in the laboratory tests and later in some of the field tests is shown in Figure VI-3. The folding mirror is mounted on an aluminum plate which can be rotated about a center axis and locked in any position required. The platform is mounted on 6 inch castors to provide mobility. The platform can be extended to any height between 7 and 14 feet.

The spectroradiometer was set up as described in Chapter IV. The photomultiplier tube was used for making energy measurements in the wavelength range of 0.33 to 0.68 microns. The lead sulfide detector was used for reading from 0.68 to 3.0 microns. The range of energies read by the sulfide detector was limited by the detector response. However, the upper limit (λ = 0.33 microns) of the readings made with the photomultiplier tube was caused by factors other than the tube responsiveness. These factors included a decrease in the reflective quality of the first surface aluminized reflector's used in the spectroradiometer and in the folding mirror, a decrease

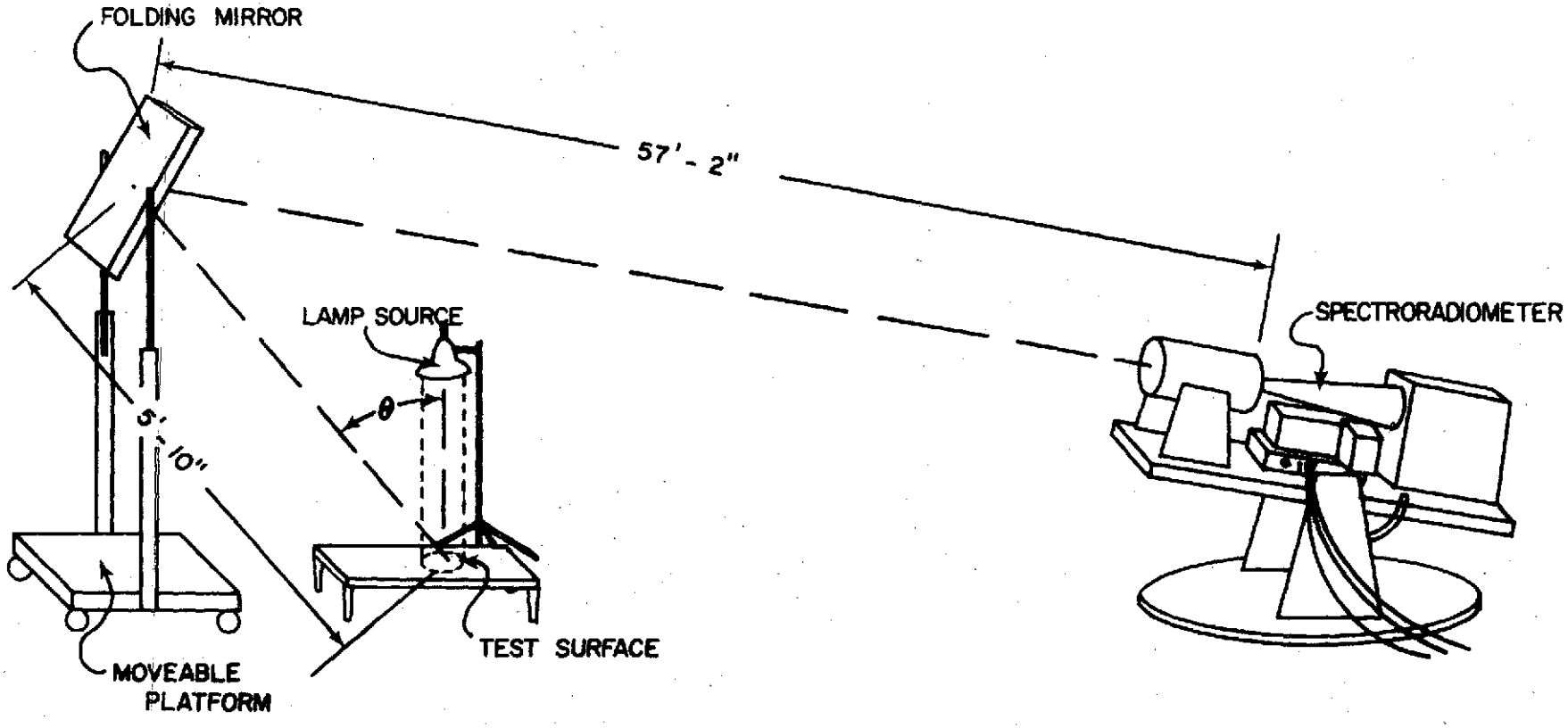

FIGURE VI-2. EQUIPMENT ARRANGEMENT USED IN LABORATORY TESTS

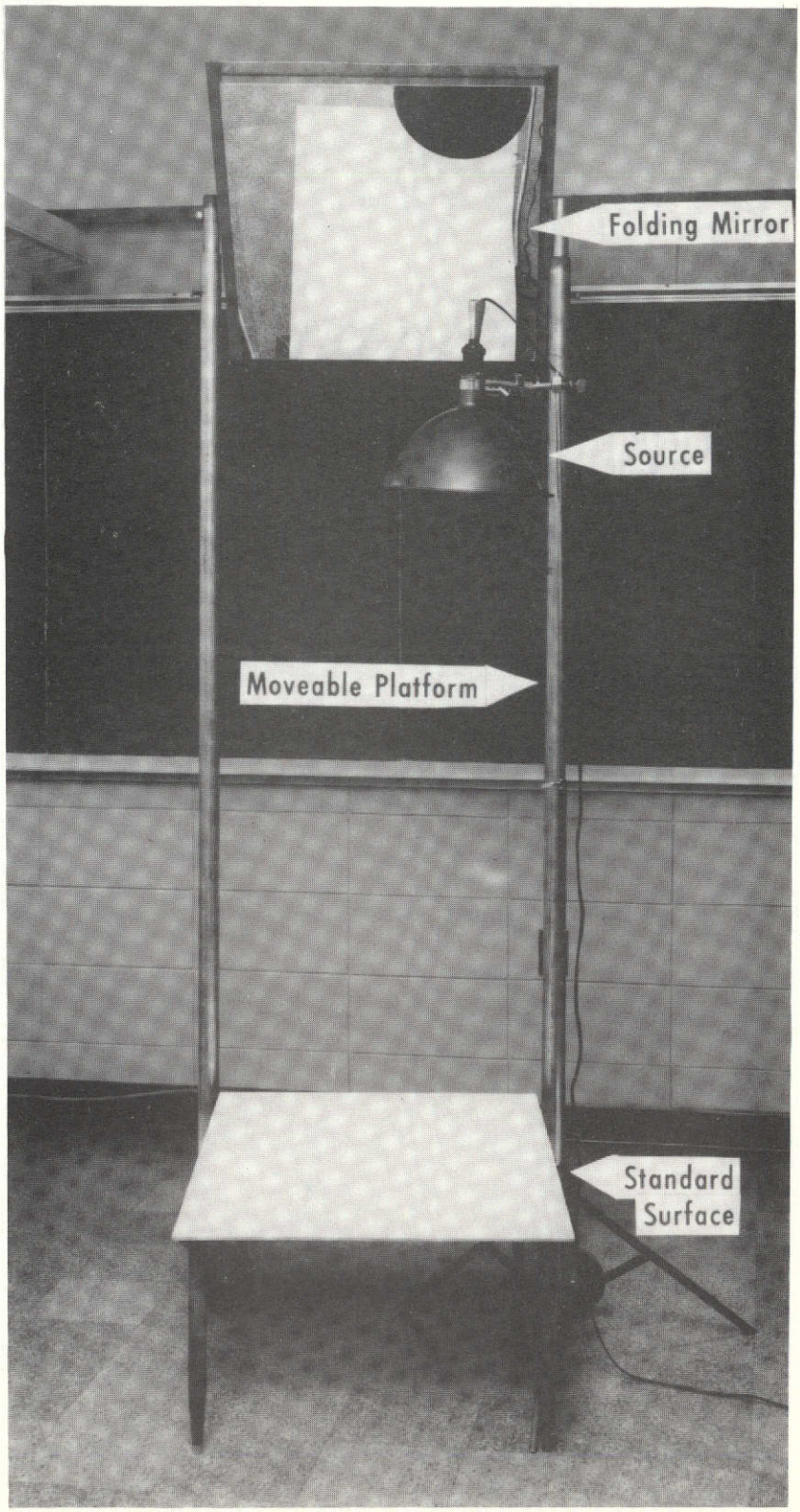

FIGURE VI-3. Photograph of Moveable Platform

in available energy from the source and the small bandwidth of energy passed by the spectroradiometer at wavelengths less than 0.35 microns.

A standard surface used as a comparison to the readings made from the test surfaces was made by painting a 2 feet by 3 feet piece of quarter inch aluminum plate with Nextel Velvet Coating 101-A10 white paint manufactured by the 3M Company. The paint used to make the standard surface was quoted by the manufacturer as having reflectance properties approaching those of a perfectly diffuse surface in the visible region.

The source used in the experiments was a 500 watt photolamp with a temperature rating of 3200 degrees Kelvin. The bulb was made by Sylvania under the brand name Photo-ECT. The bulb was placed in a standard photographers reflector made especially for this type of bulb. The reflector and bulb was mounted on a tripod as seen in Figure VI-3.

Experimental Procedures

Two different procedures were used for taking data; however, the setup used for all the laboratory tests was as shown in Figure VI-2. For the first 32 test runs a plot of Saint Augustine grass was used as the test surface. For these runs the source was set up at the angle desired and readings were first made from the standard surface through the wavelength range of the detector used in the radiometer. The standard surface was then removed and the test surface was put in its place. Readings were then taken from the test surface at the same wavelengths and under the same conditions and ratioed with the

readings taken earlier from the standard surface to give the relative bidirectional reflectance. The source was then put at another angle, the test surface removed and replaced with the standard surface and the procedure repeated.

When these data were first cross-plotted to give the changes in reflectance with source angle, scatter was noted in the data, particularly in the infrared region. Because of this, tests were made to determine more exactly the diffuse characteristics of the standard surface. The results of these tests are given in Appendix D. Another factor which contributed to the scatter was that the test surface of grass was removed and replaced again for each test run made at a different angle. Therefore, the exact same spot of grass was not necessarily being viewed for each test run made. Subsequent analysis of the data showed that this factor did not contribute greatly to the scatter in the visible region.

In order to eliminate any sources of error which might be introduced by the factors mentioned above, a second procedure was adopted. First, to obtain the bidirectional reflectance of grass and soil samples, the test sample was placed in the radiometer field of view and the light source was placed at $\zeta = 0^{\circ}$. The radiometer viewing angle (θ) was 15 degrees. The test surface was then removed and the standard surface was placed at the same distance from the lamp source as the test sample had been. Readings were then made at selected wavelengths with the spectroradiometer of the energy being reflected from the standard surface. The standard surface was then removed and replaced with the test surface. Readings at the same

wavelengths were then taken from the test surface. The readings from the test surface were divided by the readings from the standard surface to give the relative bidirectional reflectance.

After a complete wavelength scan had been made in the range of a detector to determine the relative bidirectional reflectance of the test surface at $\zeta = 0^{o}$, data was obtained to find the variations in the bidirectional reflectance of the test surface with source angle. The test surface was left exactly as positioned to obtain the data at $\zeta = 0^{o}$. The exact center of the spot being viewed with the spectroradiometer was then found. A small marker was then placed at this point. The light source was carefully placed with exactly 49 inches between the center of the area viewed and the light source. Readings were then made at selected wavelengths of the energy being reflected from the test surface with the source placed at different angles. The test surface was not moved while these test runs were made. These readings were then compared to readings that would have been obtained if the test surface were perfectly diffuse. The readings obtained with the source at $\zeta = 0^{o}$ was taken as the standard and the percent differences between the readings at the other source angles and those of a diffuse surface based on the standard were obtained (see Appendix E). These data indicate the variation in the bidirectional reflectance of the test samples with source angle.

All the laboratory and field tests were conducted with a viewing angle (θ) of 15 degrees. The relative azimuth angle (Ψ) between the radiometer and the source planes was kept at 0 or 180 degrees for all the laboratory tests. It would have been preferable to have also taken data with a viewing angle of zero degrees; however, with the

technique used this was impossible since the geometric requirements would dictate that the folding mirror be much higher than the radiometer. The folding mirror height in the laboratory was limited by the height of the ceiling so that even with the radiometer on the floor the folding mirror does not completely fill the radiometer field of view if it is adjusted to give a viewing angle of zero degrees to the test surface.

Mirror Tests

One of the key items in the development and usefulness of the techniques used in these experiments is a folding mirror which is lightweight, and a first surface reflector and which can be obtained inexpensively in large sizes. The folding mirrors used were described earlier and are available in sizes up to 4 feet by 8 feet; however, they were not originally developed or designed for scientific purposes. Therefore, several tests were made to determine if this type of mirror could be used for the purposes outlined.

In order to test the folding mirrors, the system was set up as shown in Figure VI-2. Readings from the standard surface were then recorded on the strip chart recorder while the folding mirror was rotated and moved back and forth so that the energy read was reflected from different areas of the mirror. No change was recorded in the intensity of the energy measured during these tests. The tests were conducted with the energy being recorded in the visible green region.

A second series of tests were conducted to see if winds blowing on the mirror would affect the energy readings. These tests were conducted as before except that the mirror was fixed and a fan and a

large piece of cardboard was used to simulate large gusty winds blowing across the mirror. Using this technique the mirror surface could be seen visually to move and vibrate slightly, but as in the other tests there was no effect on the intensity of the energy received by the radiometer.

Standard Surface Tests

When the first test runs were analyzed, it was found that the data for the angular variations were scattered except in the visible region. It was theorized that this was caused by one or a combination of several factors. One of these factors was that the results were affected by variations in the diffuseness of the standard surface with various source angles. For this reason a series of tests were conducted to determine if the standard surfaces showed such characteristics.

The procedure used to test the standard surface was to set up the spectroradiometer, folding mirror and standard surface as shown in Figure VI-2. The area viewed on the standard surface was then found precisely and the center marked with a small x. The source was then placed exactly at a distance of 49 inches from the x to the lamp bulb at various source angles. A distance of 49 inches was used to keep from saturating the photomultiplier detector with too much energy and still be close enough to the surface to not interfer with the line of sight between the spectroradiometer, the folding mirror, and the standard surface. The reflected energy was recorded at selected wavelengths at each source angle. The results of these tests are given in Appendix D. Each run was repeated at least twice. A 500 watt

photolamp was used at wavelengths (λ) of 0.35, 0.40, 0.75, 0.85, 1.00, 1.25, 1.50, 1.75, 2.00, 2.25 and 2.50 microns. A 150 watt bulb in a reflector was used at λ = 0.40, 0.60 and 0.65 microns. A 150 watt bulb without a reflector or shield of any kind was used at λ = 0.40, 0.45, 0.50 and 0.55 microns. Two completely separate sets of data each taken twice was obtained at λ = 0.40 using different sources. The photomultiplier tube detector was used for λ = 0.35 to λ = 0.65 microns. The lead sulfide detector was used from λ = 0.75 to λ = 2.50 microns.

In order to determine if the energy was being reflected diffusely at all source angles, it was necessary to calculate the changes in the energy impinging on the standard surface at each source angle. This analysis is shown in Appendix D. If the surface were perfectly diffuse, the changes in the reflected energy from the standard surface would be proportional to the changes in the incoming energy. In Appendix D, Figures D-5 through D-20 are plotted to show the actual energy received by the radiometer with a viewing angle of 15 degrees and the expected energy if the standard surface were perfectly diffuse.

These tests showed that the standard surface was not diffuse in the infrared region and at λ = 0.40 microns. Also the actual intensity curve did not exactly follow the predicted curve for a perfectly diffuse surface at any wavelength. However, it was noted that for the five curves made in the visible region (Figures D-7 through D-11) the results follow very closely the results that would be expected from a diffuse surface. This tends to substantiate the diffuseness claim made by the manufacturer of the paint if only the visible region is considered.

Another conclusion made from these tests was that since the data was generally consistent and repeatable that the technique of positioning the lamp as described was a valid experimental procedure. Also since the data in the visible region agreed with the manufacturer's claim made for the paint the analysis used was substantiated. Even though it was shown that the standard surface was not diffuse when considering small bandwidths of energy except in the visible region, the surface was still used as a standard so that comparisons between the reflectances of the various surfaces tested could be made.

Tests of Reflectance of Saint Augustine Grass

Using the equipment and techniques discussed, the reflectance (ratio of energy reflected from test surface to energy reflected from standard surface) and variations of the reflectance with source angle were determined for a plot of St. Augustine grass (Stenotaphrum secumalatum). The grass surface used for a test plot was dug up from a well carpeted lawn. The grass was well watered and very thick. There were no other types of grasses in the plot used except St. Augustine. The plot studied was a plug approximately 18 inches in diameter and 6 inches thick. The grass was cut at a height of 2 inches above the ground surface. The width of individual blades of grass ranged between 1/8 inch and 1/4 inch. The individual grass blades were oriented randomly in direction with some preference for a vertical direction. After the tests when the grass was allowed to grow to a greater height, there was a greater tendence for the individual grass blades to be oriented in a vertical direction.

The base soil or dirt was not visible when looking at the test sample. However, it was possible to see through the grass and see decayed vegetation beneath the green grass blades when looking at an angle of zero degrees to the surface. But when viewing the plot at an angle of 15 degrees (the radiometer viewing angle) only grass blades could be seen. The size of the field of view of the radiometer was approximately 2 inches by 6 inches at the test plot for all the laboratory tests conducted.

Figures VI-4 and VI-5 present the relative bidirectional reflectance data taken for the grass plot with a source angle of zero degrees. The soil moisture content was checked at the beginning and at the end of the runs and found to be 48 percent and 42 percent, respectively. A 500 watt photolamp source was used in the ultraviolet region and a 150 watt bulb was used in the visible region. The data was recorded on the Northrup Speedomax strip chart recorder. The wavelength drive was operated manually. The amplifier gain was adjusted at each point to give a reading close to 10 millivolts at each wavelength from the standard surface for test runs 1, 2 and 9. The data was recorded with the digital voltmeter for runs 33 and 34. The data in the visible region ($\lambda = 0.45$ to $\lambda = 0.65$) is very close to the true bi-directional reflectances which would be obtained with a perfect reference surface. The standard surface has a very low reflectance in the ultraviolet region which caused the reflectance data presented in the ultraviolet region in Figure VI-4 to be high.

The reason for the differences in the reflectance readings made with the photomultiplier tube detector and the lead sulfide detector between $0.65 < \lambda < 0.70$ is because the photomultiplier tube has a

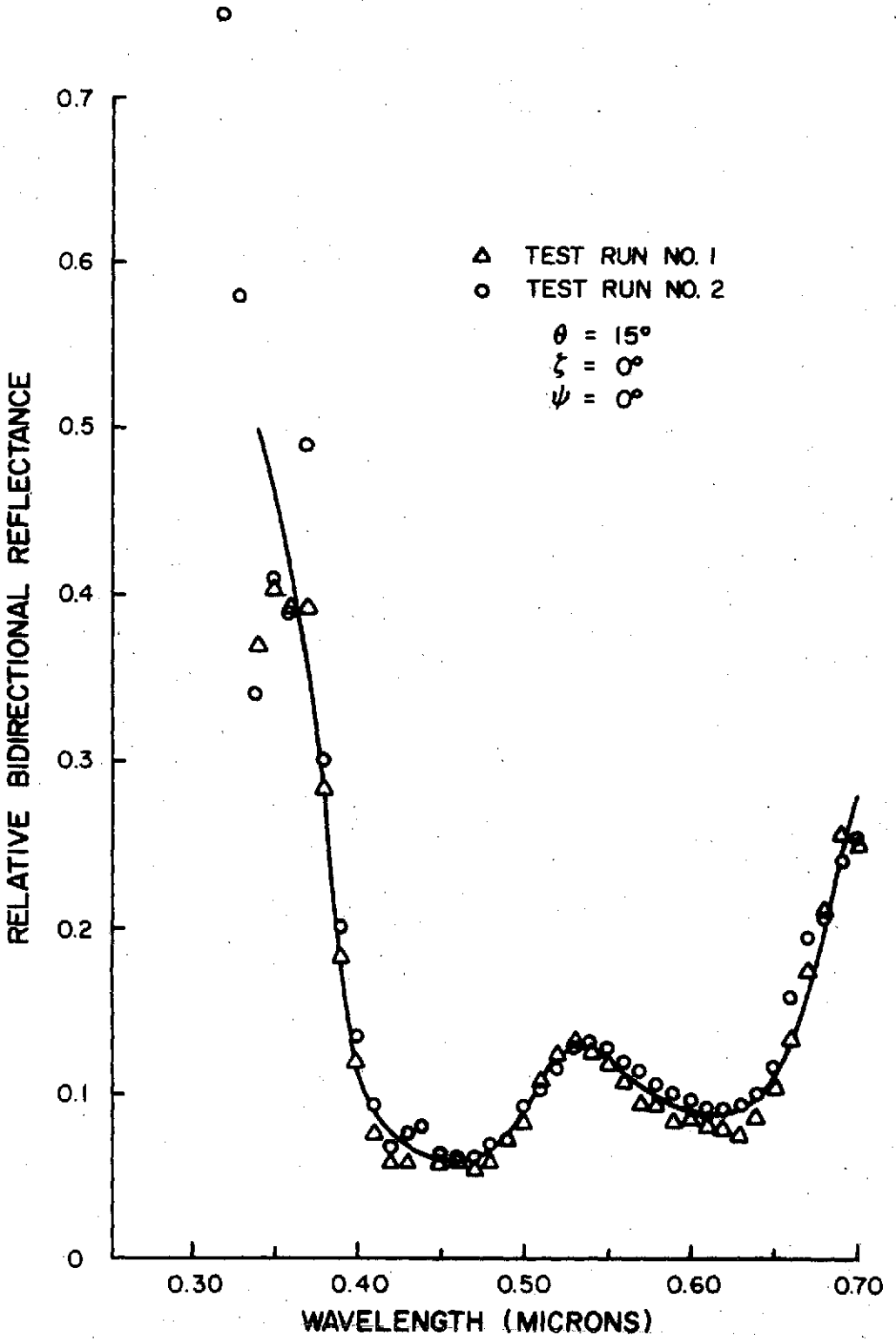

FIGURE VI-4. BIDIRECTIONAL REFLECTANCE OF SAINT AUGUSTINE GRASS IN THE VISIBLE REGION

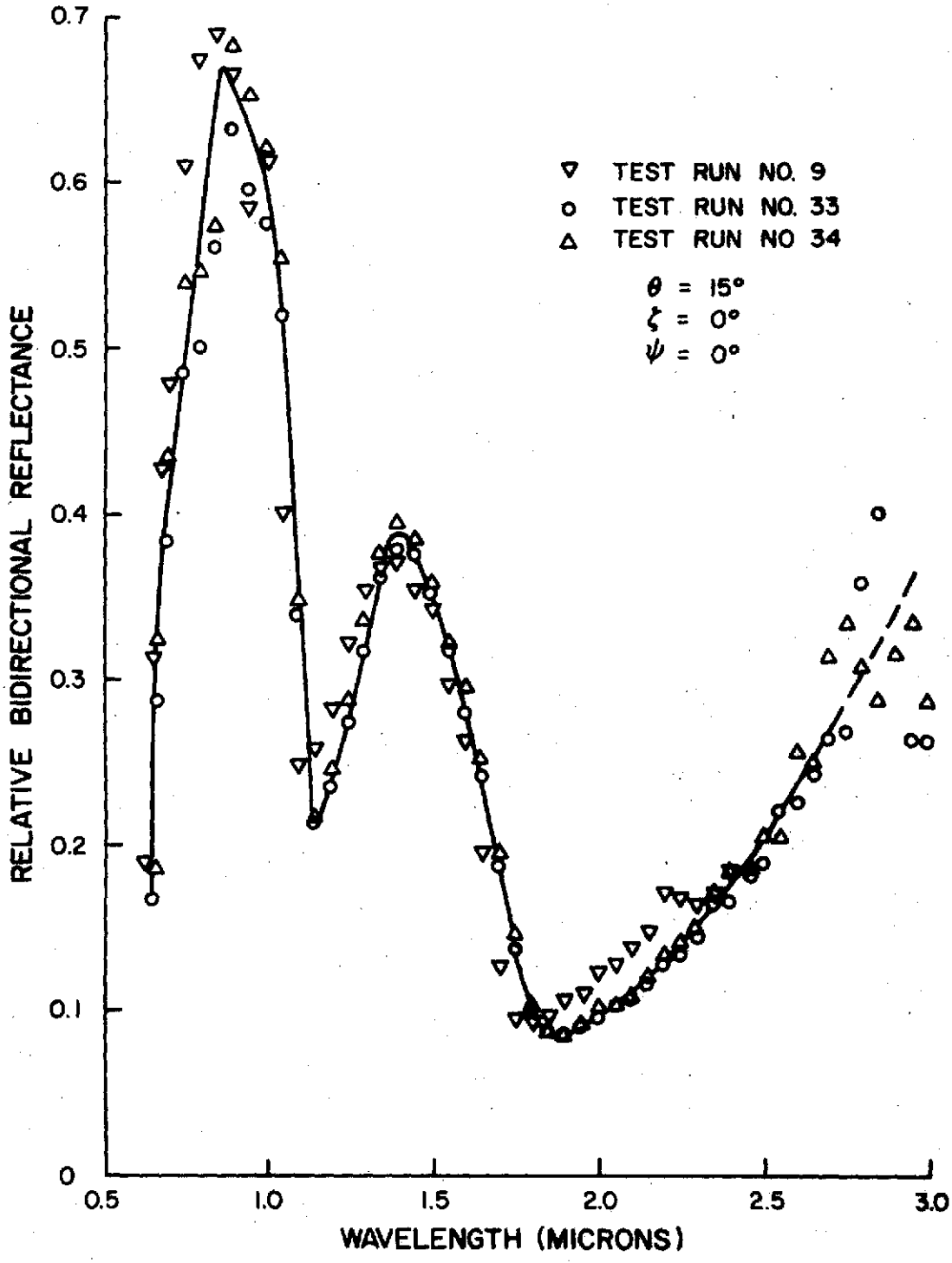

FIGURE VI-5. BIDIRECTIONAL REFLECTANCE
OF SAINT AUGUSTINE GRASS IN THE INFRARED REGION

natural cutoff point near λ = 0.68 microns and is therefore not reading through the entire bandwidth of energy available to the detector in this region. A similar drop off in detectability occurs for the lead sulfide detector at wavelength less than 0.70 microns. Therefore, the real values of reflectance read in this region are higher than those obtained with the photomultiplier tube and lower than those taken with the lead sulfide cell. The solution to getting better data in this region is to use a detector with a S-1 spectral response. This phenomenon occurs only if the reflectance is varying rapidly with wavelength in this region.

As seen from Figure VI-4, the data taken at wavelengths less than 0.35 microns is erratic. This was caused by the low level of energy being received by the detector in this region and therefore the high level of gain required to make any readings at all. The low level of energy received by the detector was caused by the lack of a source which produced energy in the ultraviolet region, the low reflectance of the surfaces used to collect and focus the energy and the narrow bandwidth of energy transmitted by the monochromator in this region (see Table IV-1).

It should be noted that the data from test runs number 33 and 34 shown in Figure VI-5 were made some two weeks after the data plotted as test run number 9. During this time period the plot was watered and recut to give a 2 inch height. The soil moisture content was checked after runs 33 and 34 were made and found to be 48 percent. For all of the test runs shown in Figures VI-4 and VI-5, a different portion of the grass plot was viewed to get the data, yet the data shows good consistency. The data in the infrared region beyond λ = 2.5

microns is erratic due to the low detectability of the lead sulfide cell in this region and the low amount of energy being produced by the source at wavelengths greater than 2.5 microns.

Figures VI-6 through VI-9 show the effects of source zenith angle on the reflectance of grass surfaces when the source and the radiometer are in the same plane. The data and analysis used to calculate these curves is given in Appendix E. A 500 watt photolamp was used as the source for taking the data. The digital voltmeter was used to record the readings which were made manually for runs 33 and 34. Two independent runs were made to get the data at each point and then averaged as detailed in Appendix E.

The results of these tests show that there is considerable variations in the bidirectional reflectance of grass surfaces. Also this variation is not the same in various regions of the electromagnetic spectrum. These variations are due both to the spectral characteristics of an individual grass blade and the structural arrangement of the blades as well as the angular relationships between the source, the test plot and the radiometer. Since the structural arrangement of the blades in the plot is a major factor in the data received, it is not inconceivable that a plot of the same type of grass at a different height and thickness might give somewhat different results.

Reflectance in the ultraviolet region is seen to vary by 50 percent for the source zenith angles studies. This variance decreases somewhat in the visible region and is down to 20 percent in the near infrared. However, Figure VI-9 shows that further out in the infrared the variance again increases. These data tends to indicate that when comparing energy levels in different portions of the spectrum in order to identify plants the solar zenith angle must be considered. The data

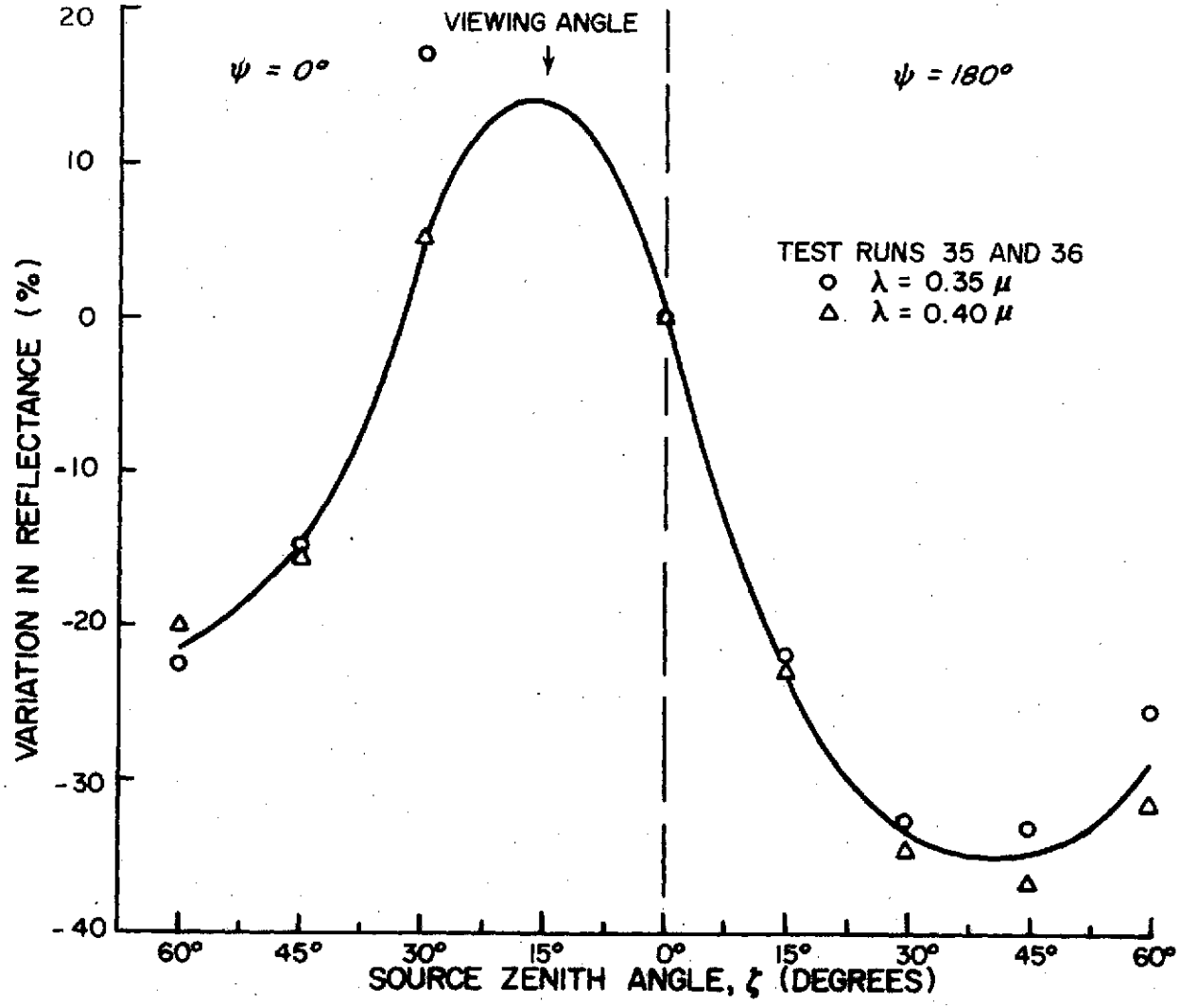

FIGURE VI-6. VARIATION IN REFLECTANCE FROM SAINT AUGUSTINE GRASS AT λ = 0.35 AND 0.40 MICRONS

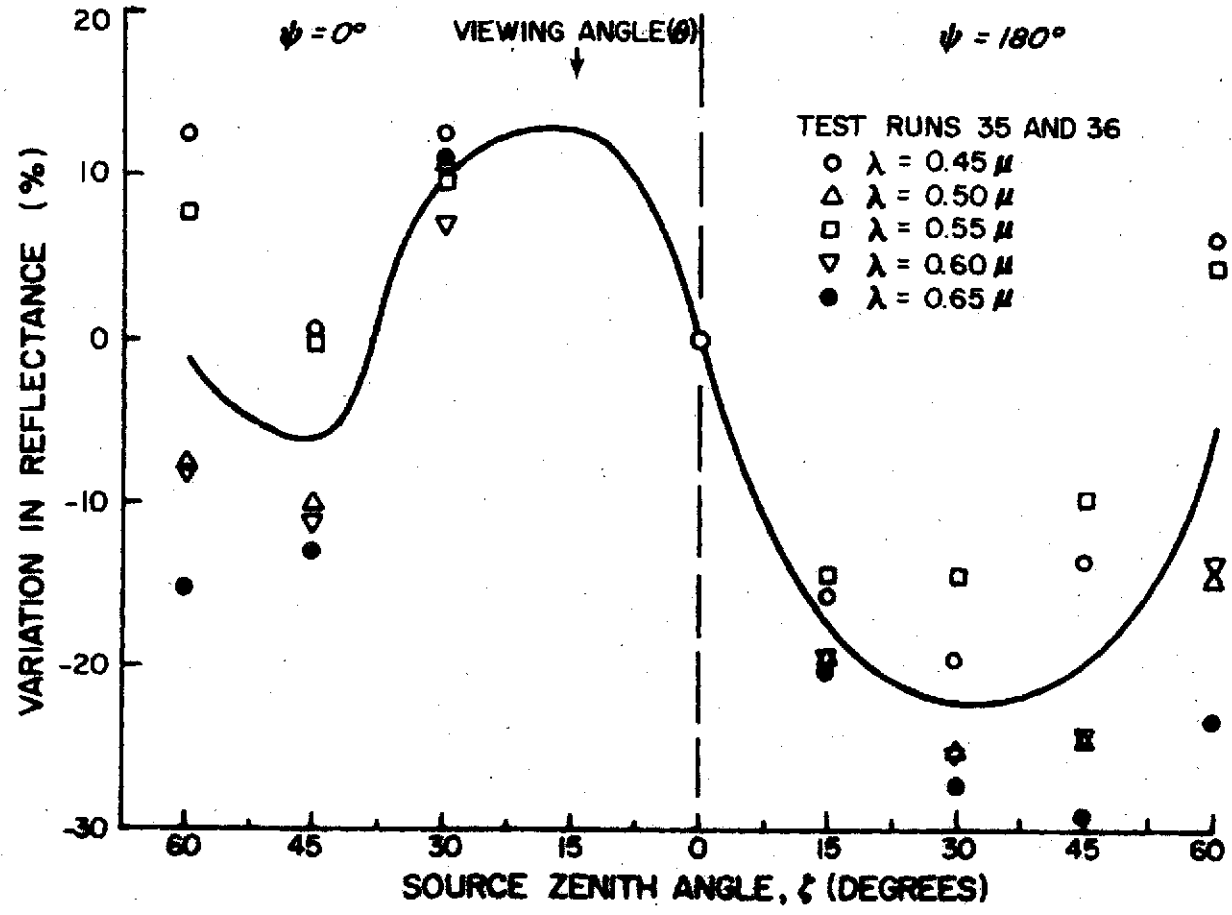

FIGURE VI-7A. VARIATION IN REFLECTANCE FROM SAINT AUGUSTINE GRASS IN THE VISIBLE REGION

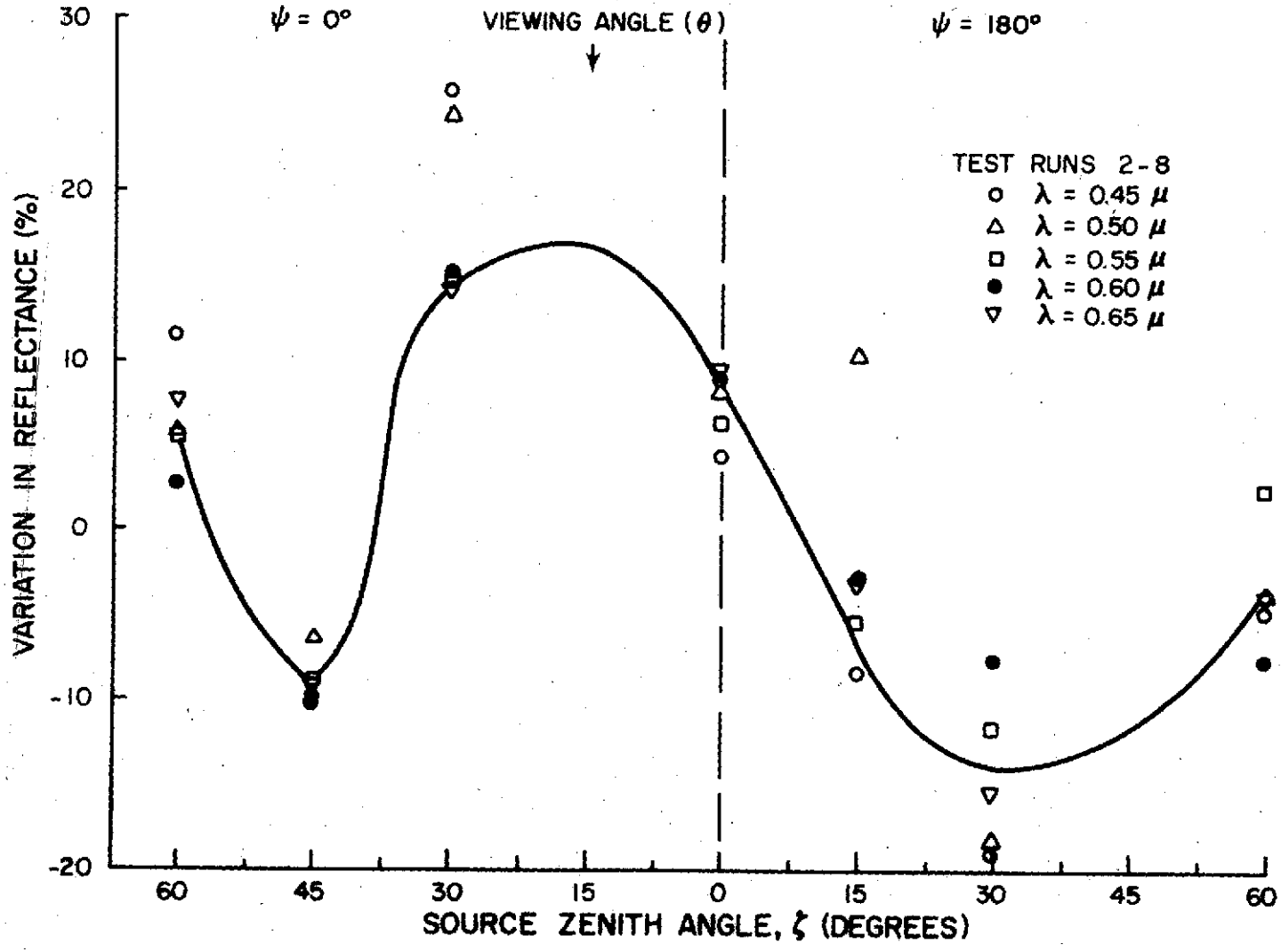

FIGURE VI-7B. VARIATION IN REFLECTANCE FROM SAINT AUGUSTINE GRASS IN THE VISIBLE REGION

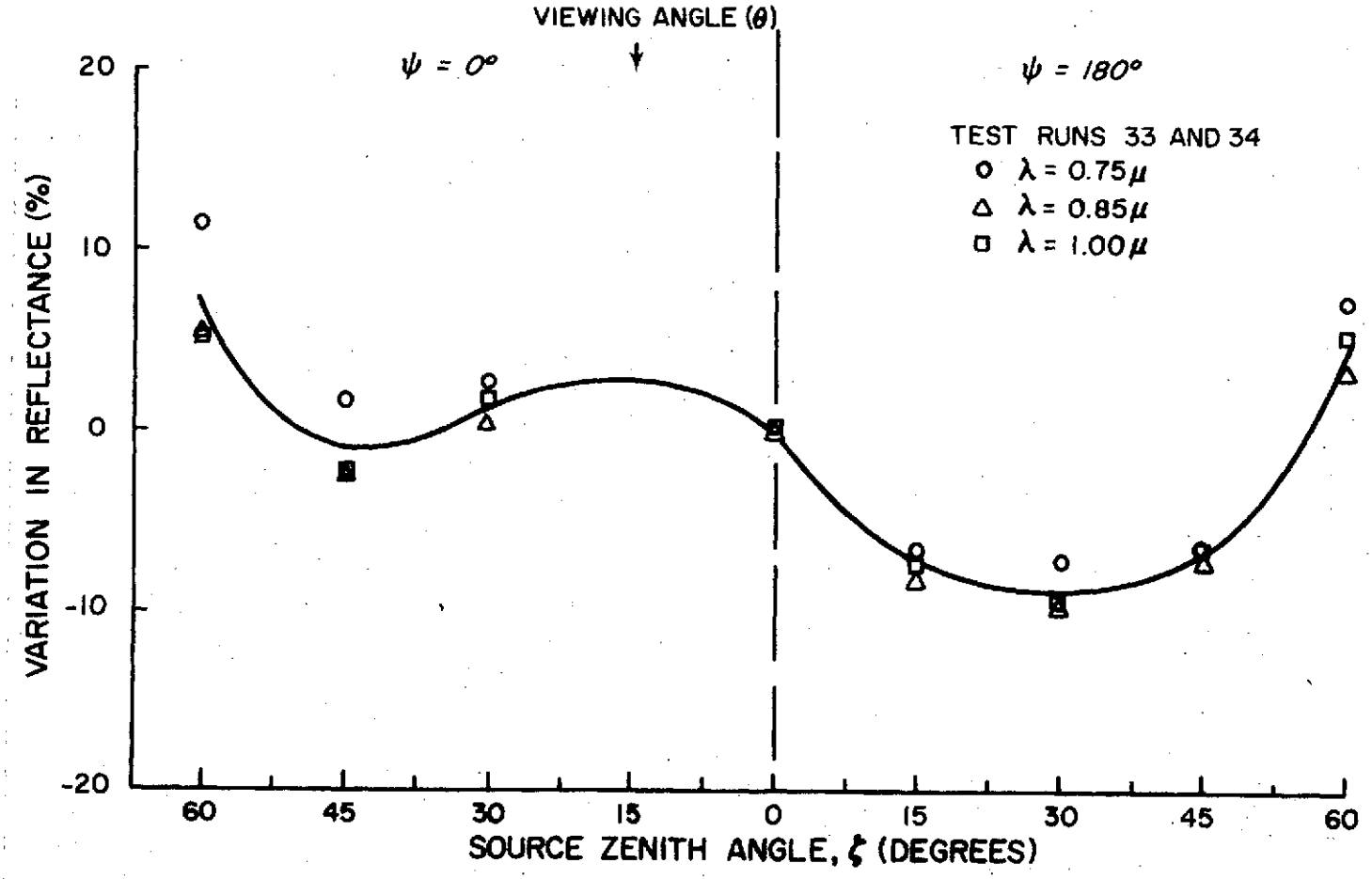

FIGURE VI-8. VARIATION IN REFLECTANCE FROM SAINT AUGUSTINE GRASS AT λ = 0.75, 0.85, AND 1.00 MICRONS

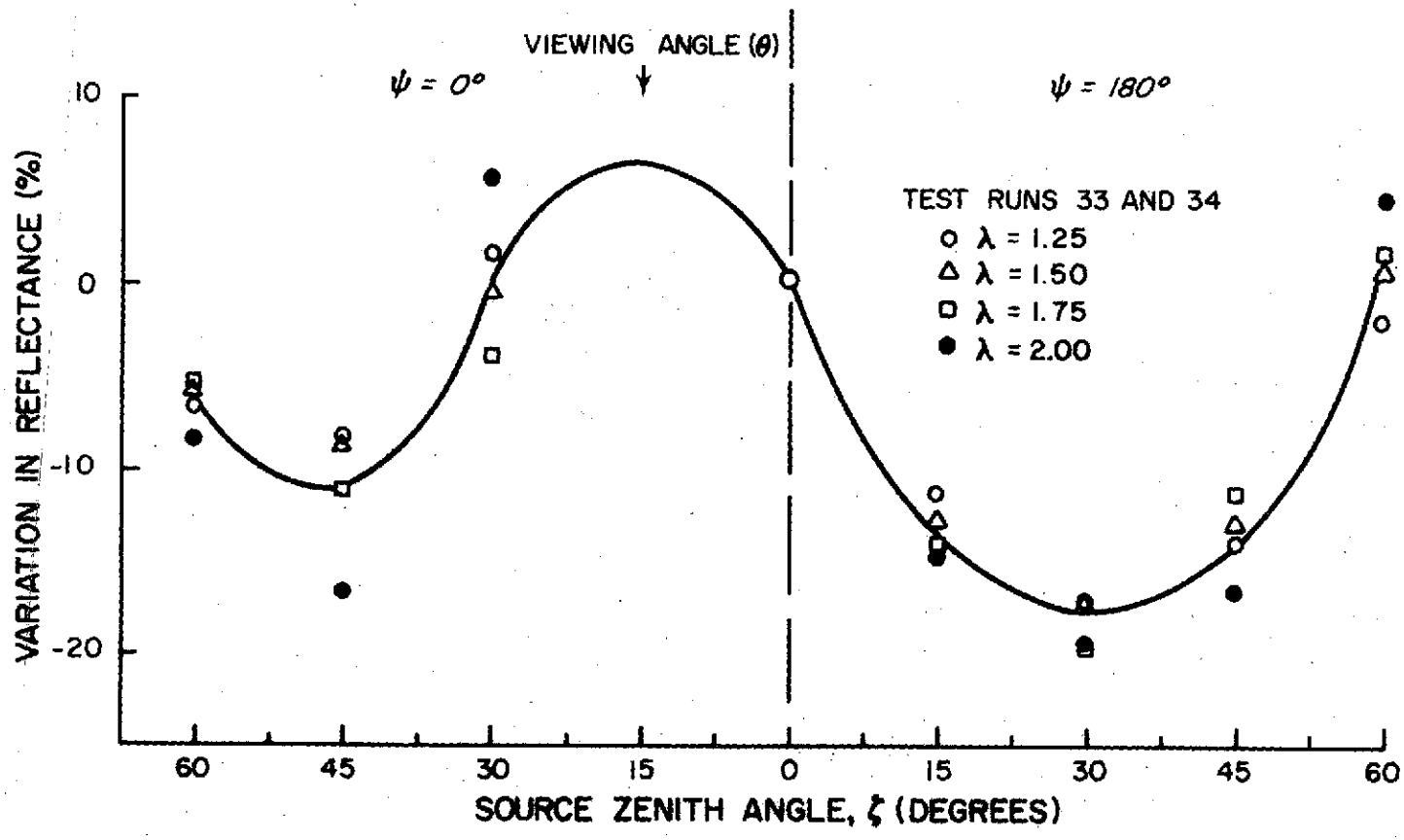

FIGURE VI-9. VARIATION IN REFLECTANCE FROM SAINT AUGUSTINE GRASS FROM λ = 1.25 TO 2.00 MICRONS

as shown is valid only for a viewing angle (θ) of 15 degrees. Since a viewing angle of zero degrees was unobtainable in the laboratory tests with the technique used, it could not be determined if these same variances still exist at viewing angles closer to zero degrees.

Figure VI-7A and VI-7B presents data in the visible region on the variation of reflectance with source angle as obtained using both procedures described earlier. The basic difference in the methods used to take these data is that the data presented in Figure VI-7A is based on looking at the same surface for each source angle and the data presented in Figure VI-7B is based on data taken two weeks earlier in which the grass surface was replaced for each source angle so that exactly the same surface was not viewed at each source angle. Also any lack of diffuseness as shown in Figures D-7 through D-11 had an effect on the data in Figure VI-7B. However, even with these differences the curves in the two figures are very similar and show exactly the same trends. As a result of these two figures it appears that the 2 inch by 6 inch area viewed in the laboratory was large enough so that randomness and integration of the individual grass blades could be assumed within this size area of St. Augustine grass. This data also shows the repeatability of the data even after the grass surface had been watered, grown and cut several times.

Tests of Reflectance of Soil

Reflectance data and data on variations of reflectance with source angle was also taken from a pan filled with black soil. The soil was taken from the floodplain of the Mississippi River on the campus of Louisiana State University. The soil had been dug up when making a

ditch in which sewer pipe was laid and contained no vegetation. The soil was black alluvium deposited by the Mississippi river. It is very finely grained with a high clay content and is very common to the area along the Mississippi River and in the Mississippi Delta. The soil was placed in a 4 inch deep pan 18 inches in diameter, and the top was leveled with a trowel. Since this process left a slick sheen, the soil surface was then heavily washed with water. This left the surface level but without the sheen. The surface was pitted during the washing process and looked very natural. After making the readings, the surface soil was scrapped off and placed in a container to determine the moisture content which was found to be 33 percent.

The equipment setup and procedure used to take the data was the same as that used for the latter test runs made on the grass surface. The viewing angle was 15 degrees and the size of the soil area from which reflectance readings were received was approximately 2 inches by 6 inches.

Figure VI-10 presents the data taken which shows the relative bidirectional reflectance of the soil sample in the visible and ultraviolet regions. The data in the region from $\lambda = 0.45$ microns to $\lambda = 0.60$ microns is not very accurate since the phototube detector was being saturated in this region when readings from the standard surface were taken. However, a number of conclusions can still be made. First the data in the ultraviolet region shows that more energy was reflected from the soil in this region than from the grass surface and that for part of the ultraviolet spectrum more energy was reflected from the soil than from the standard surface. It also appears that even though the soil appears black to the human eye it actually

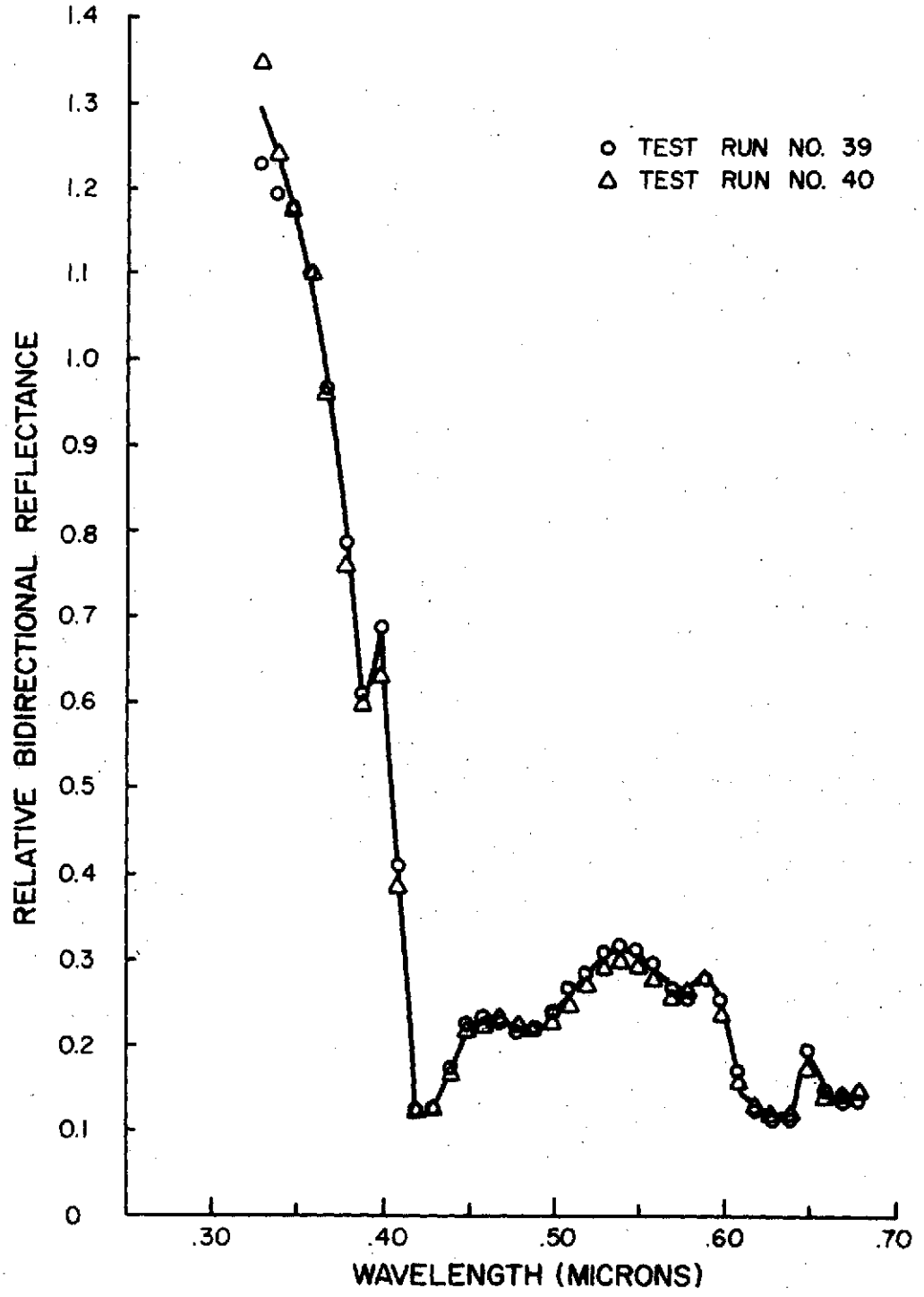

FIGURE VI-10. RELATIVE BIDIRECTIONAL REFLECTANCE OF BLACK ALLUVIUM SOIL IN VISIBLE REGION

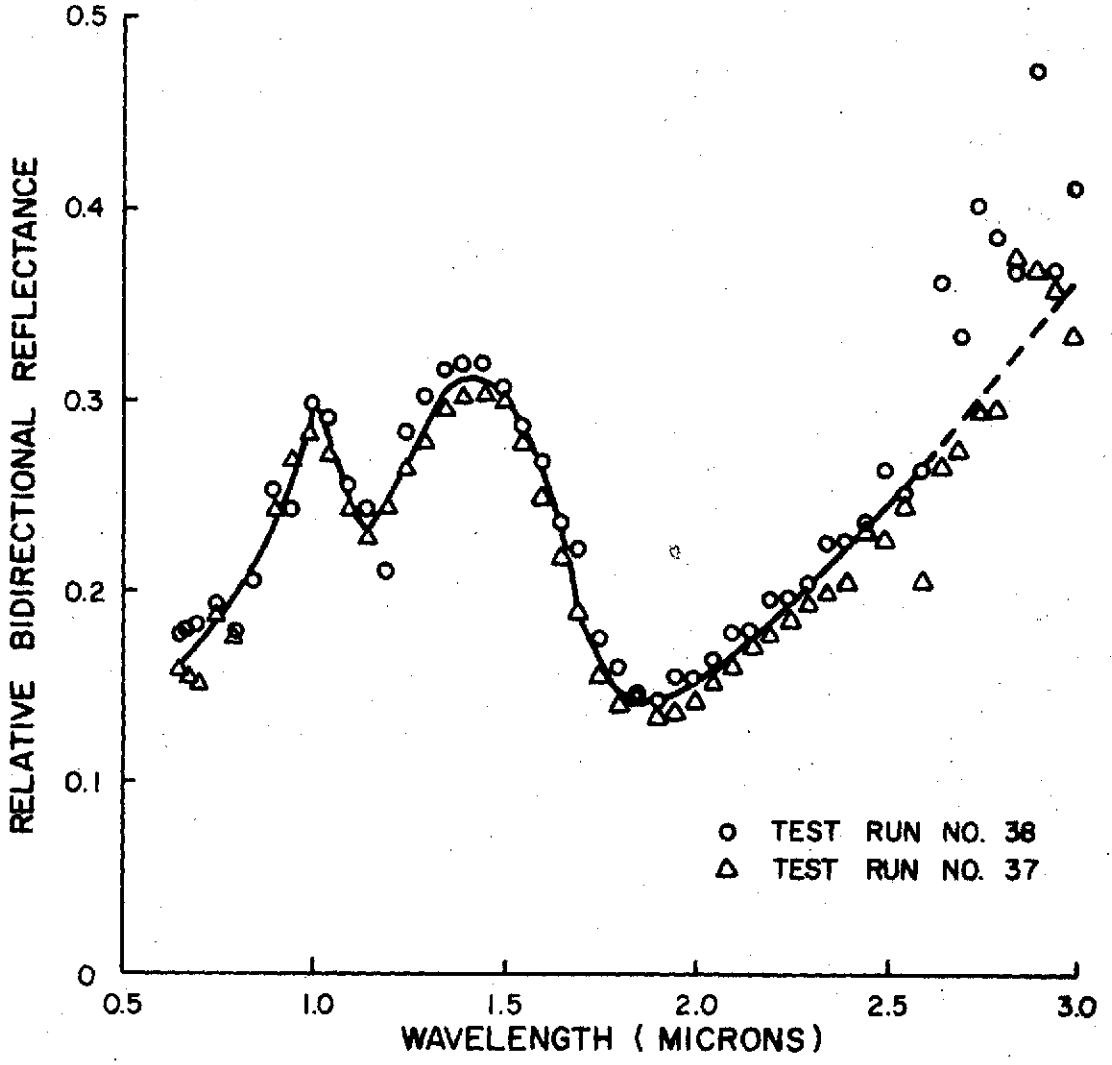

FIGURE VI-11. RELATIVE BIDIRECTIONAL REFLECTANCE OF BLACK ALLUVIUM SOIL IN INFRARED REGION

reflected more energy in the visible region than the grass surface. This is explained by the structure of the grass surface which tends to reflect the energy between several different individual grass blades so that a large portion of the incoming energy is absorbed before the energy is finally reflected back out from the surface. At wavelengths greater than 0.64 microns the energy reflected by the grass surface is greater than that reflected from the soil surface. This is seen by comparing Figure VI-11 and Figure VI-5.

Figures VI-12 through VI-16 show the effects of source zenith angle on the reflectance of a soil surface when the source and the radiometer are in the same plane. The data used to generate these curves is presented in Appendix E. The procedure used to generate the curves is also presented in Appendix E and is the same as that used for the grass surface. A 500 watt photolamp was used as the source, and the readings were recorded from the digital voltmeter of the spectroradiometer. Two separate runs were made so that, data was taken twice for each point, averaged and then used to obtain the data shown in the figures.

These data show that like the grass surface, the variation in the reflectance of the soil with source zenith angles is very dependent on the wavelength of the energy being sensed. Also these variations with wavelength show the same general trends as determined for the grass surface. The biggest differences in the variations as found for the grass and soil reflectances is that the curves for the soil surface are much smoother and that the backscatter from the soil surface is very small. That is, the amount of energy reflected in a direction back toward the source is much smaller than the amount of

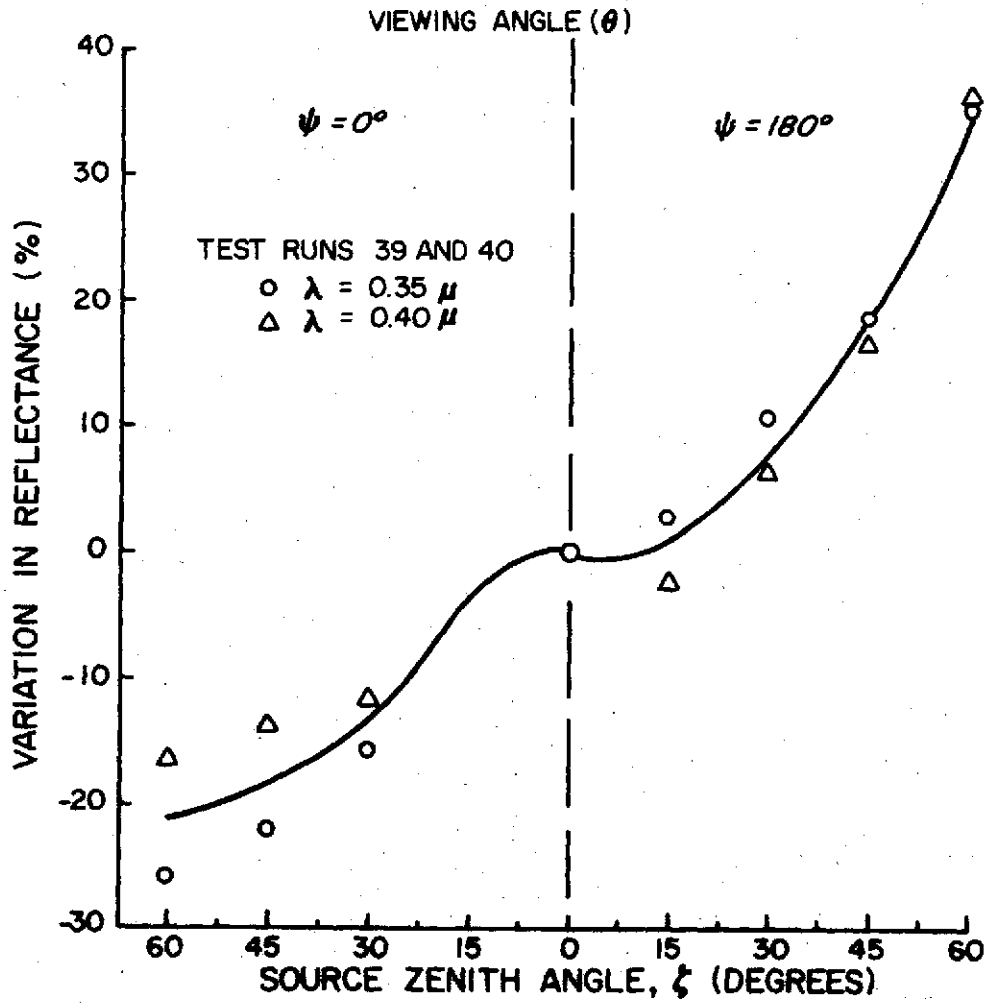

FIGURE VI-12. VARIATION IN REFLECTANCE OF BLACK ALLUVIUM SOIL IN THE ULTRAVIOLET REGION

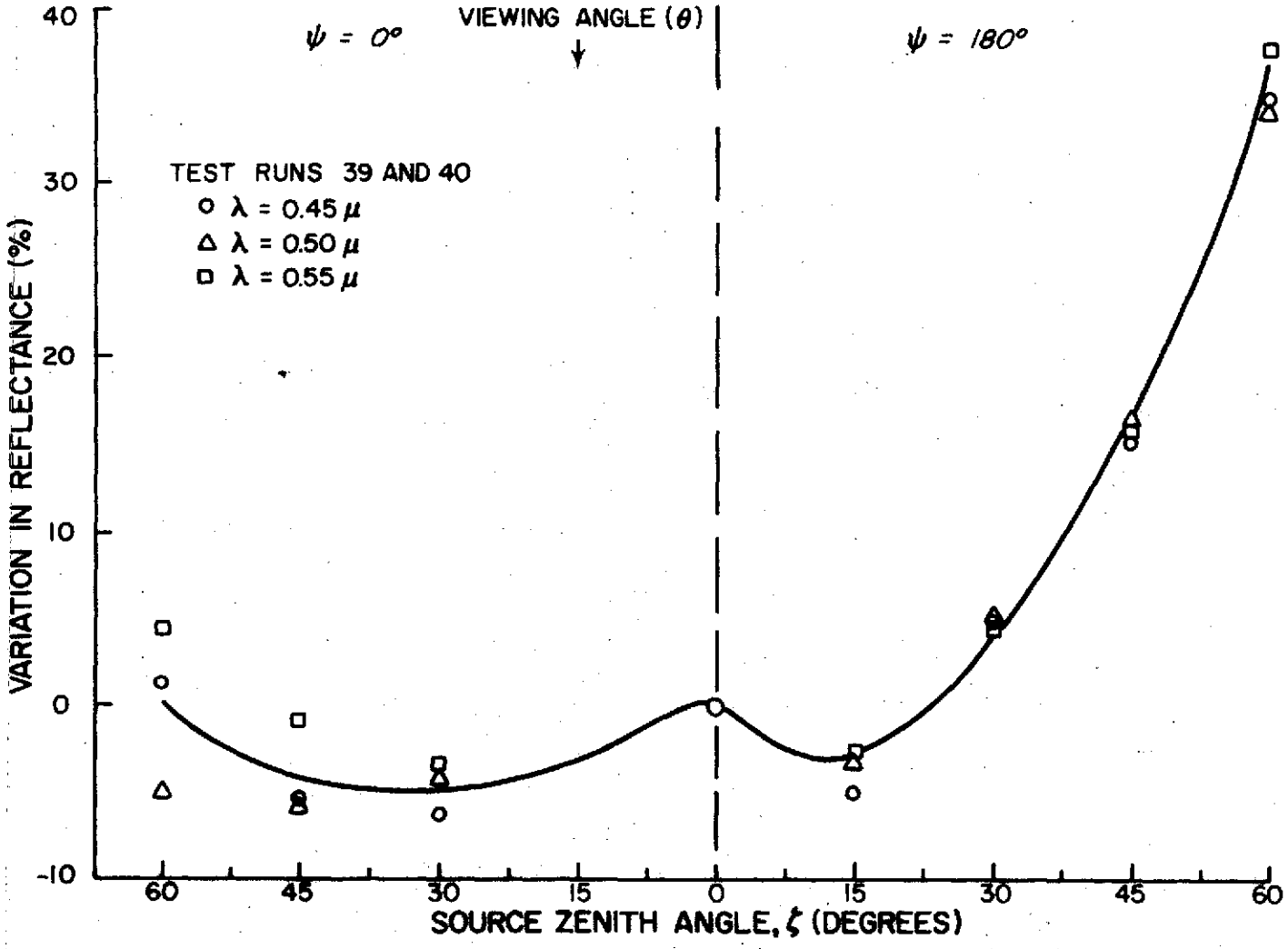

FIGURE VI-13. VARIATION IN REFLECTANCE FROM BLACK ALLUVIUM SOIL FROM λ = 0.45 TO 0.55 MICRONS

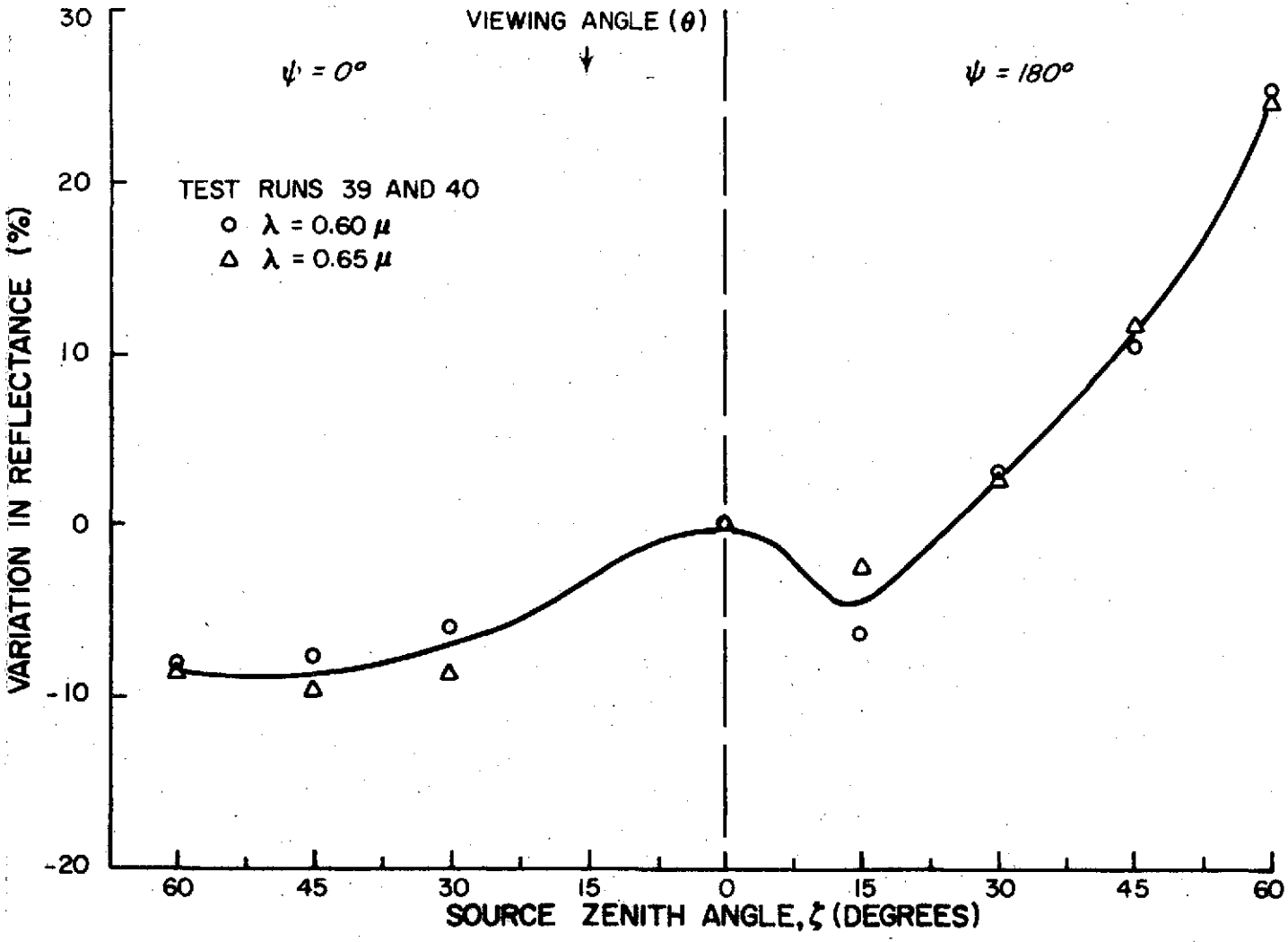

FIGURE VI-14. VARIATION IN REFLECTANCE FROM BLACK ALLUVIUM SOIL FROM λ = 0.60 AND 0.65 MICRONS

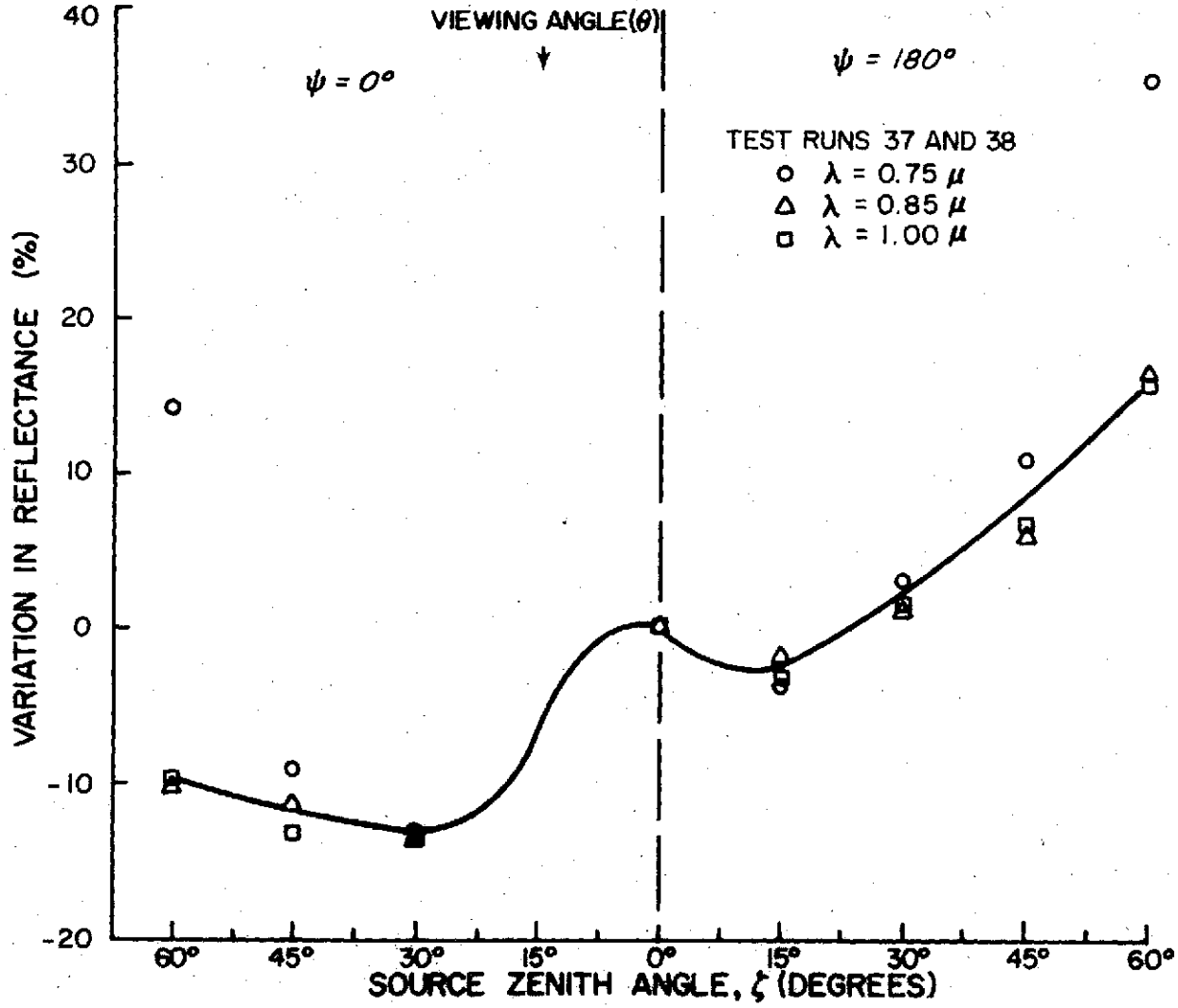

FIGURE VI-15. VARIATION IN REFLECTANCE FROM BLACK ALLUVIUM SOIL IN THE INFRARED REGION

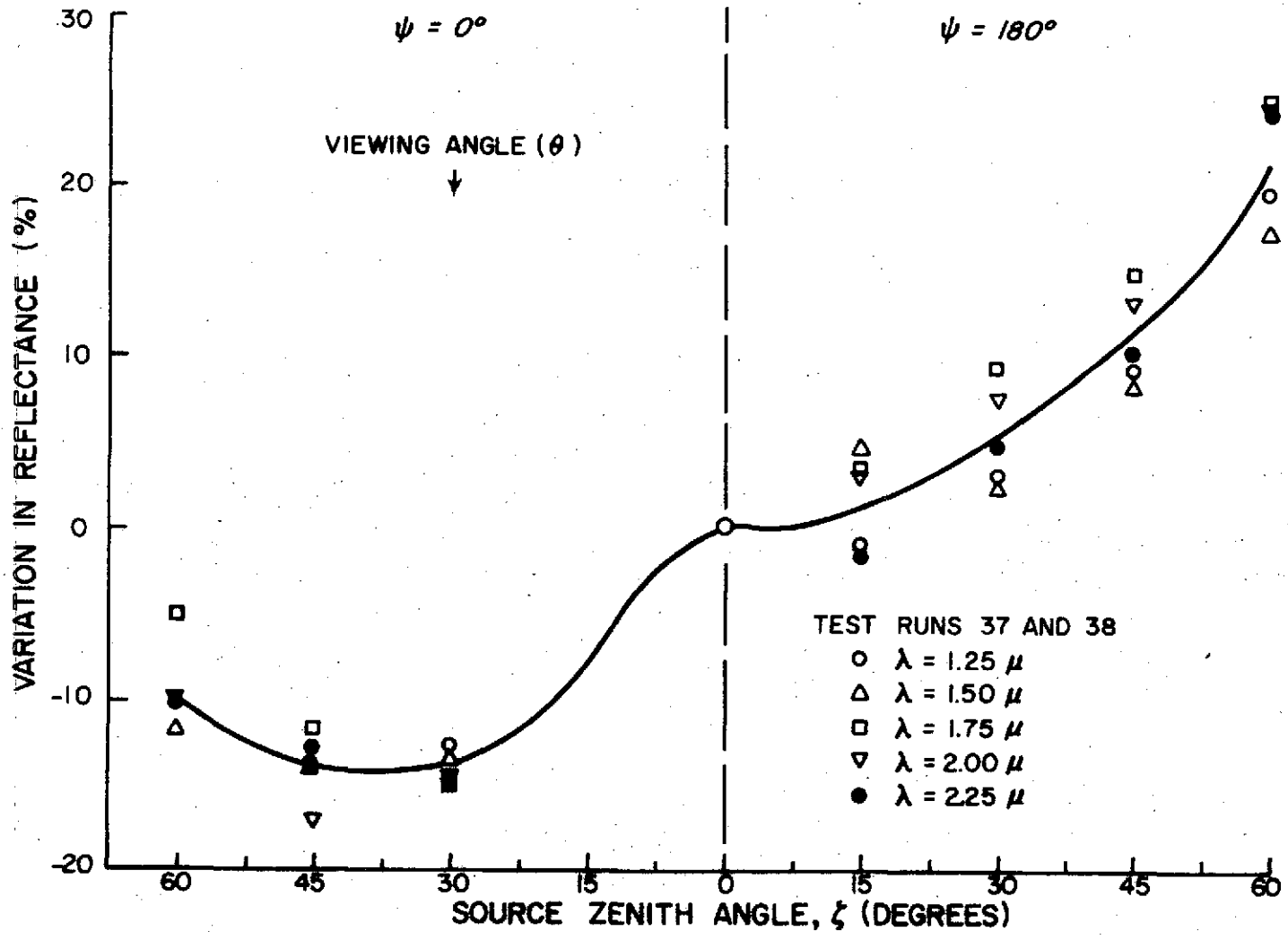

FIGURE VI-16. VARIATION IN REFLECTANCE FROM BLACK ALLUVIUM SOIL IN THE INFRARED REGION FROM λ = 1.25 TO 2.25 MICRONS

energy reflected in a direction away from the source. This effect was not found for the grass surface.

Tests of Reflectance of Bermuda Grass

After the field tests (Chapter VII) were completed, a plot of Bermuda grass (Cynoden dactylon) was taken from the area where the field tests were conducted. Reflectances were then determined for the Bermuda grass plot in the laboratory. These data were plotted to give a comparison to the field tests made on Bermuda grass and to give a comparison to the laboratory data taken from the Saint Augustine grass.

The Bermuda grass plot was dug up from the field, placed in a pan and taken directly to the laboratory for testing. The plot consisted entirely of Bermuda grass and was taken from an area where the grass was very thick. The grass was cut to a height of 2 inches above the ground before the tests were conducted. The surface appeared green and brown to the eye. The tops of the grass was mostly green whereas the underlying grass was brown. Some soil (black Mississippi delta alluvial) was visible although it was mostly covered with decayed vegetation. At least 40 percent of the plot consisted of brown or decayed vegatation. This same feature was present in the test areas from which field data was taken. The leaf structure was small and randomly oriented. The Bermuda grass structure differed from the Saint Augustine grass in that leaves formed from the main vertical structures so that some of the grass leaves had a horizontal orientation. Also the Bermuda was not a deep green like the Saint Augustine grass and was not well watered. The soil moisture

content of the test plot was found to be 26 percent.

Figures VI-17 and VI-18 present the relative bidirectional reflectance of the Bermuda grass plot. The source was normal to the surface for the data shown and the viewing angle was 15 degrees. A 150 watt light bulb was used as the source for the data shown in Figure VI-17, and a 500 watt photolamp was used for the data taken in the infrared region (Figure VI-18). The data was taken with the spectroradiometer and recorded on the Fluke digital voltmeter. Only one set of data was taken from the Bermuda grass in the laboratory.

It can be seen from comparing Figures VI-17 to VI-4 that the bidirectional reflectance for Bermuda and Saint Augustine grasses are almost identical in the visible region. It would therefore be very difficult to distinguish between these two grasses by using these curves only. In the infrared region (Figures VI-18 and VI-5) the reflectance curves for the two grasses are also very similar; however, the reflectance of the Bermuda grass in this region is higher throughout than the reflectance of the Saint Augustine grass plot. Whether this is a general characteristic of the two grasses or of just the two plots studied is not known.

Figures VI-19 through VI-22 show the effects of source zenith angle on the reflectance of the Bermuda grass plot studied in the laboratory. The data and procedure used to calculate the points shown as the curves are given in Appendix E. Only one set of data was taken to obtain these curves. The data at $\zeta = 30^{o}$ and $\Psi = 0^{o}$ were ignored in drawing the curves since the data taken at this point was very high in the visible region and low in the infrared region when compared to the other data. Also there was some difficulty in

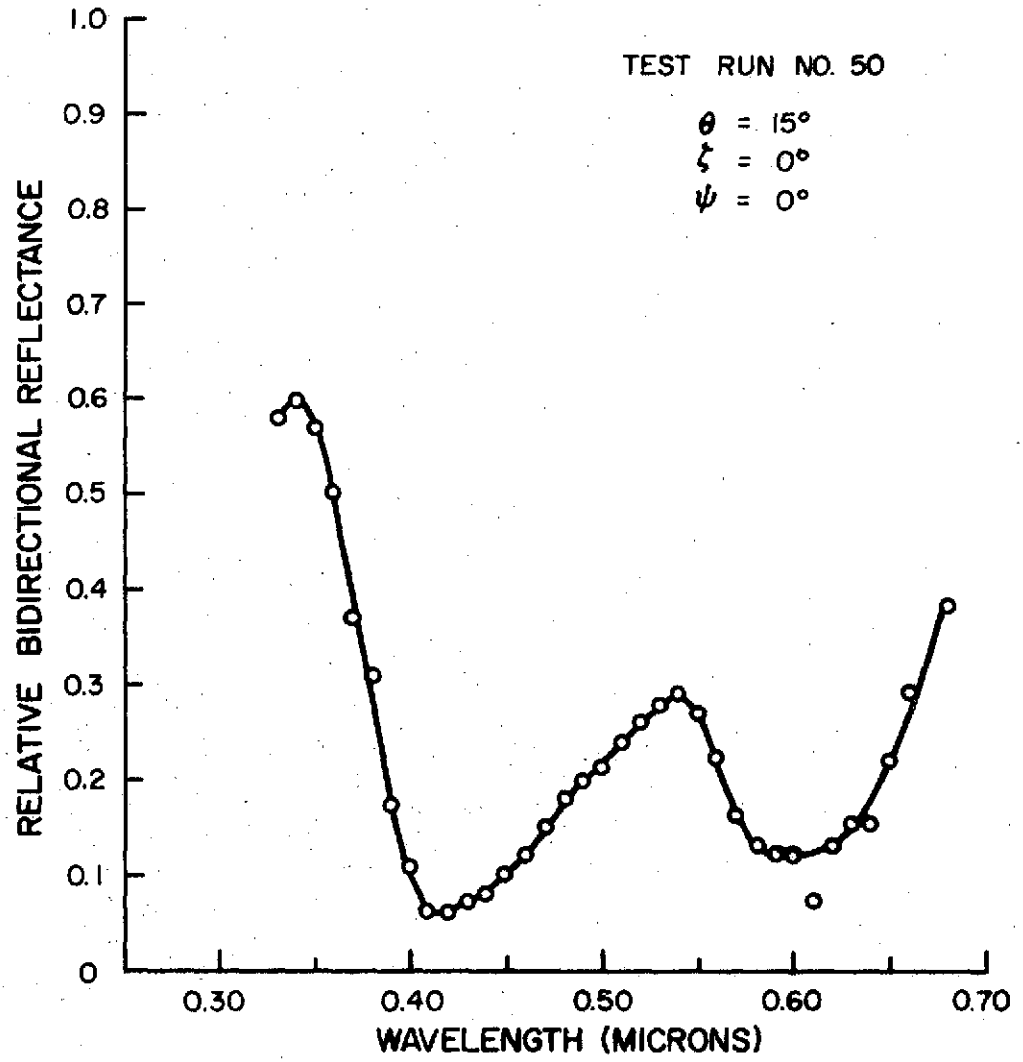

FIGURE VI-17. RELATIVE BIDIRECTIONAL REFLECTANCE OF BERMUDA GRASS IN THE VISIBLE REGION

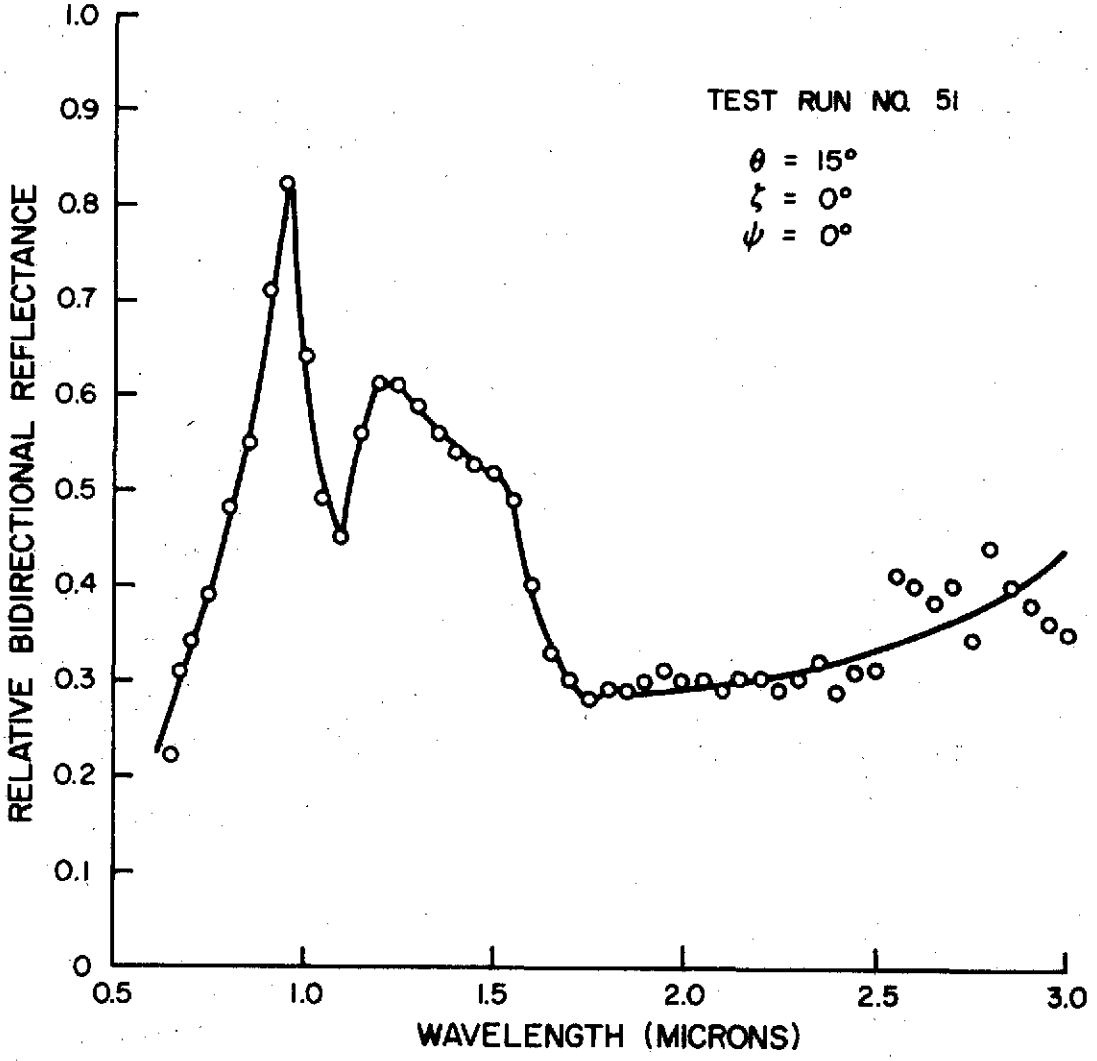

FIGURE VI-18. RELATIVE BIDIRECTIONAL REFLECTANCE OF BERMUDA GRASS IN THE INFRARED REGION

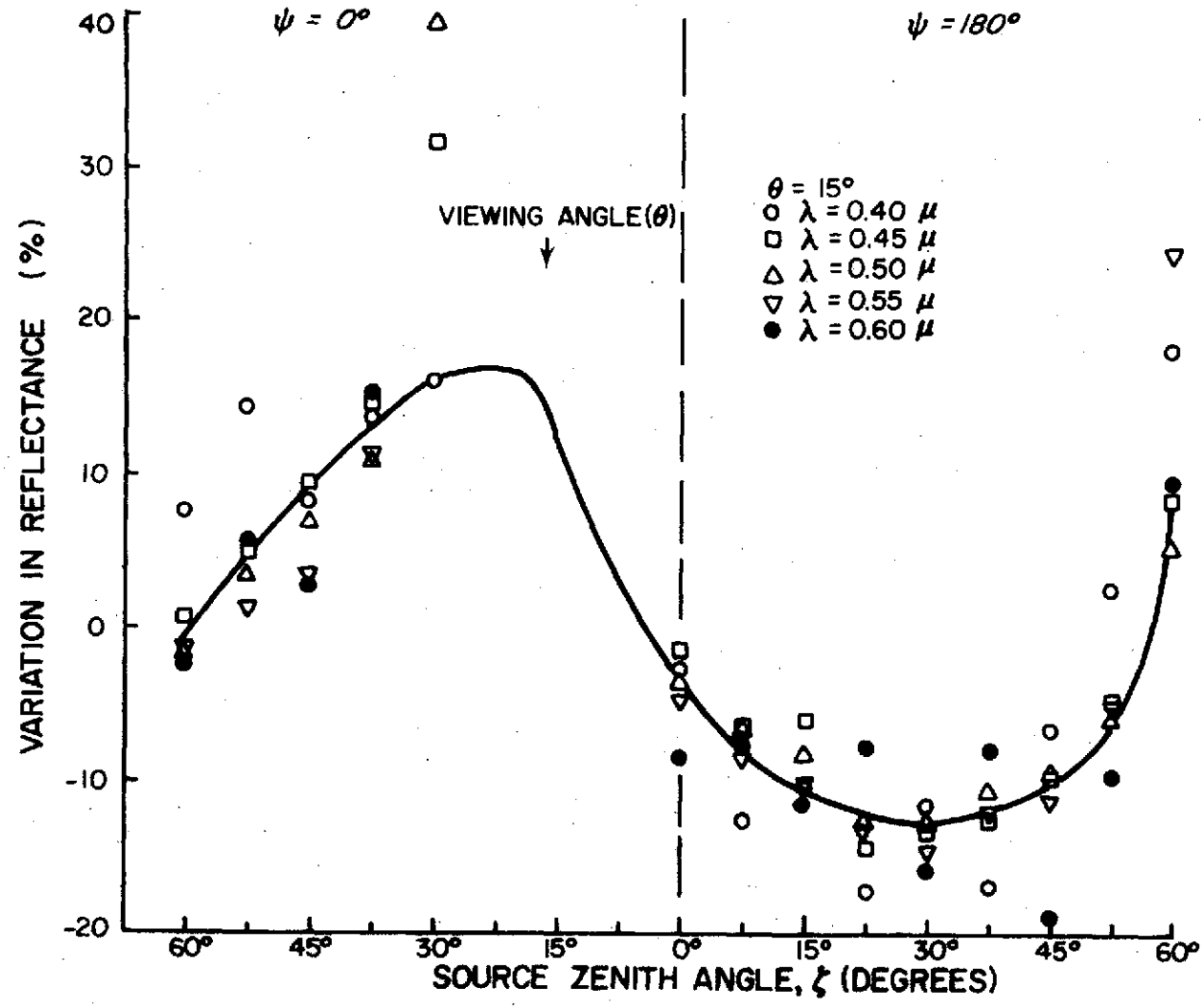

FIGURE VI-19. VARIATION IN REFLECTANCE FROM BERMUDA GRASS IN THE VISIBLE REGION

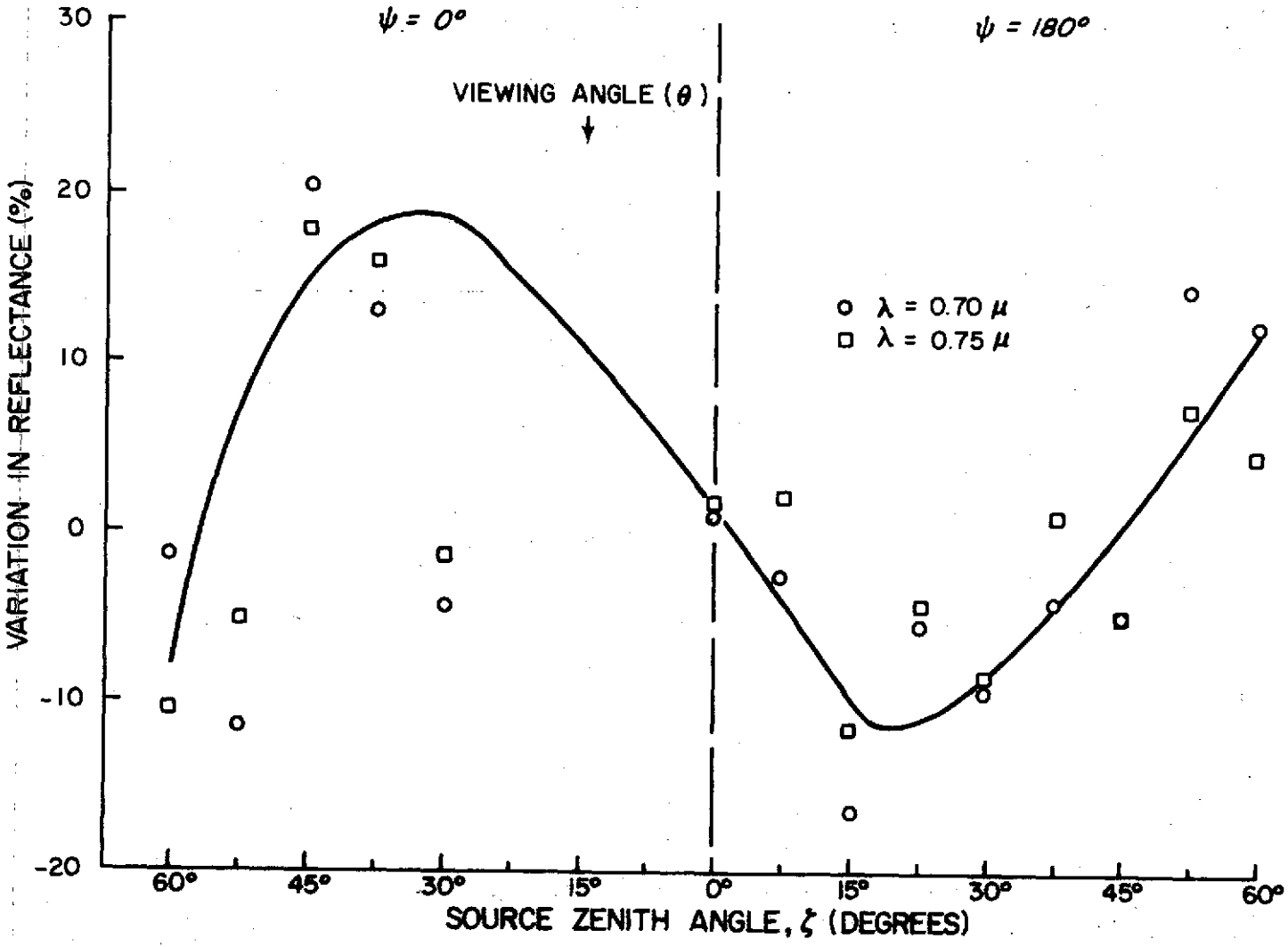

FIGURE VI-20. VARIATION IN REFLECTANCE FROM BERMUDA GRASS AT λ = 0.70 AND 0.75 MICRONS

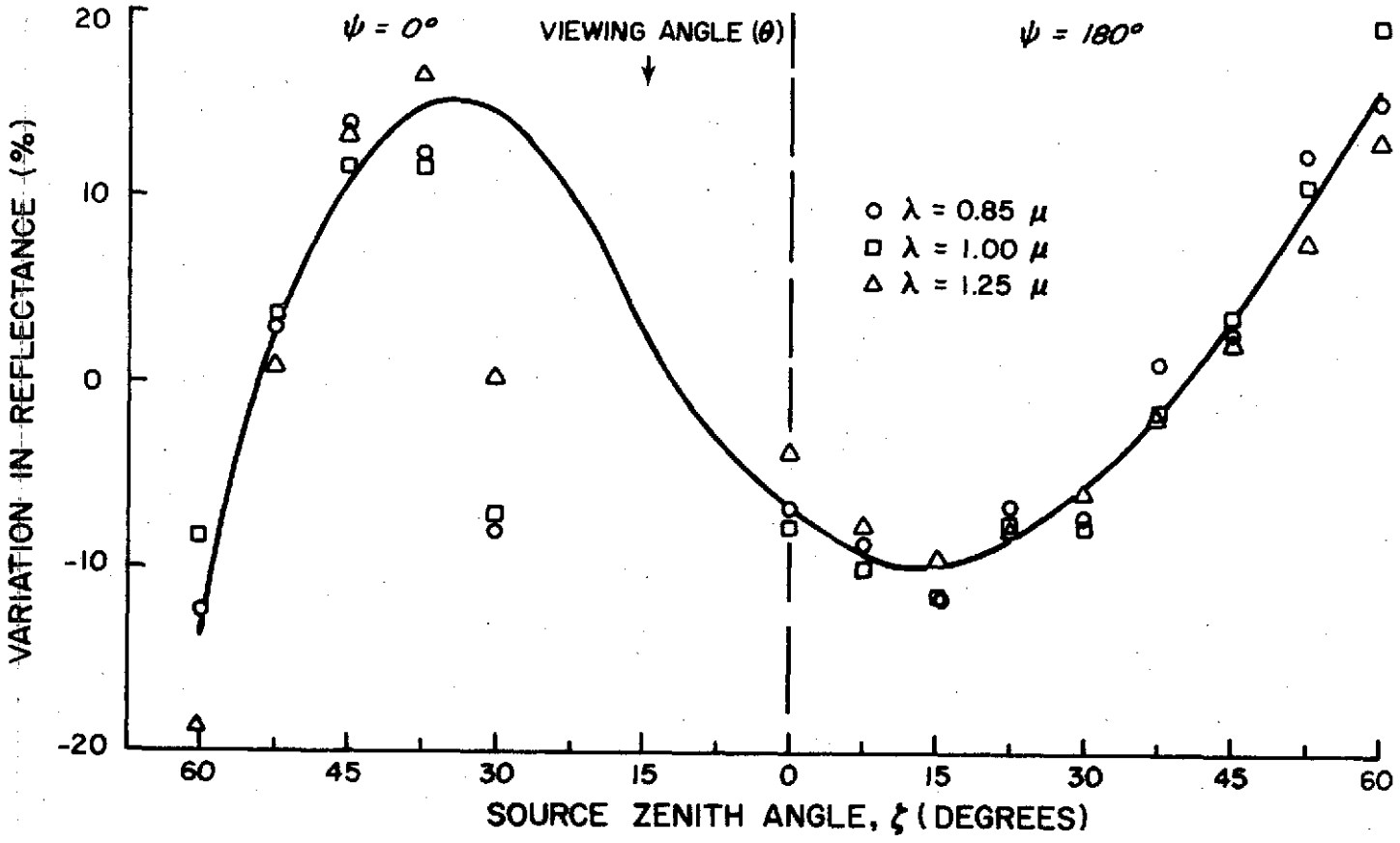

FIGURE VI-21. VARIATION IN REFLECTANCE FROM BERMUDA GRASS AT λ = 0.85, 1.00, AND 1.25 MICRONS

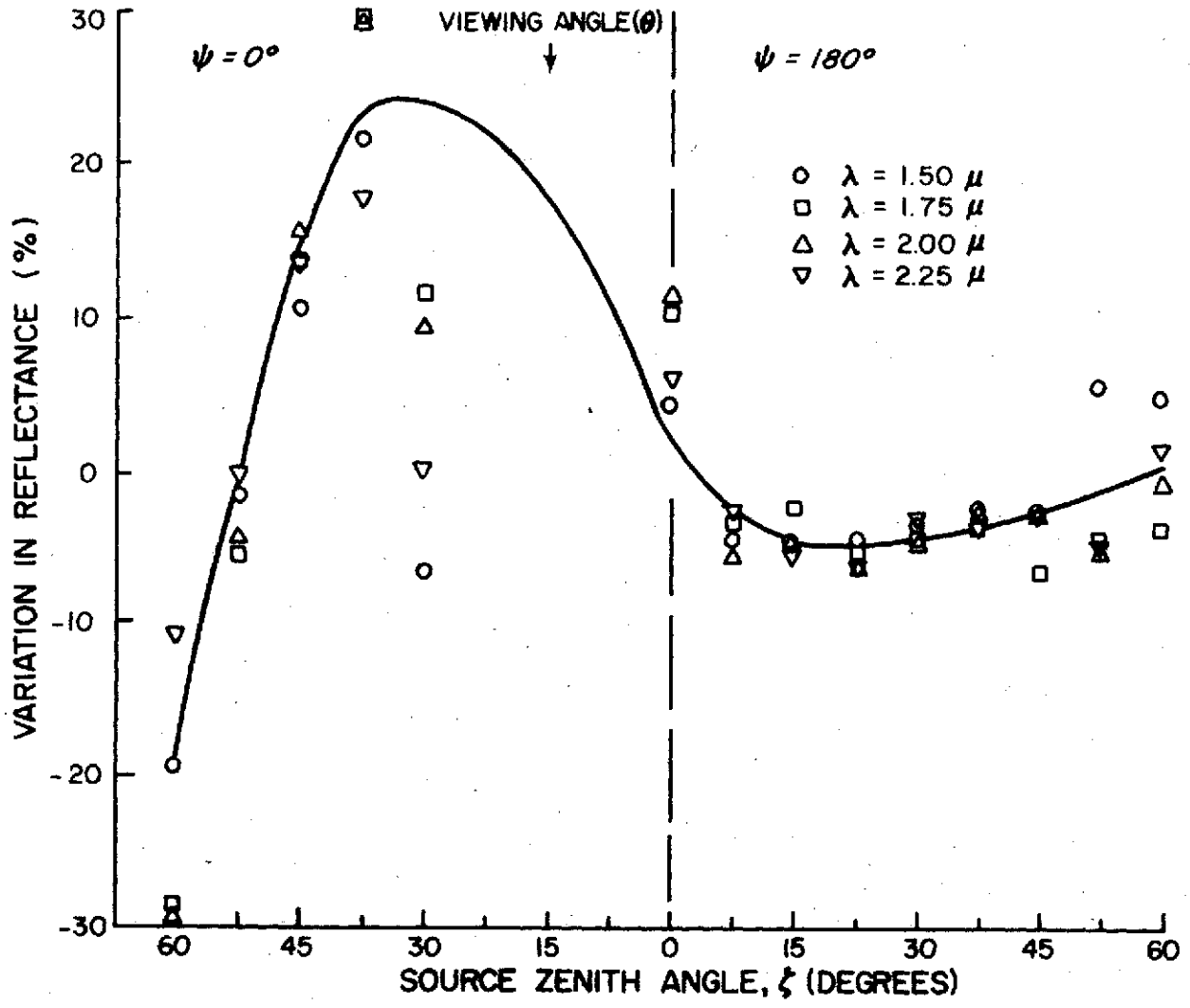

FIGURE VI-22. VARIATION IN REFLECTANCE FROM BERMUDA GRASS FROM λ = 1.50 TO 2.25 MICRONS

properly positioning the lamps for the data at this point. The general trend of the data for the Bermuda grass reflectance versus source angle is very similar to the results found for the Saint Augustine grass. The biggest difference is that for the Bermuda grass the variation in reflectance was found to be about the same for all the regions of the electromagnetic spectrum studied. There is also a slight difference in the shape of the curves. These conclusions are found from comparing Figures VI-19 through VI-22 with Figures VI-6 through VI-9.

Conclusions

The conclusions that were made from the laboratory tests fell into two categories. These categories were conclusions having to do with the technique used to make the measurements, and conclusions that could be made from the data taken.

These tests showed that the technique used to take data in the laboratory was easy to use and can result in good reflectance data from an integrated natural surface. The major disadvantages to the laboratory technique were the lack of a better standard surface to which the reflectance readings could be compared and the smallness of the plot which could be viewed. The standard surface problem could be helped by preparing a different type of surface which would be more diffuse and a more perfect reflector in the ultraviolet and infrared regions. The size of the spot viewed can only be improved by having a larger distance between the spectroradiometer and the test plot. This would require a larger laboratory. The major problem involved with the test plot sensed being so small (2 inches by 6 inches)

is that most crops consist of large plants which are spaced some distance apart so that a large area must be viewed in order to include several plants and the areas in between in the radiometer field of view. This is necessary to get the reflectance of an integrated area representing the type of plot sensed with airborne sensors.

It was also found from the laboratory tests that the photomultiplier tube is easily saturated so that the voltage output of the spectroradiometer is no longer linear with the intensity of the energy being reflected from the test surface. This is a problem only when readings are to be made from a standard surface which has a high reflectance. When reading from most natural surfaces, the reflectance in the visible region is low enough that this is not a problem.

Another area in which the laboratory technique used to take data was thought to be limited was how to vary the viewing angle. However, two ways were found to solve this problem after the laboratory tests were completed. One way is to use a laboratory with a high ceiling (25 feet or greater) where the folding mirror can be mounted high above the radiometer. The second and easiest method found was to vary the angle of the test plot while the readings are being made. This method will give good results only if the structure of the test plot is not altered by placing it at an angle with the horizontal.

The most significant results concluded from the data was that there are very significant variations in the reflectance of natural surfaces with source zenith angle and that these variations are not always the same for all regions of the electromagnetic spectrum. It was also concluded that the structure of the surface which is made up of an integration of individual plants, leaves, or particles is a

significant factor in determining the effects of the source angle on bidirectional reflectance. The final conclusion made was that in order to truely understand the bidirectional reflectances from a natural surface that data must be taken at many viewing angles, source angles, and relative azimuth angles on different plots of the same type of grass or soil and that the structural characteristics of the surface must be better understood.

CHAPTER VII

FIELD TESTS AND RESULTS

In order to fulfill the original objective of developing a technique to determine the reflectance of natural surfaces in the natural environment, field tests were conducted. Data was taken in the field in the natural environment on the reflectance of Bermuda Grass (Cynoden dactylon). Data was taken both with the folding mirror mounted on the moveable platform used in the laboratory and on the balloon system. The field in which the tests were conducted was covered with a thick stand of Bermuda grass and was cut regularly to a height of two to three inches above the ground. The data was taken in the first few weeks of August, 1974.

Experimental Techniques

The first technique used to collect reflectance data was very similar to that shown in Figure VI-1. The spectroradiometer was located at the back of a panel truck on the turntable described in Chapter IV. The folding mirror was mounted on the moveable platform used in the laboratory tests and was at a height of 12 feet above the ground. The mirror was positioned to give a viewing angle with the ground of 15 degrees. The folding mirror was at a distance of 150 feet from the spectroradiometer. The sun was used as the source. The experiment was set up so that the folding mirror was due east of the spectroradiometer. Therefore, the sun was behind the mirror in the mornings. The plot from which data was taken was composed of Bermuda grass as described in Chapter VI. The size of the plot studied with this technique was approximately 6 inches by 16 inches. A photograph

showing the arrangement of the folding mirror, standard surface and spectroradiometer is given in Figure VII-1.

The spectroradiometer was aligned and focused visually in the field. The standard surface was placed over the test plot and the optics in the radiometer was aligned by adjusting the spring mounted mirrors until the spot of visible energy from the standard surface was centered on the monochromator opening slit. The radiometer was focused by placing a black strip of cardboard across the standard surface and adjusting the focus knob on the telescope until the image was focused clearly at the monochromator opening.

Two procedures were used in collecting the field data with the platform mounted mirror. The first way in which data was collected was to keep the viewing azimuth and the test plot constant. Readings were first made from the test plot and then from the standard surface with the spectroradiometer. Runs were made throughout one day with the photomultiplier tube and then throughout another day with the lead sulfide detector. Readings were taken manually at 5 to 10 selected wavelengths for each detector used. Readings were recorded every one-half hour throughout the day. It required from ten to twenty minutes to take readings at one time period from both the standard and the test plot. Near one o'clock when the sun was at its highest elevation, a more complete spectral scan was made. Readings at this time were made at 20 to 30 different wavelengths within the response range of the detectors used.

With this first procedure used to collect data, the relative azimuth angle (Ψ) was a variable. The reason for Ψ varying was that the viewing azimuth was due east and the solar azimuth varied from

FIGURE VII-1. Photograph of Field Test Using Platform Mounted Mirror

almost due east in the early morning to south at one o'clock and then was almost due west in the late evening. The more complete spectral scan was made when the sun was near due south; therefore, Ψ was 90 degrees for the data taken at that time. It was assumed during all the tests that the solar angles did not vary sufficiently during the time period required to collect a set of data to affect the results obtained.

In order to try and collect data with the same angular relationships as the data taken in the laboratory and to see the effect if any of Ψ on the reflectance, a second procedure was used to collect data with the platform mounted mirror. With the second procedure the platform mounted folding mirror was rotated for each run so that $\Psi = 0^{o}$ or $\Psi = 180^{o}$. With this technique a slightly different plot of grass was viewed for each set of data taken; however, the laboratory test had shown that this should not have any effect on the results. The mirror had to be rotated and its angle with the horizontal adjusted for each data set made in order to give a viewing angle of 15 degrees at $\Psi = 0^{o}$ or $\Psi = 180^{o}$. Since the mirror was moved for the data taken at each solar angle, the spectroradiometer alignment with the mirror had to be checked for each run. Because of the time required to set up using this procedure not as much data was taken with this method as with the first procedure described.

To help determine where the sun was located during the day, a computer program was written and the solar elevation ($90^{o}-\zeta_{o}$) and azimuth (φ_{o}) were calculated for all the days in August versus the time of day. A description of this program and sample results are given in Appendix F. The highest elevation obtained by the sun on the days

in which data was collected was when ζ_o = 14 degrees. This position of the sun was obtained at approximately one o'clock each day. The position of the sun throughout the day can best be visualized from Figure VII-2. This figure shows the end point of the shadow of a vertical pole at the center of the chart one unit high for August 15, 1974. The shortest shadow (maximum solar elevation) was obtained when the sun was due south.

The second technique used to collect data was by utilization of the balloon/mirror system shown in Figure III-1. The mirror was positioned underneath the balloon at an altitude of 100 feet. The mirror was kept horizontal by the mirror cables and the spectroradiometer was positioned on the ground 27 feet from a spot directly beneath the mirror. The viewing azimuth was 270 degrees or due west and the viewing angle between the mirror and the test plot was 15 degrees. The distance between the radiometer and the spot viewed was 210 feet. The size of the Bermuda grass plot viewed was approximately 7.5 by 20 inches.

Since the mirror when positioned with the balloon system had a slight angular movement which caused the field of view of the radiometer to vary over an area greater than the area of the standard surface, it was not possible to read from the standard surface with the balloon/mirror system. Therefore, the standard surface was located beneath the platform mounted mirror used in the first technique. This folding mirror was located 100 feet to the east of the spectroradiometer. Readings were first made from the test surface by viewing the folding mirror mounted beneath the balloon. Then the spectroradiometer was rotated on the turntable and readings were made from the standard

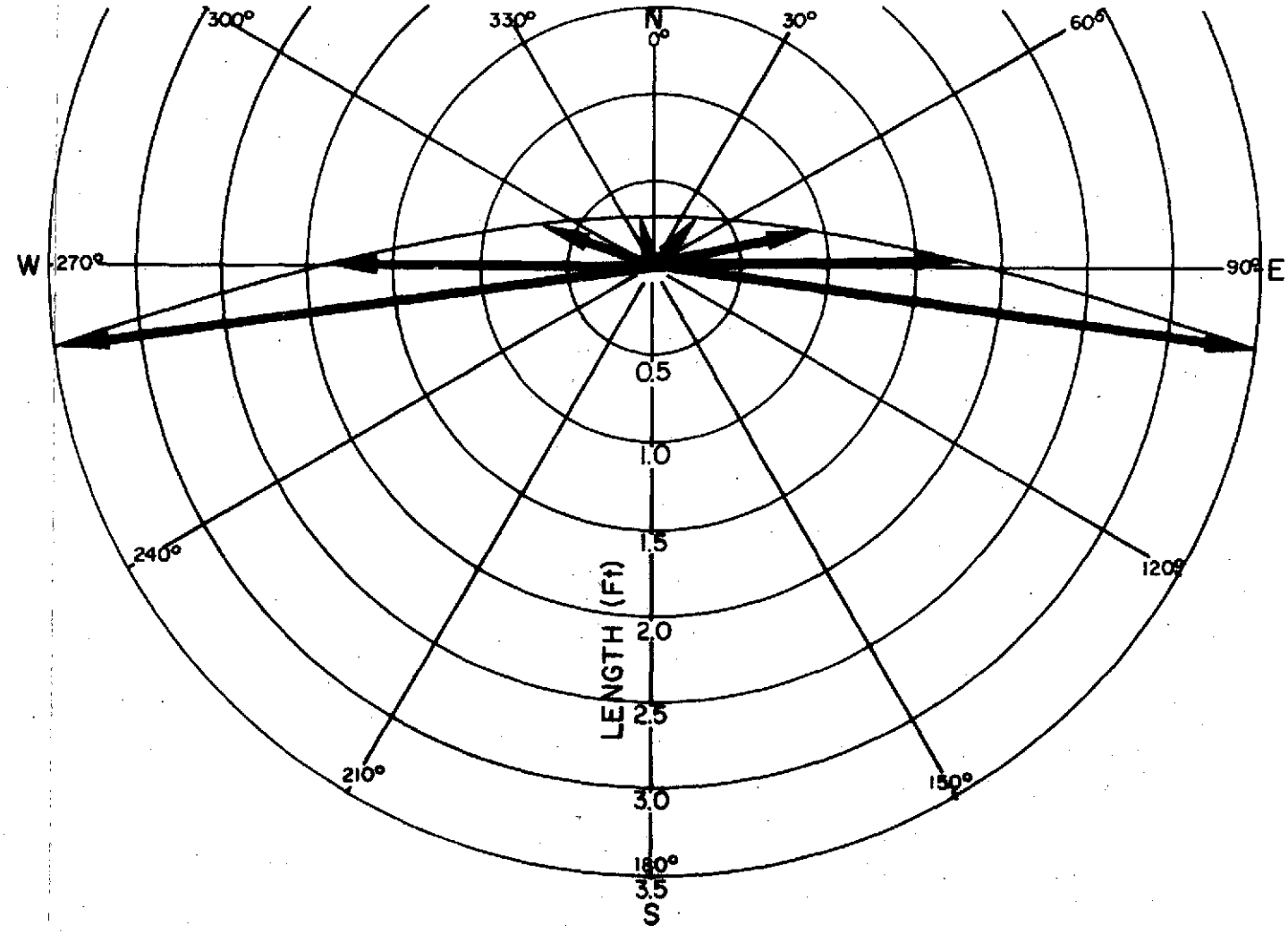

FIGURE VII-2. SHADOW OF END POINT OF ONE FOOT HIGH BAR ON AUGUST 15, 1974

surface with the platform mounted mirror.

The balloon had to be taken down and refilled every morning so that realignment of the system was necessary each day. Alignment with the folding mirrors was a problem since there was no way to see directly the spot being received by the spectroradiometer. Alignment was accomplished in the field by placing a black piece of cardboard over the platform mounted mirror and then turning the spectroradiometer with the photomultiplier tube detector until the field of view was centered on the mirror as determined by the voltage reading from the spectroradiometer. The eyepiece on the telescope was then adjusted so that the crosshairs were centered on the folding mirror. It was then assumed that by centering the eyepiece crosshairs on the folding mirror (whether under the balloon or on the platform) the field of view of the radiometer would be centered on the folding mirror. Due to time problems in trying to take field data with the balloon system, the telescope eyepiece alignment was not rechecked after the field tests with the platform mounted mirror were completed.

When using the balloon technique, it was noted that the angular movements of the folding mirror were less than $\pm$ 1/2 degree so that essentially the same spot was viewed throughout the day. However, since the balloon was taken down each day and put up again, the exact same spot was not viewed each day since the mirror was not positioned exactly the same every day. Also since the viewing azimuth was kept constant for each day, the relative azimuth (Ψ) was a variable throughout the day as was the solar zenith angle.

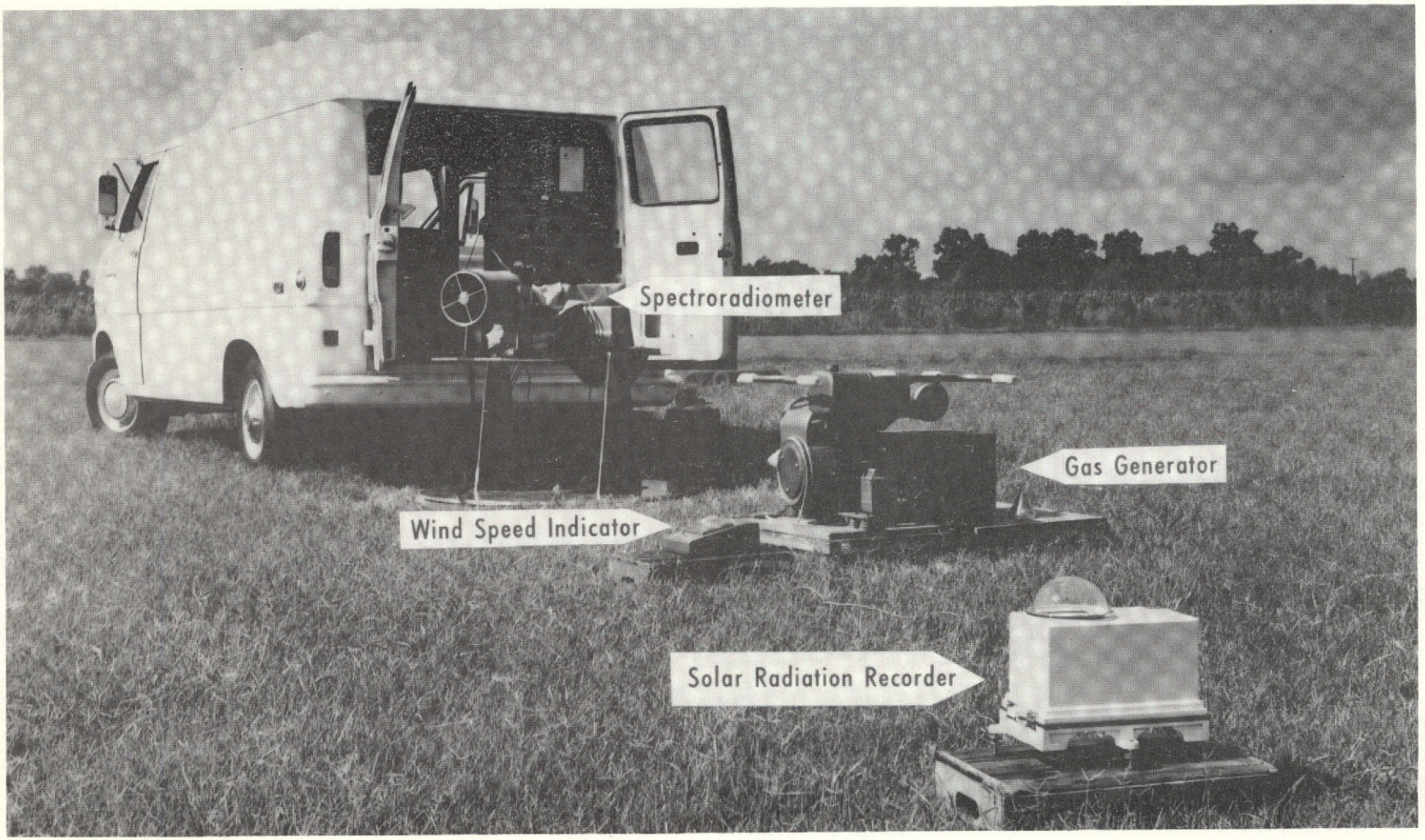

FIGURE VII-3. Photograph of Equipment Used in Field Tests

Experimental Apparatus

Most of the equipment used in the field tests has been described in other chapters. A list of the equipment used includes the balloon system, moveable platform, folding mirrors, spectroradiometer, gas generator, solar radiation recorder, wind speed and direction indicator, temperature and relative humidity recorder, standard surface, laser and plumb-bob. Some of these items are shown in Figure VII-3 as positioned for the field tests.

The only item not described previously is the solar radiation recorder. It was made by the Weather Measure Corporation. The instrument was used to indicate the presence and effect of clouds and as a general indication of the amount of solar radiation being received at the test site as a function of the time of day. Radiation is measured when it passes through a glass dome and heats black and white bimetallic strips. The difference in radiant energy absorption of the two strips in turn activates a pen which prints out a continuous record on a rotating drum.

The instrument has a slow response time so that its reading could not be correlated directly with the readings made with the spectroradiometer. However, the output of the recorder was helpful in analyzing the data from the spectroradiometer and in better understanding the readings made.

The balloon used in the field tests contained 1200 cubic feet of helium. The system was designed, launched and operated as outlined in Chapter V and Appendix B. A plumb-bob was used to position the folding mirror carried by the balloon at the right height and location. Two pounds of tension were pulled in each of the three mirror cables.

The weight of the folding mirror and its holder and attachments was six pounds. A six stake arrangement as suggested in Chapter IV was used for the cable stakes. However, once the three winches were attached to three of the stakes they were never moved. The winds during the field tests with the balloon were very light except for the fourth day when thunderstorms developed in the area. The winds from the storms were gusty and variable and caused the balloon and mirror cables to become twisted. The balloon ripped the next day after the cables were untangled, and the balloon had been refilled and was being re-launched.

Several times during field tests with the balloon system, the laser was used to test the stability of the folding mirror. It was found from these quick checks that the angular movements of the folding mirror were very small and that the laser spot after being reflected by the mirror generally stayed in an area 6 inches by 6 inches on the ground. The gas generator was used to power the laser as had been done in the tests of the smaller balloon systems (Chapter IV) and also to power the spectroradiometer and the wind speed and direction indicator.

The spectroradiometer was modified somewhat for the field tests from the configuration used in the laboratory. One of these modifications included removing the strip chart recorder and remounting the electronics in a 48 inch high rack. This was done in order that the entire system could easily be placed in the panel truck. All data was recorded manually with the digital voltmeter.

The other modifications made to the spectroradiometer were used only when readings were being made with the photomultiplier tube as

the detector. Since it was known from the laboratory tests that it was easy to saturate the photomultiplier tube, a circular piece of black cardboard was cut with an 8 inch outside diameter. A three inch hole was then cut in the center of the cardboard. The cardboard was placed inside the telescope at the face of the primary mirror. To further reduce the intensity of the energy incoming to the photomultiplier tube, the focusing optics used at the exit of the monochromator to focus all of the exiting energy on the tube was removed. This further reduced the energy recorded by the detector by a factor of five.

Data Taken With Platform Mounted Mirror

Figures VII-4 and VII-5 presents some of the field data taken with the platform mounted mirror on the relative bidirectional reflectance of Bermuda grass. These data were taken in the field two days after there had been a heavy rain. However, the field was well drained and the soil moisture content during the time in which data was taken was found to be 25 percent. Test runs 103 and 104 shown in Figure VII-4 were both made on the same day. Run 103 and 105 present the reflectance data taken with the solar plane approximately 90 degrees to the viewing plane. Run 104 presents data taken with the solar and viewing planes at approximately the same azimuth. These data were taken by first reading from the test surface at each wavelength and then reading from the standard surface at the same wavelengths.

Comparing Figure VII-4 to the data obtained for the relative bidirectional reflectance of Bermuda grass taken in the laboratory

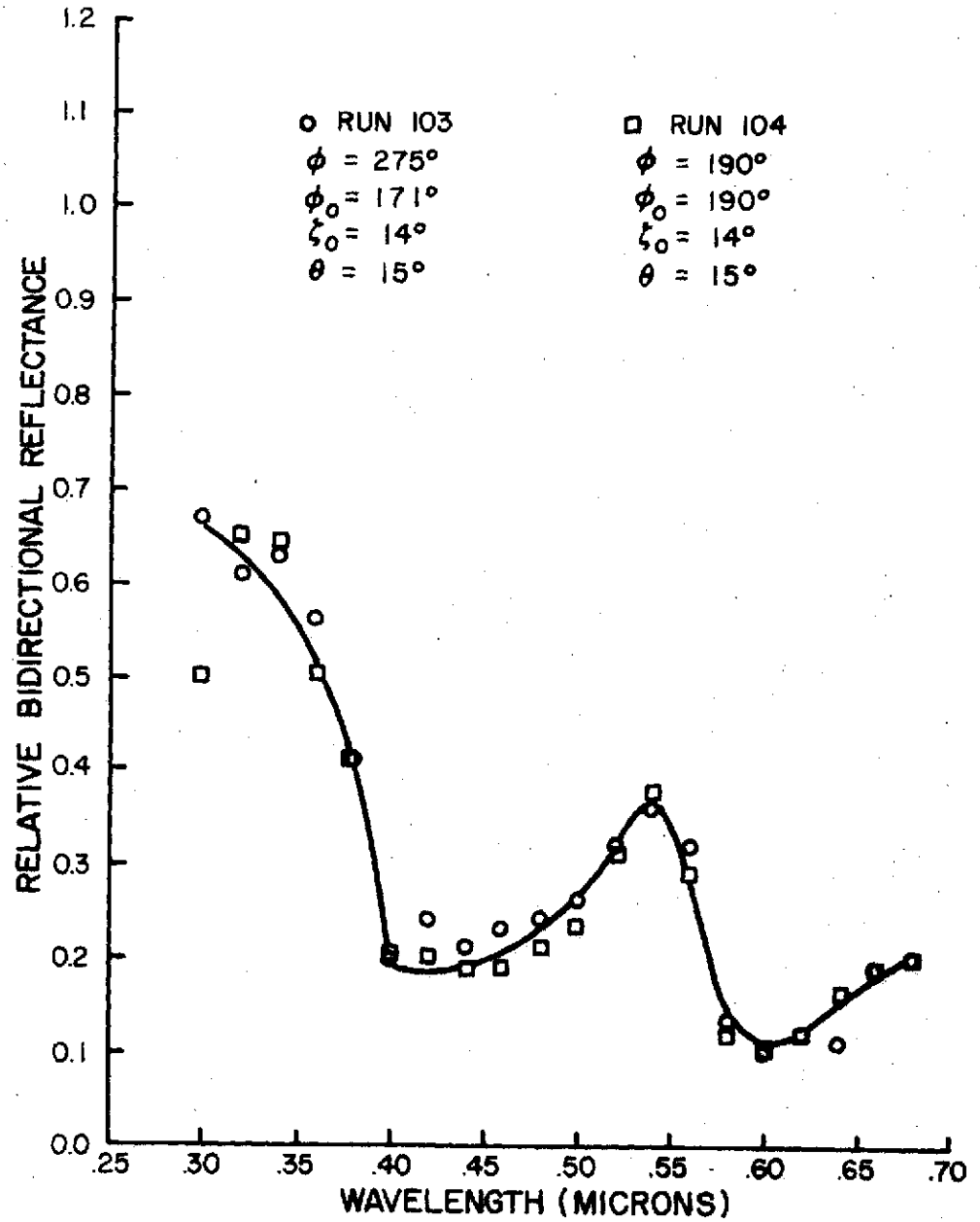

FIGURE VII-4. REFLECTANCE OF BERMUDA GRASS IN VISIBLE REGION MADE WITH PLATFORM MOUNTED MIRROR

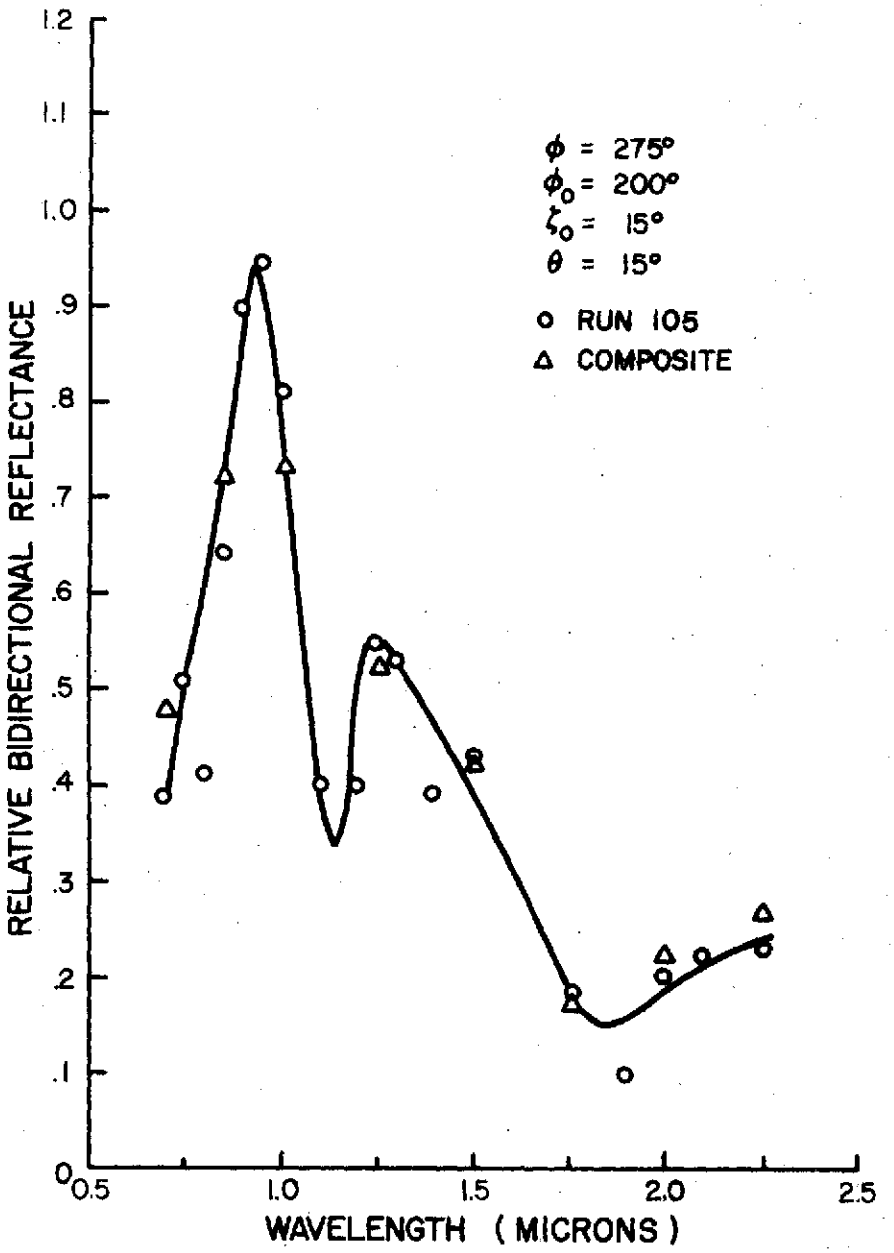

FIGURE VII-5. REFLECTANCE OF BERMUDA GRASS IN INFRARED REGION MADE WITH PLATFORM MOUNTED MIRROR

(Figure VI-17), it is seen that the general shape of the curves is the same. However, the data taken in the field is considerably higher in the region from λ = 0.40 microns to λ = 0.55 microns. It appears that this was caused by the photomultiplier tube being saturated when reading from the standard surface in this region in spite of the precautions taken to prevent this from happening. The detector was not saturated when readings were being made from the test surface. The field data was taken with a source angle of 15 degrees since this was the highest zenith angle reached by the sun whereas the laboratory data was taken at a source angle of zero degrees. From Figure VI-19 it is seen that the reflectance at a source angle of zero degrees would be expected to be 15 to 20 percent higher than that taken at a source angle of 15 degrees. It should be noted that on the day on which this data was taken, the sky was very clear and the monochramator entrance slit width had been reduced to one millimeter in order to try to keep from saturating the photomultiplier tube. It can also be seen from Figure VII-4 that there is little variation in the bidirectional reflectance of Bermuda grass with the relative azimuth angle ($\Psi = \varphi - \varphi_o$) at $\zeta_o = 15^o$ and $\theta = 15^o$.

Figure VII-5 shows the data taken in the field in the infrared region on the relative bidirectional reflectance of Bermuda grass. The composite data points shown are an average of the readings taken at various solar angles throughout the day. This data is seen to be slightly lower than that taken in the laboratory in this region. These slight differences could originate from a number of causes. One of these is the different solar zenith and relative azimuth angles used in taking these data. Other factors include experimental errors and

and possible differences in the characteristics of the two test plots from which the laboratory and the field data were taken, in particular the difference in the soil moisture content. Among the causes of experimental error which affected the data was the varying solar radiation due to clouds. The day on which the infrared data was obtained with the platform mounted mirror it was clear in the morning; however, by one o'clock when the data shown in Figure VII-5 was taken, the sky had become filled with clouds. Therefore, it was necessary to either take data while the sun was blocked by clouds or wait for openings in the clouds and take the data as quickly as possible. Because of this problem, data was not taken at as many wavelengths as had been done in the visible region. Also much of the data had to be discarded because there would be a large change in the solar radiation between the time readings were made from the test surface and the time that readings were made from the standard surface.

Data was also taken to see if the effect of the solar zenith angle on bidirectional reflectance could be obtained using the platform mounted mirror. These data were obtained by taking readings from the standard and test surfaces every one-hour from about 9 o'clock in the morning to 5:30 o'clock in the afternoon. The data for test run 103 were taken with a constant viewing azimuth so that the same plot was viewed throughout the day. Test run 104 was made by rotating the folding mirror so that the viewing and solar planes were the same or 180 degrees apart. The sky was cloudless and the solar radiation as sensed by the solar radiation recorder varied by cos ζ_o for all the data shown in these figures.

It was found when comparing the readings from the solar radiation

recorder and the readings taken with the spectroradiometer from the standard surface that the readings made with the spectroradiometer using the photomultiplier tube detector did not follow a cos ζ_o curve. Therefore, the readings made with the photomultiplier tube from the standard surface were assumed to be invalid except for those made in the early mornings and evenings when the intensity of the solar radiation was low. These readings made in the early morning and evening were then corrected by the cos ζ_o to give corrected readings from the standard surface throughout the day. These corrected readings were then divided into the readings made from the test surface to give the relative bidirectional reflectance data given in Figures G-1 through G-7 in Appendix G.

The data plotted in Figures G-1 through G-7 shows considerably more variation and a different trend from that obtained in the laboratory and is considered to be erroneous. The primary item which affected these readings was variance in the power output of the gas generator. These were the first runs made in the field and the gas generator was missing considerably and at times would cause the readings to drop or rise by 50 percent or more. The gas generator was later repaired and this problem corrected. This data was not retaken because of the weather conditions which existed for the remainder of the time available to take data with the platform mounted mirror.

Figures G-8 through G-16 present all the data taken at various solar angles in the field in the infrared region. Test run 105 was taken with a constant viewing azimuth so that the relative azimuth ($\overline{\Psi}$) was a variable. This data was taken with the platform mounted mirror but the viewing azimuth was varied so that $\Psi = 0^o$ or $\Psi = 180^o$. Test

run 112 was made with the balloon mounted mirror. For the data taken with the balloon/mirror system, the viewing azimuth was held constant. All of these data were obtained by first reading from the test surface and then reading from the standard surface. The two readings were then compared to give the relative bidirectional reflectance.

All of the data taken in the infrared region was taken on cloudy days. Because of this there was considerable variation in the solar radiation while the readings were being made. This factor introduced enough scatter in the data so that any variations in the reflectance with source angle could not be found. Therefore, only an average line is drawn through the data. At λ = 0.85, 1.00 and 1.25 microns the data taken with the balloon mounted mirror appears to show a trend which is much higher than the average calculated. Since this appears in the data only at these wavelengths and the data at all the wavelengths for a particular solar angle were collected at the same time and in the same manner for each solar angle, there is no way to explain the phenomenon.

Data Taken With The Balloon/Mirror System

Figures VII-6 and VII-7 present the field data taken with the balloon/mirror system on the reflectance of Bermuda grass as a function of wavelength. All of these data were taken with a constant viewing azimuth (φ) of 270 degrees. Two runs were made with the photomultiplier detector on different days while viewing different test plots. The data taken in the infrared region was made on a third day which was overcast. At the time these runs were made, there had not been any rain for over a week, and the field was very dry. The soil moisture content was found to be 17 percent.

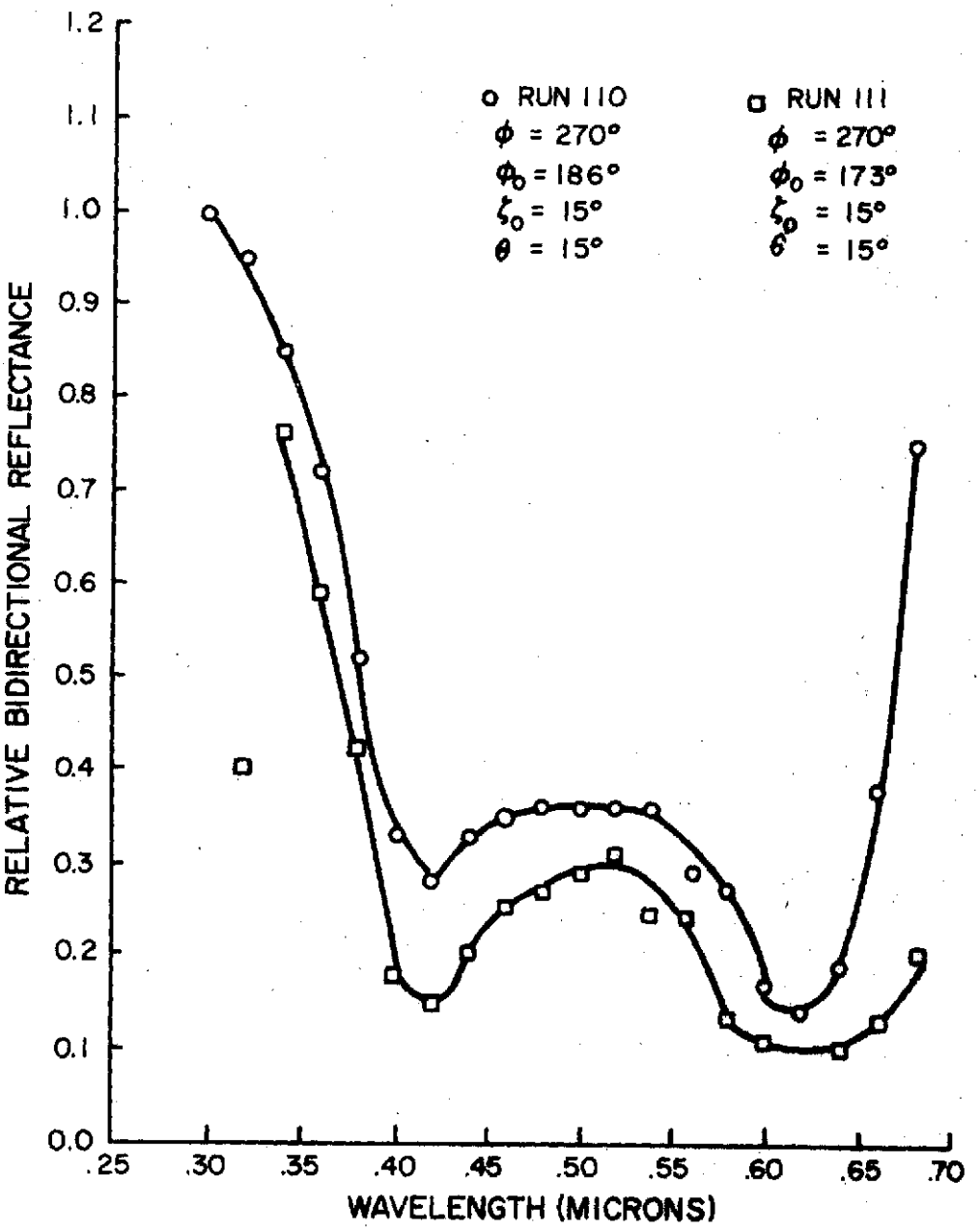

FIGURE VII-6. RELATIVE BIDIRECTIONAL REFLECTANCE IN THE VISIBLE REGION OF BERMUDA GRASS PLOT MADE WITH BALLOON MIRROR SYSTEM

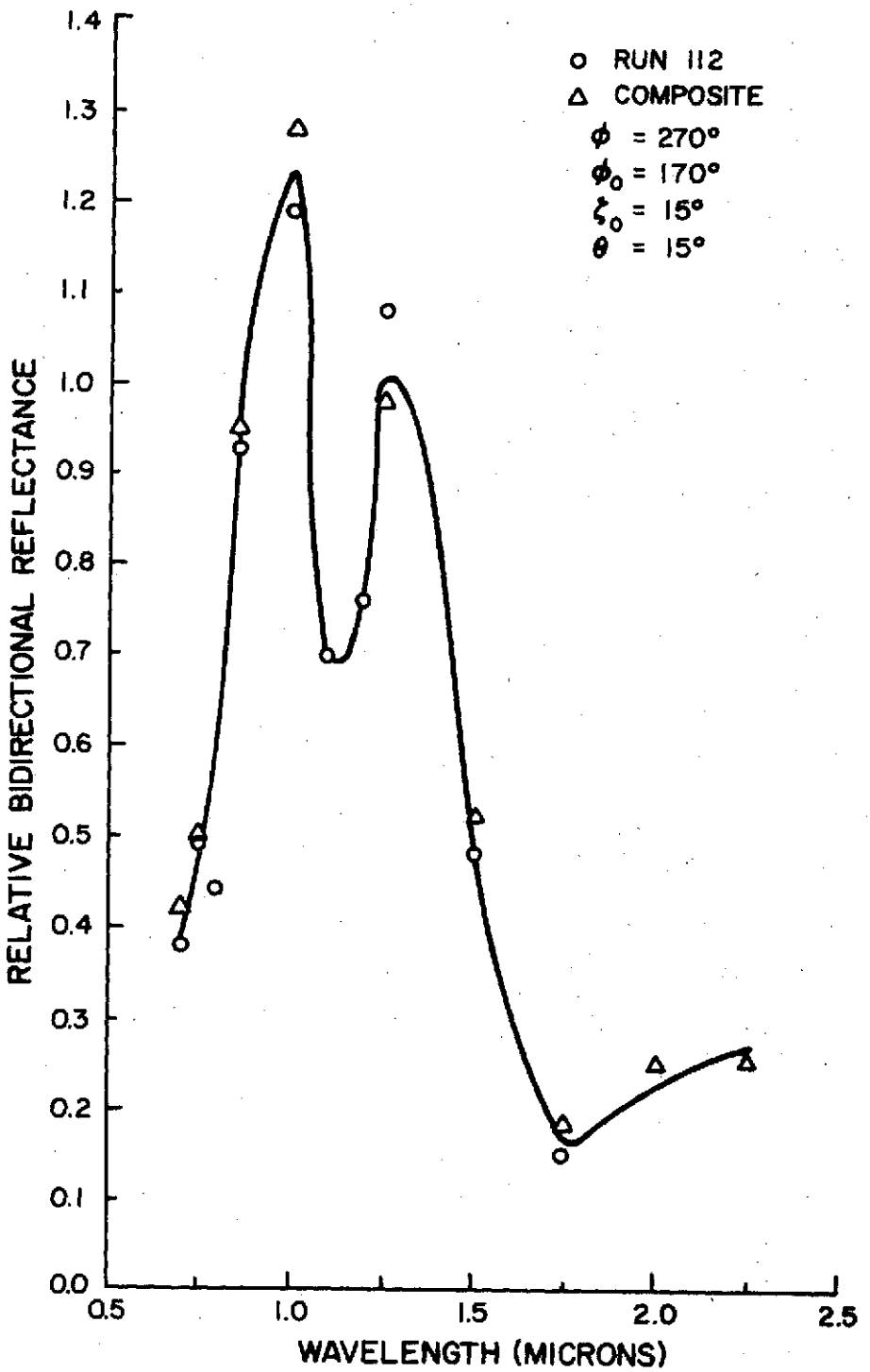

FIGURE VII-7. RELATIVE BIDIRECTIONAL REFLECTANCE IN THE INFRARED REGION OF BERMUDA GRASS PLOT MADE WITH BALLOON MIRROR SYSTEM

The data taken with the photomultiplier tube as a detector was made with an entrance and exit slit width on the monochromator of one millimeter. However, the readings taken from the standard surface from $\lambda = 0.40$ to $\lambda = 0.55$ microns used to divide into the readings taken from the test surface to get the reflectance appeared to be in error due to saturation of the detector. This caused the curves in Figure VII-6 to have a different shape in this region from the curve obtained in the laboratory. Two curves are shown in Figure VII-6 for data taken on two consecutive days. The data plotted for test run 110 is too high due to an experimental error caused by the alignment of the spectro-radiometer with the folding mirror. This problem was discovered when the spectroradiometer was brought back into the laboratory and the alignment checked with the telescope eyepiece. However, since the shape of the curves for test run 110 and 111 which were taken on two different days of two different test plots is the same, the ability to take consistant data with the technique used was substantiated.

The relative bidirectional reflectances as obtained with the balloon mounted mirror in the infrared region were higher than those found in the laboratory. There was also a slight difference in the shape of the curve in the near infrared. This effect was expected due to the difference in the soil moisture content of the test plot viewed in the field with the balloon/mirror system and the test plot viewed in the laboratory. The overall increase in the data obtained with the balloon was either due to the alignment problem or due to a variation in the solar radiation while the readings were being made due to the light clouds present in the area.

Figures VII-8 through VII-14 present the data on the variation

of the bidirectional reflectance of Bermuda grass with source angle as taken with the balloon mounted mirror. Plotted on each figure is the normalized curve obtained for the visible region in the laboratory for those data. It is seen that this data shows the same general trend as the laboratory data except for the field data taken in the afternoon (Ψ greater than 180^{o}). The data is higher in the afternoon between the source zenith angles of 10 to 30 degrees due to extraneous light being recorded by the spectroradiometer when the sun is near the alignment of the spectroradiometer and the folding mirror.

The data as shown in Figures VII-8 through VII-14 was obtained by taking the readings from the standard surface early in the day and correcting them by the cos ζ_{o}. These readings were then divided into the readings taken from the test plot with the folding mirror mounted underneath the balloon system. The standard surface readings were made using the platform mounted folding mirror. The days on which test runs 110 and 111 were made were clear. Most of the first day in which test run 110 was made was spent in launching the balloon and setting up the equipment.

Conclusions

It was shown from the field tests that the bidirectional reflectance of large test plots could be obtained using the concept of a folding mirror. This type of data was obtained both with the folding mirror mounted on a platform and with the folding mirror mounted underneath a balloon. Between the weather and difficulties with the equipment most of the data taken on the variation of the reflectance with source angle was either invalid or contained too much scatter to verify a trend in the data. In order to really understand the

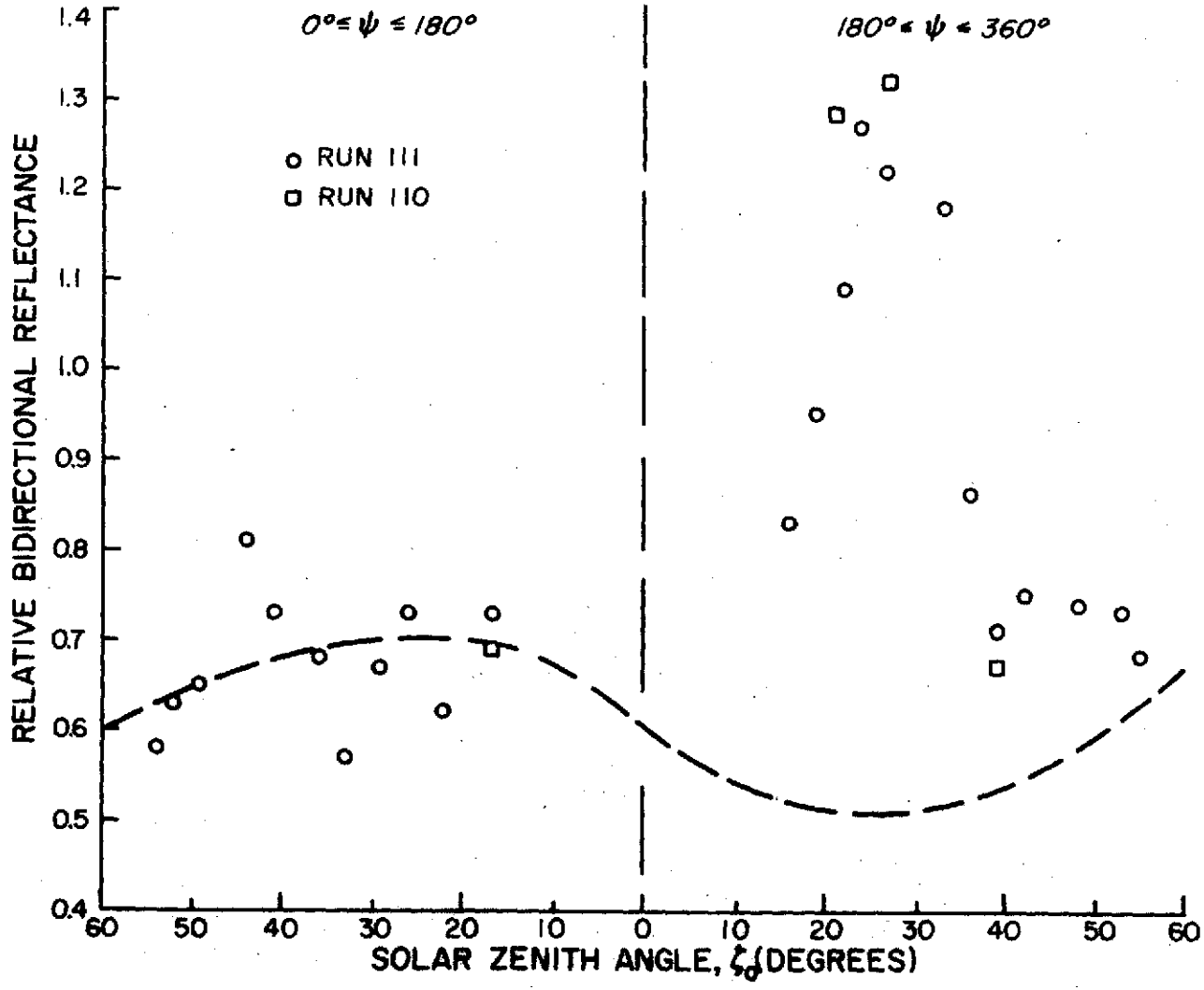

FIGURE VII-8. RELATIVE BIDIRECTIONAL REFLECTANCE OF BERMUDA GRASS PLOT AT λ= 0.35 MICRONS TAKEN WITH BALLOON MIRROR SYSTEM

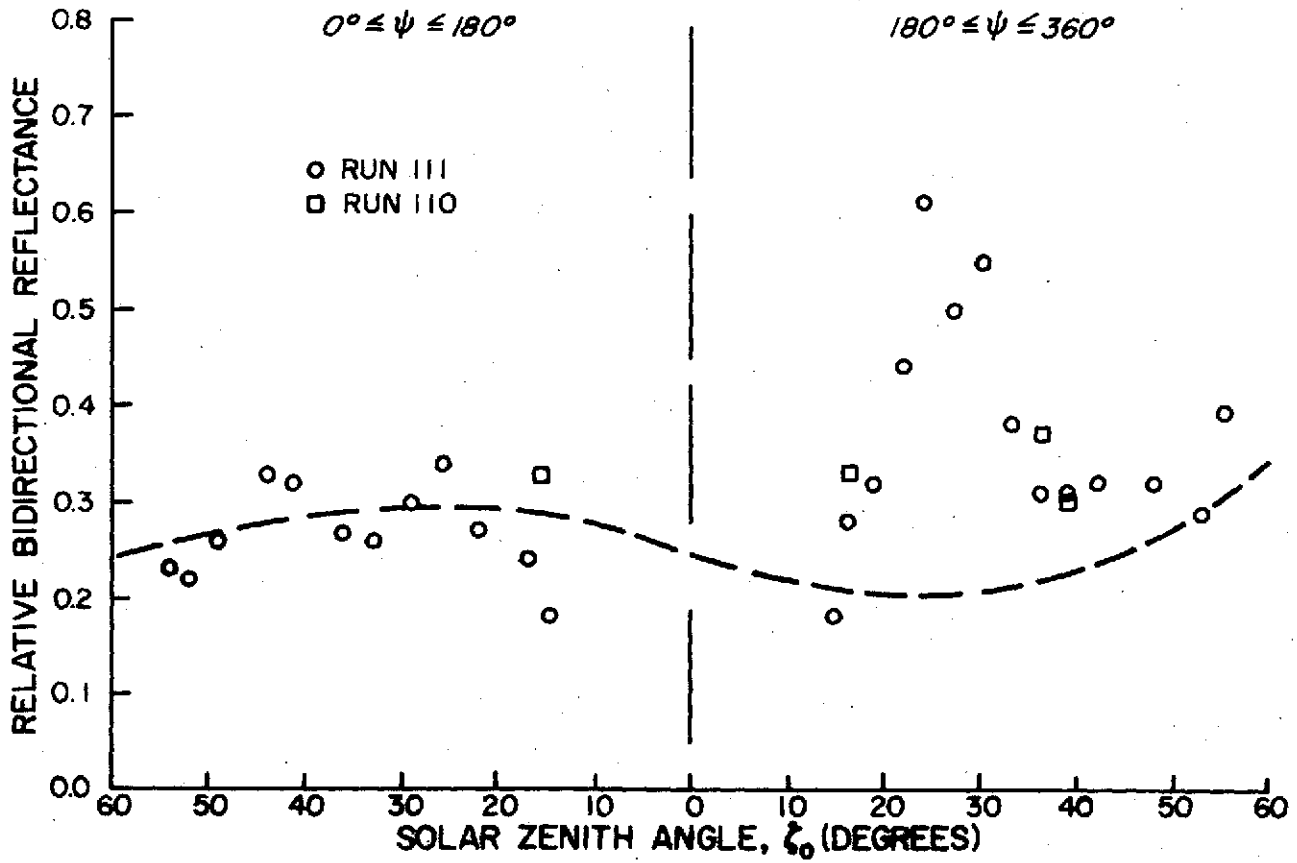

FIGURE VII-9. RELATIVE BIDIRECTIONAL REFLECTANCE OF BERMUDA GRASS PLOT AT λ=0.40 MICRONS TAKEN WITH BALLOON MIRROR SYSTEM

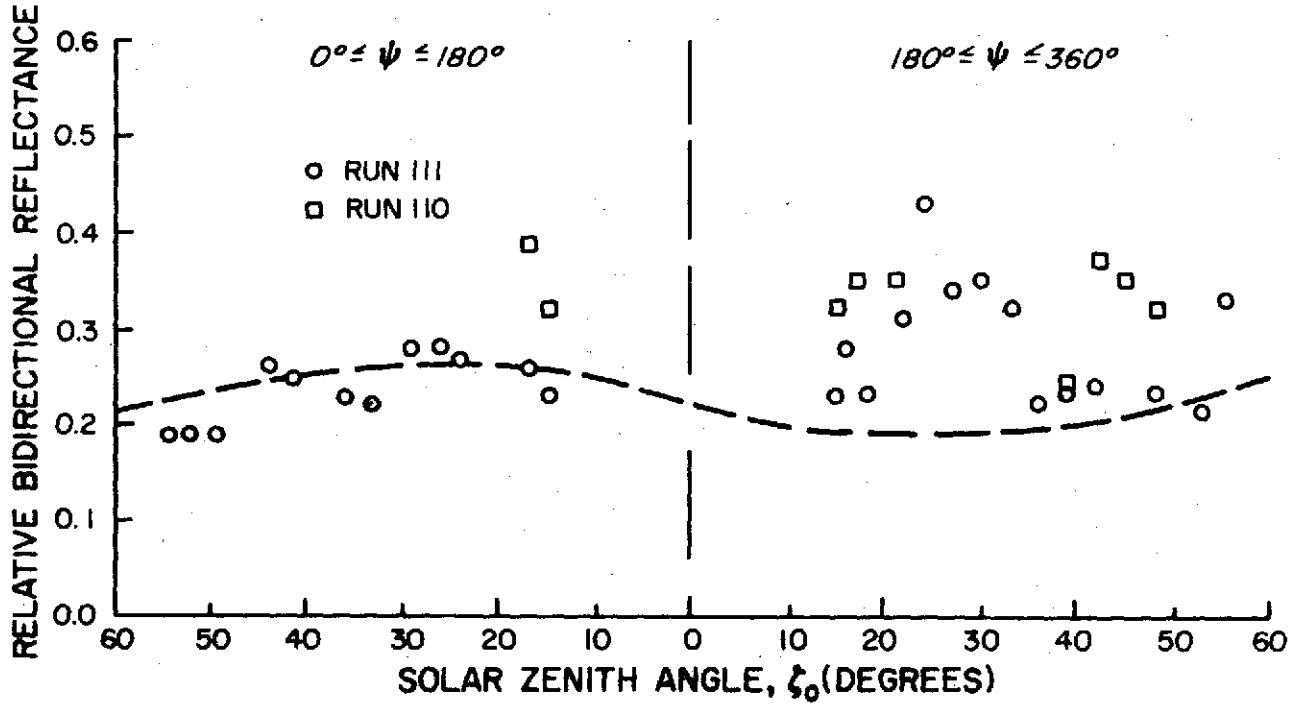

FIGURE VII-10. RELATIVE BIDIRECTIONAL REFLECTANCE OF BERMUDA GRASS PLOT AT λ = 0.45 MICRONS TAKEN WITH BALLOON MIRROR SYSTEM

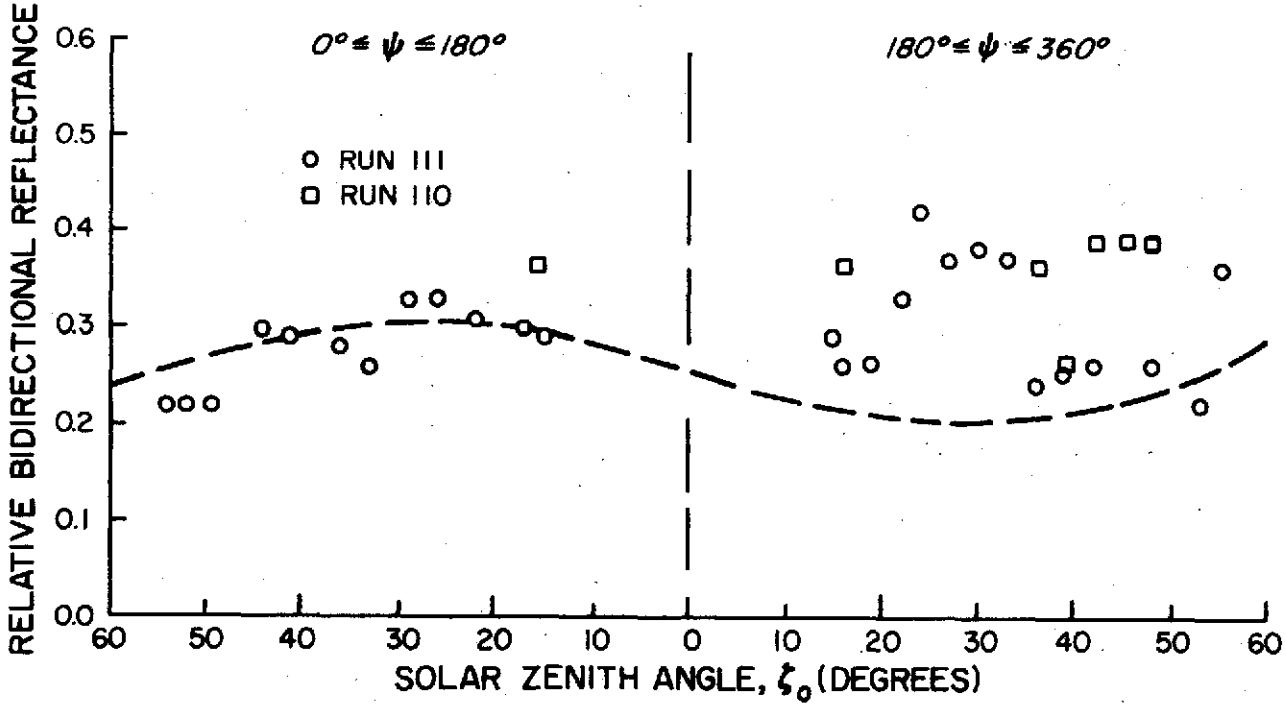

FIGURE VII-11. RELATIVE BIDIRECTIONAL REFLECTANCE OF BERMUDA GRASS PLOT AT λ = 0.50 MICRONS TAKEN WITH BALLOON MIRROR SYSTEM

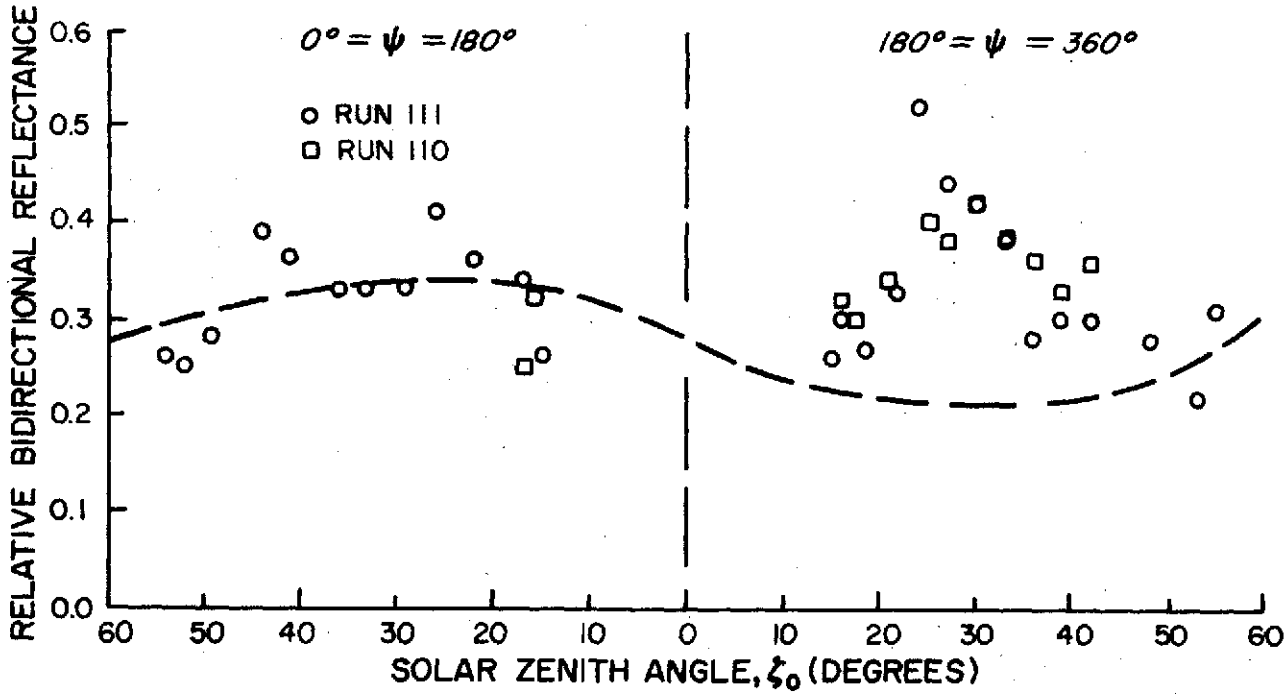

FIGURE VII-12. RELATIVE BIDIRECTIONAL REFLECTANCE OF BERMUDA GRASS PLOT AT λ = 0.55 MICRONS TAKEN WITH BALLOON MIRROR SYSTEM

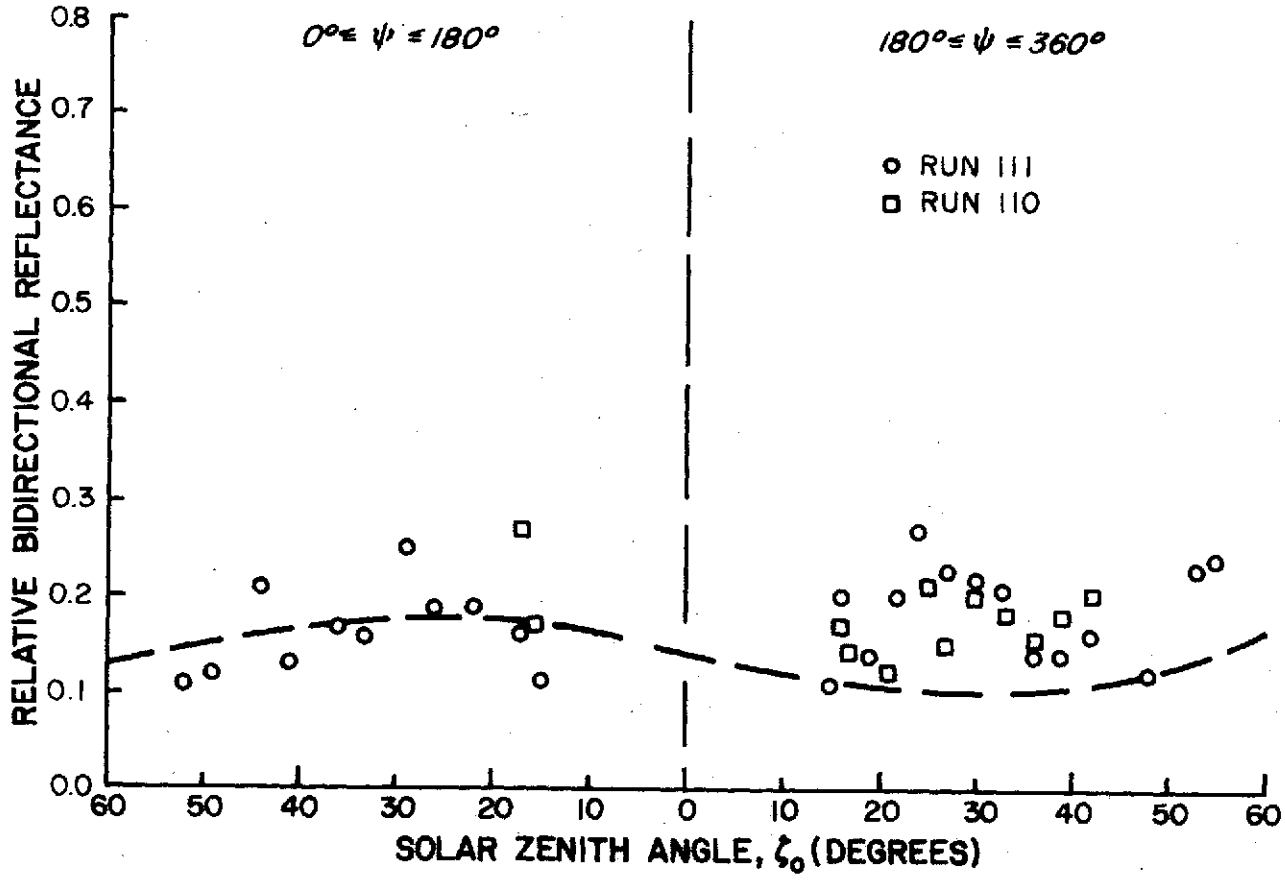

FIGURE VII-13. RELATIVE BIDIRECTIONAL REFLECTANCE OF BERMUDA GRASS PLOT AT $\lambda = 0.60$ MICRONS TAKEN WITH BALLOON MIRROR SYSTEM

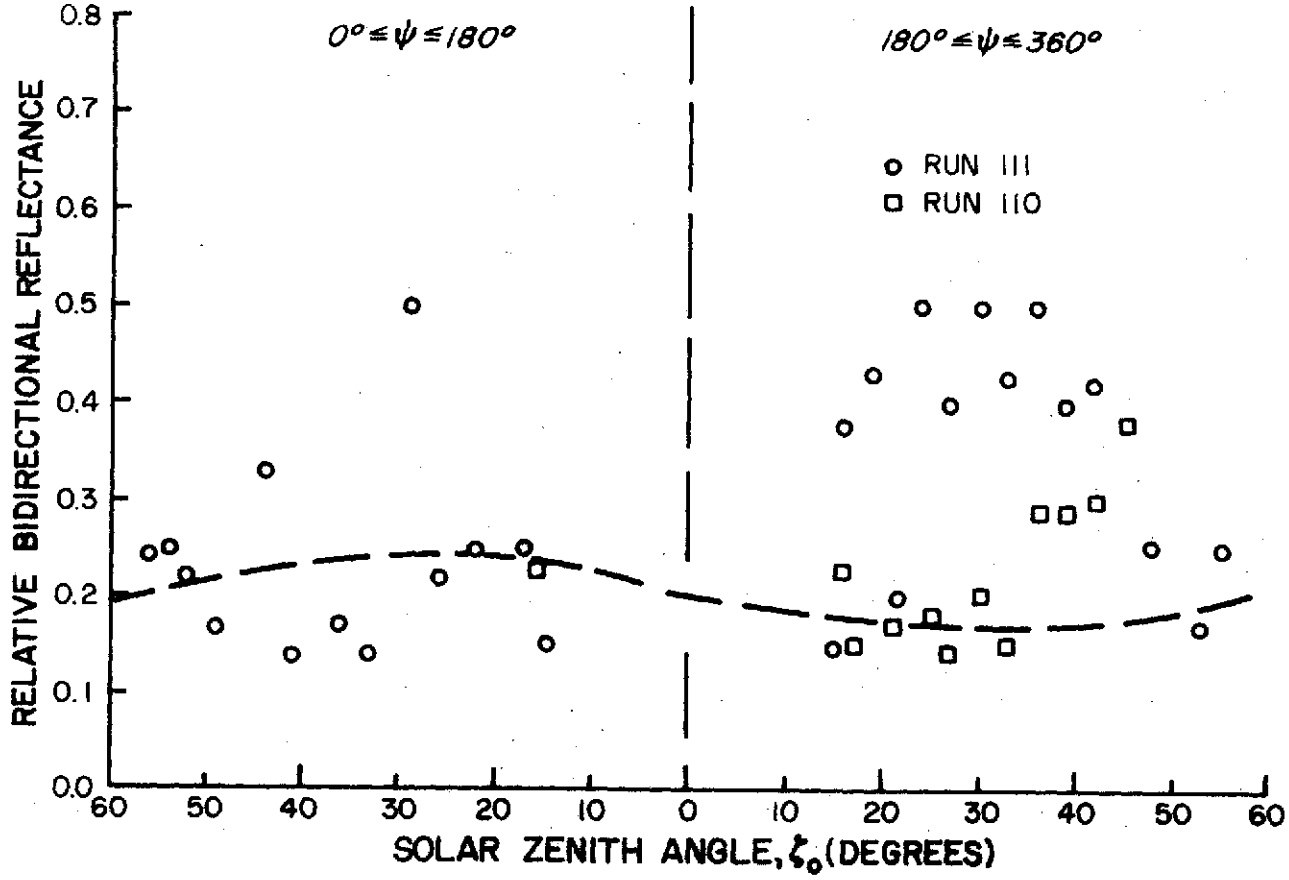

FIGURE VII-14. RELATIVE BIDIRECTIONAL REFLECTANCE OF BERMUDA GRASS PLOT AT $\lambda = 0.65$ MICRONS TAKEN WITH BALLOON MIRROR SYSTEM

effects of a variable like source angle on the reflectance of a particular natural surface much more data than was obtained in this experiment must be taken.

It was also concluded from the field tests that the spectroradiometer as described in Chapter IV was not well suited for field use. In particular, the photomultiplier tube detector has too low a saturation point to be used in natural light and especially with an eight inch collector. Another problem that arose when using the spectroradiometer in the field was alignment with the folding mirror. This was not a problem in the laboratory where there was plenty of time to use the photomultiplier detector to check the spot being viewed and to align the telescope eyepiece with that point. However, in the field when the radiometer is moved each day and must be realigned, there is not enough time available to align the system each day if runs are to be made beginning early in the morning. This is further complicated if the balloon has to be lowered and refilled also. Therefore, it was concluded that a quick way to check the alignment of the spectroradiometer with the folding mirror be devised before further field tests are conducted with the system.

Another conclusion made was that when the sun was shining through clouds that good readings could not readily be made. It had been hoped that by reading from both the standard and test surfaces that the effects of cloud cover on the solar radiation could be eliminated. However, it was found that the solar irradiation can vary as much as 50 percent within several minutes when the sun is behind clouds. Because of this it is recommended that field data be taken only on clear days and that readings from the standard surface be

checked only one or two times during the day to get an average reading after correcting by the cos ζ_o. Calculated readings from the standard surface can then be obtained for any time of the day by using the cos ζ_o where ζ_o is obtained from the program described in Appendix F.

The final conclusions are about the use of the balloon system for positioning a folding mirror. The technique was found to work well; however, it involved a great deal of time and effort to make the system work properly. It was seen that it is imperative that the balloon system be used only at times when the weather is good. This eliminates all but a few months of the year for Southern Louisiana. Also due to the difficulty found in using the balloon system, it is recommended that the platform mounted mirror method be used unless the area to be viewed is so large that this technique can not be made to work.

CHAPTER VIII

SUMMARY AND CONCLUSIONS

A technique based on the concept of using a large first surface reflector as a folding mirror was developed in order to obtain bi-directional reflectance data from large integrated natural surfaces. The technique consisted of using a spectroradiometer with a small angular field of view. The spectroradiometer is mounted on a turn-table with three degrees of freedom. Readings of reflected energy are made by positioning the radiometer to read from the folding mirror which reflects the energy from the surface being tested to the radiometer. Reflectance is obtained by dividing the readings made from a test surface by readings made from a standard surface.

The technique was used in three ways to obtain reflectance data. The first data was taken by setting up the equipment in the laboratory. In this case the folding mirror was mounted on a moveable platform which was stationed some 60 feet from the spectroradiometer. The test plots were placed in a pan beneath the folding mirror. The viewing angle for all the data taken was 15 degrees from the normal. This method was used to take bidirectional reflectance data on Saint Augustine and Bermuda grass and black alluvium soil. Data was taken in a wavelength range from 0.33 microns to 3.0 microns and at aource angles from -60 degrees to +60 degrees from the normal. Photolamps were used as the source for the data taken in the laboratory.

A second set of data on the reflectance of Bermuda grass was taken in the field. This data was taken in a similar manner to that described above except that the folding mirror mounted on the moveable

L-3

platform was 150 feet from the spectroradiometer. Also the sun became the source in the field tests, and the radiometer was powered by an electrical gas-powered generator. A third set of data on the reflectance of Bermuda grass was obtained by mounting the folding mirror 100 feet in the air with a tethered balloon system. Data was taken in the same manner as before except that the folding mirror was located at a different place, and there was small variation in the exact plot of grass viewed due to slight oscillations of the folding mirror (test runs 110, 111 and 112).

In order to make reflectance readings a spectroradiometer was designed around existing laboratory equipment and built. An eight inch Celestron 8 telescope was available and was used as the collecting optics. A Perkin Elmer Model 99 monochromator was also available and was used as the wavelength and bandwidth selector. Focusing and matching optics to transfer the energy from the telescope to the monochromator were designed and built. A 1P28 photomultiplier tube was used as the detector in the ultraviolet and visible portions of the electromagnetic energy spectrum. A lead sulfide detector was used in the region from 0.68 microns to 3.0 microns. All of the optical and detector portions of the spectroradiometer were mounted on a turntable to give three dimensional freedom to the system. The entire device was placed in the back of a truck when taking field data.

A Perkin-Elmer Model 13 amplifier was used with the spectro-radiometer. The amplified signal was recorded either on a Leeds and Northrup Speedomax G strip chart recorder or read from a digital voltmeter. Control of the spectroradiometer was made through the electrical system which was mounted in a 19 inch rack. Cables which

were easily disconnected were used to connect the rack mounted and turntable mounted portions of the spectroradiometer.

Another major system designed for this investigation was a tethered balloon system used to position the folding mirror above the ground. This system was designed and tested using 800 cubic foot balloons. From these tests it was found that a mirror could be positioned with a tethered balloon system with little lateral movement. However, it was found that one to two degrees of angular oscillations could be expected from the folding mirror. A final balloon system was launched and used to take reflectance data. The final system utilized a 1200 cubic foot balloon. Three main cables were used to position the balloon. These cables were wound on winches which were attached to iron stakes in the ground. Three smaller cables were used to position the folding mirror which was attached underneath the balloon. The oscillations of the folding mirror used on the final system was found to be less than one degree.

Data was obtained on the relative bidirectional reflectance (ratio of readings taken from a test surface to the readings taken from a standard surface under the same conditions) of Saint Augustine grass, Bermuda grass and black Mississippi delta alluvium soil. This data was taken with a viewing angle of 15 degrees from the normal and at source angles of zero and 15 degrees. Data was also obtained on the variations in the bidirectional reflectance with source angle for the test surfaces mentioned. This data was taken both in the laboratory and in the field for Bermuda grass.

There were a number of conclusions which resulted from the investigation. These conclusions fell into four categories; those

having to do with the technique developed; those about the design and use of the spectroradiometer; those dealing with the tethered balloon system; and those that resulted from the reflectance data taken. All of these areas are discussed in the following paragraphs.

The technique of taking reflectance data by using a large first surface reflector as a folding mirror was found to work extremely well. The data received using this technique was consistent and repeatable. The reflectance data generated from the grasses also agreed in general with the data presented in current literature for similar substances. The major advantage to the technique is that it allows large areas of a natural surface to be used in obtaining reflectance data. The technique of using a folding mirror also allows the spectroradiometer or other type of detector system to be placed on the same general level as the surface viewed and still to take data on the energy being reflected above the surface.

It was found, as expected, that much better data can be obtained when the technique is used in the laboratory. It is therefore recommended that the technique be used entirely in the laboratory to receive data unless atmospheric or solar effects are to be studied. It will also be necessary to take data in the field if the laboratory is not large enough that the distance between the detector system and the surface viewed allows a large enough field of view to include a well integrated sample of the surface to be studied. It is not recommended that the balloon system be used to position the folding mirror in the field unless it is the only way possible to obtain the data required due to the complexities and difficulties encountered when using this system.

The spectroradiometer that was designed and built was also found to work extremely well in the laboratory. It was possible with the system to record reflectance data for very narrow bandwidths of energy from 0.30 to 3.0 microns. The system also recorded the energy in a very small angular field of view. The biggest problem encountered with the system was saturation of the photomultiplier tube detector. This problem was easily remedied in the laboratory tests by using a lower intensity source. Because of this problem it is not recommended that the spectroradiometer as presently configured be used in field tests due to the high intensity of the solar radiation. However this problem could be solved by using a different type of detector in the visible region or by using some type of transmission filter to reduce the intensity of the energy received in the visible region.

The use of a tethered balloon system to position an object such as a folding mirror at a point in the sky worked only as long as the balloon stayed fully inflated and the winds were not too severe. When the system worked as designed, the mirror could be positioned with lateral movements of less than one inch and with angular movements of less than one or two degrees. The biggest problem with the system used in these investigations was that the balloons used did not meet the specifications of the original design study. The balloons had a high leak rate, did not maintain their aerodynamic shape during gusty winds and the stabilizers did not operate properly. It is not recommended that further work be done in this area unless it is found that balloons can be purchased or built which are better designed to meet the requirements of a tethered system as outlined in this report.

A considerable amount of reflectance data was obtained on grasses and soils during the investigations. It was found that soils and grasses have a low reflectance in the visible region. In the infrared region, the reflectance of grass is very high from 0.75 to 0.90 microns, whereas the reflectance of soils is low in this area. Further out in the infrared region (1.5 microns to 3.0 microns) the bi-directional reflectance curves of the two surfaces are very similar. It was found from the laboratory tests that in the ultraviolet region the reflectance of the soil was much higher than the reflectance of the grasses. As expected, there was a characteristic peak in the reflectance of the grasses in the visible region near 0.54 microns which is associated with the green color of the grasses.

Data was also taken on the variations in the bidirectional reflectance with source angle. It was found that significant variations did exist and that these variations were very different for the soil and grasses. It was found that for one of the grasses and the soil studied that the variations in the reflectance data showed significant changes as a function of wavelength.

BIBLIOGRAPHY

1. Knipling, Edward B. "Physical and Physiological Basis for the Reflectance of Visible and Near-Infrared Radiation from Vegetation," Remote Sensing of Environment, vol. 1 (1970), pp. 155-159.

2. Coblentz, W. W. "Radiometric Investigation of Infrared Absorption and Reflection Spectra," National Bureau of Standards Bulletin, vol. 2 (1906), pp. 457-462.

3. Coblentz, W. W. "Selective Radiation from Various Solids," National Bureau of Standards Bulletin, vol. 6 (1910), pp. 301-319.

4. Aldrich, L. B. "The Reflecting Power of Clouds," Smithsonian Miscellaneous Collections, vol. 69, No. 10 (1919),

5. Angstrom, A. "On the Albedo of Various Surfaces of Ground," Geogr. Ann., Stockh., vol. 7 (1925) pp. 323-342.

6. O'Neal, A. M. "Effects of Moisture on Soil Color," Soil Science, vol. 16 (1923) pp. 275-279.

7. Richardson, Lewis F. "The Reflectivity of Woodland, Fields, and Suburbs between London and St. Albans," Quarterly Journal of the Royal Meteorology Society, vol. 56 (1930), p. 31.

8. Krinov, E. L. "Spectral Reflectance of Natural Formations," Akad. Navk SSSR, Laboratoriia Aerometodov, Moscow, 1947 (Natl. Research Council of Canada, Techn. Transl. TT 439 by G. Belkov), Ottawa, 1953.

9. Fritz, Sigmund. "The Albedo of the Ground and Atmosphere," Bulletin of the American Meteorological Society, vol. 29 (1948), p. 303.

10. Neiburger, M. "The Reflection of Diffuse Radiation by the Sea Surface," Trans. Ameri. Geophys. Un., vol. 29 (1948) pp. 647-652.

11. Colwell, R. M. "Platforms for Testing Multi-Sensor Equipment," Proceedings of the Second Symposium on Remote Sensing of Environment, University of Michigan, Ann Arbor, Feb., 1963.

12. Ashburn, E. V. and Weldon, R. G. "Spectral Diffuse Reflectance of Desert Surfaces," Journal of the Optical Society of America, vol. 46 (1956) p. 583.

13. Graham, W. G. and K. M. King, "Short-Wave Reflection Coefficient for a Field of Maize," Quarterly Journal of the Royal Meteorology Society, vol. 87 (1961), pp. 425-428.

14. Boileau, A. R. and J. I. Gordon, "Atmospheric Properties and Reflectances of Ocean Water and Other Surfaces for a Low Sun," Applied Optics, vol. 5, No. 5 (May 1966) pp. 803-805.

15. Gordon, J. I. and G. V. Church, "Sky Luminances and the Directional Luminious Reflectances of Objects and Backgrounds for a Moderately High Sun," Applied Optics, vol. 5, No. 5 (May 1966), pp. 793-801.

16. Winkler, E. M. "Relationship of Air Photo Tone Control and Moisture Content in Glacial Soils," Proceedings of Second Symposium of Remote Sensing of Environment, Institute of Science and Technology, The University of Michigan, Ann Arbor, Feb., 1963.

18. McClellan, W. D., J. P. Meiners and D. G. On, "Spectral Reflectance Studies on Plants," Proceedings of Second Symposium of Remote Sensing of Natural Environment, Institute of Science and Technology, University of Michigan, Ann Arbor, Feb., 1963.

19. Watson, Robert D. "Spectral Reflectance and Photometric Properties of Selected Rocks," Remote Sensing of Environment, vol. 2 (1972), pp. 95-100.

20. Howard, J. A., R. D. Watson, and T. D. Hessin, "Spectral Reflectance Properties of Pinus Ponderosa in Relation to Copper Content of the Soil-Malachite Mines, Jefferson County, Colorado," Proceedings of the Seventh Symposium on Remote Sensing of Environment, University of Michigan, Ann Arbor, May, 1971.

21. Chia, Lin S. "Albedos of Natural Surface in Barbados," Quarterly Journal of the Royal Meteorology Society, vol. 93 (1967), pp. 116-120.

22. Salomonson, V. V. "Aniosotropy of Reflected Solar Radiation from Various Surfaces as Measured with an Aircraft-Mounted Radiometer," Proceedings of the Fourth Symposium of Remote Sensing of Environment, University of Michigan, Ann Arbor, Dec., 1966.

23. Salomonson, V. V. and W. E. Marlatt, "Airborne Measurements of Reflected Solar Radiation," Remote Sensing of Environment, vol. 2 (1971) pp. 1-8.

24. Salomonson, V. V. and W. E. Marlatt, "Anisotropic Solar Reflectance over White Sand, Snow, and Stratus Clouds," Journal of Applied Meteorology, vol. 7, pp. 475-483.

25. Suits, Gwynn H. and G. R. Safir, "Verification of a Reflectance Model for Mature Corn with Applications to Corn Blight Detection," Remote Sensing of Environment, vol. 2 (1972), pp. 183-192.

26. Lyon, R. J. P. "Analysis of Rocks by Spectral Infrared Emission (8 to 25 μ)," Economic Geology, vol. 60 (1965) pp. 715-736.

27. Lyon, R. J. P. and J. W. Patterson, "Infrared Spectral Signatures-A Field Geological Tool," Proceedings of the Fourth Symposium on Remote Sensing of Environment, University of Michigan, Ann Arbor, December, 1966.

28. Yost, Edward. "The Reflectance Spectra of Mineralized Trees," Proceedings of the Seventh International Symposium on Remote Sensing of Environment, University of Michigan, Ann Arbor, May, 1971.

29. Miller, L. D. and R. L. Pearson, "Area Mapping Program of the IBP Grassland Biome: Remote Sensing of the Productivity of the Shortgrass Prairie as Input into Biosystem Models," Proceedings of the Seventh Symposium on Remote Sensing of Environment, University of Michigan, Ann Arbor, May, 1971.

30. Marshall, R. E., N. Thomson, F. Thomson, and F. Kriegler, "Use of Multispectral Recognition Techniques for Conducting Rapid, Wide-Area Wheat Surveys," Proceedings of the Sixth Symposium on Remote Sensing of Environment, University of Michigan, Ann Arbor, October, 1969.

31. Earing, D. L. and I. W. Ginsbey, "A Spectral Discrimination Technique for Agricultural Applications," Proceedings of Sixth Sympsoium on Remote Sensing of Environment, University of Michigan, Ann Arbor, October, 1969.

32. Tanguay, M. G., R. M. Hoffer, and R. D. Miles, "Multispectral Imagery and Automatic Classification of Spectral Response for Detailed Engineering Soils Mapping," Proceedings of the Sixth Symposium on Remote Sensing of Environment, University of Michigan, Ann Arbor, October, 1969.

33. Kolipinski, M. C., A. L. Higer, N. S. Thomson, and F. J. Thomson, "Inventory of Hydrobiological Features using Automatically Processed Multispectral Data," Proceedings of the Sixth International Symposium on Remote Sensing of Environment, University of Michigan, Ann Arbor, October, 1969.

34. Block, Myron J., "Emissivity of Granular Surfaces at Resonance Frequencies," Proceedings of the Third Symposium of Remote Sensing of Environment, Institute of Science and Technology, University of Michigan, Ann Arbor, November, 1965.

35. Buettner, K.J.K., C.D. Kern, and J.F. Cronin, "The Consequences of Terrestrial Surface Infrared Emissivity," Proceeding of the Third Symposium on Remote Sensing of Environment, Institute of Science and Technology, The University of Michigan, Ann Arbor, November, 1965.

36. Gates, David M. and W. Tantraporn, "The Reflectivity of Deciduous Trees and Herbaceous Plants in the Infrared to 25 Microns," Science, vol. 115 (1952), p. 613.

37. Gansman, H. W., W. A. Allen, R. Cardenas, and A. J. Richardson, "Relation of Light Reflectance to Cotton Leaf Maturity," Proceedings of the Sixth Symposium on Remote Sensing of Environment, University of Michigan, Ann Arbor, October, 1969.

38. Oshiver, A. H., R. B. Stone, J. R. Clark, and G. A. Besberisn, "Factors in Measurement of Absolute Sea Surfaces Temperature by Infrared Radiometry," Proceedings of the Third Symposium on Remote Sensing of Environment, Institute of Science and Technology, University of Michigan, Ann Arbor, November, 1965.

39. Rose, H. M., D. C. Anding, and J. Walker, "A Computer Program to Calculate Atmospheric Effects on Infrared Wavelength Radiation," Proceeding of the Seventh Symposium on Remote Sensing of Environment, University of Michigan, Ann Arbor, May, 1971.

40. Turner, R. E., W. A. Malila, and R. F. Kalepka, "Importance of Atmospheric Scattering in Remote Sensing, or Everything You've Always Wanted to Know about Atmospheric Scattering but Were Afraid to Ask," Proceedings of the Seventh Symposium on Remote Sensing of Environment, University of Michigan, Ann Arbor, May, 1971.

41. Hisim, D. H. "Detection of Air Pollution by using a Hohlraum Spectral Analyzer," M. S. Thesis, Department of Mechanical Engineering, Louisiana State University, December, 1972.

42. Hapke, Bruce and Hugh Van Horn, "Photometric Studies of Complex Surfaces with Applications to the Moon," Journal of Geophysical Research, vol. 62 (August 1, 1963), No. 15, pp. 4546-4569.

43. Shockley, W. G., S. J. Knight, and E. Libscomb, "Identifying Soil Parameters with an Infrared Spectrophotometer," Proceedings of Second Symposium on Remote Sensing of the Environment, Institute of Science and Technology, University of Michigan, Ann Arbor, February, 1963.

44. Chen, Hsi-shu and C. R. N. Rao, "Polarization of Light on Reflection by Some Natural Surfaces," British Journal of Applied Physics, vol. 1, Ser. 2 (1968), pp. 1191-1196.

45. Stockhoff, E. H. and R. T. Frost, "Polarization of Light Scattered from Moist Soils," Proceedings of the Seventh Symposium on Remote Sensing of the Environment, University of Michigan, Ann Arbor, May, 1971.

46. Coulson, K. L. "Effect of Surface Reflection on the Angular and Spectral Distribution of Skylight," Journal of Atmospheric Sciences, vol. 25 (September, 1968), pp. 759-770.

47. Coulson, K. L. "Effects of Reflection Properties of Natural Surfaces in Aerial Reconnaissance," Applied Optics, vol. 5 (June 1966), No. 6, pp. 905-917.

48. Coulson, K. L., G. M. Bouricius, and E. L. Gray, "Optical Reflection Properties of Natural Surfaces," Journal of Geophysical Research, vol. 70 (1965), pp. 4601-4611.

49. Hodarev, Y. K., B. S. Dunaev, B. N. Rodionev, A. L. Aerebryakyan, Y. M. Tchesnokov, and V. S. Etkin, "Some Possible Uses of Optical and Radio-Physical Remote Measurements for Earth Investigations," Proceedings of the Seventh Symposium on Remote Sensing of Environment, University of Michigan, Ann Arbor, May, 1971.

50. Maples, D. and J. F. Hagewood, "Design and Construction of a Remote Sensing Apparatus," Final Report NGR-19-001-068, Louisiana State University, 1972.

51. Holmes, R. A. "Field Spectroscopy," Remote Sensing with Special Reference to Agriculture and Forestry, National Academy of Sciences, 1970.

52. Foster, Ronald B. "A Stable Platformed Tethered Balloon," Department of Mechanical, Aerospace, and Industrial Engineering, Louisiana State University, August 9, 1972 (unpublished report).

53. Hoerner, Sighard F., Fluid Dynamic Drag, Great Britain, 1958.

54. Jakob, Max, Heat Transfer, John Wiley and Sons, Inc., 1949, pp. 23-58.

55. Wiebelt, J. A., Engineering Radiation Heat Transfer, Holt, Rinehart and Winston, Inc., 1966.

56. Thekaekara, M. P., Extraterrestrial Solar Spectrum, NASA Goddard Space Flight Center.

57. Fowles, G. R., Introduction to Modern Optics, Holt, Rinehart and Winston, Inc., 1966.

58. Holter, M. R. "Infrared and Multispectral Sensing," Bio Science, vol. 17 (1967) pp. 376-383.

59. Boucher, Paul E., Fundamentals of Photography, D. Van Nostrand Company, 1963.

60. Scherz, J. P. and Alan R. Stevens, An Introduction to Remote Sensing of Environmental Monitoring, University of Wisconsin, August, 1970.

61. Anderson, R.M., Letter from the 3M Company, Decorative Products Division, July 26, 1974.

62. Escobal, P. R., Methods of Orbit Determination, John Wiley & Sons, Inc., New York, 1951.

63. American Ephermis and Nautical Almanac, U. S. Government Printing Office, Washington, DC, 1974.

64. Chapman, S., The Earth's Magnetism, John Wiley & Sons, Inc., New York, 1951.

APPENDIX A

STATE OF THE ART SURVEY OF REMOTE SENSING TECHNIQUES IN THE THERMAL-ORIGINATED ENERGY REGION

Characteristics of Thermal Radiation

All bodies at a temperature above absolute zero emit energy due to the temperature of the body. This energy is normally referred to as thermal radiation. Thermal radiation is associated with the molecular vibration and/or rotation of a system and as such is a function not only of the temperature of the system but also the substance and molecular structure of which the system is made. Energy emitted in the same wavelength range as thermal radiation due to non-thermal effects is possible but is negligible for most cases.

The total amount of thermal energy emitted from a body can be obtained from the Stefan-Boltzmann law, $E = \epsilon\sigma T^4$ [54]. In this relationship, E is the total amount of energy emitted by the body, ϵ is the total emittance of the body, σ is the Stefan-Boltzmann constant and T is the absolute temperature. The total emittance is defined as the ratio of the total energy emitted from a real body to that emitted from a black or perfect body at the same temperature.

A black body is an ideal body or surface which is a perfect radiator and a perfect absorber of thermal energy. Therefore, for a black body the energy emitted is a function only of the temperature of the body and is the maximum amount of thermal energy which a body at that temperature can emit. This ideal case is called a black body since such a surface would appear black to the eye at room temperature. Surfaces which appear black, however, are not black bodies. For instance soot which appears black to the eye absorbs only 95 percent of the thermal radiation rather than 100 percent which would be necessary to classify it as a black body. A black body is best

represented naturally by using a hollow enclosure with only a small hole in it. The hole can then be considered a black body.

Max Planck, near the turn of the century, developed theoretically an equation for the intensity of the thermal energy being emitted from a black body as a function of wavelength. Planck using the quantum theory that radiation is made up of a multitude of finite parts found that the distribution of monochromatic, unpolarized thermal energy emitted by a perfect system of dipole oscillators (that is, a perfect emitter which is a black body) is

$$E_{b\lambda} = \frac{C_1}{\lambda^5}\left[\frac{1}{\exp\ (C_2/\lambda T) - 1}\right]$$

where

$E_{b\lambda}$ = monochromatic energy emitted normal to the surface

λ = wavelength of emitted energy

$C_1 = 5.889 \times 10^{-6}$ erg^{-1}-cm^2/sec

$C_2 = 1.43879$ cm-^{o}K

This distribution is shown plotted in Figure A-1. By differentiating with respect to λ and setting equal to zero, it can be shown that this relationship obeys Wien's displacement law that $\lambda_{max}T$ is a constant [55]. Performing the calculations results in

$$\lambda_{max}T = 0.2883 \text{ cm-}^{o}\text{K}$$

which corresponds to experimental results. This line is shown plotted in Figure A-1. The monochromatic linear polarized radiant energy normal to the radiating surface is $E_{b\lambda}/2$. The monochromatic radiation in the hemispherical space above a radiating surface element is $\pi E_{b\lambda}$.

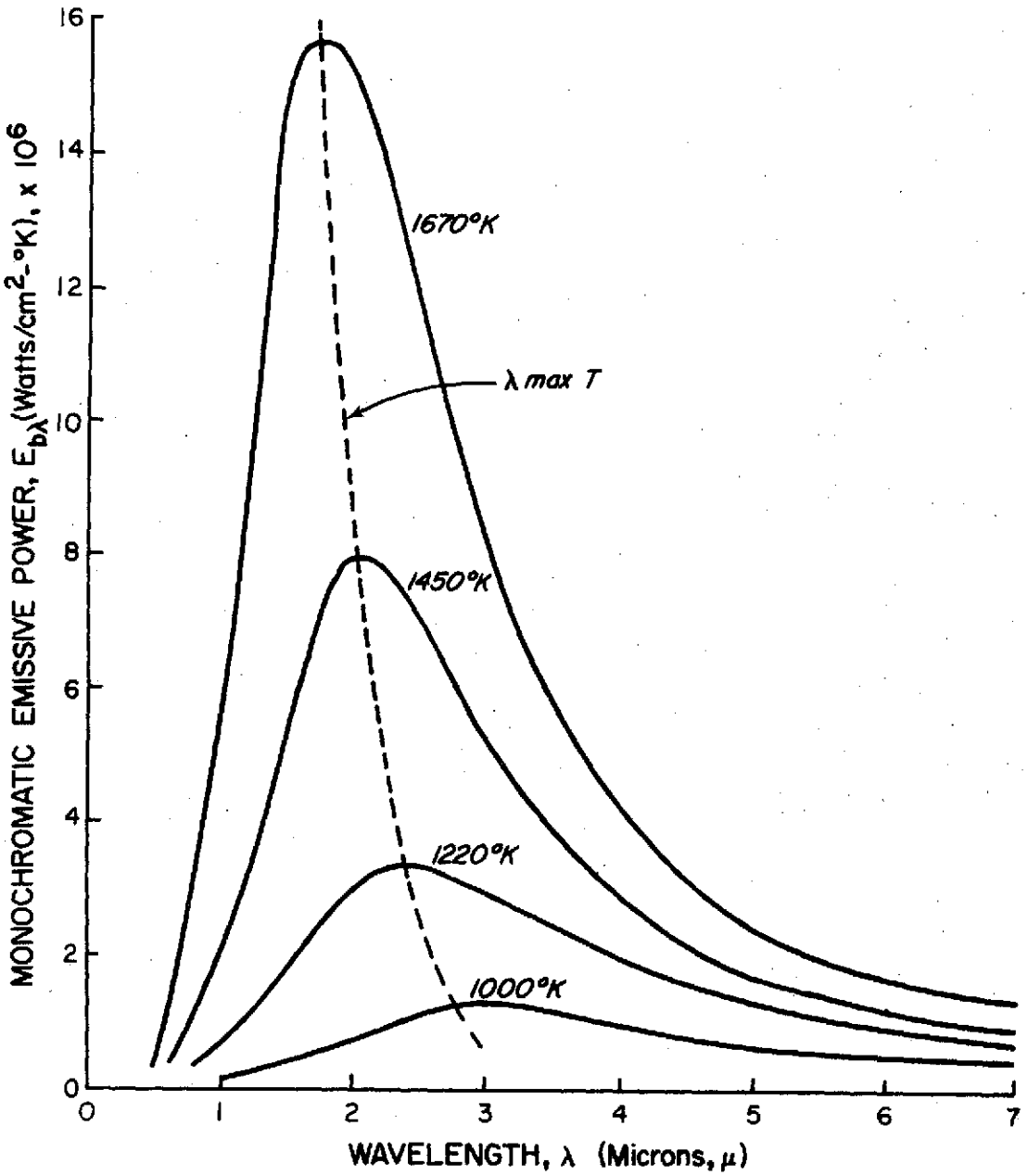

FIGURE A-I. EMISSIVE POWER OF A BLACK BODY AS A FUNCTION OF TEMPERATURE AND WAVELENGTH

By integrating to find the area under the curves in Figure A-1, the total energy (E) emitted from a black body can be found. This gives the same results as for the total energy radiating from a surface as obtained with the Stefan-Boltzmann equation when the emittance (ϵ) is unity. Therefore,

$$E_b = \int_o^\infty E_{b\lambda}\, d\lambda = \sigma T^4$$

It is noted from Figure A-1 that as the temperature of a black body increases the peak of the energy radiated is shifted to a shorter wavelength. Also there is a sharp decline in the intensity of the energy emitted at wavelengths shorter than the wavelength at which the maximum energy is emitted. This accounts for an object not flowing or emitting radiation in the visible region until a certain temperature is reached. An object as it is heated will first glow dull red as it gets hot enough to just emit in the visible region. As the temperature is increased, the object will glow more intensely and become yellow, white, and then bluish in color.

Most thermal radiation received on the earth comes from the sun. A plot of the solar spectral irradiance is given in Figure A-2. This curve was originated by NASA [56] and at present is considered the best estimate of the solar spectral irradiance of the earth at the average sun-earth distance in the absence of the earth's atmosphere. Using the standard curves developed by NASA, the integrated value of the solar energy received by the earth is 135.1 mw/cm^2.

Using the NASA data the effective black body temperature of the sun was found to be 5630.7°K. This was calculated by finding the temperature of the normalized blackbody curve which minimized the area

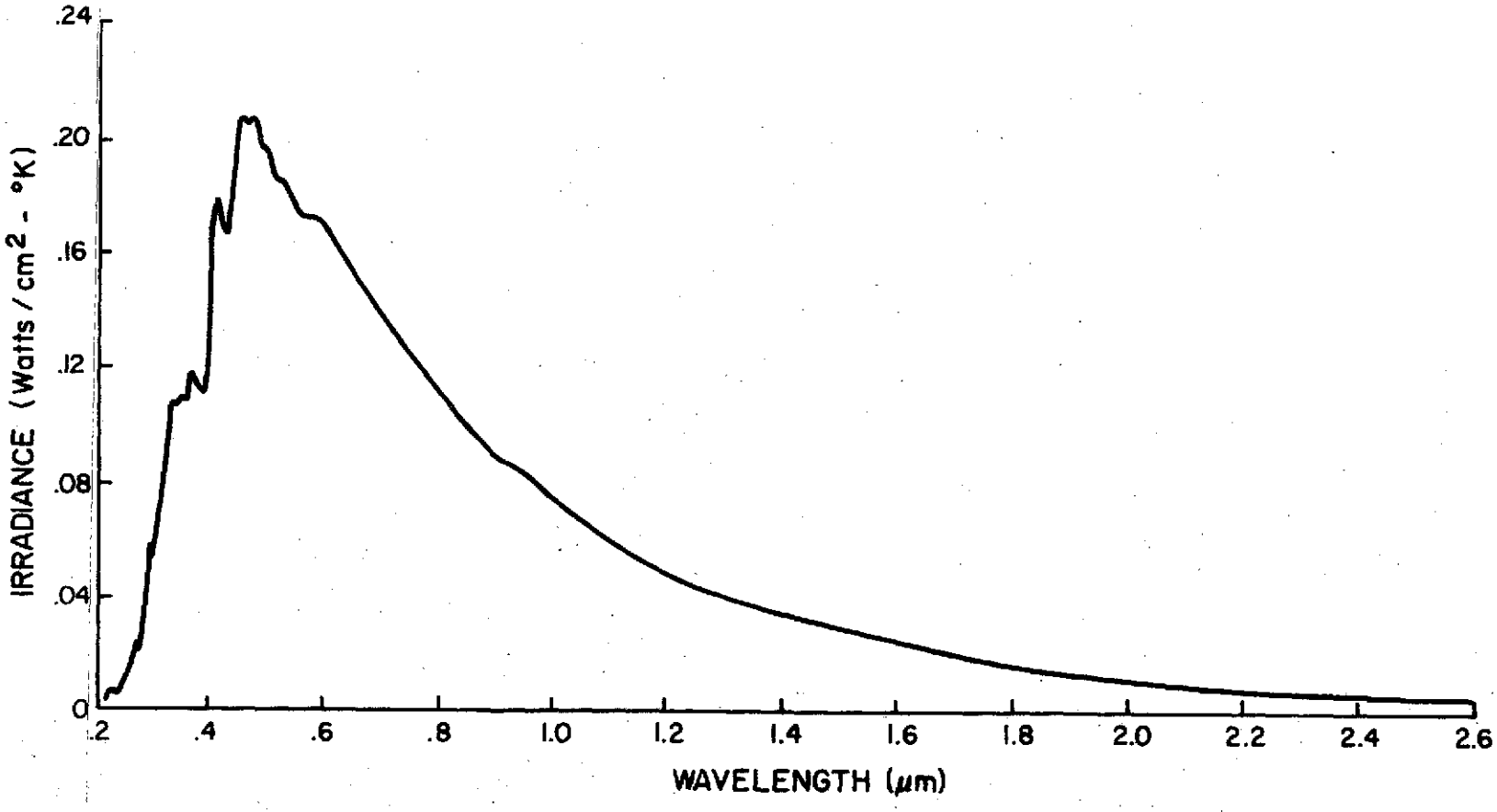

FIGURE A-2. SOLAR SPECTRAL IRRADIANCE

enclosed between the blackbody curve and the standard solar curve. If the temperature of the sun is computed by Wien's displacement law; that is, $\lambda_{max}T$ = constant from Figure A-2, the sun's temperature is found to be 6166°K. λ_{max} was taken to be at 0.47μ. Using the Stefan-Boltmann equation, the temperature of the sun is calculated to be 5762°K. The Stefan-Boltmann constant, σ, has a value of 5.6699×10^{-12} watts per sq cm-$^{o}K^{4}$ [57].

Thermal energy is categorized according to the wavelength of the emitted or reflected energy. The visible region is from 0.4 to 0.7 microns and is so called because the human eye is responsive to energy in this region. It is interesting to note from Figure A-2 that the solar energy peaks in this region. In the visible region, the eye and mind interpret energy in the wavelength range of 0.4 to 0.5 microns as blue, 0.5 to 0.6 microns as green and 0.6 to 0.7 microns as red. Energy with a wavelength less than 0.4 microns is called ultraviolet, and energy with a wavelength greater than 0.7 microns is called infrared. The infrared region is considered to end at 1000 microns and the microwave region begins. Energy in the infrared region can be focused with mirrors, lenses, and other optical devices like visible light. It can also be transmitted through some materials which are opaque to visible light. Forty per cent of the sun's energy conveyed to the earth is in the infrared region. Energy with a wavelength longer than 1000 microns is not considered thermal in origin. The infrared region is often divided into three arbitrary regions; 0.7 to 1.5 microns is the near infrared, 1.5 to 6 microns is the middle infrared and 6 to 1000 microns is the far infrared region.

As a body is heated, the frequency of propagation of the emitted energy increases and the peak of the energy distribution curve is shifted to shorter wavelengths. Thus all bodies emit energy in the infrared region, but it is only when they are heated to a relatively high temperature that they emit energy in the visible region. The normal temperature of the earth is $300^{o}K$ in which case the energy peaks at approximately 10μ and can only be detected with sensitive instruments called thermal detectors [58].

Figure A-3 shows a representation of the emitted energy from a black, gray, and real body such as a natural surface, all at the same temperature. For the Stefan-Boltzmann Law, $E = \epsilon\sigma T^4$ we can find the energy emitted by a black body by letting $\epsilon = 1.0$. However, for real surfaces the emittance can range from 0.05 to 0.95. If we assume that the emittance, ϵ, is not a function of the wavelength, then the surface is considered to be a gray body and the emitted energy is as shown. Actually, the emittance of a real surface is also a function of wavelength and causes the monochromatic emissive power curve of natural surfaces to look somewhat as shown for the real body in Figure A-3. The term monochromatic or spectral refers to the fact that most thermal properties are a function of wavelength as well as temperature. The monochromatic emittance (ϵ_λ) of a surface is defined as the energy emitted at a temperature T and a specific wavelength to the energy that would be emitted at that wavelength if the surface were a black body at temperature T [55]. Written symbolically,

$$\epsilon_\lambda(T, \text{ system}) = \frac{E_\lambda(T, \text{ system})}{E_{b\lambda}(T)}$$

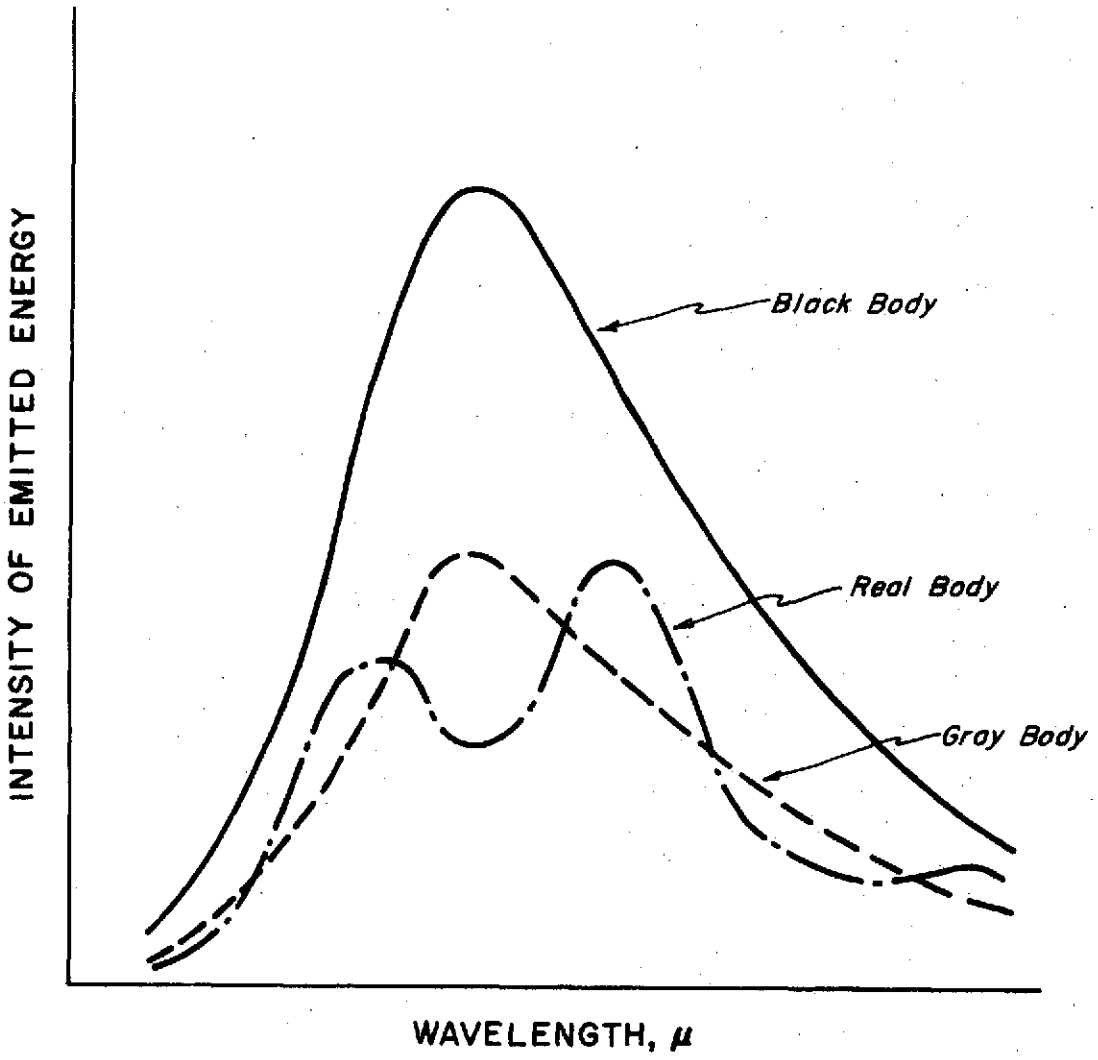

FIGURE A-3. EFFECT OF EMITTANCE ON EMITTED ENERGY

The overall or total emittance is

$$\epsilon(T, \text{system}) = \frac{\int_o^\infty \epsilon_\lambda(T, \text{system})\, E_{b\lambda}(T)\, d\lambda}{\int_o^\infty E_{b\lambda}(T)\, d\lambda}$$

Like emittance, reflectance is also a function of wavelength and surface temperature. Reflectance is defined as the ratio of the incoming radiation to the outgoing radiation if the emitted energy is omitted. Reflectance can also be defined totally or monochromatically. Therefore, curves similar to those shown in Figure A-3 are representative of the reflected as well as the emitted energy. Due to the natural situation that exists on the earth, most measurements made in the visible and near infrared region of natural surfaces in a natural environment are of the reflected energy originating from the sun. Measurements made in the far infrared are generally from the emitted energy from the terrain. A representation of this is given in Figure A-4. The relative intensity of the energy sensed in the different regions is not shown to scale.

Reflectance and emittance as defined are still incomplete in their definitions due to the angular characteristics of these properties for natural surfaces. Total hemispherical reflectance was defined as the inverse of the ratio of the total energy ingoing to a surface element (dA) through a hypothetical hemispherical surface enclosing the surface element to the total amount of energy being reflected outgoing through the hemisphere (see Figure A-5d). Bidirectional reflectance is the ratio of the intensity of the reflected energy outgoing from a surface at a particular angle to the intensity of the incoming energy at any other angle (Figure A-5a). Directional emittance is similarly defined in terms of the intensity of the energy emitted

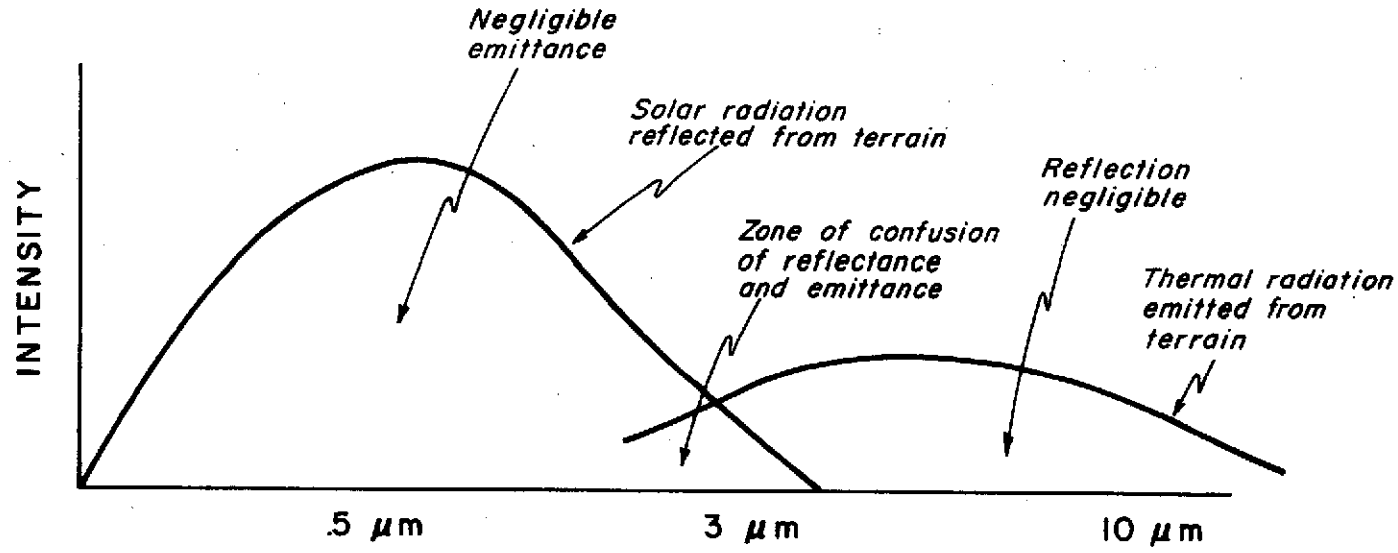

FIGURE A-4. SCHEMATIC OF ENERGY SENSED IN REMOTE SENSING

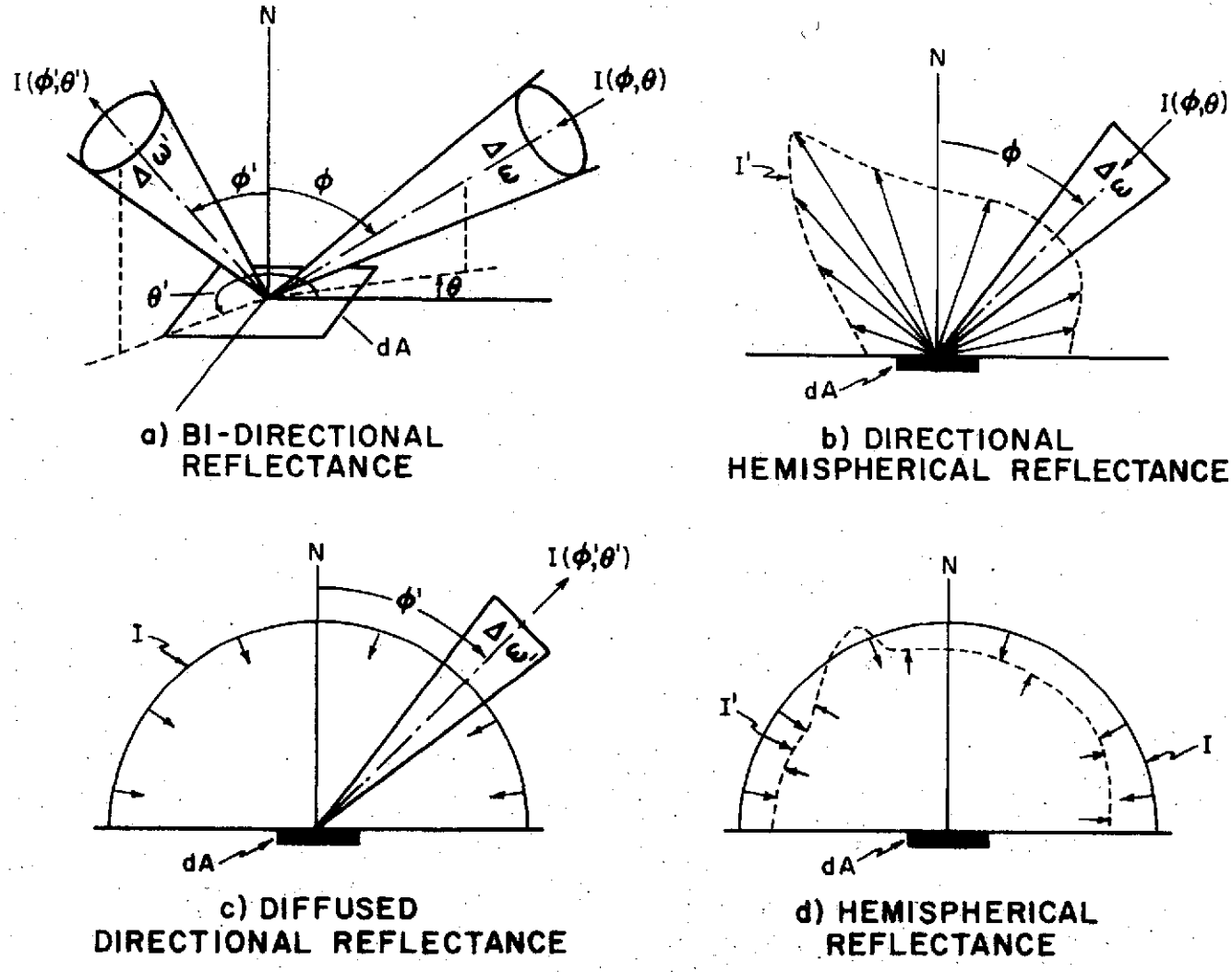

FIGURE A-5. REFLECTANCE TERMINOLOGY

at a particular angle to the intensity of energy that would be produced by a black body at the same temperature at that angle. Diffuse directional reflectance is defined as the ratio of the energy being reflected in a particular direction to the total diffuse energy incoming to the system (Figure A-5c). None of these definitions for reflectance fit exactly the conditions that exist when doing remote sensing of natural surfaces in the natural environment since solar radiation after passing through the atmosphere contains both spectral and diffuse components. Therefore, reflectance as used in remote sensing is based on a combination of the definitions as given in Figure A-5a and A-5c and like the emittance is a directional quanity.

Since the directional characteristics of reflectance and emittance are used in remote sensing, reflectance and emittance are functions not only of the temperature and wavelength, but also the directional quantities. Thus the reflectance and emittance is a function of the temperature of the surface, wavelength, nature of the incoming energy, angle at which the energy is being read, as well as the molecular structure of the surface.

One of the problems involved in measuring the reflectance and emittance characteristics of natural surfaces in the natural environment is determining the characteristics of the solar irradiation. Figure A-1 gives a best estimate of the solar irradiance on the earth assuming the earth has no atmosphere. However, the atmosphere acts as an attenuation of this incoming radiation in many ways. Also since atmospheric conditions are a variable, there will be a variable effect on the radiation received on the surface of the earth.

Lord Rayleigh was the first to theorize about light being scattered by dust particles and molecules of air. He stated that the intensity of the light scattered by suspended particles in the atmosphere is inversely proportional to the first power of the wavelength. Therefore, the effect of scattering is much greater in the ultraviolet region than in the visible region. Also since the violet and blue wavelengths are shorter, energy represented by these colors is scattered more and results in a red sunset since the light is traveling a greater distance through the atmosphere.

Solar radiation is also attenuated by the atmosphere due to the presence of gases which block out or absorb the solar energy at various wavelengths. These effects are shown in Figure A-6. The transmittance (τ_λ) as shown is defined as the per cent of energy transmitted through the atmosphere to the total amount incoming. In some regions the transmissions is blocked almost completely by water vapor, carbon dioxide or a combination of the other gases present in the atmosphere. The regions which are relatively open are often called windows. It is noted that the visible region is one such open region. Due to the water vapor in the air, the atmosphere virtually closes energy transmission beyond the 25 micron wavelength region to the microwave region. Because of this effect, measurements made in the infrared region are generally limited to the infrared windows.

The question must now arise as to what it is that we measure when we use a remote sensing device. This is best represented by Figure A-7. The energy measured is that incoming at a specific angle from a natural surface to a remote sensing device on board an aircraft or satellite. This energy is a function of the solar irradiance (G_{sun}), atmospheric

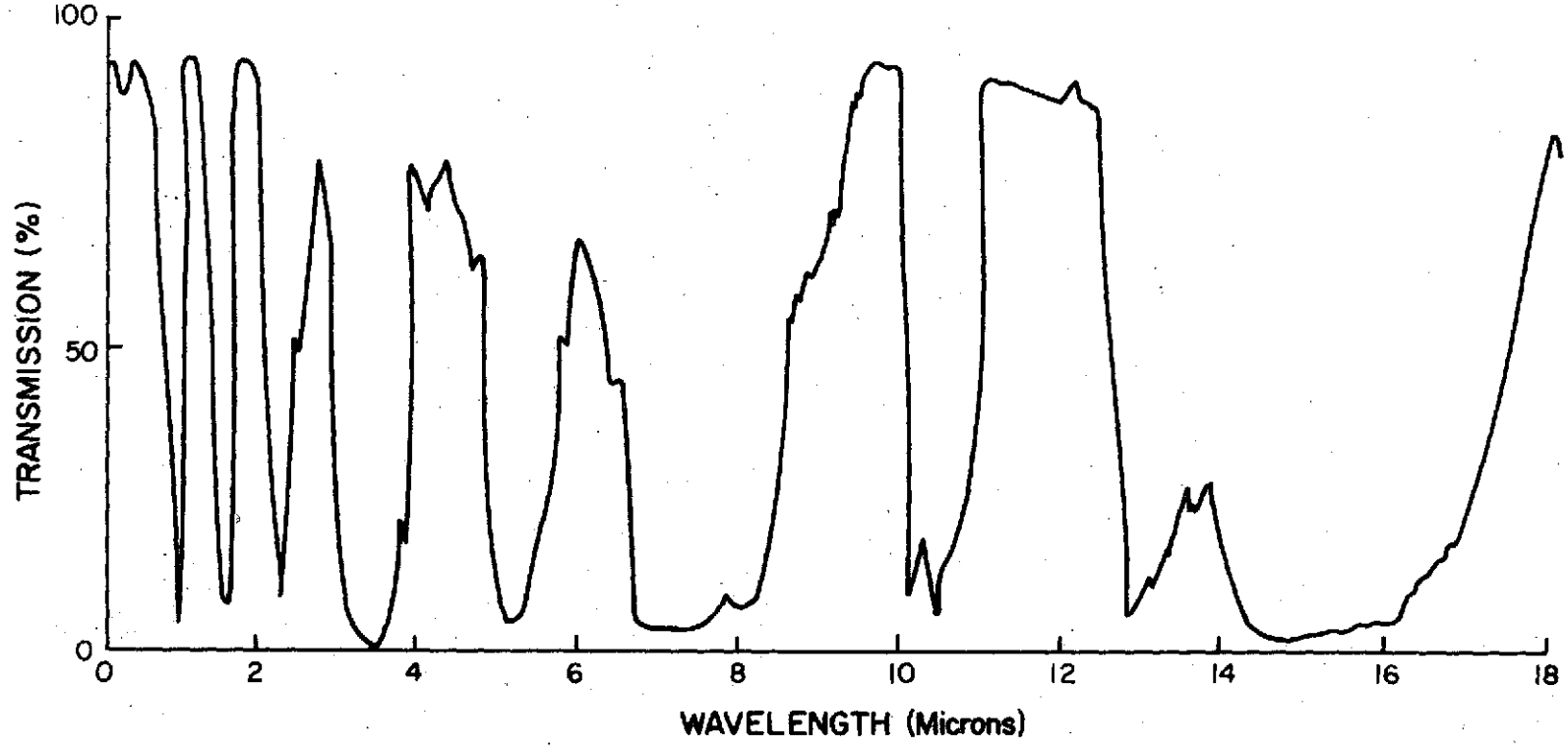

FIGURE A-6. TRANSMISSIVITY OF THE ATMOSPHERE

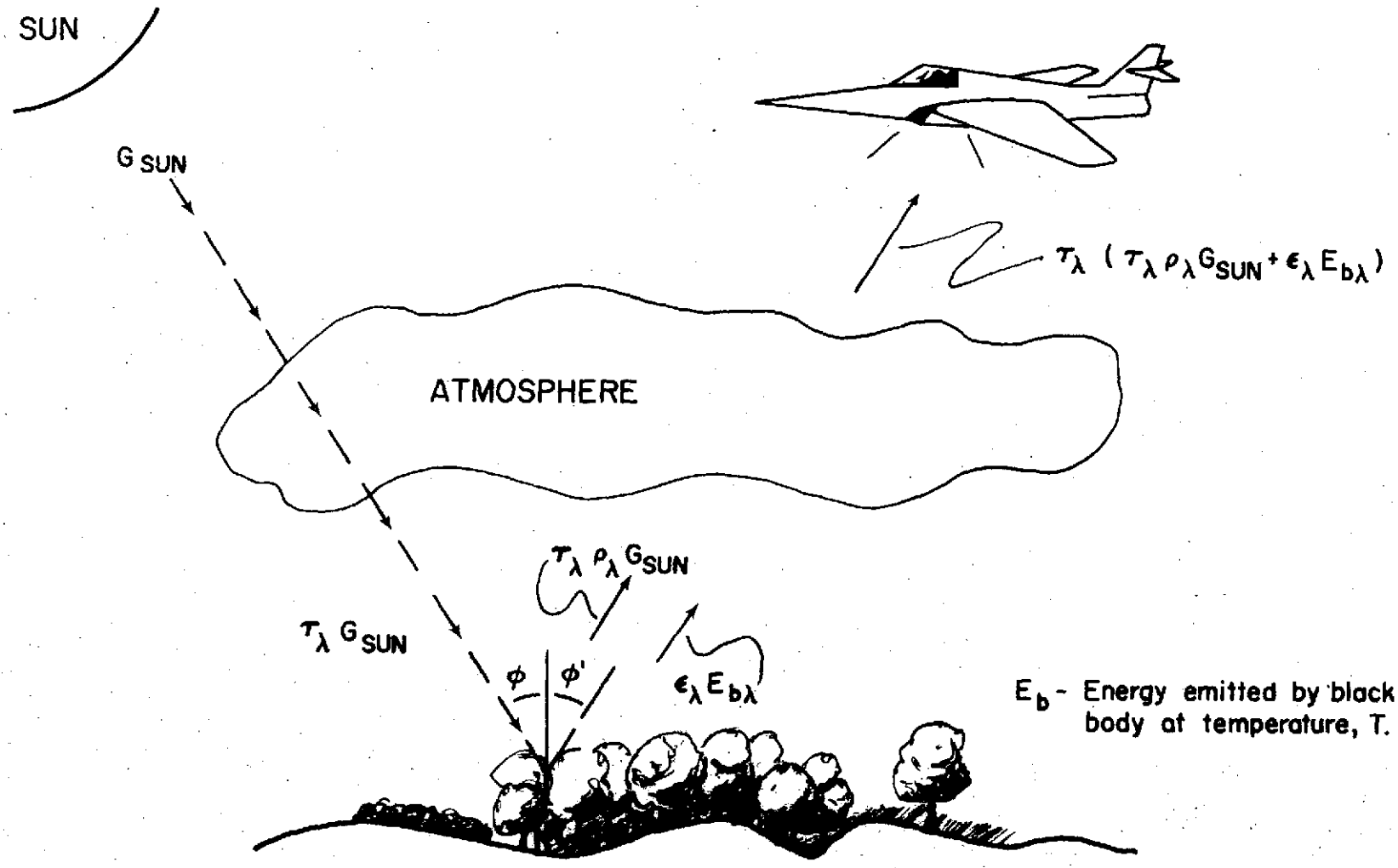

FIGURE A-7. WHAT IT IS WE MEASURE.

transmissivity (τ_λ), and the reflectance (ρ_λ) and emittance (ϵ_λ) properties of the surface, all functions of wavelength (λ). The reflectance and emittance are also functions of the orientation of the irradiance (φ',θ'), the sensing angle (φ,θ), the temperature of the surface, the surface conditions and the surface itself. Other factors which are involved include the effects of the atmosphere in scattering the solar energy so that both a diffuse and a spectral component result and the difference between the transmissivity effects on the incoming solar energy and the reflected energy outgoing from the terrain to the aircraft. All of these factors make it rather difficult to interpret the information received by remote sensing.

Simply stated, the energy measured by remote sensing is that energy reflected and emitted by the surface transmitted to the sensing device. However, in order to interpret this information so that identification of the surface is possible, knowledge of the effects of all the factors mentioned in the paragraph above must be known. In many practical applications now being made of remote sensing, these problems are minimized by sensing on days when atmospheric conditions are similar and by maintaining the sensing angles and the sun's angular orientation the same. Ground truth measurements are then made to determine specific spectral characteristics of the reflectance properties of the surfaces to be identified.

If we consider measuring the incoming energy from a natural surface to a remote sensing device as a function of wavelength, then the data received can be called a spectral characteristic of the surface measured. However, in order for this characteristic to be useful in identifying the surface, the effect of all major variables on this characteristic

may be required unless ground truth measurements are obtained which can be used to eliminate these variables or a unique pattern is found independent of the variables. The larger the wavelength spectrum over which spectral data can be obtained, the more likelihood a unique identifying pattern can be found. Thus each natural surface may have a unique spectral pattern which if known can be used to identify the surface. By using the entire thermal spectrum and dividing it into small enough wavebands, the effect of many of the natural and system variables may also be determinable. If so, identification of natural surfaces and surface characteristics can be more easily made and under less strenuous conditions than now required.

Figure A-8 shows the type of instruments which are used in remote sensing and the wavelength range in which they can be used. Photography is a common means of remote sensing but does not readily lend itself to automatic processing and is limited in the wavelength range of the energy it records.

Thermal scanners are used to record data in the infrared region. These devices convert the intensity of the energy measured in a small wavelength spectrum into a voltage reading which is recorded. These devices can be operated day or night. They are described in greater detail in a later section.

A multispectral scanner is a series of measuring instruments of the same nature as the thermal scanner except that the entire thermal energy spectrum is divided into as many as eighteen regions, and the energy in each of these regions is recorded. This type of technique can be used to make a complete spectral recording of a natural surface

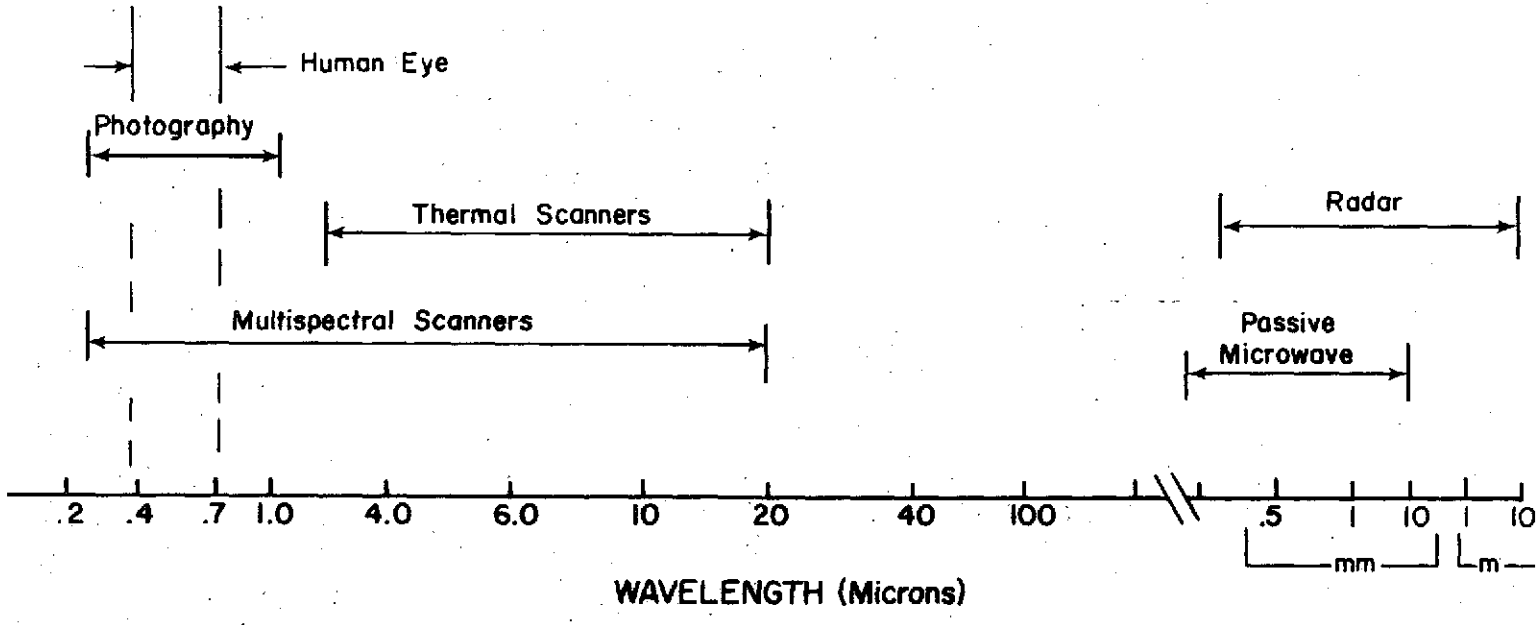

FIGURE A-8. RANGE OF OPERATION OF COMMON REMOTE SENSING INSTRUMENTS

if enough devices are used to divide the thermal wavelength spectrum into small waveband regions.

Radar and microwave systems are based on energy measurements using sources that are not thermal in origin and are not considered in this report. However, they do have an advantage over methods based on thermal radiation in that longer wavelength energy in this region is not blocked by the atmosphere. Therefore, they can be used day or night and in any weather conditions since the longer wavelength energy used in radar is not affected by cloud cover.

Photographic Systems

The most widely used remote sensing device is aerial photography. Photographic systems range from small hand-held cameras used with light aircraft to complicated multiple cameras that photograph in different regions of the electromagnetic spectrum which are carried in the bay or cargo area of large multi-engine aircraft. These systems record on photographic film the selective reflection of the sun's energy from the terrain. Just as each object has its own particular color, so will each terrain feature have a particular reflectance curve in the ultraviolet and infrared region as well. Many times with an aerial camera system, selective terrain features can easily be identified from the resulting photographs.

Remote sensing by photography is relatively cheap and simple and is generally the most advantageous method of doing remote sensing if the information one is seeking can be obtained this way. However, photography has not been developed that responds to energy emissions throughout the electromagnetic spectrum. Perhaps the biggest

disadvantage to photographic techniques is that they are a qualitative rather than a quantitative method. That is, photography records the intensity of the energy reflected from the terrain in large bandwidths and only approximately. A photograph will not tell you in exact terms the amount of energy received nor what is its exact wavelength. Because of this, a photograph will not look exactly like the original terrain. Photographs are also not readily amendable to automatic processing. For these reasons, the information which can be recorded by photography is limited in nature and use. However, photography is still the most common method used in remote sensing.

The two variables which are important in photography are the sensitivity of the film and the bandwidth and amount of energy allowed to reach the film. The fundamental mechanism used to control the amount and type of energy reaching the film is the camera. In its simplest form, it is no more than a darkened box with a pinhole in one side. The film is fixed in place on the opposite side of the box. The only disadvantage to this simple type of arrangement is that a pinhole does not admit much light, and therefore an unduly long time would be required for exposure. Therefore, a lens which admits more light and focuses the light onto the film is generally used instead of a pinhole.

The most important element of photography from the standpoint of the engineer or scientist involved in remote sensing is the film. The camera is basically an optical mechanical device used to project the energy coming from an image onto the film. The film however must record this energy in a manner that is as reproducible and as consistent as possible. Since most photographs obtained in remote sensing are analyzed

by the human eye, the response of the film and resulting picture should also match that of the eye as closely as possible.

Modern ordinary films use silver salts or halides as the light sensitive emulsion. This is fixed on a backing or support which is generally cellulose nitrate or acetate. This coating of emulsion ranges from 0.0012 to 0.0016 inches thick. Emulsions can be made sensitive to many different ranges of the electromagnetic energy spectrum as shown in Figure A-9. Printing paper is an example of a type of film which is sensitive only to the ultraviolet and blue region of the spectrum. Because of this, a red or yellow light will not expose printing paper. Orthochromatic film is film that is sensitive to ultraviolet, blue, and green light. Therefore, this film will not respond to a red light. Many earlier films were of this type.

The most common film in use today is called panchromatic. It is sensitive to ultraviolet as well as all of the energy in the visible range. Because its sensitivity range is very similar to that of the human eye, it is considered the optimum for most uses. The image produced is shades of black and white corresponding generally to the intensity of the energy received in the visible range from the object or terrain photographed.

Panchromatic film is developed and used in a manner similar to that discovered by Tolbert. The image to be photographed is focused through the camera lens onto the film and the shutter opened for a predetermined amount of time. The light entering the camera sensitizes the grains of silver salt in the emulsion. The grains of silver salt that have been acted upon by the light will be turned to silver when the film is emmersed in a developer solution. Next, the film is washed in an

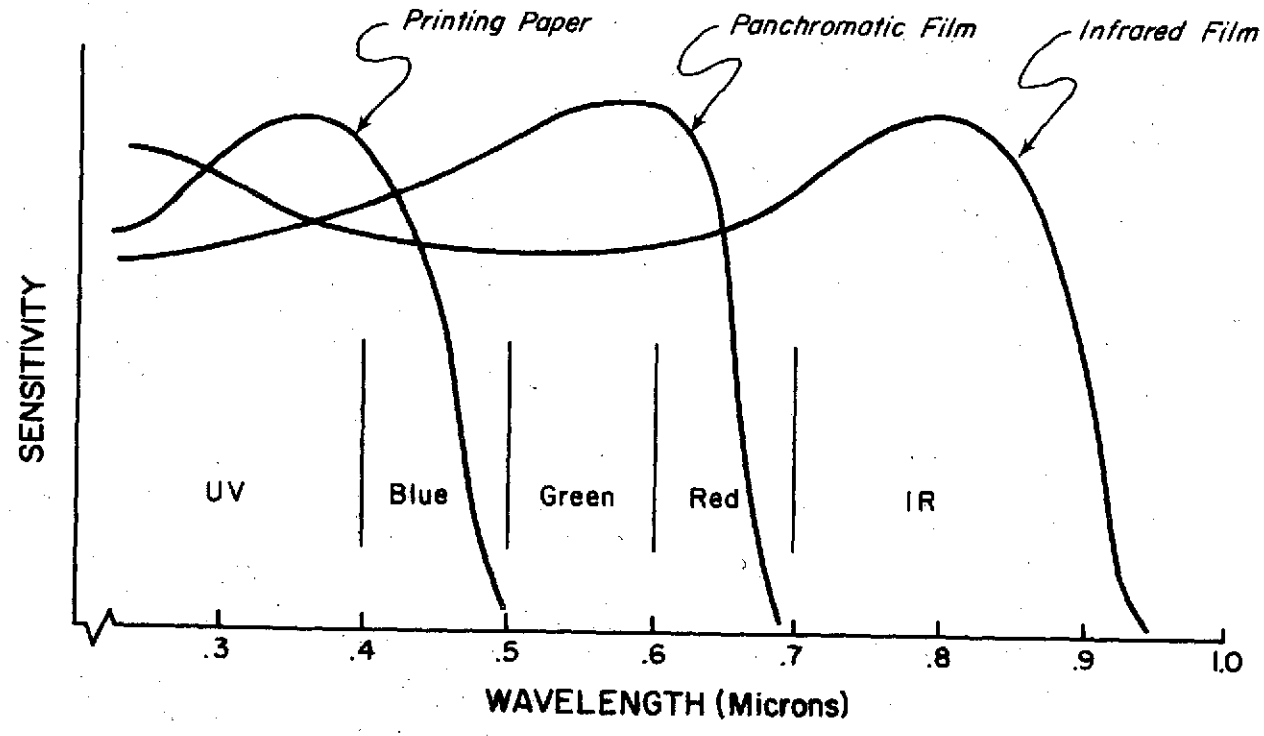

FIGURE A-9. SENSITIVITY OF VARIOUS BLACK AND WHITE FILMS EMULSIONS

acidic stop bath to stop the action of the developer. The film is then bathed in a solution called hypo which washes the unaffected silver salts away, and finally it is rinsed in water and dried [59].

The film is then left with blackened silver where the light activated the film and clear where there was no light. Since this is the reverse of the photographed image, it is called a negative. A positive is made by putting the negative over similar light sensitive paper and passing light through the negative in such a manner that it exposes the emulsion on the other piece of light sensitive paper. The second film will be the reverse of the negative and is called positive since its tones correspond to tones or intensity of reflected energy as they existed in reality. The positive is developed and processed in much the same manner as the negative.

Resolution of the film is determined by the grain size of the silver salts. If we consider the picture pattern as made up of individual grains or clusters, no smaller details could be represented than the grain size. In the actual case, location and light intensity affect resolution as well as film processing. However, grain size is a limiting factor and for this reason the silver salt crystals are very numerous. For example, in the case of panchromatic film the grain size is of the order of 0.2 microns.

One problem involved in film is the halation effect which is the reflection of light from the emulsion support layers after the light has passed through the emulsion. This effect can produce a halo effect around the object if long exposure times are required. Halation is reduced by using a dye coating on the film support that absorbs any energy transmitted through the emulsion.

Another problem involved with films is that during developing the emulsion swells when it is wetted and then shrinks when dried. In order to counterbalance this effect, a hardened gelatin is put on the back of the film support in order to keep the film from curling.

One of the problems involved with the use of black and white film is that the image formed represents the total energy reflected throughout the ultraviolet and visible spectrum without regard to color. This means that a green object that reflects as much total energy as a red object will look the same. Therefore, with black and white film, most objects must be distinguished by shape rather than color. In the case of the reflectance curves shown in Figure A-10, the intensity or lightness of an object in the terrain in a photograph will be the same if the area under the energy reflected curve is the same in the visible region and if panchromatic film is used. However, if the range of the sensitivity of the film is extended into the infrared region as shown in Figure A-9, the tones will be different for live green vegetation as compared to green netting. If a filter or blocking lens is used that allows only the infrared energy to enter the camera, the tones on black and white infrared film will be even more distinctive for the reflectance curves shown in Figure A-10c.

Black and white infrared film is made similar to panchromatic film. Most silver salt emulsions are sensitive only to ultraviolet and blue light and must be treated with special dyes to make the film sensitive to the longer wavelength energy. By further treating the emulsion, film manufacturers have been able to extend the sensitivity of the emulsions to energy in the near infrared region. The response of this type of film is shown in Figure A-9. Increasing the sensitivity of

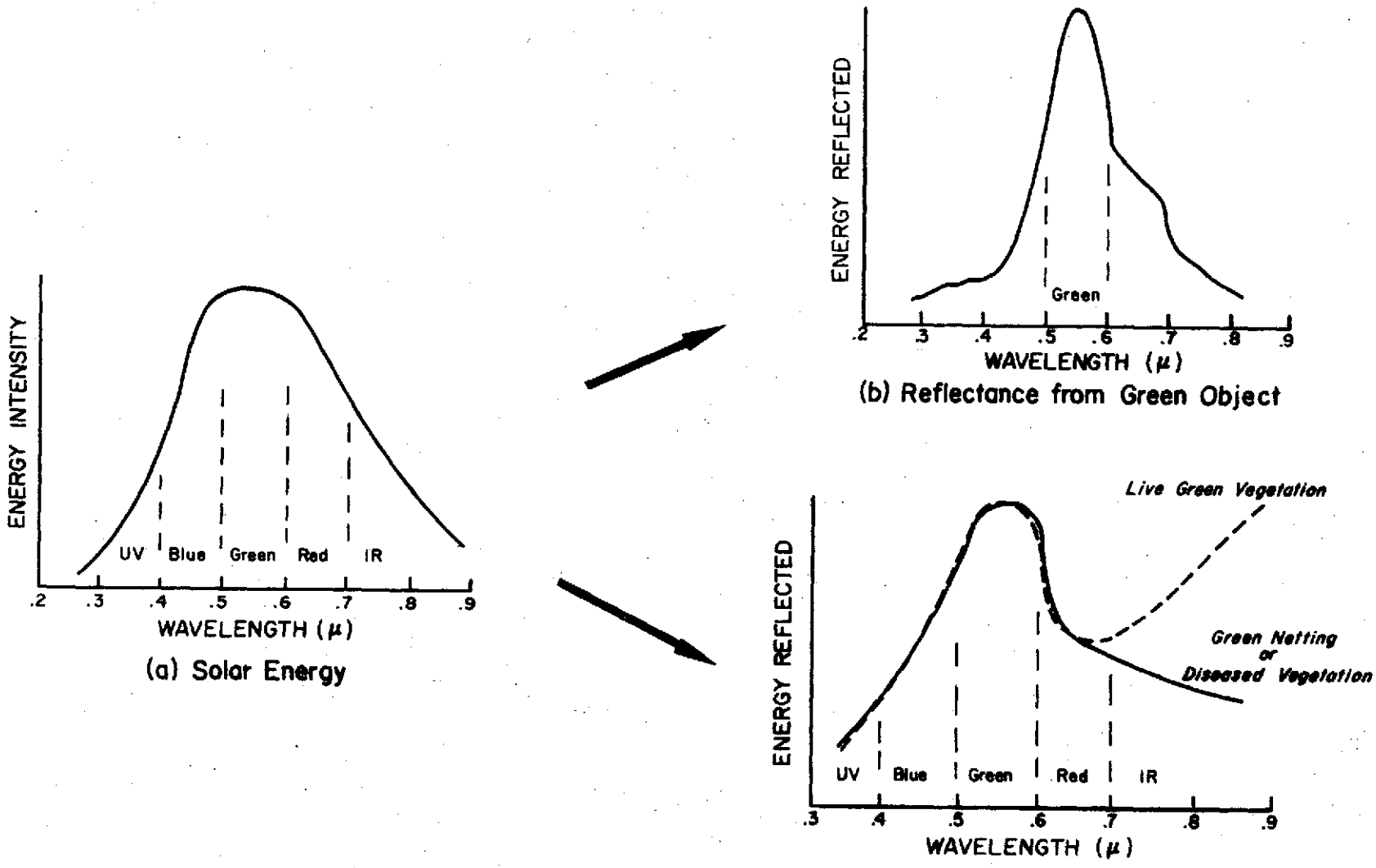

FIGURE A-10. TYPICAL REFLECTANCE CURVES

the film to wavelengths much beyond 1.2 microns appears to be impractical since it would be difficult to keep the film from being exposed by the emitted energy from the film's surrounding or by the camera itself [60].

Infrared photographs of radiation in the middle and far infrared wavelength range can also be made by electronic means. The photograph is made from a recording of an electrical signal produced by an infrared detector. The recorded electrical signal is used to vary a light source which point by point exposes a segment of photographic film. Thus, an image of the infrared radiation is produced.

Another improvement that increased the usefulness of photography for remote sensing was the manufacture of normal color film. With color film, the incoming radiation can be recorded in three different bandwidths corresponding roughly to blue, green, and red light (see Figure A-11). The emulsion of color film is similar to that of black and white film in that it also consists of silver salts; however, three layers instead of one are used as shown in Figure A-11 [60]. Each layer reacts the same as for black and white film except that by special treatment during manufacture each layer is made sensitive to only a certain portion of the visible region of the energy spectrum. Also a blue blocking filter is used as shown. The results are film in which the top layer reacts to blue light, the second layer to green light, and the bottom layer to red light.

The exposure of color film with a camera is the same as in black and white film. Light is captured on each layer in response to the intensity of the light in the region in which each layer is sensitive. In the first step of development, the exposed halides in each layer

are turned to black crystals of silver salts. This is the same as for black and white film. There are two types of processes from this point on in the development of color film. One process, the color negative process produces a negative prior to making a print. The second process is called color reversal and results directly in a correct tone color transparency from the film. The second process is generally used in making color slides.

In the color negative process, the black silver salts in each layer are replaced by complimentary colors to the basic colors of blue, green, and red. That is, the silver grains in the blue layers are replaced by a yellow dye. The silver grains in the green layers are replaced by magenta dye, and the silver grains in the red region are replaced with a cyan dye. The complimentary colors are used since yellow is composed of red and green light which is the absence of blue. Similarly magenta is composed of red and blue wavelengths and cyan is composed of blue and green light. The resulting negative is a true color negative in that the opposite or compliment of each color has been used in the layer sensitized by light with the wavelength of the original color. Therefore, when white light is shown back through the color negative and a similar type film is exposed, a positive corresponding to the original colors of the object photographed will be produced.

Therefore, the color negative process is very similar to the black and white film process. In summary, the silver salts of the three sensitized layers are developed and replaced by the complimentary colors of the colors of the original object. The unused salts are washed away, and the negative is then used to make a positive by

exposing through the negative a piece of color printing paper similarly sensitized. The accuracy of this technique in color representation that is, the amount of energy being reflected in each region, is dependent on the sensitivity of the film (see Figure A-11) and the characteristics of the dyes used. For scientific purposes the final color tone should be matched as closely as possible to that of the original object or terrain photographed. For art photography this may be of little importance.

With the color reversal process, the partially developed film itself is exposed so the complimentary layers are activated. The salts in the original sensitized layers are then washed away leaving only the compliments of the layers which were washed away. This results in the original colors of the object on the original film which is usually used as a color transparency.

During World War II another type of film was developed call Camouflage Detection film. This film was the first use of color infrared film. It was given this name, since camouflage could readily be identified using this type film. The sensitivity of a typical color infrared film is shown in Figure A-12. With this type film the ultraviolet region is usually eliminated by using a filter which blocks out all energy with a wavelength shorter than 0.4 microns.

In order to see the energy in the infrared region in a color photograph, a color must be assigned to the energy in this region. When this is done, only two colors remain to be assigned to the energy in the visible spectrum. This means for example that for the film shown in Figure A-12, blue and green reflected energy is photographed as blue, red is photographed as green and infrared energy is photographed as red.

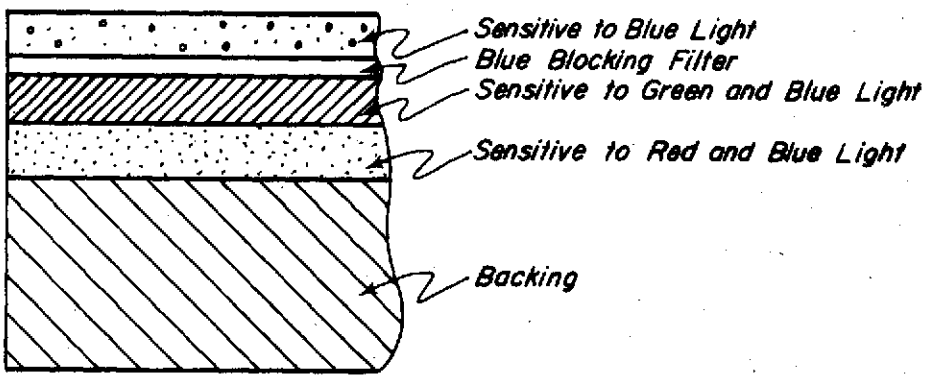

CROSS SECTION OF FILM

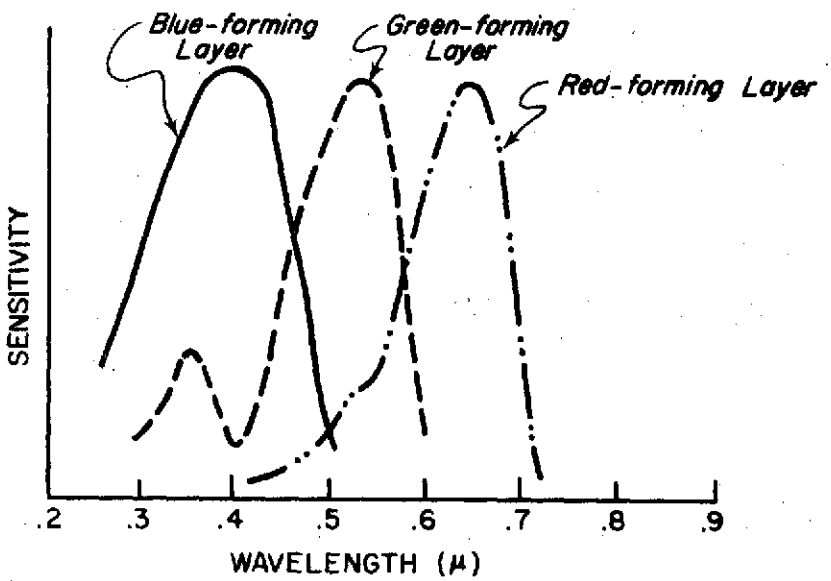

FILM SENSITIVITY

FIGURE A-11. TYPICAL NORMAL COLOR FILM

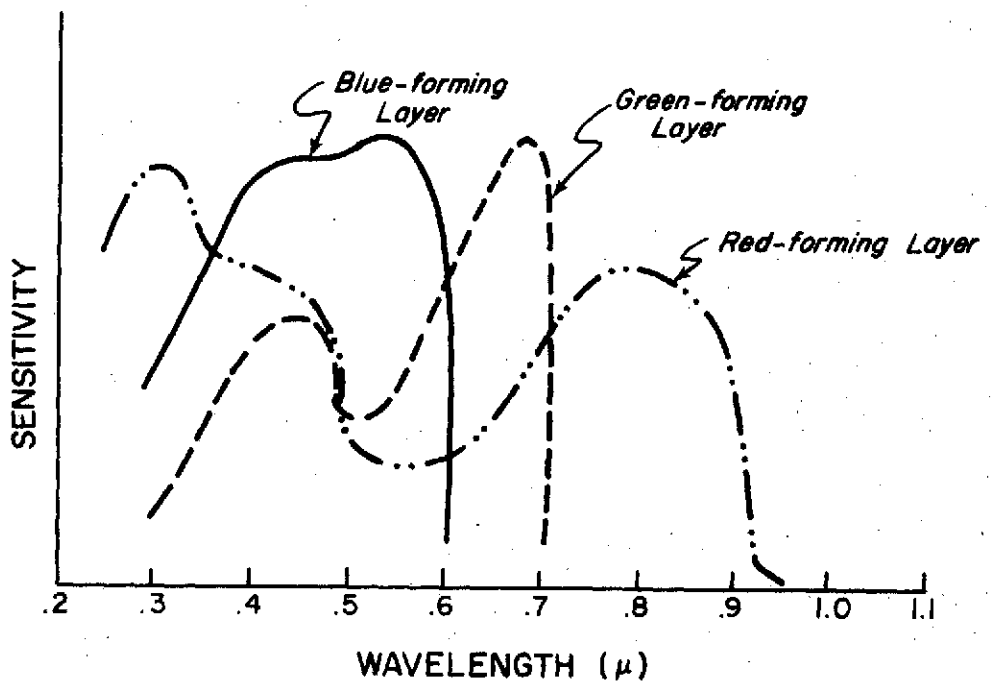

FIGURE A-12. SENSITIVITY OF TYPICAL INFRARED COLOR FILM

Since the colors are switched, this is referred to as false coloring. Different color combinations are possible so that color infrared film is not restricted to the color combinations given in the example. False coloring can also be produced with regular color film by switching the chemical dyes used in the different layers of the film.

Infrared photography is important and useful when the reflectance of the object to be sensed is very different in the infrared region from the surrounding even though the surroundings, or similar objects, may have the same or similar energy reflectance curves in the visible region and thus look the same. A typical example is shown in Figure A-10 for camouflage and healthy vegetation. The same type reflectance curves often result for diseased and healthy vegetation. In a regular color photograph the two may look the same but in a color infrared photo the live green vegetation will be a bright red, whereas diseased vegetation will be a dull purple. It has also been found that moisture content effects the reflectance in the infrared region to a great extent. The objective is therefore to use the film or film combination that distinguishes energy in the region where there is the most difference.

Another item which can be attached to a camera when used in remote sensing is a filter. This gives another variable to be used in conjunction with the film to obtain a desired result. A filter is in essence a device which is put between the film and the object viewed which governs the wavelengths of the energy which reaches the film. In this respect filters act to control the wavelengths of the energy received in much the same respect that the diaphragm acts to control the amount of energy received on the film.

Filters are often used to block unwanted parts of the reflected energy from reaching the film. For example, in the detection of camouflage or diseased vegetation the only difference in the spectral characteristics of the object being detected and its surroundings may be in the infrared region. In this case the subject will be more easily identified if the visible and ultraviolet portions of the energy spectrum are blocked by a filter, and only the infrared energy is received on the film. Also, it has been noted that atmospheric haze is caused by scattering of the ultraviolet and shorter wavelength light. Therefore, if a filter is used which blocks energy in this region, the haze will not show up in the photograph.

Narrow band pass filters are also available with which it is possible to select only a particular band such as 0.4 to 0.5 microns and record only the image of the energy reflected in this region. By using combinations of filters and films, energy can be recorded in any narrow region of the ultraviolet, visible or near infrared region desired. Therefore, the bandwidth which best distinguishes the terrain feature or object that is to be sensed can be selected. An example of this, is the detection of oil slicks where the ultraviolet part of the spectrum is the best for identification.

The three most commonly used types of camera systems for remote sensing are the conventional single lens camera, panoramic and strip cameras, and multiband or multilens camera systems.

The single lens aerial camera is an airborne camera consisting of a magazine, a drive mechanism, a cone and lens. The magazine is the light tight box that holds the film. The magazine of most modern aerial cameras utilizes a continuous roll of 9-1/2" by 200' roll of film.

With this film about 250 exposures can be made. Each exposure is approximately 9" x 9". The drive mechanism is used to position the film for each exposure. During an exposure, suction is created at the back of the film by means of a vacuum to hold the film flat against the back plate at the instant of exposure to eliminate wrinkling of the film and subsequent distortion in the photograph. The cone is a light tight mechanism which holds the lens correctly in relationship to the film. The length of the cone is a function of the focal length of the lens. The lens is compound and gives a fixed focus with the focus at infinity. In most aerial cameras the shutter is between the front and the rear elements of the lens. The shutter speeds are as high as 1/500 to 1/1000 of a second. The drive mechanism recocks the shutter after each exposure. Any type of film can be used with the single lens aerial camera which can also be fitted with filters if desired.

Relatively accurate measurements of terrain feature can be made with single lens aerial cameras; however, they only make photographs of a narrow strip of the territory over which the camera is flown. Therefore, strip or panoramic camera systems may be more useful to the investigator than a single lens camera if photographs of a large amount of territory is needed.

One type of panoramic camera consists of nine lens. The main lens is located in the center with eight other lens surrounding it in a circle with their optical axes parallel to the main lens. A series of mirrors focus the view of the surrounding lens so that in effect the optical axis is changed to look outward at the boundary of the area that the main lens views. The effect is a panoramic view which looks

like one image but is in effect composed of nine photographs. The angular coverage of this type of camera is 130°.

Another type of camera is the strip camera. This type of camera presents the results as a single strip rather than individual frames. Instead of a round aperture a slit is used which is perpendicular to the line of flight. The film is generated to move at a speed consistent with the ground speed of the aircraft. The shutter then remains open from the time the film is fed into the camera until the time the camera runs out of film. If the aircraft followed a level straight path, the resulting photograph would be relatively free of distortion. However, this is practical only in theory.

A third type of panoramic camera often used in remote sensing is a strip panoramic camera. The use of this type of camera makes it possible to photograph a large area in a single exposure with high resolution. A narrow field is required to minimize aberration of the lens. A narrow slit parallel to the camera platform line of flight is used and the camera is equipped to pan perpendicular to the flight line to make a panoramic picture. The optical train of the system is designed to make such movements. In order to maintain a clear focus on the film while the camera is panning, the film must be held in an arc while it is exposed. This makes the photographic scale become progressively smaller as the distance to the objects on the left and right of the flight path are increased. However, for some applications the advantages of this type of system outweighs the disadvantages.

A third type of camera system and the one most applicable to problems involving identification of natural objects by remote sensing is the multiband or multilens camera. A multiband camera system makes

several simultaneous black and white photographs in different bands of the electromagnetic energy spectrum. A variety of film and filter combinations are used to get the bands desired. They provide the user with the possibility of photographing in many narrow portions of the energy spectrum at a single point in time and space. Since multiple photographs with black and white film are made, this technique gives higher spatial resolution than any of the other systems mentioned. Also by multiple projection through the film transparencies with light shown through color filters a color projection can be made which is more true in tones and color than in regular color photography. Similarly, false color projections can easily be made. This technique can also be used to convert the imagery on the photographs to electrical signals which can fairly readily be adapted to automatic processing by a computer.

An example of a multiband camera is the U. S. Army C.R.R.E.L. Four Camera System. The system uses 70 mm film and has four Hasselblad cameras mounted on a platform that simultaneously operates the cameras. This system is relatively inexpensive and easy to use. A more complex multiband system is the ITEK Nine-Lens Multiband Camera. Three strips of 70 mm film are simultaneously exposed with this camera which has nine separate lens. Caution must be made when using this type of system to calibrate each image. Whenever different films are used in systems such as these, care must be exercised in interpreting the results since the spectral sensitivity of each batch or type of film may be different.

The simplest, cheapest, and easiest multiband camera system to use is to mount several small 35 mm cameras on a common frame and

operate them simultaneously. This type of system was used by the University of Wisconsin in their remote sensing studies. The system can be hand-held and carried aboard a small aircraft for minimum economy. For many applications in remote sensing, this type of system will probably prove the most economical if general differences in spectral responses are all that is required in interpreting the data.

Photography and in particular, multiband photography has several advantages as well as limitations when used for remote sensing of the natural environment. A major advantage of photographic systems is the spatial resolution which results from the photograph. This gives the analyst a great deal of ground detail to be used in analyzing the data. Photography as now developed also covers a range in the energy spectrum three times that of the human eye. Compared to other types of systems employed for remote sensing, photography is the least complicated and expensive to operate. This appears to be the main reason for its being the primary technique employed in remote sensing.

There are a number of limitations to photography which must be considered when using photography for remote sensing. For one thing photography is limited to detection of energy with a wavelength between 0.3 and 1.2 microns. If remote sensing by detection in an energy region other than this is required, another type of system must be used. Also photography records the energy received in large bandwidths such as the entire visible portion of the spectrum or the blue portion. This limits greatly the amount of true spectral data which can be obtained.

The response of the photographic method is not the same as the response to the human eye. Therefore, the tones or colors in

a photograph will not be exactly like the object photographed as viewed by the human eye. This does not necessarily present a problem unless the photographic response is not repeatable. However, the density of grains exposed when subjected to a constant intensity of energy is not a linear function of the exposed time. This function is called the characteristic curve of the emulsion and is not only non-linear but also changes somewhat from batch to batch due to handling, atmospheric conditions and other causes. Therefore, repeatability of the photographic process is somewhat questionable if a high degree of accuracy is required. The characteristic curve of films (density of grains exposed versus energy intensity) is also different for different types of films and wavelength of the energy recorded.

Also the truth and repeatability of the photograph depends not only on the sensitivity of the emulsion itself but the entire photographic process as well. Thus the amount and color of the light, the spectral energy sensitivity of the emulsion, the type of developer, method of developing, fixing and drying as well as the physical conditions of humidity and temperature, contribute to the final result. For this reason photography may be considered a qualitative rather than a quantitative technique.

Finally, photographs generally have to be interpreted manually which is slow and time consuming since it is rather difficult to convert the output from a photographic system to a form which can be input to a computer or automatic data processing machine. This difficulty is partially overcome by making black and white transparencies with multiband systems. However, a great deal of equipment and effort

is still required in the automating process, and the discrete number of accurate voltage levels corresponding to the original irradiation as depicted by the shades of gray in the photograph appears limited to twenty or less in most cases.

Electronic Detection Systems

One of the disadvantages of photography for remote sensing is its limitation to sensing in only the visible and near infrared regions. However, electronic sensing systems have been developed which can operate in the middle and far infrared regions as well as the visible and near infrared region. Another advantage of electronic detector systems is that their output is generally in a form readily adaptable to automatic processing. For this discussion these systems will be categorized into two groups. One is thermal scanning systems which operate in the infrared region from 3 to 14 microns and multispectral scanning systems which record energy in bands throughout the ultraviolet, visible, and the infrared regions as well.

When considering the entire wavelength region of energy originating from a thermal origin, the spectrum extends from 0.2 or 0.3 microns to 1000 microns. However, the practical limit for measuring energy in this region in the natural environment ranges from 0.3 microns to approximately 15 microns. Fifteen microns defines the longest wavelength energy in the far infrared window (8-15 microns). The entire region from 0.3 to 15 microns is still very broad and, therefore several different types of electronic detectors must be employed in sensing energy throughout this region. The type of system used is also dependent upon the application and the response required of the

system. For this reason only a general description of the electronic detection systems used in remote sensing will be given. A more detailed discussion of the detector elements available will be made. The type of detector element used in a particular sensing system will generally depend on the application.

The basic element or building block of electronic detector systems is the radiometer, which is an instrument for measuring electromagnetic or acoustic radiation in a specific bandwidth. It measures the intensity of the energy being emitted or reflected from an object electronically. Its basic components are shown in Figure IV-1.

An optical device collects and focuses the energy from the object being sensed. In the laboratory this device may be a fiber optic probe or, as generally used in field work, may be a telescopic device. A wavelength selector selects the median wavelength of the energy to be sensed and width of the band. The selector may consist of filters, prisms and/or diffraction grating devices. If different wavelengths of energy are to be sensed over a time interval, a device such as a monochromater may be used which consists of prism and mirror devices which can be adjusted to select only the desired wavelength of energy required. The detector is used as the device which converts the photons of electromagnetic energy into an electrical signal. The signal is then amplified and recorded.

The radiometer can be used to measure energy throughout the electromagnetic spectrum if the proper detectors are used. This device can be used to measure temperature directly if the emissivity of the object being sensed is known. If the system is designed to operate in the middle or far infrared region, it is often called a

thermal or infrared sensing system. If put on board an aircraft and used to scan laterally across the flight path of the aircraft, the system becomes a thermal scanner. In this application, the recorder is generally photographic film. If a series of radiometers are integrated so that measurements are made in several different portions of the energy spectrum simultaneously and the system is put on board an aircraft and used in a scanning mode, the system is called a multispectral scanner.

The most commonly used electronic detection systems in remote sensing are the thermal and multispectral scanners carried on board aircraft. In the future it is expected that greater use will be made of these systems in many varying fields of applications. Also it is expected that systems of this type will be deployed in satellites.

A thermal scanner consists of a radiometer made to sweep side to side perpendicular to an aircraft line of flight and which senses energy in the 3-5 microns or 8-14 microns region. Figure A-13 shows the sweep characteristics of a thermal scanner carried on board an aircraft. The resolution is the smallest area which can be sensed by the system and corresponds to one data point in a scan. The area shown shaded in Figure A-13 represents the resolution which depends on the optics of the system, the angular field of view, and the altitude at which the aircraft is flying. The data received can be recorded on electromagnetic tape for automatic processing at a later time, displayed on a cathode ray tube, used to make an infrared photograph or all three may be done simultaneously. A typical schematic of a thermal scanning system is shown in Figure A-14 [60].

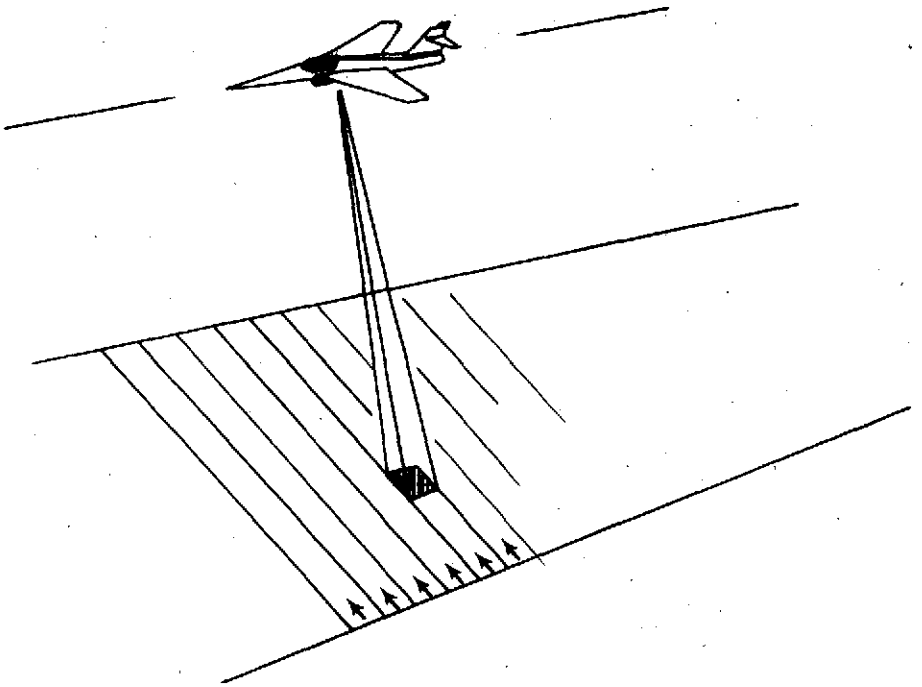

FIGURE 13. METHOD OF SCANNING

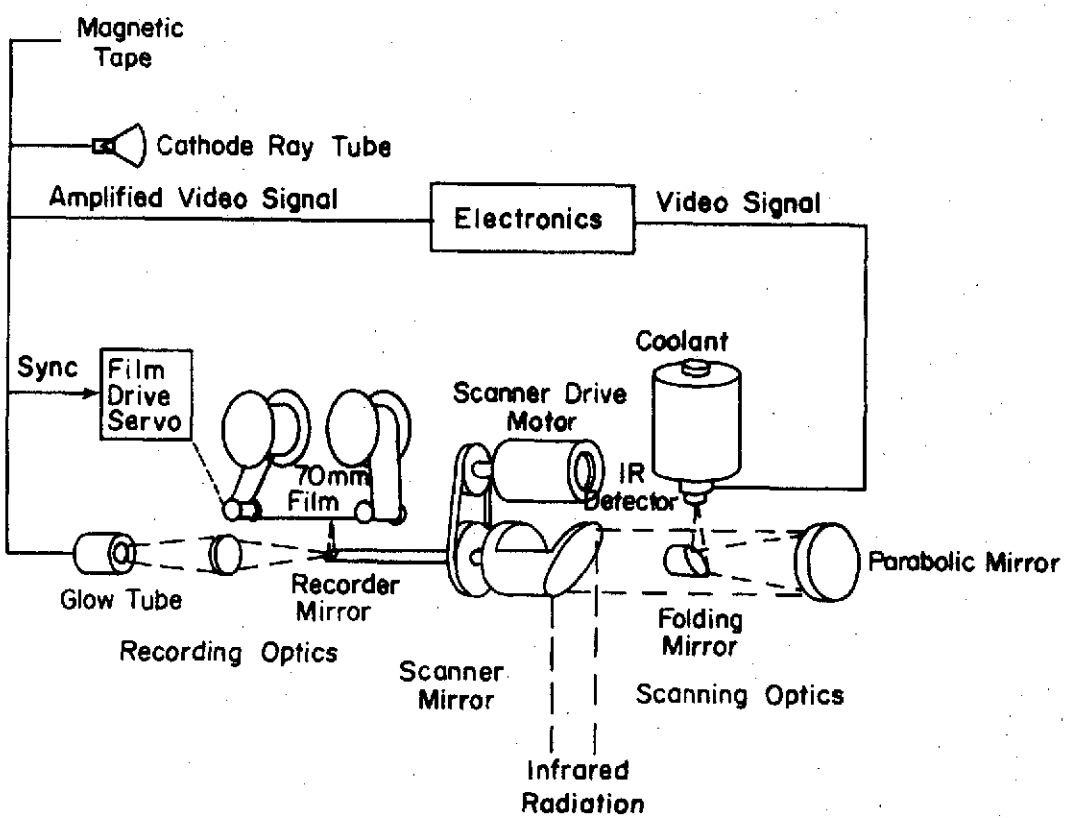

FIGURE 14. SCHEMATIC OF THERMAL SCANNING SYSTEM

The radiation from the ground is received onto a scanning mirror located on a revolving shaft. The energy is reflected by the scanning mirror through an optical arrangement such as shown in Figure A-14 which focuses the incoming rays on the active element of an infrared detector. When sensing is done in the 3 to 5 micron region, the active element is generally indium antimonide crystals. The area surrounding the detector and the detector must be cooled with liquid nitrogen to reduce the background radiation to an acceptable level. If sensing is being done in the 8 to 14 micron region, crystals of doped germanium are generally used. The coolant used in this case is liquid helium. The detector, which is mounted in a Dewar flask with the coolant to prevent heat transfer to the coolant, converts the infrared radiation to an electrical signal. The variations in the electrical signal will be proportional to differences in the radiation received by the detector as the scanning mirror revolves.

Filters or wavelength, bandwidth selections are not generally used with thermal scanning systems since the range of the detectors plus the phenomenon of the transmissivity of the atmosphere in effect selects the wavelength and bandwidth of the energy detectable by these systems.

If a photographic type of image is to be made, the electrical signals from the detector are amplified and used to modulate a variable intensity light source such as a glow tube as shown in Figure A-14. In the case of a glow tube printer, the output of the tube is focused onto a moving strip of film by a rotating mirror on the same shaft as the receiving mirror. This produces a strip of film similar to a photograph taken with a strip camera. The output can also be displayed

on a cathode ray tube and monitored inflight. In some cases infrared photographs are made directly from the cathode ray tube display.

The reason this system is commonly called a thermal rather than an infrared scanner is that the temperature of the objects being sensed is generally the primary factor affecting the amount of radiation received. Therefore, the lighter areas in an infrared photograph made in this fashion are assumed to correspond to the areas with the highest temperature. However, warmer and colder as seen in the infrared photograph does not necessarily correspond directly to temperature but rather to the apparent radiation which is also affected by the emissivity of the object being sensed. In the case of readings or photographs made over water where the emissivity is constant, the thermal scanner will detect directly the temperature patterns in the water. Presently, this capability has been developed to a point where temperature differences in water less than a tenth of a degree can be detected.

One of the advantages of thermal scanners is that they can be used day or night. During the day the reflected solar energy in the infrared regions beyond 5 microns is negligible compared to the emitted energy so that the prime difference in day and night measurements made in this region are due only to diurnal temperature differences. This fact leads to the use of the differences in the tones of objects at different times of the day as a method of identifying objects. This is due to the difference in heat capacity and thermal conductivity of objects which if known can be used as identifying characteristics.

A recently developed system which shows great promise for future use as a remote sensing system is multispectral scanning systems. A

figurative layout of this type of system is given in Figure A-15. The resolution and scanning characteristics of the system are the same as for the thermal scanner shown in Figure A-13. The multispectral scanner is much like the thermal scanner in operation except that instead of recording energy in only one bandwidth a number of channels or bandwidths are used. These channels in which energy is recorded may be in the ultraviolet, visible or infrared regions.

The mechanics of the multispectral scanners is similar to the thermal scanner except that the incoming radiation is divided into discrete bandwidths by diffraction gratings and prisms after which it is focused upon separate detectors. The output from each detector is amplified and recorded simultaneously.

The multispectral scanning system which has received the most attention is one developed by the Willow Run Laboratory of the University of Michigan. This system consists of 18 channels. Twelve of these channels are in the visible region, one is in the ultraviolet region and the remaining five are in the infrared region. A great deal of effort is presently being made to develop computer techniques for automatic processing of the data produced by this system in order to identify crops and soils. Presently there are numerous arguments pro and con about the usefulness of the techniques being developed as well as arguments about the optimum number of channels to use in multispectral scanning.

One of the advantages of a multispectral scanning system is the versatility which it allows the interpreter in displaying his results. Black and white photographs can be made from each channel of information. Also any three channels can be combined to make false or real color

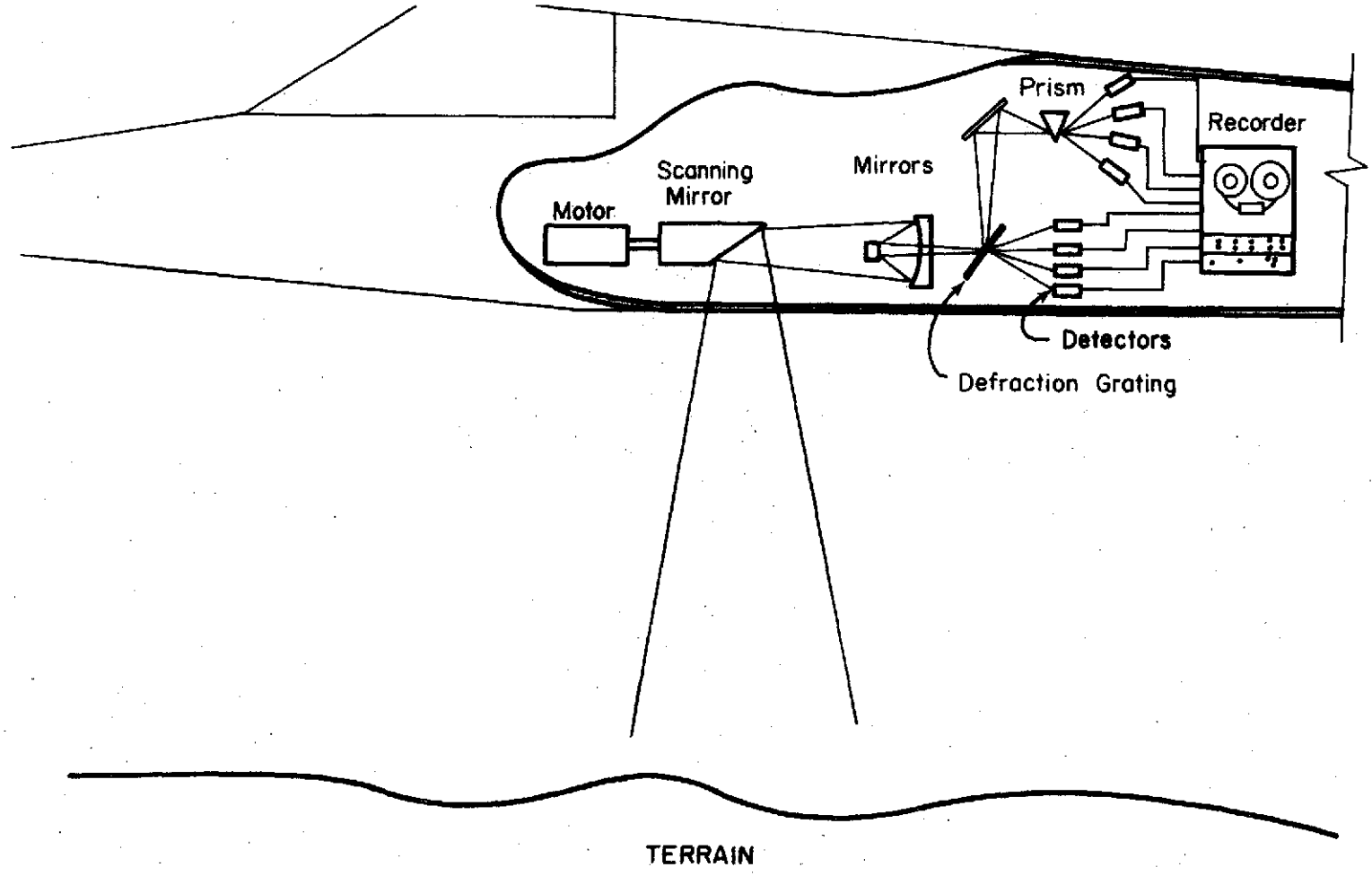

FIGURE A-15. SCHEMATIC OF MULTISPECTRAL SCANNER

photographs. Since the recorded data is electronic in nature, the output of the system can readily be inputted to a computer which can display the results in several ways. Numerous channels of data are also available for comparison for use in automatic identification by a computer. Due to the volume of data that is rapidly becoming available from remote sensing, some type of automatic processing technique is required and multispectral data is the most amenable to automatic interpretation. As the number of bands is increased the chances of finding an identifying pattern for each object received becomes more likely and more reliable. However, this does increase the amount of data to be processed.

There are several disadvantages to multispectral scanning systems. The main problem with such systems is their expense and complexity. Also the spatial resolution is poor when compared to similar data obtained with photographic systems.

The basic element involved in any of the systems discussed is the detector which converts the received electromagnetic energy into a measurable electrical signal. There are many different types of detectors and the one or ones used in any system will depend on the application and the wavelength of the energy to be measured. There are a number of parameters involved in the selection of a particular detector for a particular application. These parameters or characteristics of detectors can be divided into five groups as discussed below.

1. The minimum radiant flux which will generate a signal. That is, the signal must be high enough to be detected above the noise which is generated due to background radiation and electronic noise

from the associated circuitry.

2. The wavelength range in which the detector will generate a useful signal. The signal may be a direct voltage output or a resistance change which can be converted into a voltage reading and amplified.

3. The linearity and output of the detector per unit of incident radiant flux.

4. The time lag in the detector and circuitry from time of incident energy on the detector to signal output. If the signal is to be amplified by an A.C. circuit, the circuit frequency must be less than the time constant frequency of the detector.

5. The spectral characteristics of the detector. The same level of incident radiation will not generate the same signal level from a detector if the energy wavelength is different. Therefore, calibration may be required at several points in the spectrum.

Detectors can be broken down into two groups. Those used primarily in the infrared region and those used in ultraviolet, visible, and near infrared regions. The detectors used in the infrared region include two basic types - those whose output depends on a heating effect of the element and those that have a property change because of direct absorption of photons to generate charged pairs of electrons. This later group must be cooled to operate effectively. Figure A-16 shows the sensitivites of detectors used in infrared sensing. The detectors used in the visible and adjacent region are photomultiplier tubes and as such are based on the photoemissive effect.

Thermal detectors are used primarily for sensing in the infrared region. These type of detectors depend on the heating effect of the

energy being received in order to give a reading. The thermocouple detector is the most common type of thermal detector used in infrared energy measurements. A typical representation of a thermocouple circuit is shown in Figure A-17.

In the case of a thermocouple detector, the active junction is attached to a blackened low mass plate which is used as a receiver. The receiver is normally protected by a case which has an opening through which the incident radiation reaches the receiver. The opening is enclosed by a substance such as a NaCl, KBr or fused silica crystal. The type of substance used for the opening will limit the range of incident radiant energy that will impinge on the receiver. This is one of the characteristic factors involved in picking a thermocouple. The receiver is attached to the case by thin support fibers made of a material with as low a thermal conductivity as possible.

The cold junction is attached to the wall of the case. Thus the output of the device is a function of the temperature difference between the case and the receiver which is assumed to be in thermal equilibrium with the object whose radiant energy is being measured. Therefore, in order for a thermocouple detector to be used in the far infrared range, the case will generally have to be cooled to lower the temperature of the cold junction and to minimize the energy which might be emitted to the receiver by the case.

In order to eliminate as much as possible the heat transfer due to connection between the case and receiver, the case may be evacuated if very small irradiation measurements are to be made. However, for amplification purposes it may not be desirable to minimize the resistance to energy losses from the receiver since the time constant

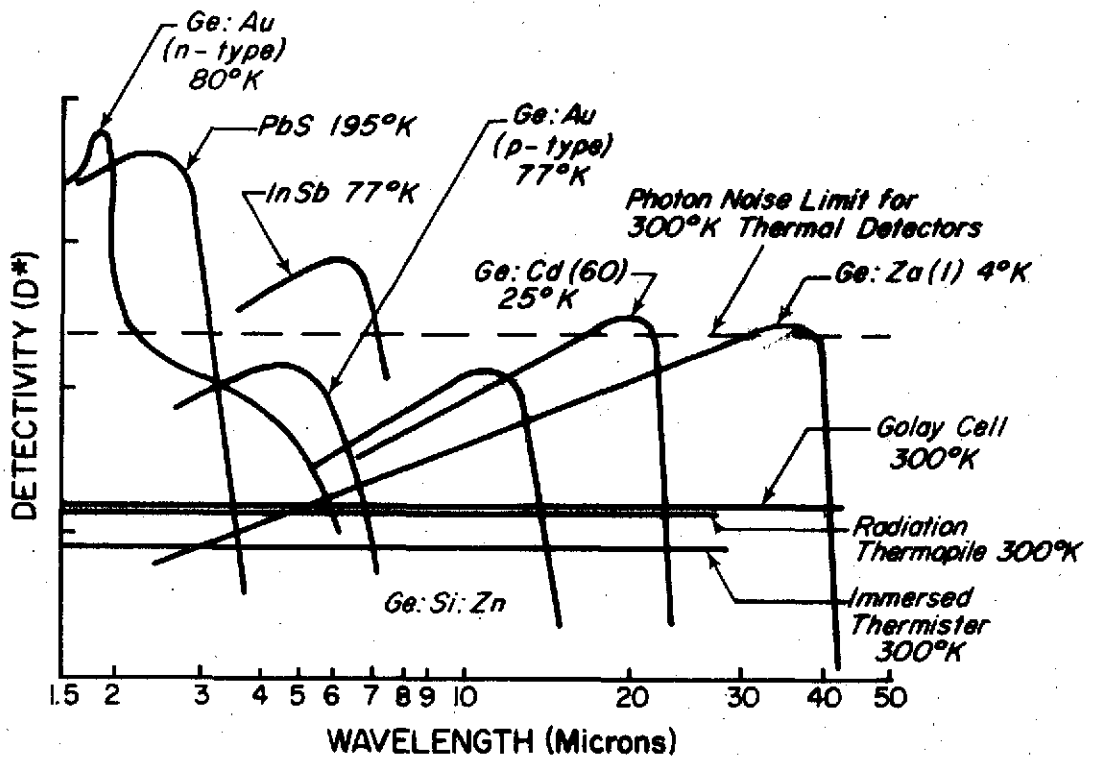

FIGURE A-16. DETECTOR SENSITIVITIES

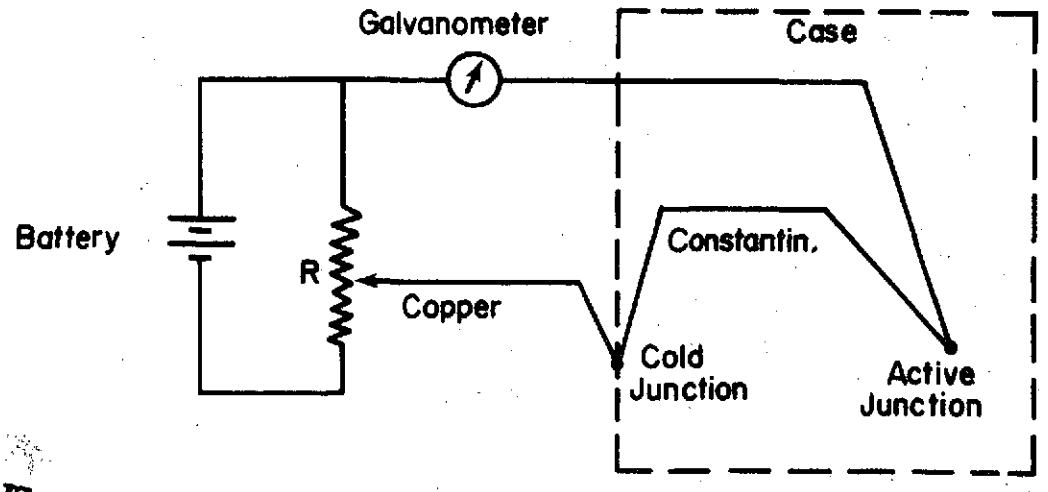

FIGURE A-17. THERMOCOUPLE CIRCUIT

for a thermocouple detector is proportional to this resistance times the heat capacity of the receiver [55]. Again the design of the detector will depend on the application.

Another type of thermal detector is the bolometer which has been adapted for detection of infrared energy. The bolometer detector is similar to a thermocouple detector except that the voltage producing element of the thermocouple is replaced by a resistance producing element with the resulting change in circuitry. Irradiation of the active element causes a temperature rise in the element which produces a corresponding change in resistance. Therefore, like the thermocouple detector, the response of the detector is based on the heating of the active element by the irradiation. Thus for small values of irradiation to be measured in the far infrared region, the best results will be obtained if the bolometer case is cooled.

Other types of thermal detectors can be produced which convert the heating effect of the irradiation into a mechanical movement which can be sensed. One way this is done is by expansion of a gas against a bellows connected to a variable resistor.

Thermal detectors are not generally used in airborne remote sensing because the response time involved in the receiver element reaching thermal equilibrium with the object being sensed is longer than the viewing time. Therefore, detectors are used which depend on the photoconductive or photovoltaic effect. Materials which exhibit these properties and which are used in infrared detectors are shown in Figure A-16. Photon detectors are based on the effect of photon collision with these materials. Photoconduction takes place when the photons cause electrons to be excited from the valance band of the

material to the conduction band thus changing the conductive characteristics of the material. The photovoltaic effect takes place when a voltage potential is introduced in a material due to bombardment by photons. Most infrared detectors used in airborne remote sensing use the photoconductive effect.

Since these effects are based on the energy of the photons which is a function of the wavelength, detectors made using photon effects show a quite definite cutoff point as seen in Figure A-16. This cutoff point corresponds to the wavelength at which not enough energy is available in the photon to move the electron into the conduction band.

The detectors generally used to measure energy emissions in the ultraviolet and visible regions are based on the photoemissive effect. Photoemission takes place in a material where the incoming photons have enough energy to cause the material to release electrons. Since the energy required for the photoemissive effect (removal of electrons from the atomic structure) is relatively high, detectors based on this technique are not usable except in the shorter wavelength region where the energy per photon is higher than in the infrared region. Detectors of this type also exhibit sharp cut-off points and the response is strongly affected by the wavelength of the energy. This is because the effect of the photon impingement is a function of the number of photons and not the energy involved if the energy involved with a photon is above a certain threshold level.

The most common type of photoemissive device is a photomultiplier tube. Examples are RCA 1P21 and 1P28 tubes. The response of this type of tube is shown in Figure A-18. These tubes operate on a cascade effect which is produced by a series of secondary plates. The primary

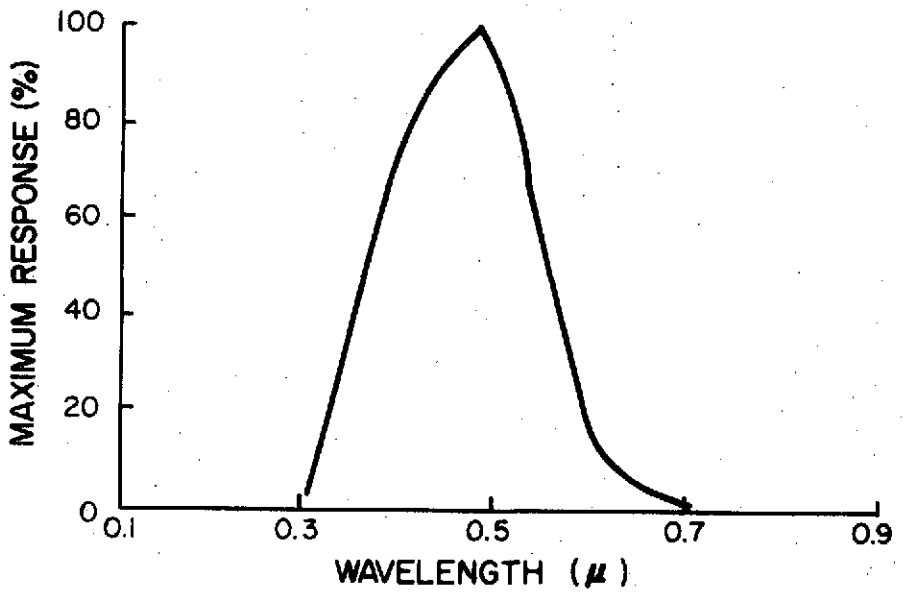

FIGURE A-18. RESPONSE OF IP21 RCA PHOTOMULTIPLIER DETECTOR

cathode is photoemissive which sets up a chain reaction type of effect when electrons are emitted from it after being hit by photons. Because of the multiplying effect, a readily detectable signal can be produced.

Once a radiation measurement system is set up it must be calibrated which can be a difficult and frustrating task since systems calibrated in a laboratory under ideal conditions do not often function the same under less ideal conditions. One way to overcome this is to build an internal calibration system into the instrument [51]. In order to calibrate the systems, a standard radiant source is often used. The source should emit energy in the wavelength of interest and in a manner similar to the object whose radiation is to be detected but with a known intensity.

In remote sensing monochromatic measurements are generally taken. Several sources may be required to cover the range of interest. In the ultraviolet and visible region, a gas discharge tube enclosed in quartz may be used as a source. In the visible and near visible regions tungsten strips may be used. The intensity of the energy output will be determined by the voltage across the strips. Since the tungsten strips must be enclosed in an inert gas, a glass envelope is required which makes standard measurements with this source impossible in much of the infrared region. Therefore, in the infrared region beyond 2 microns a Globar heating element is often used. A Globar consists of a sintered tungsten carbon rod which can be heated in air up to $2700^{\circ}R$. Since the element can be heated in the air, infrared readings can be made. The sources described are only a few of those available.

Anyone interested in standard sources should first outline his requirements before deciding on the type of system he will use.

The advantages of electronic detection systems can be divided into three groups. The first is that with electronic detectors radiant energy can be measured throughout the wavelength regions of thermal originated energy which are available in the atmospheric windows. Secondly, the spectral distribution of the radiation is discernable. Thirdly, the output from electronic detector systems is readily amenable to computer systems and automatic interpretive procedures. The disadvantages of these systems can be summed in two words -- cost and complexity.

APPENDIX B

BALLOON LAUNCH PROCEDURE AND TEST LOG

The following is an outline of the procedure used to launch the balloon/mirror system used for making stability tests

I. Assemble all equipment
   - A. Obtain use of suitable field
   - B. Rent truck
   - C. Assemble all equipment for balloon system
   - D. Assemble instrumentation and measuring equipment
   - E. Load truck
   - F. Carry all equipment to test site

II. Prepare to launch balloon
   - A. Place a marker near center of field
   - B. Drive stakes into the ground
     1. From marker lay off a circle with a radius which will give the balloon cable the required angles when attached to stakes on the circle
     2. On circle drive six stakes 60° apart
   - C. Attach winch and cable to stakes nearest direction of the prevailing wind
   - D. Attach other two winches so that all three are 120° apart
   - E. Drive three stakes for mirror system into ground
     1. Place so that cable angle will be 60°
     2. Place 120° apart
   - F. Set up electrical generator and check out
   - G. Check out all other electrical equipment
   - H. Roll out balloon cables to marker

I. Snap cables together

J. Pull cables tightly with winches so that balloon snaps are located over marker

III. Launch Balloon

A. Locate helium bottles near marker

B. Roll out balloon

C. Attach cables to balloon apex ring

D. Attach safety line to balloon apex ring

E. Connect regulator valve and quick disconnect to helium bottles and fill balloon

1. Hold balloon by strap at nose

2. Fill balloon until arrows meet

F. Using safety line let balloon rise until ring is approximately 6 feet above the ground

G. Attach mirror and target to ring

H. Attach mirror cables to mirror holder

I. Roll out mirror cables to stakes and leave free to unroll as balloon is raised

J. Attached marked plumb-bob line to mirror corner with slip knot

K. Slowly let balloon rise until safety line is loose

L. Locate workers at each winch and slowly unwind until mirror is at desired height

M. Attach plumb-bob at point marked on line and adjust cables until plumb-bob shows mirror to be directly over marker and at right height.

N. Lock winches and tie off safety line to a stake so that it hangs loose but doesn't drag on mirror

O. Detach plumb-bob and plumb-bob line

IV. Stabilize Mirror System

A. Pull mirror cables to the stakes

B. Attach fasterners so that cables when attached to stakes just begin to eliminate sag

C. Check tension in cables with spring scales

D. Adjust tension in cables so that they are equal and give desired downward pull on mirror system.

V. Begin Tests

The following is a log of the launch and testing of the four 800 cubic feet balloons used in the stability tests.

First Balloon Launch - June 5, 1973

The first balloon was launched generally in accordance with the procedure outlined. However, a safety line was not attached since it was thought at the time of the first launch that the cables were strong enough to hold the balloon under any conditions. The balloon launch was completed by 10:00 A.M. Weather was clear with only scattered clouds. Three and one half containers of helium were required to fill the balloon. The mirror appeared to be very stable, however, no target was attached to the mirror. No tests of the stability of the mirror system was planned for several days since the first test was mostly to determine the flight characteristics and operational lift of the balloon.

Because of the build up of thunderstorms, the balloon was lowered at 2:00 P.M. This was accomplished by cranking in on the three tether lines to the balloon. The three lines to the mirror were set free.

When the balloon was lowered to the point where the mirror was six feet above the ground, the snap on the balloon end of one of the cables broke. This was caused by pulling too much tension in the lines while trying to bring the balloon down. The ballon was then tied down by using only one of the original cables. This was done by cranking in on one of the remaining cables and letting the other go free. The nose of the balloon was then roped and tied down to another stake a few feet from the ground.

At 3:30 P.M. a large gust of wind from the south-southwest hit the balloon from a thunderstorm. The balloon was then forced downwards into the front stake and destroyed.

Second Balloon Launch - June 7, 1973

A second balloon was launched at 7:35 A.M. on June 7, 1973. In order to eliminate the problems encountered with the first balloon, a safety line was attached to the nose of the balloon and stronger snaps were obtained to replace the ones used in the first test. The safety line was attached primarily to help lower the balloon if needed. The line was made of nylon with a breaking strength of 500 pounds. The cabling arrangement was as determined in the initial study with the lead cable in a southeast direction which was supposed to be the direction of the prevailing winds. At the time of launch the winds were calm and the sky clear. As the day progressed the winds picked up from the northeast at 3 to 7 miles per hour. Again it was noted that the mirror appeared stable. A film clip of the launch was made.

At 3:30 P.M. storms begain to build in the area. The balloon was then lowered to approximately 75 feet. The mirror was at 50 feet. Lightning got close so the balloon was left unattended. The nose was

loosely tied with nylon cord to a stake in the east direction from the apex of the balloon.

At 3:30 P.M. rain and high winds along with intense lightning began. The balloon was tossed about a great deal. It was noted that some helium had been lost and that the balloon was wrinkling somewhat in the high winds. After approximately 15 minutes hail began to fall. At times the balloon was driven almost to the ground before rising back up. Storm intensity and hail increased until the balloon was driven so low at one time that the mirror and later the balloon itself was driven to the ground. Winds were from the north-northwest. The balloon then whipped back up and with a jerking motion and snapped the line lying to the north. The line to the west then snapped when all the force was put on it. The nylon line then also broke after being weakened by rubbing across the stake to which it was attached. The balloon then moved to the southeast and was last seen over University Lake. The line attached to the southeast held long enough to keep the balloon low so that the mirror rigging caught in a tree and was ripped from the balloon. The balloon then escaped when the last cable broke.

Third Balloon Launch - March 30, 1974

A third 800 ft^3 balloon was launched on March 30, 1974. The weather was clear. Winds were light and variable mostly from the west or southwest. All equipment was assembled in the field by 8:00 A.M. The center marker was placed and the stakes were set up. The first stake was set up to give the balloon cable an angle of 30^o with respect to the horizontal and was oriented into the expected prevailing wind direction as seen on Figure B-1. The other two balloon cables were placed to give 120^o between all cables and to give cable angles of 45^o.

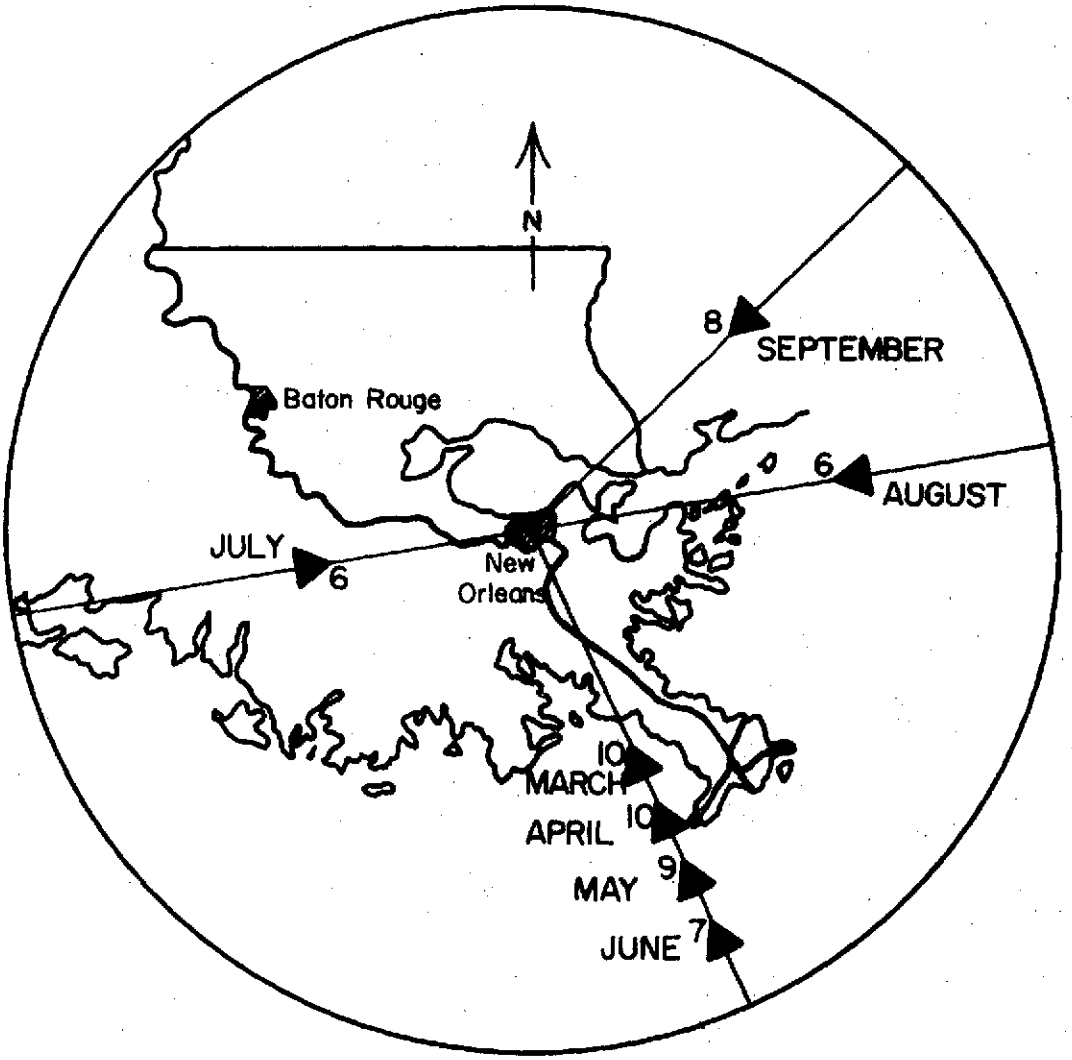

FIGURE B-1. PREVAILING WIND DIRECTION AND MEAN SPEED

Stakes for the mirror system were placed inside the balloon cable stakes and positioned so that the mirror cable angles would be the same as the balloon cable angles. The winches were then attached to the stakes and the launch proceeded as outlined with the exception that the plumb-bob line was not detached after positioning of the mirror. The launch was completed at 10:15 A.M. with the mirror positioned at an altitude of 100 feet. A photograph of the balloon being launched is given in Figure B-2. The mirror cables were then pulled in tension and attached to stakes. The tensions pulled were five pounds force on the two short cables and four pounds on the long cable. These forces were calculated to give 15 pounds of downward pull on the apex from the mirror system. It was noted that when the mirror cables were pulled in tension as stated that the main balloon cables sagged more than the mirror cables. Since the balloon cables were much heavier this could occur when the tension on the balloon cables were about the same or less than the tension in the mirror cables. This could happen only if the balloon had a net lift of 39 pounds of force or less.

Initial stability tests were conducted on the balloon/mirror system at 11:00 A.M. Winds were light with some gusts but not enough to be recorded by the wind speed indicator. Wind direction was between west and southwest. The laser mounted vertically was shown on the mirror target and the resulting spot was viewed with binoculars. A maximum movement of the target of 1/2 inch was noted. There seemed to be no oscillations of the spot on the target. The 1/2 inch movement was a gradual floating motion. Viewing was for approximately 30 minutes. The laser was then shown on the mirror and the laser beam reflected back to a target on the ground. The beam hit the ground at a point

FIGURE B-2. Photograph of Balloon Being Launched

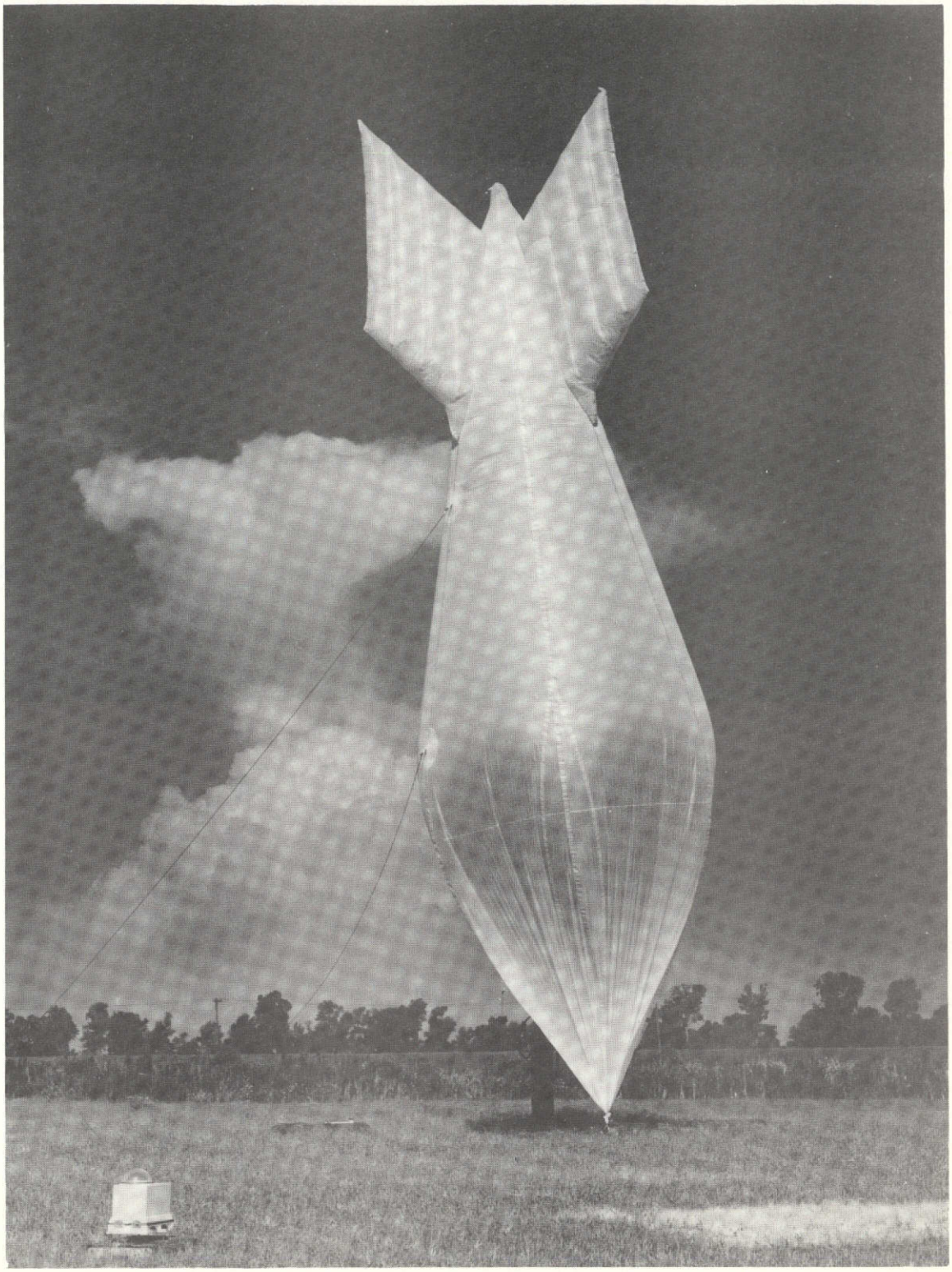

FIGURE B-2. Photograph of Balloon Being Launched

along the line of the leading cable 14 feet from the laser location directly under the balloon. The movement of the laser spot on the ground was greater than the two foot by two foot target used. The maximum movements of the spot were in the direction of the lead cables and were estimated at $\pm$ 3 feet. Therefore, the angular variations in this direction were approximately $\pm$ 1.7°. In the perpendicular direction the movements were much less and were less than $\pm$ 1 foot. These variations were therefore $\pm$ 0.6°. Similar tests conducted during the afternoon showed the same type of results.

At 6:30 P.M. it was decided to move the leading mirror so that all the angles of the mirror cables would be equal and thus try to reduce the angular variations. However, at this time, the winds had increased to an average of 3-5 miles per hour with gusts of up to 10 miles per hour. The wind direction had also changed to a more southerly direction which meant it was blowing directly between two cables. This tended to slacken the cable directly opposite the wind direction. When the laser was turned on the target, the spot was stationary for a while then the mirror jumped wildly when a wind gust hit the balloon. The target came back to its original position but continued to swerve wildly whenever the balloon was hit by wind gusts above 10 MPH. Further testing therefore was discontinued.

It was noted at this time that the balloon was losing helium and was somewhat limp. Also the ballon was not nosing into the wind as it had done previously. Instead the ballon would bend near the tail section as the stabilizers attempted to make the ballon respond to the winds. This condition caused the aerodynamic characteristics of the system to fail and thus produced high side forces at the apex of the

system. In turn this caused the cable opposite the wind to become completely slack at times, and therefore the mirror was no longer held in a stable position. However, as long as there was tension in all the cables the mirror remained stable with little movement.

The balloon was allowed to stay up through the night under the conditions given. The next morning the balloon was lowered and an attempt was made to refill the balloon. However, the balloon had lost 1/4 to 1/3 of its original supply of gas and not enough helium was available to completely fill it up again. Therefore, the mirror system was removed and the balloon was sent up again. No observations were made of the balloon between 9:30 A.M. and 1:30 P.M. at which time the balloon was found on the ground with very little helium remaining in it. No gashes or holes were found in the balloon skin, therefore, it is thought that the valve used for filling the balloon must have not been completely sealed when the balloon was launched the second time.

Subsequent analysis of the forces expected for the balloon system used during this test revealed the data given in Table B-1. Comparing this data with the side force/vertical tension required to buckle any cable for the arrangement used (see Figure B-3) it was calculated that at wind speeds higher than nine miles per hour from the west or southwest the system would be unstable. The worst condition is when the winds come from the southwest. This data compared extremely well with the results obtained under actual flight conditions.

Fourth Balloon Launch - April 9, 1974

On April 9, 1974, a fourth balloon was launched. The launch procedure was started at 8:00 A.M. and completed by 9:00 A.M. The balloon cable arrangement was the same as used in the third test except that

TABLE B-1

FORCE TABLE FOR BALLOON SYSTEM OF TEST #3

Wind Velocity	0 ft/sec	10 ft/sec	20 ft/sec
Balloon Static Lift @ 80°F	44 lb	44 lb	44 lb
Balloon Dynamic Lift	0	1.5 lb	6.0 lb
Gross Lift	44 lb	45.5 lb	50.0 lb
Balloon Weight	12.5 lb	12.5 lb	12.5 lb
Lift at Apex	31.5 lb	33.0 lb	37.5 lb
Drag or Side Force	0	0.7 lb	2.3 lb
SF/Lift	0	.031	.084
Angle of Balloon Cable at Apex with the Vertical	0°	1.7°	4.8°
Mirror System Weight	6 lb	6 lb	6 lb
Total Vertical Force in Mirror Cables	9 lb	9 lb	9 lb
Total Downward Pull at Apex Due to Payload	15 lb	15 lb	15 lb
Total Vertical Component of Tension in Balloon Cables $-T_v$	16.5 lb	18 lb	22.5 lb
SF/T_v	0	.039	.10

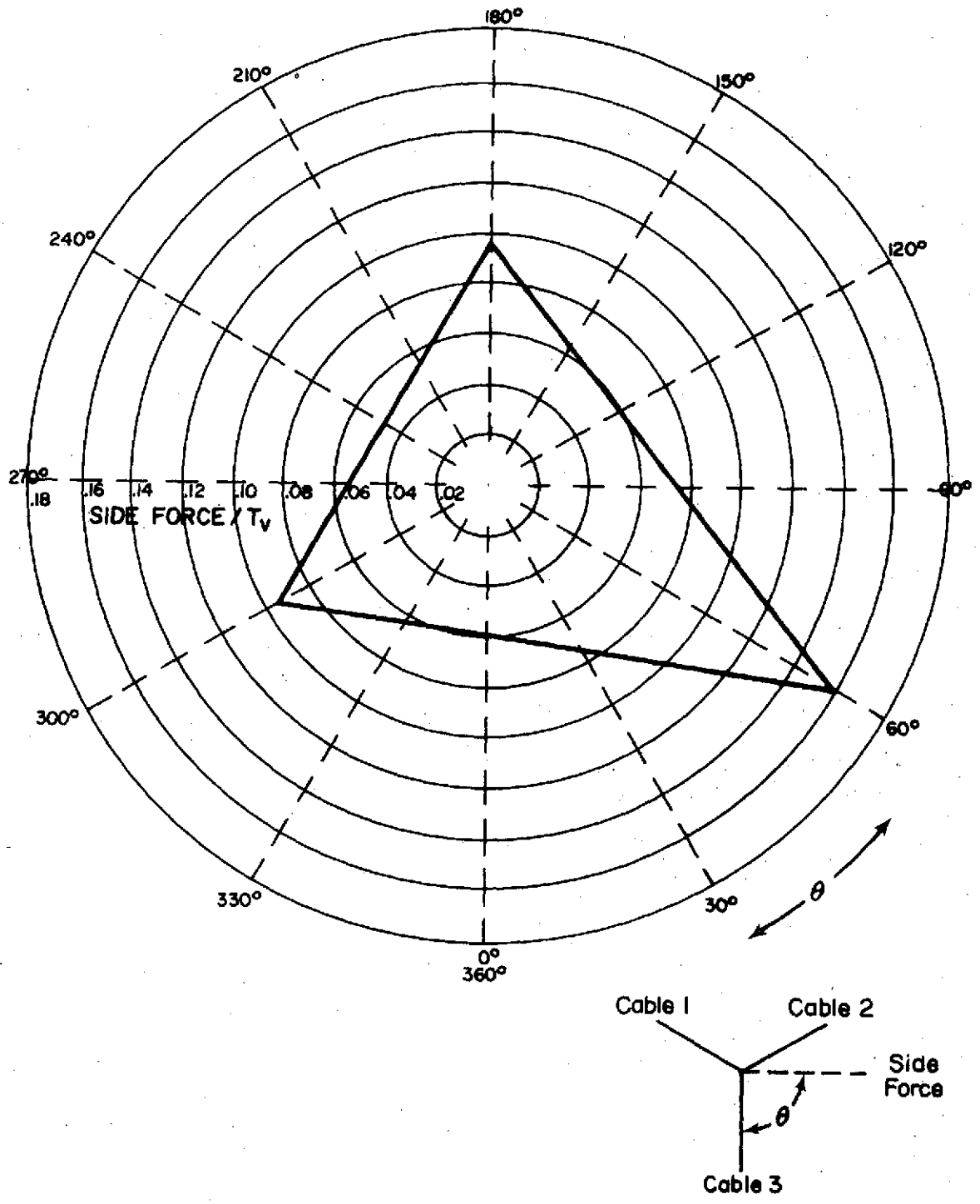

FIGURE B-3. SIDE FORCE/T_v REQUIRED FOR BUCKLING ANY CABLE FOR THE SYSTEM USED IN THE THIRD TEST

the first stake had been moved in so that all the balloon cables made angles of forty five degrees with respect to the ground. After launching the balloon, it took over an hour to attach the mirror and mirror cables, to position the mirror and adjust the tension in the mirror cables. The mirror was positioned at a height of ninety five feet. The laser was then set up and testing began at 11:00 A.M. Only two people were used throughout the launch, adjusting the mirror system and the testing. The data taken during the tests is given in Appendix C.

The day was clear, winds were variable and somewhat gusty. Winds in the morning were from the northeast but by the time tests were begun had shifted to the northwest where they stayed with only slight variation throughout the remainder of the day. The average wind speed appeared to be five miles per hour with gusts up to ten miles per hour. In general, the winds during the tests were between two and eight miles per hours from the northwest.

Three tests were completed before 1:00 P.M. For these three tests all mirror cables were at sixty degrees and all balloon cables at forty five degrees. Mirror tensions of one pound of force, two pounds of force and four pounds of force in each mirror cable were tested. Testing was begun again at 3:00 P.M. with the same cable arrangement and with mirror cable tensions of three pounds of force and two pounds of force. The mirror cables were then changed to give angles of seventy degrees with respect to the ground. Three tests with mirror cable tensions of one pound of force, two pounds of force and three pounds of force were then made. Testing was concluded at 5:30 P.M. At this time the balloon appeared to have lost little if any helium and was working extremely well. The skin was not wrinkling in the wind and the nose was flying up into

the wind apparently with a six degree angle of attack as designed. A later check at 9:00 P.M. also showed that the balloon was still operating satisfactorily.

It was noted during these tests that the shape of the laser beam after being reflected from the mirror frequently changed. One possibility was that this was caused by curvature changes in the mirror surface due to changing pressure on the mirror face caused by wind forces. It was therefore concluded that the type of mirror being used for these tests should be tested in the laboratory before reflectance readings using a balloon system and this type of mirror.

The next day was also clear but the wind speed had increased to ten to twelve miles per hour with gusts up to twenty miles per hour. The wind was from the southeast with variations in the direction of $\pm$ 30°. Due to the high winds, the system had become unstable; that is, one of the balloon cables would frequently become slack. This in turn caused the mirror system to become tangled due to the frequent jerks experienced as a cable would go slack in a high wind gust and then become tight as the balloon straightened up. It was also very noticeable that the balloon had lost helium. The nose was bowed in due to the winds and the ballon was bent near the tail where the stabilizers were acting to turn the balloon into the wind.

At 9:30 A.M. the balloon was lowered using the safety line. The system was then tied off close to the ground and the balloon refilled. Approximately two-fifths of a bottle of helium (95 cubic feet) were required to fill the balloon at this time. The mirror system was then cut free from the balloon. All of the mirror cabling had to be cut in

order to untangle the system. The cables were then rolled up and the mirror untangled from the wires wrapped around it.

At 11:00 A.M. it was decided to rebuild the mirror system and then to try to relaunch the balloon to an altitude of sixty feet. This would give the balloon cables an angle of thirty degrees. It was hoped that the system could be stabilized in this configuration. Therefore at 11:15 the balloon was again refilled and the mirror system was taken to the laboratory for repairs. In the refilling process 40 cubic feet of helium was used.

At 1:00 P.M. the mirror system was returned to the field. The balloon was again showing signs of deflating and was refilled with 100 cubic feet of helium indicating that the leakage rate of the balloon was increasing. However, it was decided to try and launch the balloon again.

The mirror system was reattached and the balloon launched at 1:30 P.M. to an altitude of sixty feet for the apex. The mirror was mounted ten feet below the apex. However, while attaching the mirror cables to stakes, the balloon became unstable and again tangled the mirror system. By this time the winds had increased to a speed of fifteen miles per hour with gusts above twenty miles per hour. Also, after launching, the balloon quickly showed signs of deflating. The tail section was bending in the winds and the nose was wrinkling and was blunted in shape. It was therefore decided to lower the balloon.

The balloon was lowered at 2:30 P.M. and a quick disconnect attached to open the fill valve at the nose. The balloon was then slowly rolled up from the tail section. This process took two and one half hours to complete. The stakes were then pulled up and the equipment removed and

stored. When the balloon was lowered it was noted that a 2 inch gash had developed near the nose of the balloon. It was assumed that this accounted for the rapid deflation of the balloon in the final launch attempt.

APPENDIX C

DATA FROM BALLOON/MIRROR STABILITY TESTS

DATA SHEET

Test Number 1 Date 3/30/74

Geometric Data

Mirror altitude 100 feet

Cable compass readings 30°, 150°, and 270°

Angle of balloon cables with ground 30° and 45°

Angle of mirror cables with ground 30° and 45°

Tension in mirror cables 4 lbs, 5 lbs, and 5 lbs

Lateral Movement Test

Time of test 11:00 A.M.

Duration of test 30 minutes

Maximum movement of laser beam on target 1/2 inch

Average movement of laser beam on target 0

Average wind speed 1 MPH

Variations in wind speed ± MPH

Average wind direction WSW

Variation in wind direction ± 30° (2)*

Angular Movement Test

Time of test 11:30 A.M.

Duration of test 5 minutes

Distance, target to laser 14 feet

Azimuth angle of line between laser and target 150°

Maximum movement of spot in azimuth plane ± 3 feet (1)*

Average movement of spot in azimuth plane ± 1 foot (1)*

Maximum movement of spot in perpendicular plane ± 3 feet (1)*

Average movement of spot in perpendicular plane ± 1 foot (1)*

(*) Refers to number in comment statement

Angular Movement Test (Continued)

Average wind speed 1 MPH

Variations in wind speed $\pm$ 1 MPH

Average wind direction WSW

Variations in wind direction 30° (2)*

Atmospheric Data

Barometric pressure 30.0 in Hg

Temperature 77°F

Comments:

[1]Target used was only 2 foot by 2 foot and therefore a rough guess had to be made of the beam movement when it went off of the target

[2]The winds were very light but quite variable in direction

DATA SHEET

Test Number 2 Date 3/30/74

Geometric Data

Mirror altitude 100 feet

Cable compass readings 30°, 150°, and 270°

Angle of balloon cables with ground 30° and 45° (1)*

Angle of mirror cables with ground 30° and 45° (1)*

Tension in mirror cables 4 lbs, 5 lbs, and 5 lbs

Lateral Movement Test

Time of test 2:00 P.M.

Duration of test 10 minutes

Maximum movement of laser beam on target 1/2 inch (4)*

Average movement of laser beam on target 0

Average wind speed 0 (3)*

Variations in wind speed + 1 MPH

Average wind direction West

Variation in wind direction ± 15°

Angular Movement Test

Time of test 3:30 P.M.

Duration of test 7 minutes

Distance, target to laser 14 feet 8 inches

Azimuth angle of line between laser and target 150°

Maximum movement of spot in azimuth plane ± 3 feet (2)*

Average movement of spot in azimuth plane ± 1 foot

Maximum movement of spot in perpendicular plane ± 3 feet (2)*

Average movement of spot in perpendicular plane ± 1 foot

(*) Refers to number in comment statement

Angular Movement Test (Continued)

Average wind speed 0 MPH (3)*

Variations in wind speed 2 MPH

Average wind direction WSW

Variations in wind direction $\pm$ 15°

Atmospheric Data

Barometric pressure 30.3 in Hg

Temperature 80°

Comments:

[1]Lead balloon cable was very slack; all balloon cables were more slack than mirror cables

[2]Target used was 2 feet by 2 feet and therefore a rough guess had to be made of the beam movement when it went off of the target

[3]Winds were light and variable; wind speed was so low that it could not be picked up by anomometer

[4]Gradual movement from initial spot; no oscillations seen

DATA SHEET

Test Number 3 Date 3/30/74

Geometric Data

Mirror altitude 100 feet

Cable compass readings 30°, 150°, and 270°

Angle of balloon cables with ground 30° and 45°

Angle of mirror cables with ground 30° and 45°

Tension in mirror cables 4 lbs, 5 lbs, and 5 lbs

Lateral Movement Test (3)*

Time of test 6:50 P.M.

Duration of test 10 minutes

Maximum movement of laser beam on target ± 1 foot (1)*

Average movement of laser beam on target ± 1 foot (1)*

Average wind speed 3 MPH

Variations in wind speed + 5 MPH / - 3 MPH (2)*

Average wind direction SSW

Variation in wind direction ± 15°

Angular Movement Test

Time of test _____

Duration of test _____

Distance, target to laser _____

Azimuth angle of line between laser and target _____

Maximum movement of spot in azimuth plane _____

Average movement of spot in azimuth plane _____

Maximum movement of spot in perpendicular plane _____

Average movement of spot in perpendicular plane _____

(*) Refers to number in comment statement

Angular Movement Test (Continued)

Average wind speed _____

Variations in wind speed _____

Average wind direction _____

Variations in wind direction _____

Atmospheric Data

Barometric pressure 30.08 in Hg

Temperature 76°

Comments:

[1]System was completely unstable; balloon had gone down and was somewhat limp; also wind gusts would make cable to the north east go completely slack moving the mirror wildly.

[2] Winds came in gusts

[3]Balloon would not turn nose into the wind; always seemed to be getting side forces which pulled one cable tight and the other two cables slack.

DATA SHEET

Test Number 4 Date 4/9/74

Geometric Data

Mirror altitude 95 feet

Cable compass readings 30°, 150°, and 270°

Angle of balloon cables with ground 45°

Angle of mirror cables with ground 60°

Tension in mirror cables 1 lb, 1 lb, and 1 lb

Lateral Movement Test

Time of test 11:00 A.M.

Duration of test 15 minutes

Maximum movement of laser beam on target ± 1 inch (1)*

Average movement of laser beam on target ± 1/2 inch

Average wind speed 5 MPH

Variations in wind speed ± 5 MPH

Average wind direction NNE

Variation in wind direction ± 45°

Angular Movement Test

Time of test 11:15 A.M.

Duration of test 15 minutes

Distance, target to laser 3 feet 6 inches

Azimuth angle of line between laser and target 150°

Maximum movement of spot in azimuth plane ± 3 feet

Average movement of spot in azimuth plane ± 6 inches

Maximum movement of spot in perpendicular plane ± 2 feet

Average movement of spot in perpendicular plane ± 6 inches

(*) Refers to number in comment statement

Angular Movement Test (Continued)

Average wind speed 5 MPH

Variations in wind speed $\pm$ 5 MPH

Average wind direction NNE

Variations in wind direction $\pm 60^{\circ}$ (2)*

Atmospheric Data

Barometric pressure 30.61 in Hg

Temperature 60°F

Comments:

[1]Exception to this was one time when side wind hit balloon and made one cable go loose. Mirror moved $\pm$ 1 foot at that time but quickly came back to rest at original location.

[2]Wind directions very changeable in gusts

DATA SHEET

Test Number 5 Date 4/9/74

Geometric Data

Mirror altitude 95 feet

Cable compass readings 30°, 150°, and 270°

Angle of balloon cables with ground 45°

Angle of mirror cables with ground 60°

Tension in mirror cables 4 lbs, 4 lbs, and 4 lbs

Lateral Movement Test

Time of test 11:40 A.M.

Duration of test 5 minutes

Maximum movement of laser beam on target ± 2 inches (1)*

Average movement of laser beam on target ± 1/2 inches

Average wind speed 5 MPH

Variations in wind speed ± 5 MPH

Average wind direction NW

Variation in wind direction ± 30°

Angular Movement Test

Time of test 11:50 A.M.

Duration of test 5 minutes

Distance, target to laser 5 feet

Azimuth angle of line between laser and target 150°

Maximum movement of spot in azimuth plane _____ (2)*

Average movement of spot in azimuth plane ± 2 feet

Maximum movement of spot in perpendicular plane _____ (2)*

Average movement of spot in perpendicular plane ± 2 feet

(*) Refers to number in comment statement

Angular Movement Test (Continued)

Average wind speed 3 MPH

Variations in wind speed $\begin{matrix} +\ 5\ \text{MPH} \\ -\ 3\ \text{MPH} \end{matrix}$

Average wind direction NW

Variations in wind direction $\pm\ 100^{\circ}$ (3)*

Atmospheric Data

Barometric pressure 30.61 in Hg

Temperature 60°

Comments:

[1]However, during angular movement test, the laser beam went off of the mirror at one time during a wind gust

[2]The movement of the beam was too great to be determined

[3]The winds were very gusty and variable in direction

DATA SHEET

Test Number 6 Date 4/9/74

Geometric Data

Mirror altitude 95 feet

Cable compass readings 30°, 150°, and 270°

Angle of balloon cables with ground 45°

Angle of mirror cables with ground 60°

Tension in mirror cables 2 lbs, 2 lbs, and 2 lbs

Lateral Movement Test

Time of test 12:05 P.M.

Duration of test 10 minutes

Maximum movement of laser beam on target ± 1/2 inch

Average movement of laser beam on target ± 1/2 inch

Average wind speed 5 MPH

Variations in wind speed + 3 MPH, - 5 MPH

Average wind direction NW

Variation in wind direction ± 30° (1)*

Angular Movement Test

Time of test 12:15 P.M.

Duration of test 15 minutes

Distance, target to laser 6 feet

Azimuth angle of line between laser and target 150°

Maximum movement of spot in azimuth plane ± 2 feet (2)*

Average movement of spot in azimuth plane ± 1 foot (2)*

Maximum movement of spot in perpendicular plane ± 2 feet (2)*

Average movement of spot in perpendicular plane ± 1 foot (2)*

(*) Refers to number in comment statement

Angular Movement Test (Continued)

Average wind speed 5 MPH

Variations in wind speed + 3 MPH / - 5 MPH

Average wind direction NW

Variations in wind direction $\pm 30^{o}$

Atmospheric Data

Barometric pressure 30.54 in Hg

Temperature 62^{o}

Comments:

[1]Winds very constant from NW at 5 MPH

[2]Spot very steady; stayed entirely on target 3½ feet by 4½ feet

C-4

DATA SHEET

Test Number 7 Date 4/9/74

Geometric Data

Mirror altitude 95 feet

Cable compass readings 30°, 150°, and 270°

Angle of balloon cables with ground 45°

Angle of mirror cables with ground 60°

Tension in mirror cables 3 lbs, 3 lbs, and 3 lbs

Lateral Movement Test

Time of test 3:00 P.M.

Duration of test 10 minutes

Maximum movement of laser beam on target ± 1/2 inch (1)*

Average movement of laser beam on target 0

Average wind speed 2 MPH

Variations in wind speed + 5 MPH, - 2 MPH

Average wind direction NNW

Variation in wind direction ± 30°

Angular Movement Test

Time of test 3:10 P.M.

Duration of test 15 minutes

Distance, target to laser 6 feet 6 inches

Azimuth angle of line between laser and target 170°

Maximum movement of spot in azimuth plane ± 3 feet

Average movement of spot in azimuth plane ± 10 inches

Maximum movement of spot in perpendicular plane ± 3 feet

Average movement of spot in perpendicular plane ± 10 inches

(*) Refers to number in comment statement

Angular Movement Test (Continued)

Average wind speed 3 MPH

Variations in wind speed + 4 MPH / - 3 MPH

Average wind direction NNW

Variations in wind direction ± 30°

Atmospheric Data

Barometric pressure 30.58 in Hg

Temperature 68°F

Comments:

[1]Only a gradual shift, no oscillations

DATA SHEET

Test Number 8 Date 4/9/74

Geometric Data

Mirror altitude 95 feet

Cable compass readings 30°, 150°, and 270°

Angle of balloon cables with ground 45°

Angle of mirror cables with ground 60°

Tension in mirror cables 2 lbs, 2 lbs, and 2 lbs

Lateral Movement Test

Time of test _____

Duration of test _____

Maximum movement of laser beam on target _____

Average movement of laser beam on target _____

Average wind speed _____

Variations in wind speed _____

Average wind direction _____

Variation in wind direction _____

Angular Movement Test

Time of test 3:30 P.M.

Duration of test 15 minutes

Distance, target to laser 8 feet 6 inches

Azimuth angle of line between laser and target 175°

Maximum movement of spot in azimuth plane $\pm$ 2.5 feet

Average movement of spot in azimuth plane $\pm$ 10 inches

Maximum movement of spot in perpendicular plane $\pm$ 2.5 feet

Average movement of spot in perpendicular plane $\pm$ 10 inches

(*) Refers to number in comment statement

Angular Movement Test (Continued)

Average wind speed 3 MPH

Variations in wind speed + 7 MPH / - 3 MPH

Average wind direction NNW

Variations in wind direction $\pm 30^{\circ}$

Atmospheric Data

Barometric pressure 30.58 in Hg

Temperature $68^{\circ}F$

Comments:

[1]Wind conditions and beam movement on mirror looked the same as for test number 7

DATA SHEET

Test Number 9 Date 4/9/74

Geometric Data

Mirror altitude 95 feet

Cable compass readings 30°, 150°, and 270°

Angle of balloon cables with ground 45°

Angle of mirror cables with ground 70°

Tension in mirror cables 1 lb, 1 lb, and 1 lb

Lateral Movement Test

Time of test 4:10 P.M.

Duration of test 10 minutes

Maximum movement of laser beam on target ± 3 1/2 feet

Average movement of laser beam on target ± 1 1/2 feet

Average wind speed 7 MPH

Variations in wind speed ± 5 MPH

Average wind direction NNW

Variation in wind direction ± 30°

Angular Movement Test

Time of test 4:20 P.M.

Duration of test 15 minutes

Distance, target to laser 11 feet 4 inches

Azimuth angle of line between laser and target 220°

Maximum movement of spot in azimuth plane ± 3.0 feet (1)*

Average movement of spot in azimuth plane 10 inches (1)*

Maximum movement of spot in perpendicular plane ± 2 feet (1)*

Average movement of spot in perpendicular plane ± 8 inches (1)*

(*) Refers to number in comment statement

Angular Movement Test (Continued)

Average wind speed 5 MPH

Variations in wind speed + 5 MPH / - 3 MPH

Average wind direction NNW

Variations in wind direction $\pm 30^{\circ}$

Atmospheric Data

Barometric pressure 30.52 in Hg

Temperature $68^{\circ}F$

Comments:

[1]Maximum angular movement noted in light variable direction breezes

DATA SHEET

Test Number 10 Date 4/9/74

Geometric Data

Mirror altitude 95 feet

Cable compass readings 30°, 150°, and 270°

Angle of balloon cables with ground 45°

Angle of mirror cables with ground 70°

Tension in mirror cables 2 lbs, 2 lbs, and 2 lbs

Lateral Movement Test

Time of test 4:40 P.M.

Duration of test 10 minutes

Maximum movement of laser beam on target ± 1/2 inch (1)*

Average movement of laser beam on target 0

Average wind speed 4 MPH

Variations in wind speed + 3 MPH / - 2 MPH

Average wind direction NW

Variation in wind direction ± 30°

Angular Movement Test

Time of test 4:50 P.M.

Duration of test 15 minutes

Distance, target to laser 7 feet 6 inches

Azimuth angle of line between laser and target 210°

Maximum movement of spot in azimuth plane ± 2 feet (2)*

Average movement of spot in azimuth plane ± 8 inches (2)*

Maximum movement of spot in perpendicular plane ± 1 1/2 feet (2)*

Average movement of spot in perpendicular plane ± 6 inches (2)*

(*) Refers to number in comment statement

Angular Movement Test (Continued)

Average wind speed 3 MPH

Variations in wind speed + 4 MPH / - 2 MPH

Average wind direction NW

Variations in wind direction $\pm$ 30°

Atmospheric Data

Barometric pressure 30.52 in Hg

Temperature 66°

Comments:

[1]Moved linearly 1 inch from initial spot

[2]Beam location very stable; moved about 1 foot to 1 1/2 feet in strong gusts

DATA SHEET

Test Number 11 Date 4/9/74

Geometric Data

Mirror altitude 95 feet

Cable compass readings 30°, 150°, and 270°

Angle of balloon cables with ground 45°

Angle of mirror cables with ground 70°

Tension in mirror cables 3 lbs, 3 lbs, and 3 lbs

Lateral Movement Test

Time of test 5:00 P.M.

Duration of test 2 minutes

Maximum movement of laser beam on target ± 1/2 inch

Average movement of laser beam on target 0

Average wind speed 4 MPH

Variations in wind speed ± 2 MPH

Average wind direction NW

Variation in wind direction ± 30°

Angular Movement Test

Time of test 5:05 P.M.

Duration of test 10 minutes

Distance, target to laser 5 feet 2 inches

Azimuth angle of line between laser and target 225°

Maximum movement of spot in azimuth plane ± 3 feet

Average movement of spot in azimuth plane ± 10 inches

Maximum movement of spot in perpendicular plane ± 1 1/2 feet

Average movement of spot in perpendicular plane ± 8 inches

(*) Refers to number in comment statement

Angular Movement Test (Continued)

Average wind speed 4 MPH

Variations in wind speed $\pm$ 2 MPH

Average wind direction NW

Variations in wind direction $\pm 30^{\circ}$

Atmospheric Data

Barometric pressure 30.51 in Hg

Temperature 66°

Comments:

APPENDIX D

STANDARD SURFACE REFLECTANCE AND DIFFUSENESS

A surface composed of Nextel Velvet Coating 101-A10 white paint manufactured by the 3M Company was used as a standard throughout the experiments. Using this standard the relative bidirectional reflectances of various test surfaces were obtained by comparing the readings taken with the spectroradiometer from a test surface to the readings taken from the standard surface. Since a surface composed of 101-A10 white paint is not perfectly reflecting or perfectly diffuse, true values of the bidirectional reflectances of the test surface were not obtained. However, the true values of bidirectional reflectance can be obtained if the reflectance and diffuseness of the standard surface is known and are used to correct the relative reflectances. The procedure and analysis used to make these corrections are given in Appendix E.

The total hemispherical reflectance of 101-A10 white paint is presented in Figure D-1. This information was received from the manufacturer (Reference 61) and covers the spectral range in which readings were taken. Figures D-2 and D-3 give the manufacturer's data on the diffuseness of a surface of 101-A10 white paint. This information is based on the light being reflected in the total visible region of the electromagnetic spectrum.

Since the energy recorded with the spectroradiometer used in the experiments was in narrow bandwidths as opposed to the data given in Figures D-2 and D-3, laboratory tests were made to determine the diffuseness of the surface as obtained with the spectroradiometer. Data were recorded with the source and the mirror in the same plane.

Figure D-4 shows the method used to determine the intensity of the light impinging on the standard surface. If the surface were

perfectly diffuse, the amount of energy reflected at different source angles (ζ) would be proportional to the incoming intensity. The intensity at various angles was rationed to the intensity impinging on the surface at ζ = 0 degrees. It is seen that the intensity of the energy received by the surface is proportional to cos ζ if the distance between the source and the test area is kept constant.

Figures D-5 through D-20 give the results of the data taken for the standard surface tests at different wavelengths. The intensity of the energy received by the radiometer from the standard surface was amplified and recorded as millivolts as seen in the figures. Two separate runs were made for each curve. At λ = 0.40 microns, two types of sources were used so that two curves were obtained. These results are shown in Figure D-6. The viewing angle (θ) for all the data taken was 15 degrees. All angles were measured according to the geometry shown in Figure III-2. Correction factors for the lack of diffuseness of the standard surface based on a viewing angle of 75^{o} and with $\zeta = 0^{o}$ as a standard can be obtained by ratioing the differences between the predicted and the actual curves to the values obtained for the predicted curves.

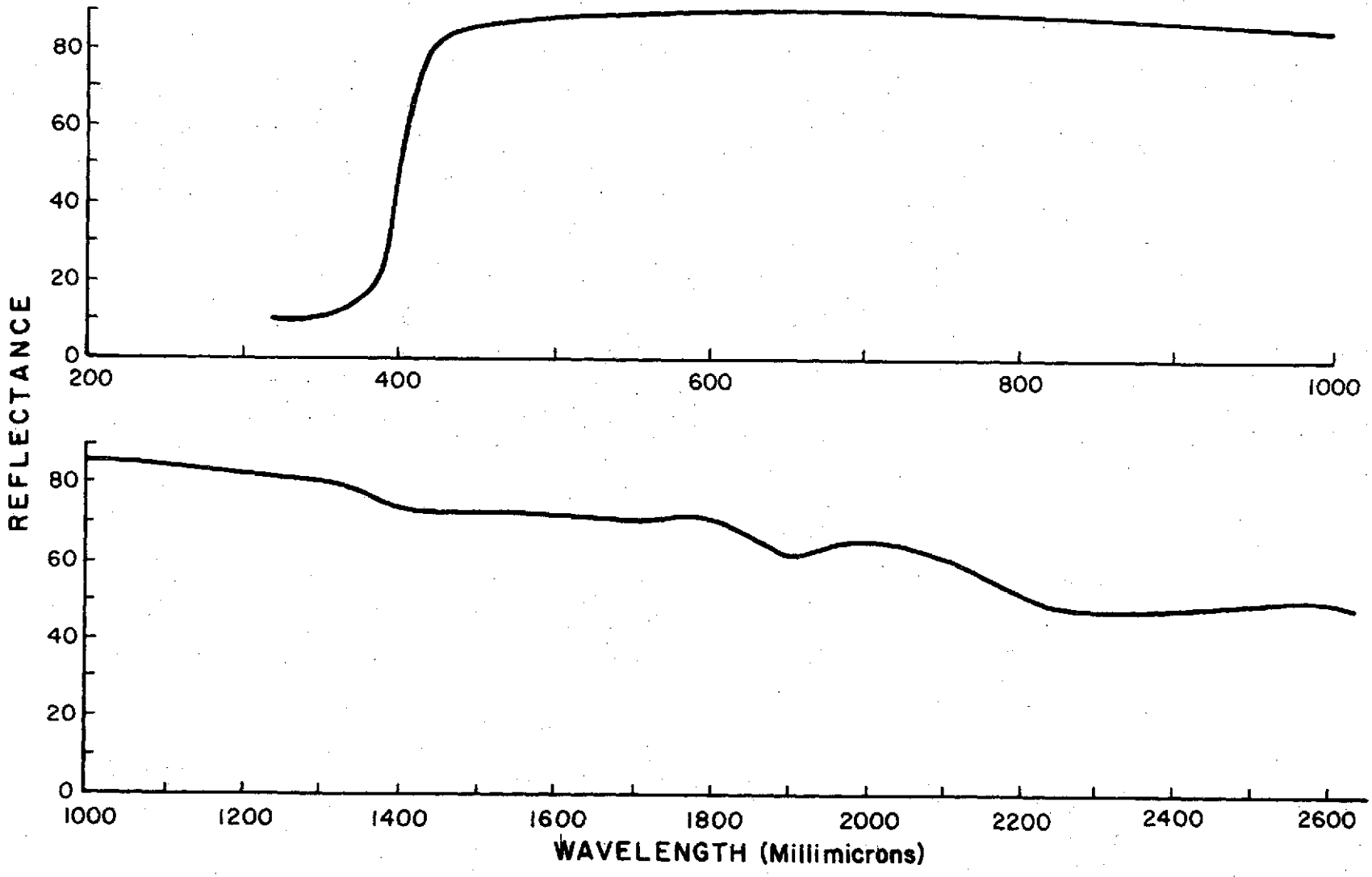

FIGURE D-1. TOTAL HEMISPHERICAL REFLECTANCE OF 101-A10 WHITE

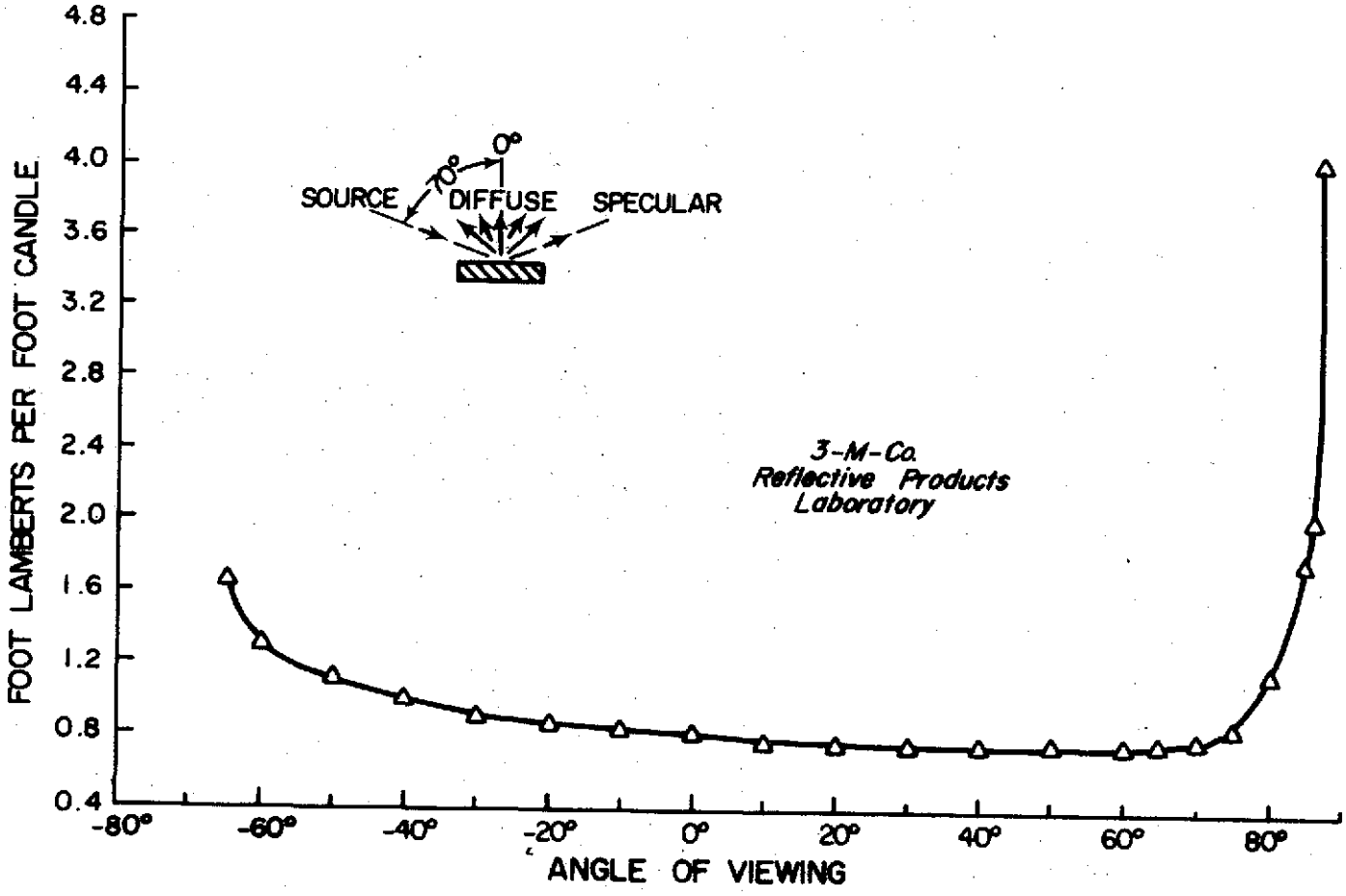

FIGURE D-2. DIRECTIONAL REFLECTANCE OF 101-A10 WHITE PAINT
LIGHT SOURCE AT -70° INCIDENCE

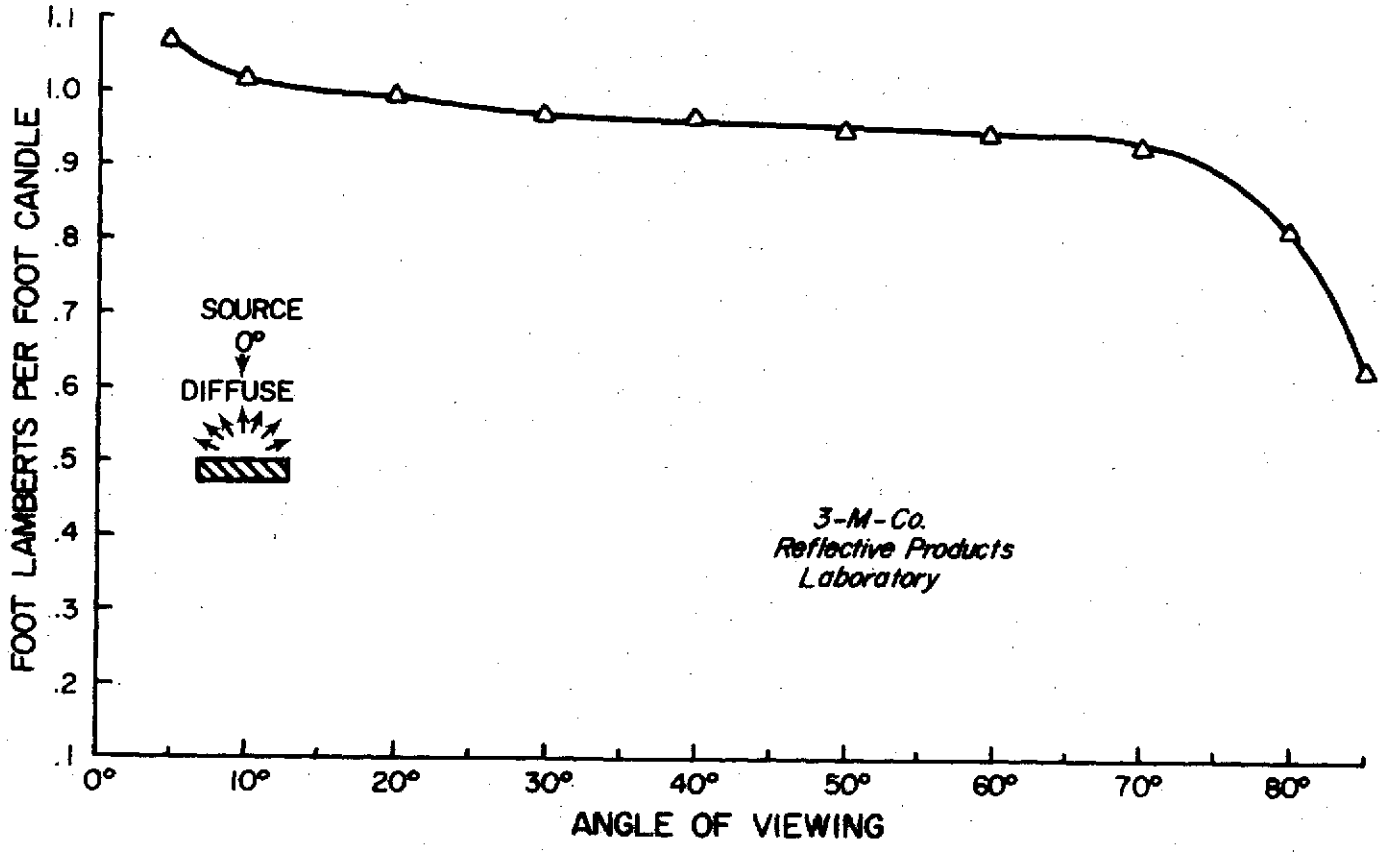

FIGURE D-3. DIRECTIONAL REFLECTANCE OF 101-A10 WHITE PAINT LIGHT SOURCE AT 0° INCIDENCE

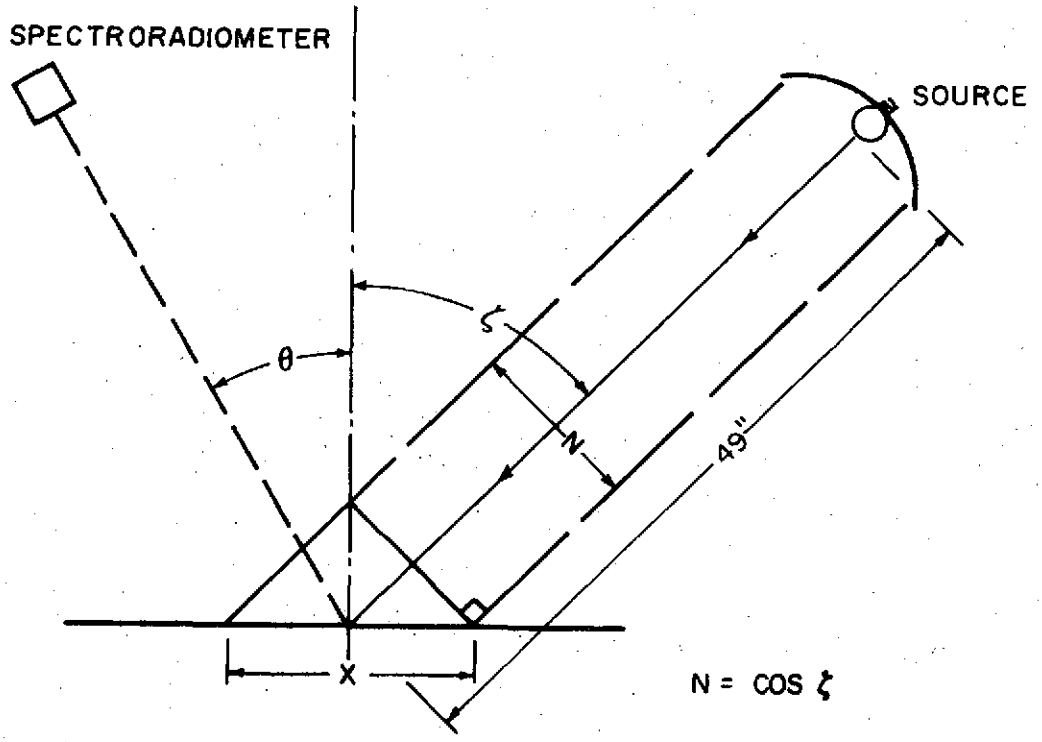

FIGURE D-4. SCHEMATIC OF TECHNIQUE USED TO TEST STANDARD SURFACE

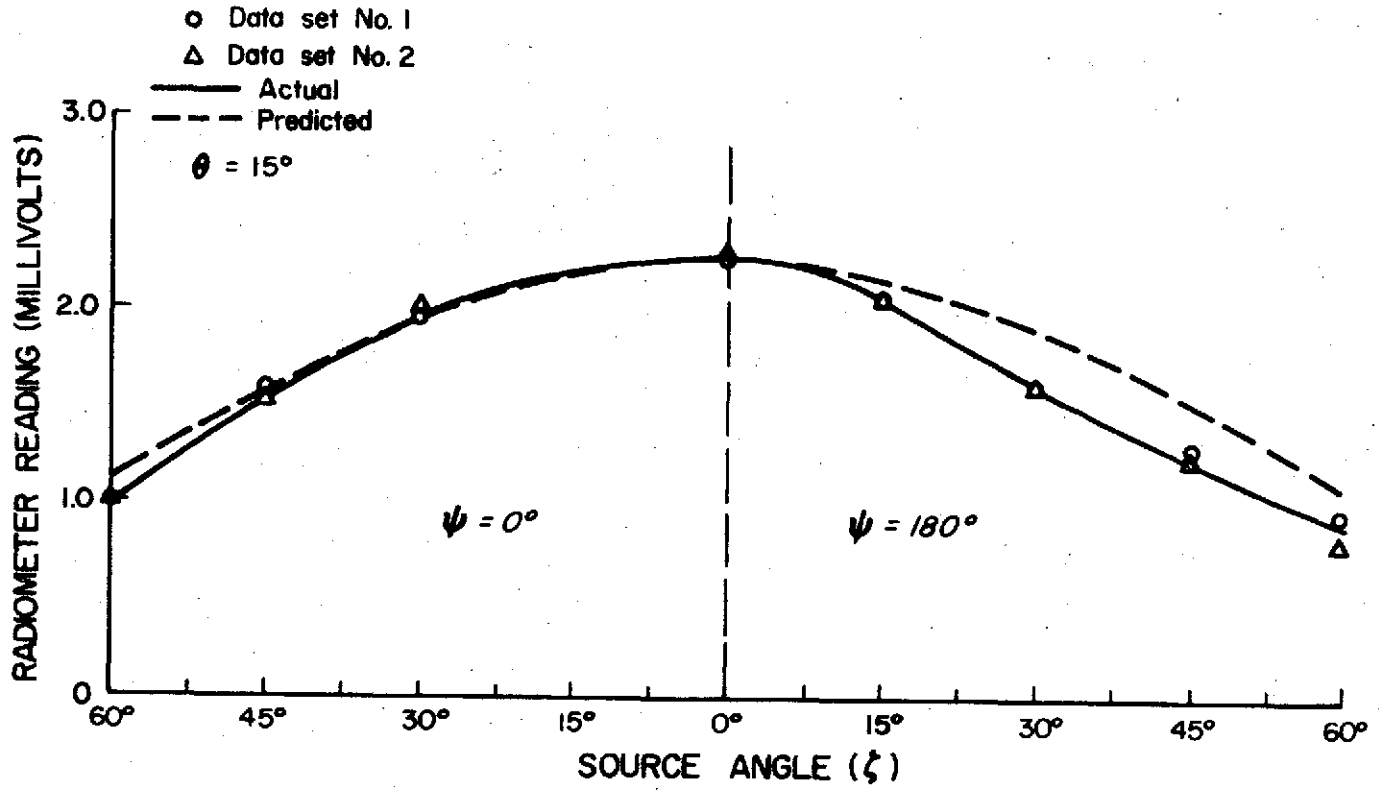

FIGURE D-5. ENERGY REFLECTED FROM STANDARD SURFACE AT $\lambda = 0.35$ MICRONS

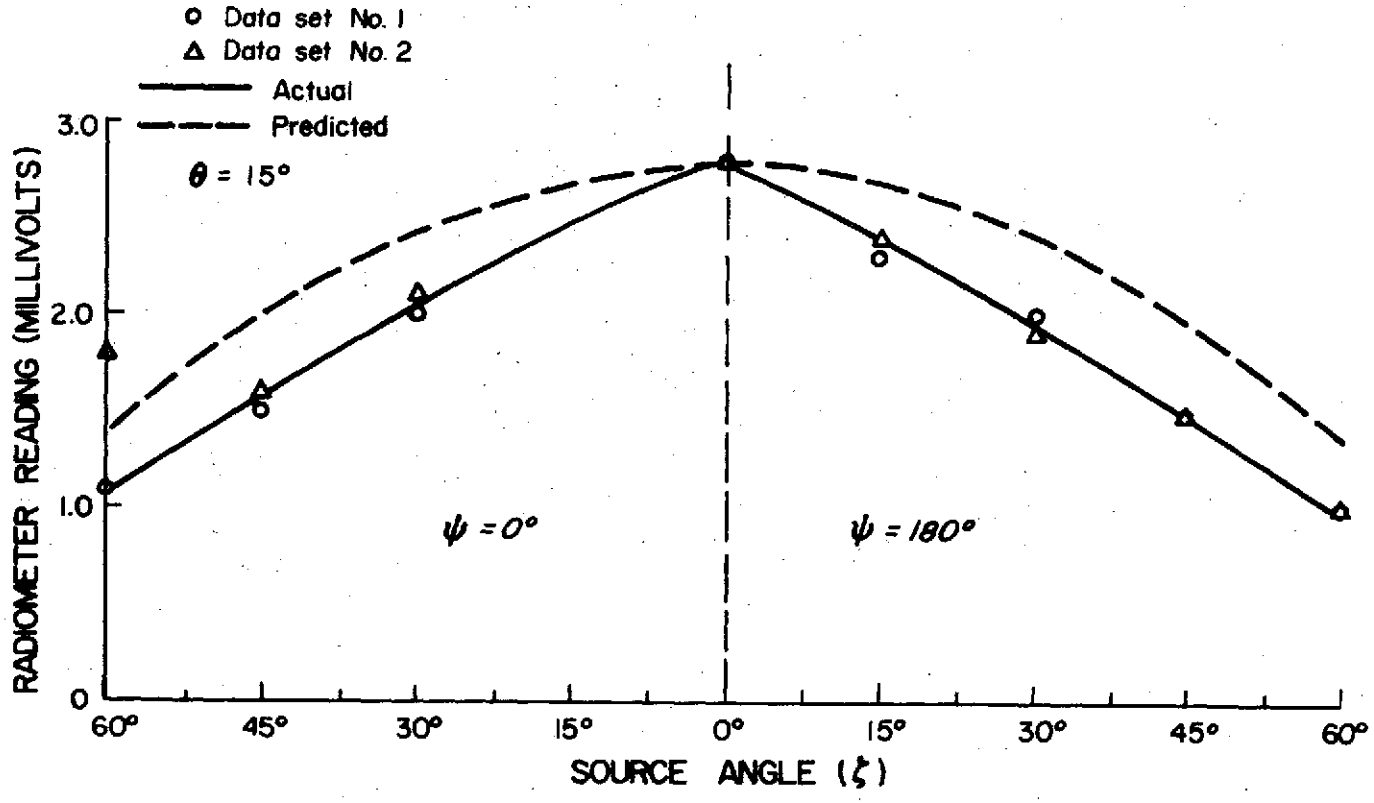

FIGURE D-6A ENERGY REFLECTED FROM STANDARD SURFACE AT λ=0.40 MICRONS

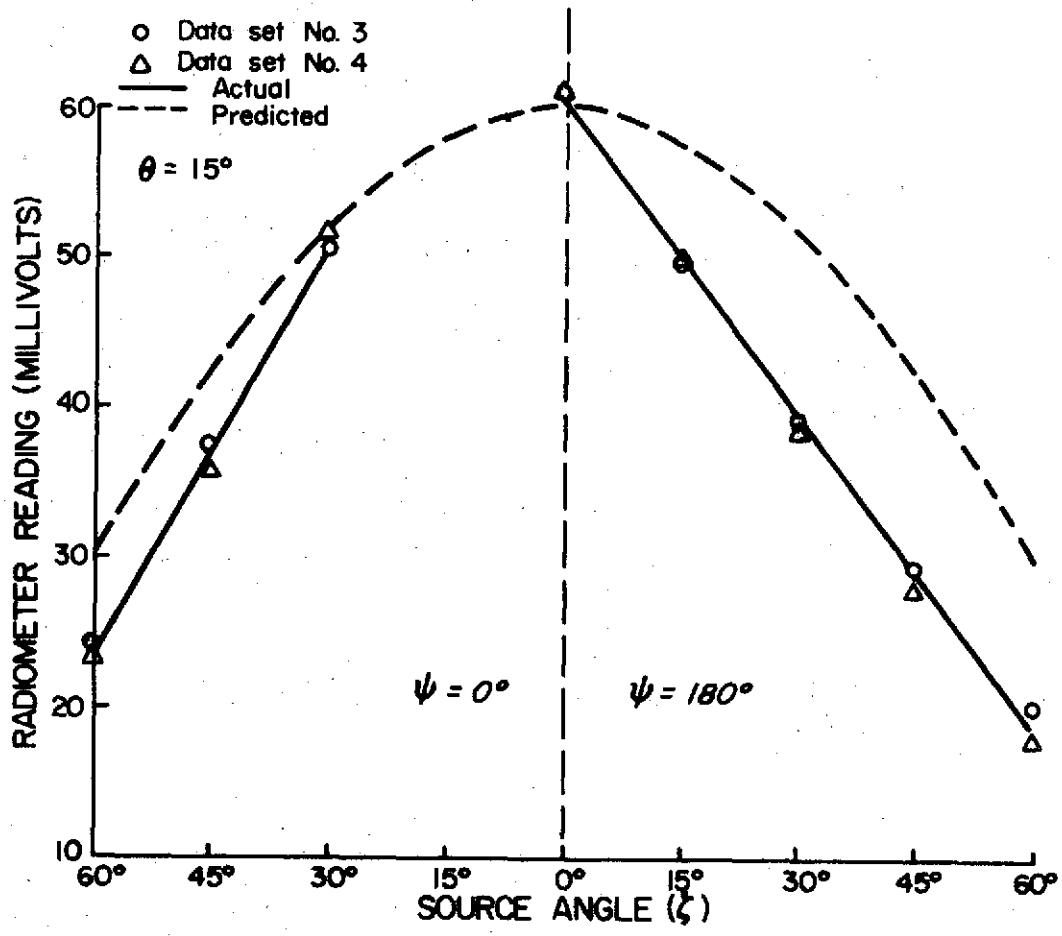

FIGURE D-6B. ENERGY REFLECTED FROM STANDARD SURFACE AT $\lambda = 0.40$ MICRONS

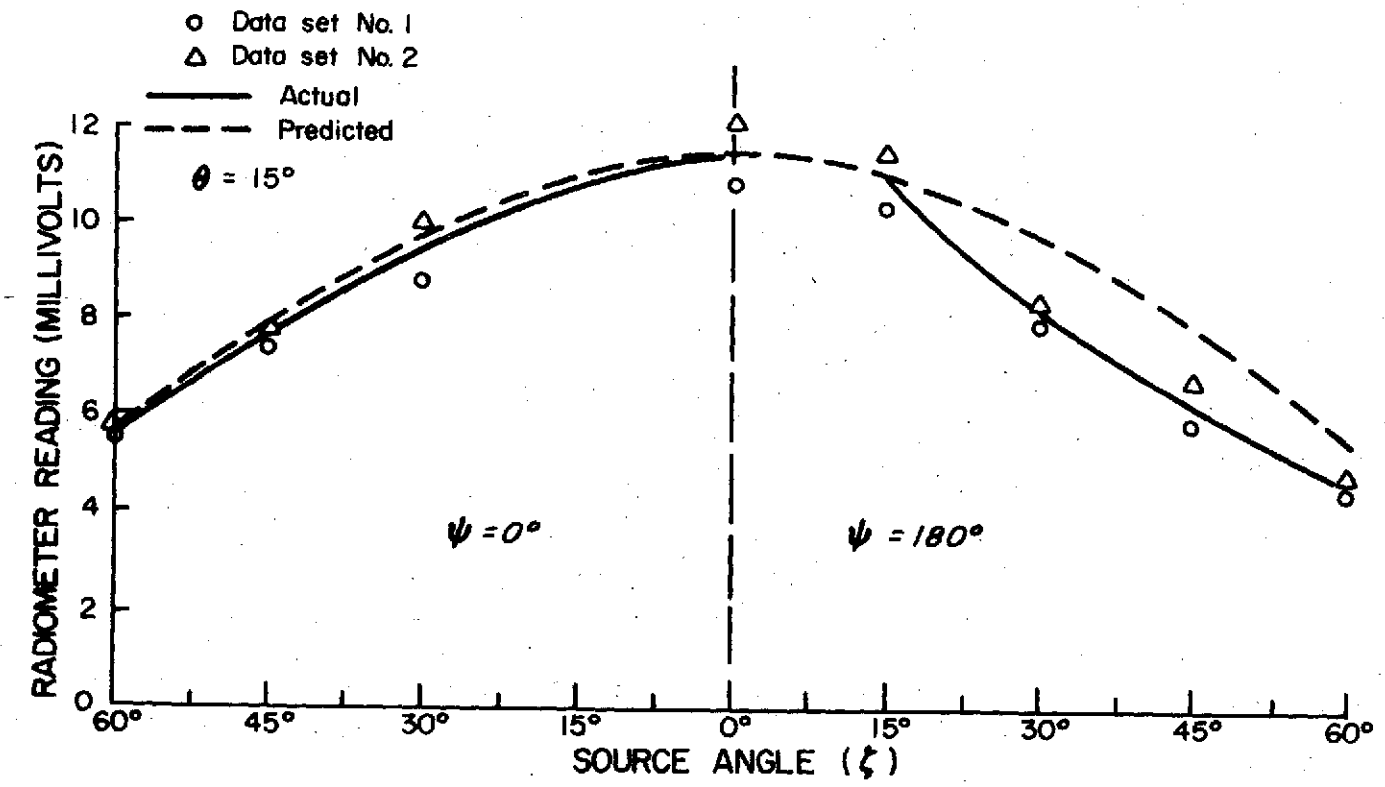

FIGURE D-7. ENERGY REFLECTED FROM STANDARD SURFACE AT λ=0.45 MICRONS

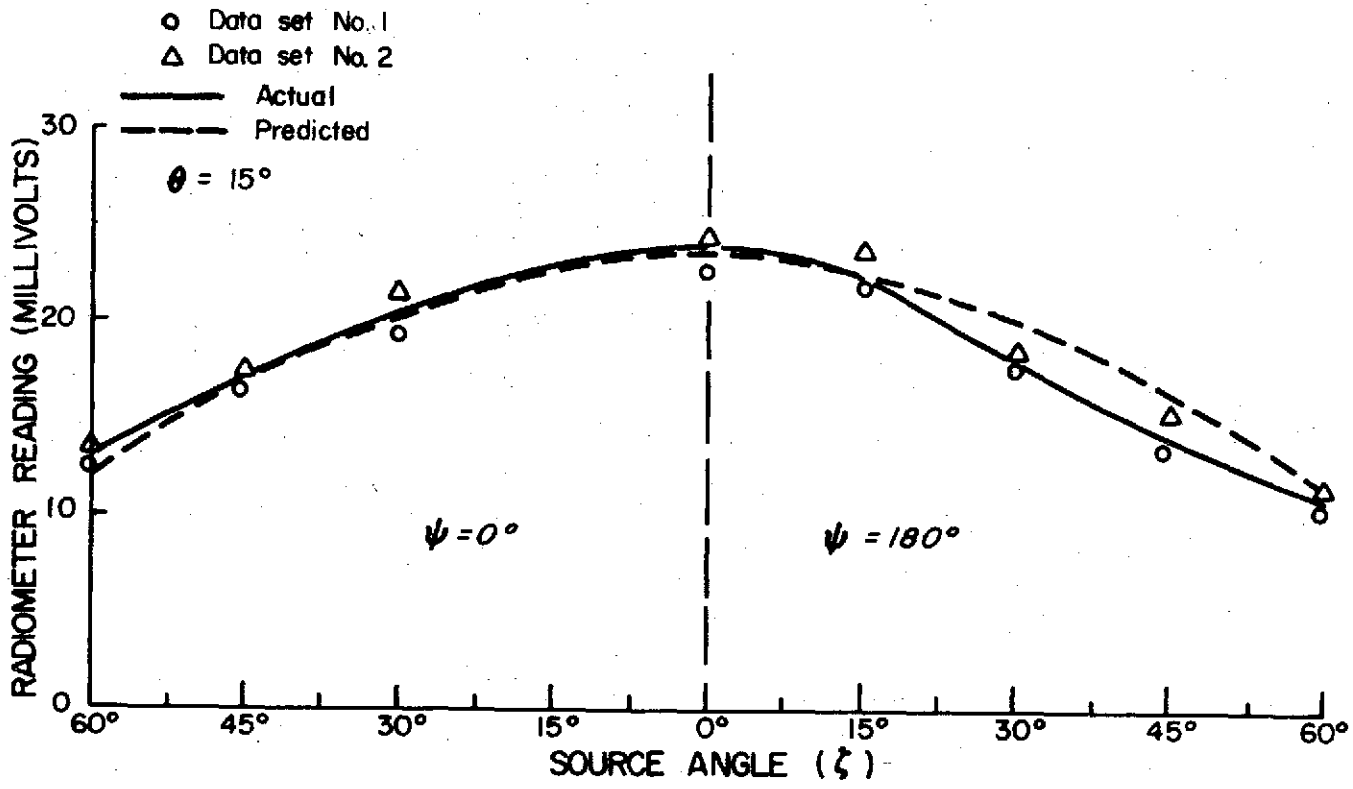

FIGURE D-8. ENERGY REFLECTED FROM STANDARD SURFACE AT λ=0.50 MICRONS

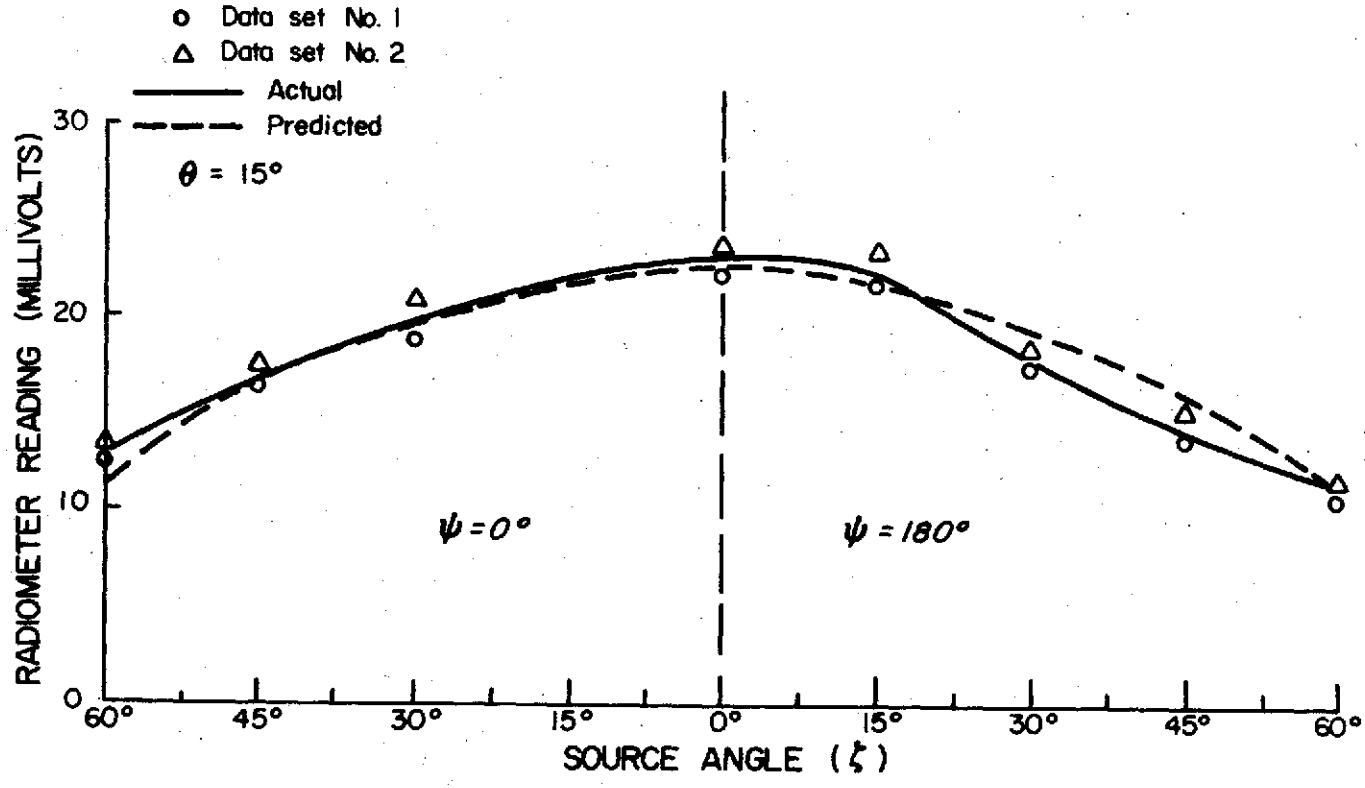

FIGURE D-9. ENERGY REFLECTED FROM STANDARD SURFACE AT λ=0.55 MICRONS

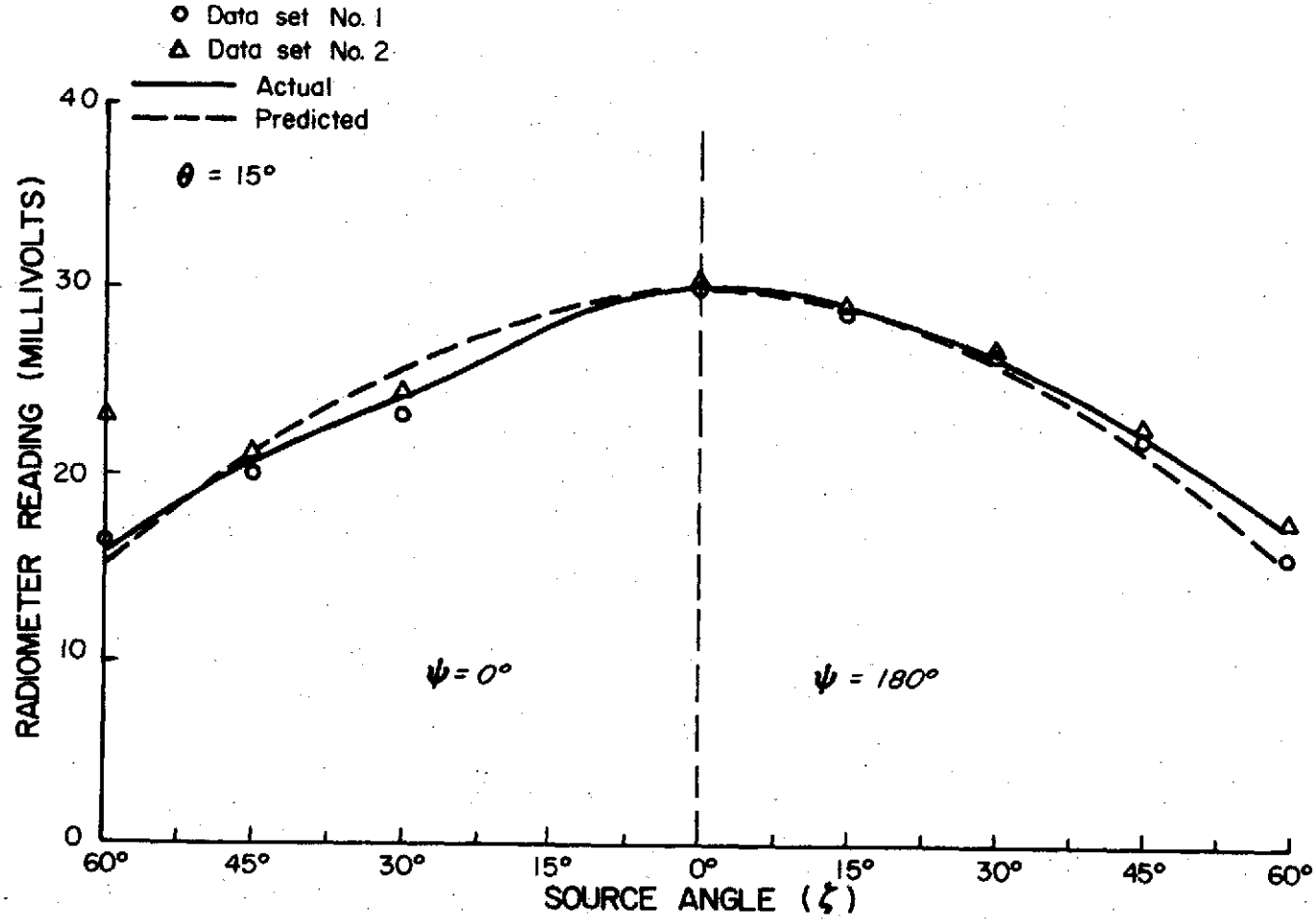

FIGURE D-10. ENERGY REFLECTED FROM STANDARD SURFACE AT λ=0.60 MICRONS

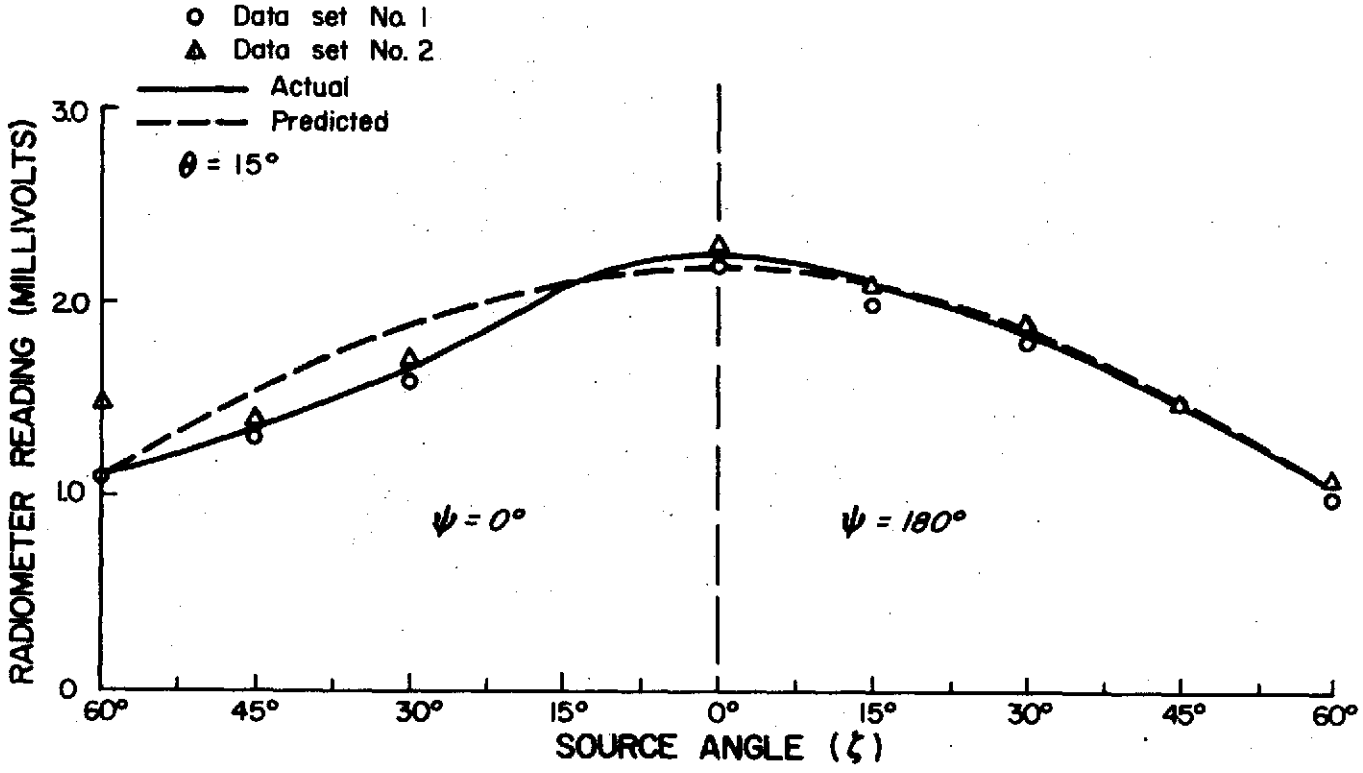

FIGURE D-11. ENERGY REFLECTED FROM STANDARD SURFACE AT λ=0.65 MICRONS

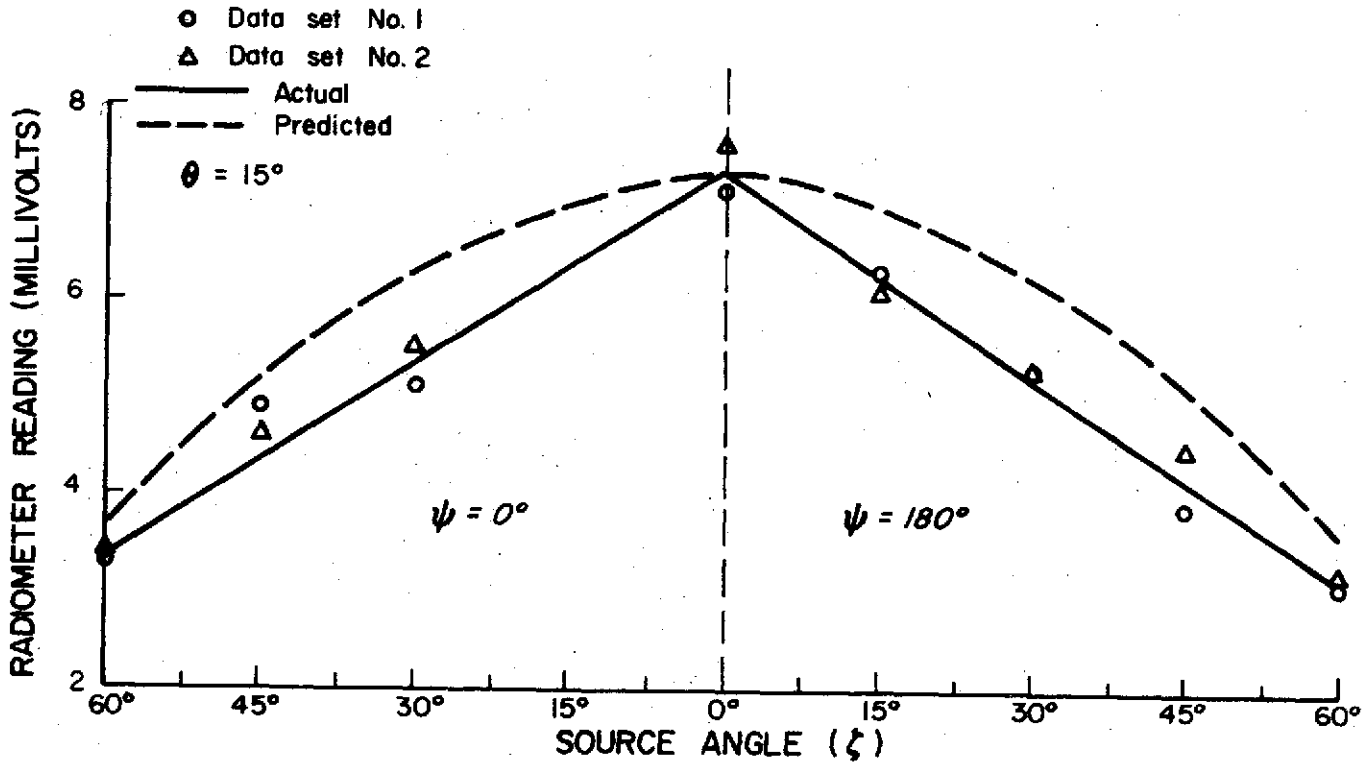

FIGURE D-12. ENERGY REFLECTED FROM STANDARD SURFACE AT $\lambda = 0.75$ MICRONS

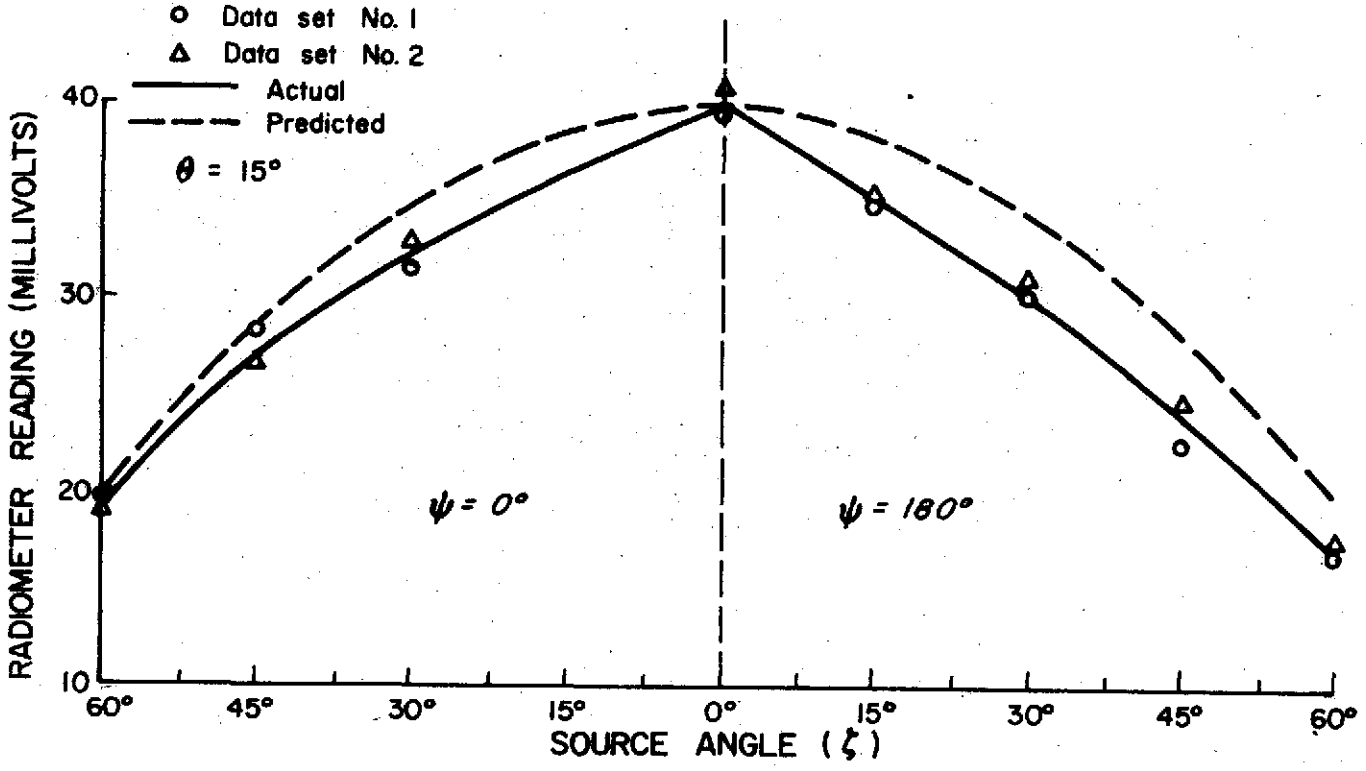

FIGURE D-13. ENERGY REFLECTED FROM STANDARD SURFACE AT λ= 0.85 MICRONS

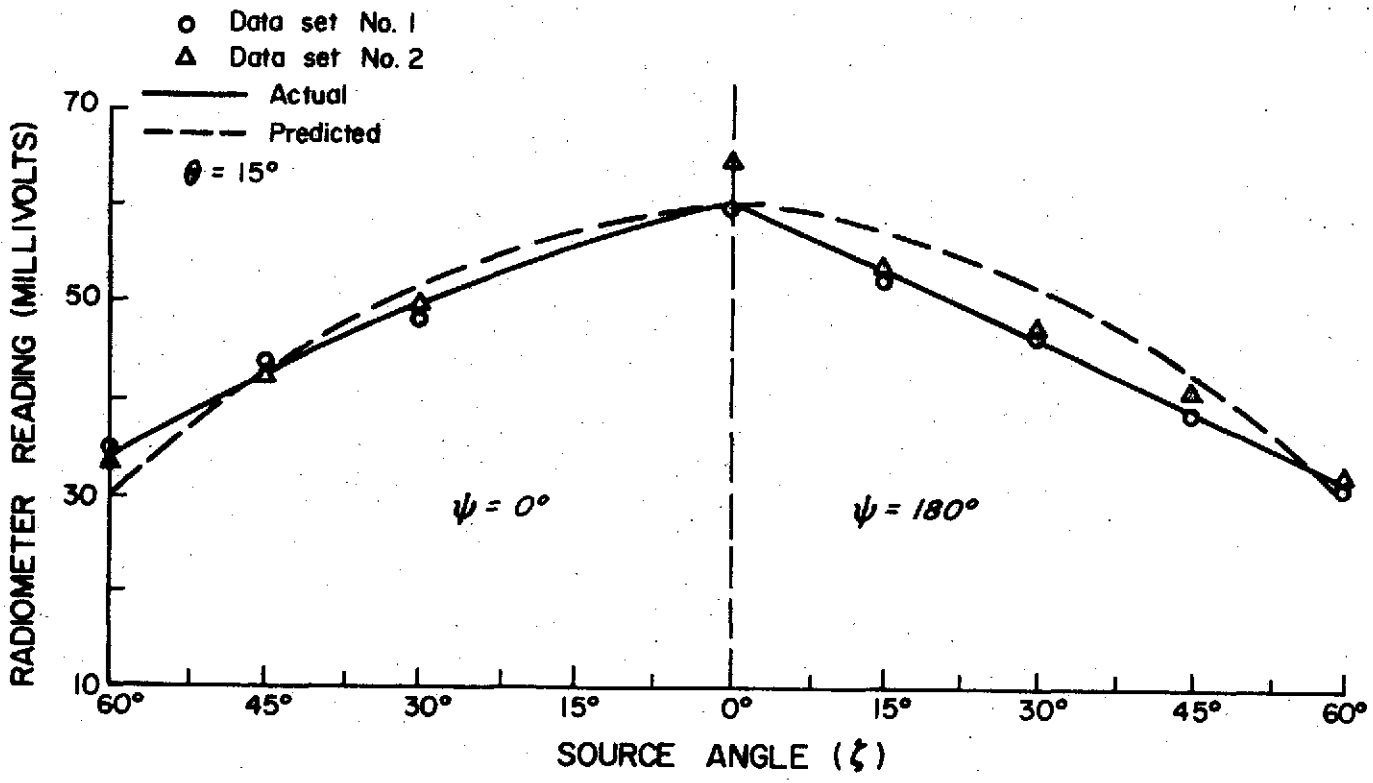

FIGURE D-14. ENERGY REFLECTED FROM STANDARD SURFACE AT λ= 1.00 MICRONS

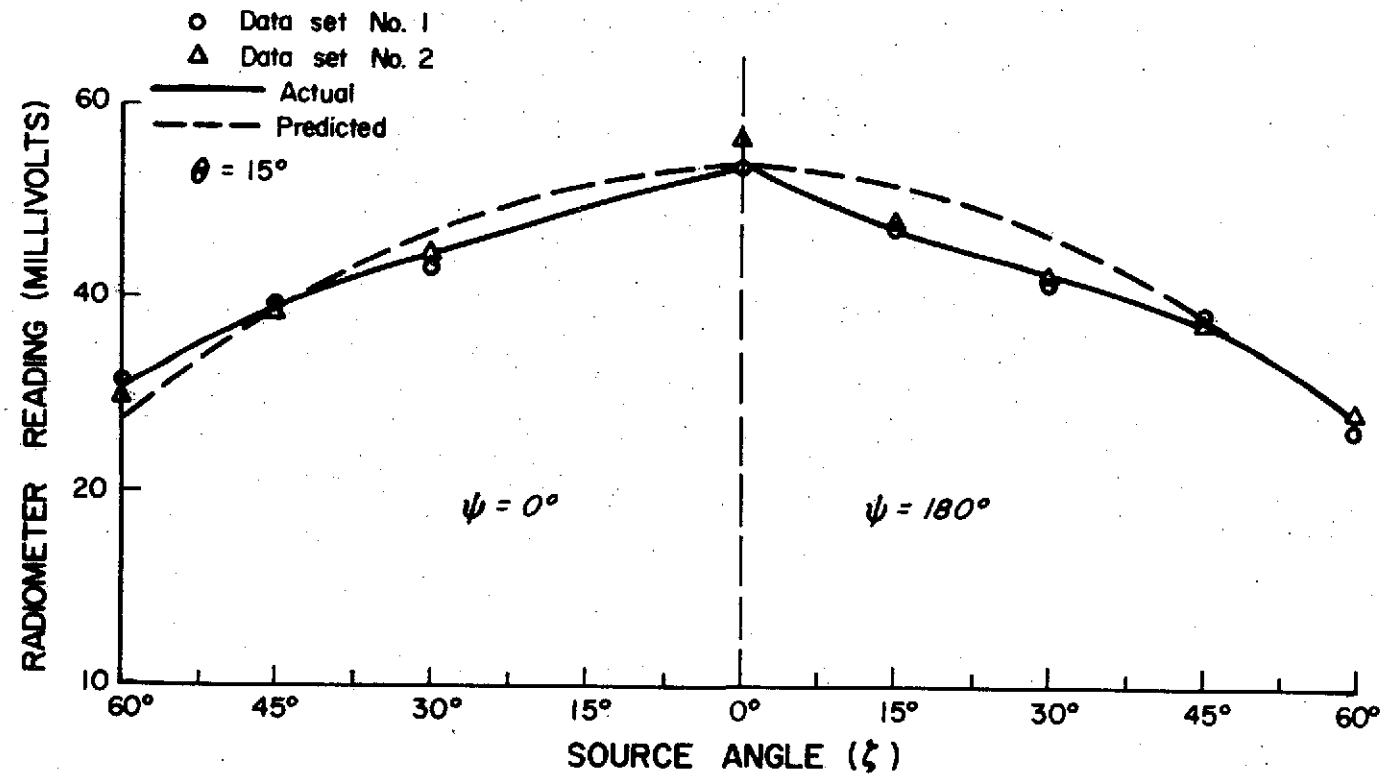

FIGURE D-15. ENERGY REFLECTED FROM STANDARD SURFACE AT $\lambda = 1.25$ MICRONS

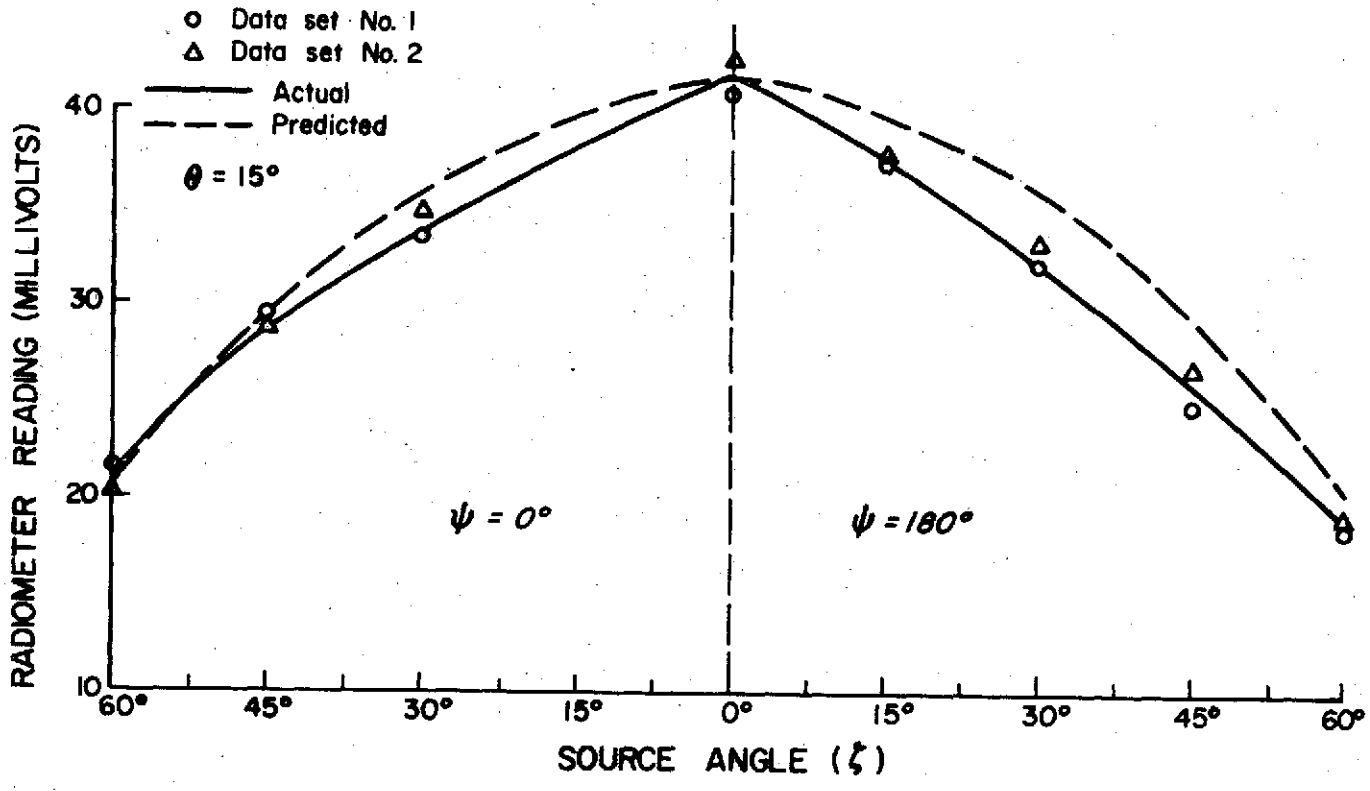

FIGURE D-16. ENERGY REFLECTED FROM STANDARD SURFACE AT $\lambda = 1.50$ MICRONS

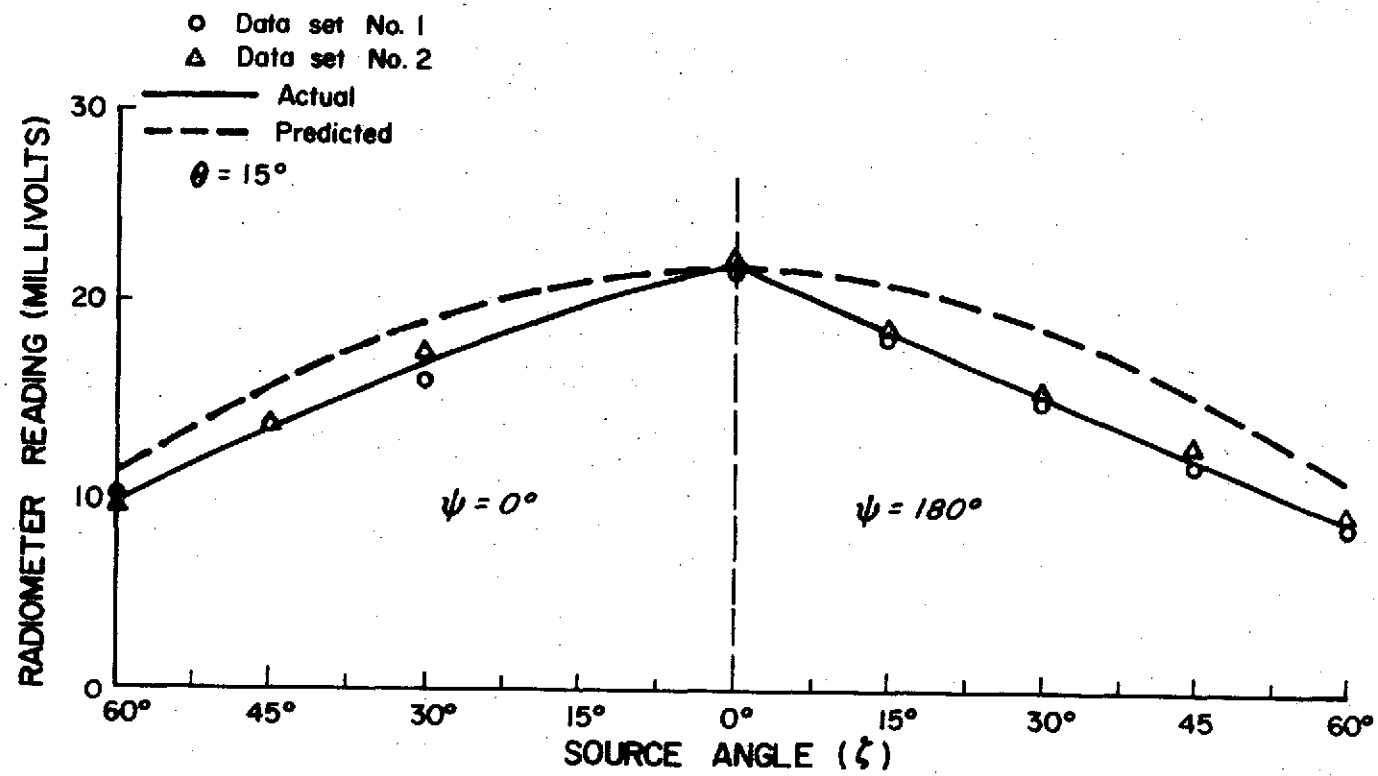

FIGURE D-17. ENERGY REFLECTED FROM STANDARD SURFACE AT λ=1.75 MICRONS

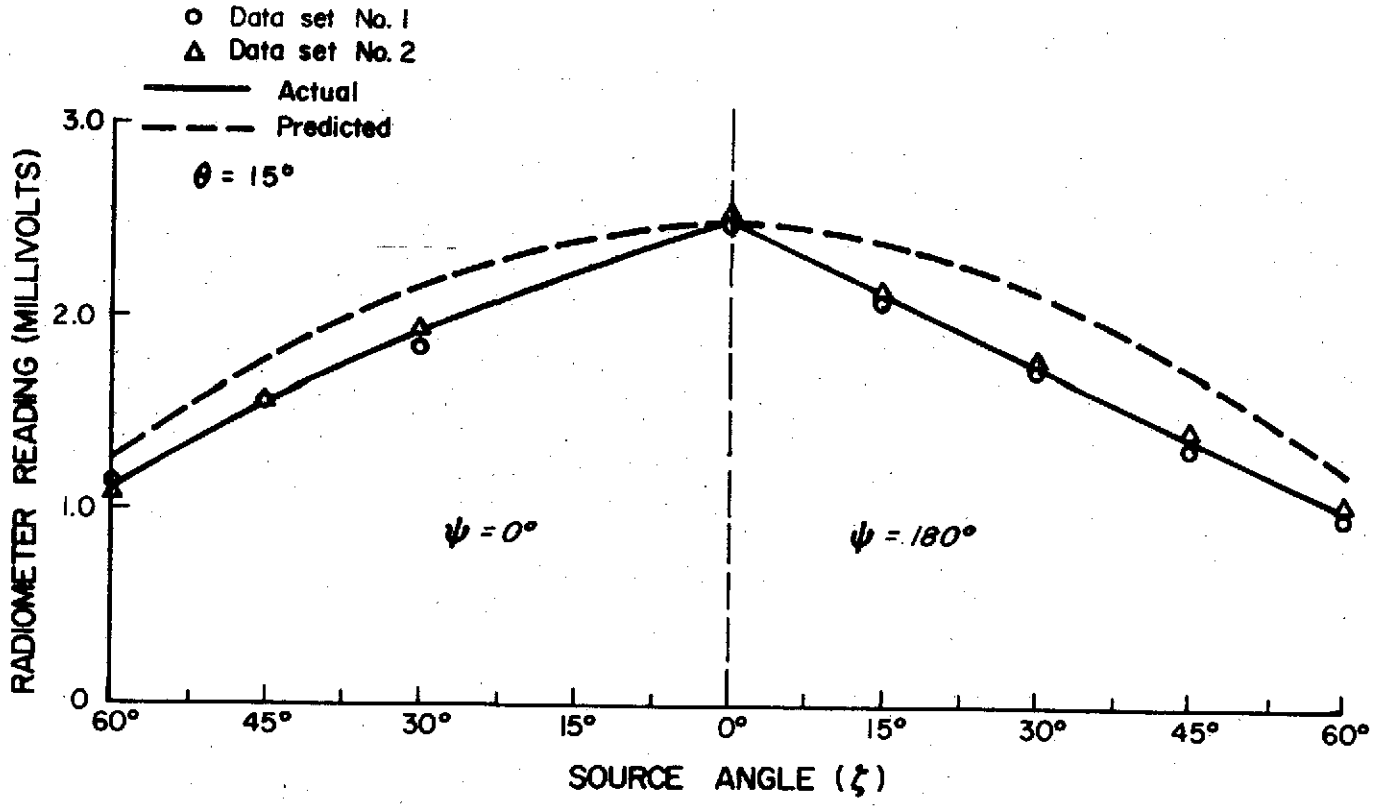

FIGURE D-18. ENERGY REFLECTED FROM STANDARD SURFACE AT λ=2.00 MICRONS

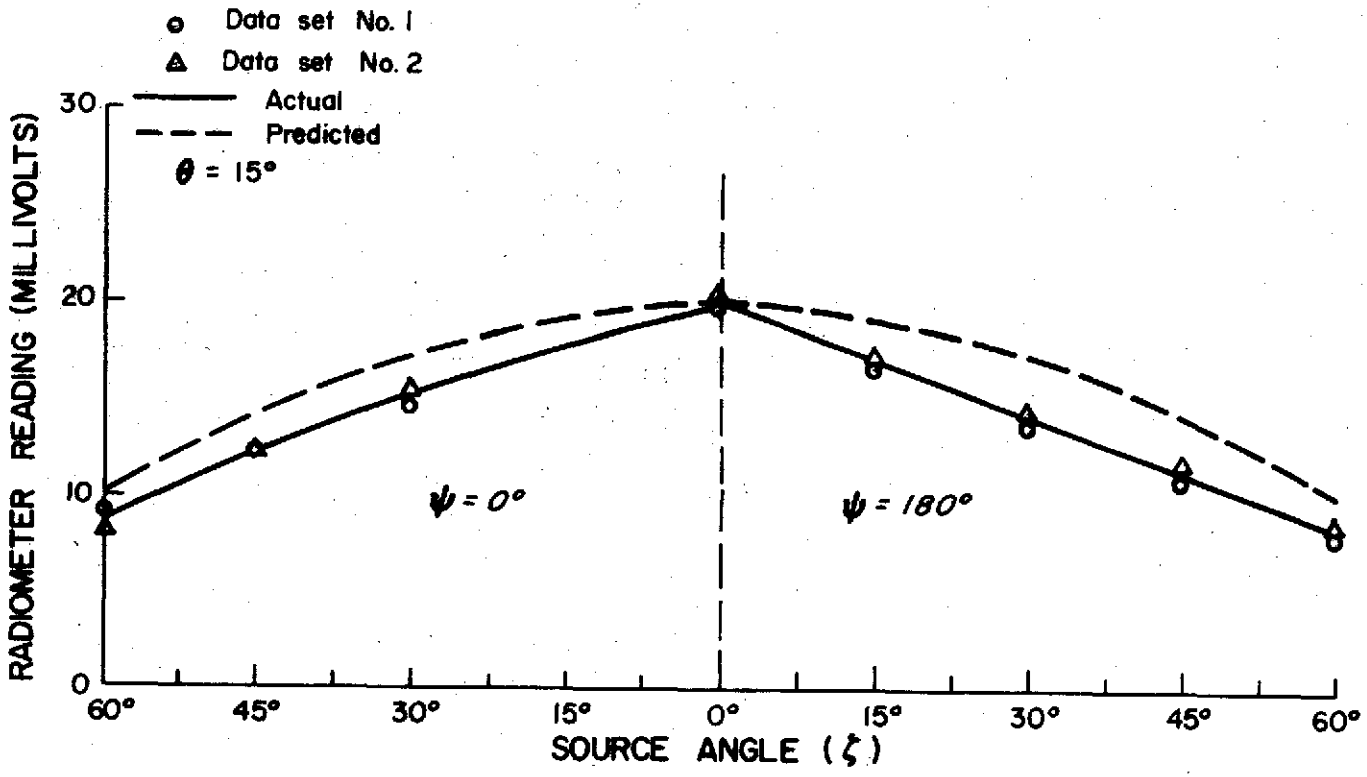

FIGURE D-19. ENERGY REFLECTED FROM STANDARD SURFACE AT $\lambda = 2.25$ MICRONS

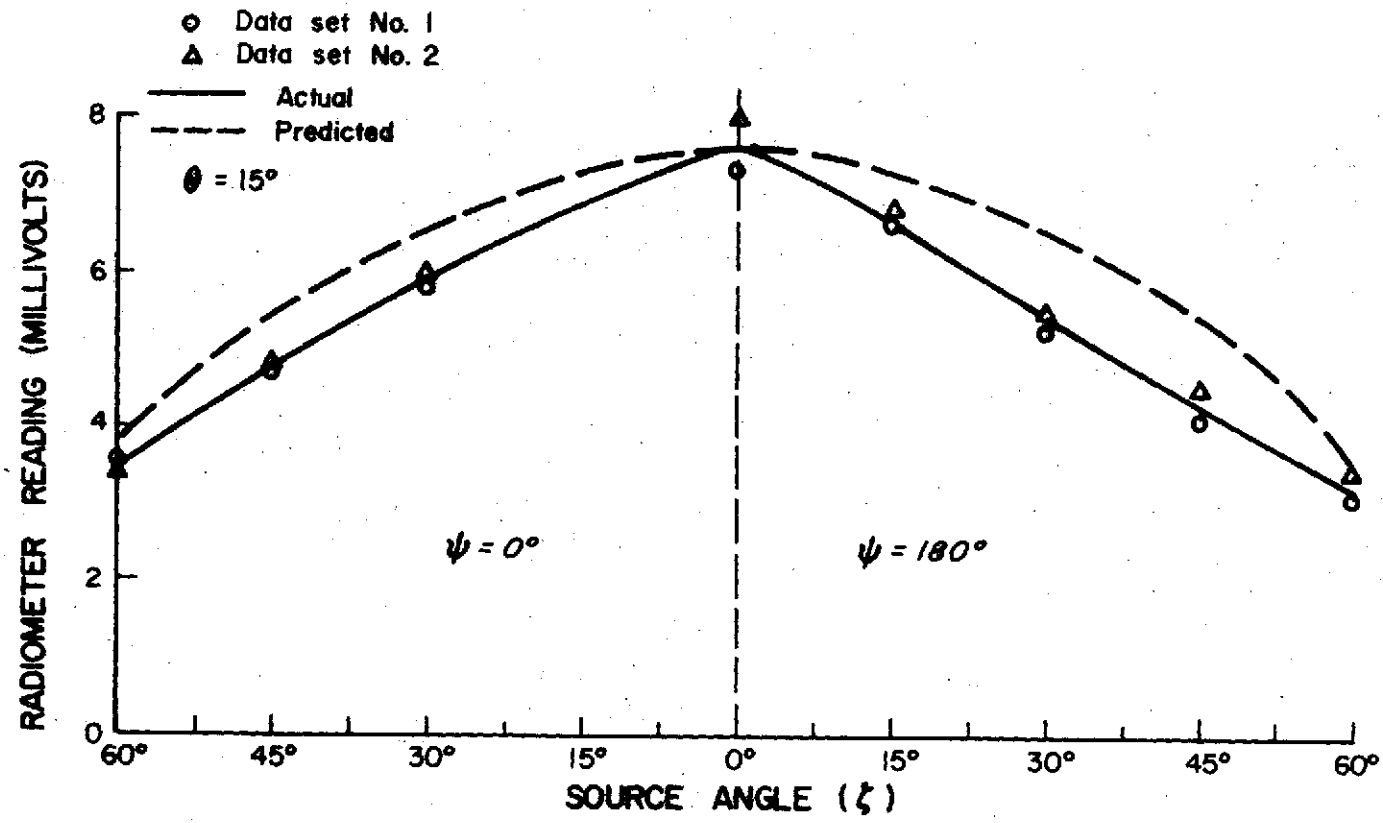

FIGURE D-20. ENERGY REFLECTED FROM STANDARD SURFACE AT λ=2.50 MICRONS

APPENDIX E

PROCEDURE AND DATA FROM LABORATORY REFLECTANCE TESTS

Several different procedures were used to obtain reflectance data and variations in the reflectance with source angle in the laboratory. In the tests numbered 1-32, runs were made to determine the reflectance of St. Augustine grass. The procedure used to obtain these data was to first read the energy being reflected from the test surface and then to read the energy being reflected from the standard surface at the same angle under the same lighting conditions. All readings were made at night so that the only energy incoming to the surface was from the lamp source. After making tests on the standard surface of 101-A10 white paint which showed that it had variations in its diffuseness with source angle, all of this data was considered invalid for determining variations in reflectance with source angle except for that taken in the visible region. In the visible region the data taken showed that the standard surface was close to perfectly diffuse. Therefore, this data was retained and is presented in Table E-1 and Figures VI-4 and VI-5. In order to obtain the variations in the reflectance with source angle, the percent difference at each angle to the average reflectance as given in Table E-1 was plotted. The final results are shown in Figure VI-7B.

The main emphasis of the study was not only to accurately determine the reflectances of the test surfaces but also to find the angular dependence of the reflectance on source angle. Since finding the angular dependence of the reflectance by taking reflectance readings at different source angles was not practical without a diffuse surface if the first procedure was used, a new procedure was developed. The second procedure was based on knowing the relationship between the intensity of the incoming energy to the test surface at each source

angle during the tests. For these tests this relationship was the cos ζ as seen in Figure D-1. This factor was based on positioning the source at the exact distance from the test plot for all the source angles at which data was taken. Greater accuracy was also obtained by using a reflector to help collimate the light beam so any inaccuracies in positioning the source were minimized. Putting this factor into Equation VI-1, the bidirectional reflectance becomes

$$\bar{\rho}(\lambda, \theta, \zeta, \Psi) = \frac{I_{out}(\lambda, \theta_{out}, \zeta_{out}, \Psi_{out})}{\cos \zeta \; I_{in}(\lambda, \theta_{in}, \zeta_{in}, \Psi_{in})} \qquad \text{E-1}$$

Since the same source was used for each test, I_{in} normal to the surface is a function of wavelength and source angle only. Therefore, even though I_{in} is unknown the variations in the reflectance with source angle (ζ) can easily be found by using the correction factor cos ζ for the readings of intensity obtained from the test surface with the spectroradiometer. The data obtained with this procedure is given in Tables E-2 through E-7. The reflectances of the test surfaces at $\zeta = 0^{\circ}$ was used as the reference in order to obtain the variances. Complete curves showing the relative bidirectional reflectances versus wavelength of each test surface were made from $\lambda = 0.3$ to $\lambda = 3.0$ microns at a source angle of zero degrees and with a viewing angle of 15 degrees.

Tables E-2 through E-5 present the actual data readings taken for St. Augustine grass and Mississippi Delta alluvial soil. Two sets of data were taken for each of these surfaces. The viewing angle was kept constant at 15 degrees for all the data taken. Complete spectral data was taken at a source angle of zero degrees from both the standard

surface and test surface and then ratioed to give the relative bidirectional reflectance. This data is shown plotted in Chapter VI. The data given in Tables E-2 through E-5 was used to find the variations in the reflectances with source angle. The data presented in the tables for the two runs was first averaged for each source angle, then based on the readings taken at $\zeta = 0^{\circ}$, the expected readings if there were no variations in the reflectance with source angle were calculated by multiplying the values at $\zeta = 0^{\circ}$ by the cos ζ. The differences between the actual and the predicted values were then calculated and the curves normalized to give percent of variation with source angle. These data are shown plotted in Chapter VI.

The same type of data was obtained for Bermuda grass in the laboratory except that only one test run was made. However, the data taken to obtain variational effects was obtained every $7\frac{1}{2}$ degrees instead of every 15 degrees as done for the St. Augustine grass and the soil. This data is shown in Tables E-6 and E-7. The procedure used to normalize the data was to divide each reading by cos ζ and then to average the results. The deviations and percent variation at each source angle were then calculated and are shown plotted in Chapter VI. The relative bidirectional reflectance data at $\zeta = 0^{\circ}$ as obtained for the Bermuda grass by reading from both the test surface and the standard surface is also given in Chapter VI.

ζ	Between Bidirectional Reflectance				
	λ=0.45	λ=0.50	λ=0.55	λ=0.60	λ=0.65
60^{o}	0.062	0.079	0.118	0.080	0.103
45^{o}	0.050	0.070	0.102	0.070	0.087
30^{o}	0.070	0.093	0.128	0.089	0.109
0^{o}	0.058	0.081	0.110	0.085	0.105
15^{o}	0.051	0.067	0.106	0.076	0.093
30^{o}	0.045	0.061	0.099	0.072	0.081
45^{o}	--	--	--	--	--
60^{o}	0.053	0.072	0.115	0.072	0.092
Ave.	0.0556	0.0747	0.112	0.078	0.957

TABLE E-1: Source Zenith Angle Influence on Saint Augustine Grass Reflectance in Visible Region

Runs 2-8

$\theta = 15^{o}$

ζ	Spectroradiometer Readings ~ Millivolts								
	λ =0.75		λ = 0.85		λ = 1.00		λ = 1.25		λ = 1.50
	Run 33	Run 34	Run 33	Run 34	Run 33	Run 34	Run 33	Run 34	Run 33
60°	2.0	1.95	11.5	11.4	18.6	18.7	6.9	6.8	6.6
45°	2.8	2.3	15.2	14.7	24.9	24.3	9.7	9.4	9.2
30°	3.2	3.1	18.9	18.8	31.2	31.2	13.0	12.8	12.1
0°	3.7	3.4	22.9	20.5	37.1	33.8	15.5	13.9	14.9
15°	3.4	3.0	19.8	18.6	32.4	30.8	13.1	12.1	12.4
30°	2.8	2.9	17.1	16.9	27.9	27.6	10.7	10.4	10.3
45°	2.4	2.3	14.2	14.3	23.6	23.4	9.1	8.8	8.8
60°	1.9	1.9	11.3	11.1	18.7	18.6	7.1	7.3	7.0

TABLE E-2: Spectroradiometer Readings From Saint Augustine Grass Taken With Lead Sulfide Detector

$\theta = 15^{\circ}$

ζ	Spectroradiometer Readings ~ Millivolts								
	λ = 1.50	λ = 1.75		λ = 2.00		λ = 2.25		λ = 2.50	
		Run 33	Run 34	Run 33	Run 34	Run 33	Run 34	Run 33	Run 34
60°	6.8	1.4	1.4	1.0	1.1	1.3	--	0.8	--
45°	9.2	1.8	1.9	1.3	1.4	1.7	--	1.0	--
30°	12.3	2.5	2.4	2.2	2.0	2.3	--	1.5	--
0°	13.5	3.1	2.8	2.4	2.2	2.7	2.5	1.5	1.4
15°	11.5	2.6	2.3	1.9	1.9	2.2	--	1.2	--
30°	10.1	2.2	1.9	1.7	1.5	1.8	--	1.1	--
45°	8.7	1.8	1.9	1.4	1.3	1.5	--	1.0	--
60°	7.1	1.6	1.4	1.3	1.1	1.3	--	0.8	--

TABLE E-2: (Con't.) Spectrodadiometer Readings from Saint Augustine Taken with Lead Sulfide Detector

$\theta = 15^{\circ}$

ζ	Spectroradiometer Readings ~ Millivolts							
	λ = 0.35		λ = 0.40		λ = 0.45		λ = 0.50	
	Run 35	Run 36	Run 35	Run 36	Run 35	Run 36	Run 35	Run 36
60°	3.4	3.5	4.9	4.95	2.8	2.8	6.2	6.3
45°	5.4	5.3	7.5	7.2	3.5	3.5	8.65	8.6
30°	9.3	8.8	12.5	11.9	4.9	4.8	13.1	12.9
0°	8.7	9.1	11.9	12.7	4.95	5.0	13.4	13.7
15°	6.7	6.7	9.15	9.1	4.1	4.0	10.6	10.45
30°	5.3	5.1	7.1	6.85	3.65	3.4	9.1	8.5
45°	4.2	4.2	5.5	5.5	3.1	3.0	7.3	7.1
60°	3.35	3.2	4.3	4.1	2.0	2.6	5.95	5.65

TABLE E-3: Spectroradiometer Readings from Saint Augustine Grass Taken with Photomultiplier Tube

$\theta = 15^{\circ}$

ζ	Spectroradiometer Readings ~ Millivolts					
	$\lambda = 0.55$		$\lambda = 0.60$		$\lambda = 0.65$	
	Run 35	Run 36	Run 35	Run 36	Run 35	Run 36
60°	15.5	15.8	3.3	3.3	1.65	1.65
45°	20.5	20.4	4.5	4.5	2.4	2.4
30°	27.7	27.4	6.6	6.7	3.8	3.7
0°	28.8	29.3	7.15	7.2	3.9	3.9
15°	24.5	24.3	5.7	5.5	3.1	2.9
30°	22.0	21.1	4.8	4.5	2.6	2.3
45°	18.6	18.4	3.9	3.8	2.0	1.9
60°	15.7	14.7	3.2	3.0	1.6	1.4

TABLE E-3: (Con't) Spectroradiometer Readings from Saint Augustine Grass Taken with Photomultiplier Tube

$\theta = 15^{\circ}$

ζ	Spectroradiometer Reading ~ Millivolts							
	λ = 0.65		λ = 0.70		λ = 0.75		λ = 0.85	
	Run 37	Run 38	Run 37	Run 38	Run 37	Run 38	Run 37	Run 38
60°	0.5	0.6	0.7	0.7	0.8	0.8	4.0	3.7
45°	0.7	0.7	0.8	0.8	0.9	0.9	5.5	5.2
30°	0.9	0.8	0.8	0.9	1.1	1.0	6.5	6.3
0°	1.0	0.9	1.1	1.05	1.5	1.3	9.2	7.9
15°	1.0	0.75	1.1	1.0	1.3	1.3	8.4	7.8
30°	0.9	0.9	1.0	1.1	1.2	1.3	7.9	7.1
45°	0.8	0.8	0.85	1.0	1.1	1.1	6.5	6.3
60°	0.5	0.7	0.8	0.7	1.1	0.8	5.2	4.8

TABLE E-4: Spectroradiometer Readings from Mississippi Delta Alluvial Soil Taken with Lead Sulfide Detector

$\theta = 15^{\circ}$

ζ	Spectroradiometer Readings ~ Millivolts							
	λ = 1.00		λ = 1.25		λ = 1.50		λ = 1.75	
	Run 37	Run 38	Run 37	Run 38	Run 37	Run 38	Run 37	Run 38
60°	9.1	8.4	7.4	7.0	6.1	5.7	2.0	1.8
45°	12.2	11.6	10.1	9.5	8.4	7.9	2.5	2.5
30°	14.7	14.4	12.3	12.0	10.2	9.9	3.0	2.9
0°	20.9	17.9	17.1	15.0	14.3	12.5	4.2	3.8
15°	19.1	17.1	15.9	14.8	13.1	14.0	4.2	3.8
30°	17.7	16,4	14.8	13.9	12.2	11.6	3.7	3.6
45°	15.0	14.3	12.7	12.1	10.5	10.0	3.3	3.2
60°	11.6	10.7	9.9	9.3	8.2	7.5	2.6	2.4

TABLE E-4:(Con't) Spectroradiometer Readings from Mississippi Delta Alluvial Soil Taken With Lead Sulfide Detector

θ = 15°

ζ	Spectroradiometer Readings ~ Millivolts					
	λ = 2.00		λ = 2.25		λ = 2.50	
	Run 37	Run 38	Run 37	Run 38	Run 37	Run 38
60°	1.8	1.8	1.8	1.9	1.0	1.0
45°	2.3	2.4	2.6	2.45	1.3	1.25
30°	2.9	2.95	3.0	3.1	1.5	1.45
0°	4.2	3.8	4.4	3.8	2.2	2.0
15°	4.1	3.85	4.0	3.8	1.8	1.8
30°	3.8	3.65	3.8	3.65	1.8	1.7
45°	3.2	3.2	3.2	3.2	1.5	1.6
60°	2.5	2.5	2.6	2.5	1.3	1.2

TABLE E-4 (Con't): Spectroradiometer Readings from Mississippi Delta Alluvial Soil Taken with Lead Sulfide Detector

$\theta = 15^{\circ}$

ζ	Spectroradiometer Readings ~ Millivolts							
	λ = 0.35		λ = 0.40		λ = 0.45		λ = 0.50	
	Run 39	Run 40	Run 39	Run 40	Run 39	Run 40	Run 39	Run 40
60°	9.4	9.0	12.2	11.6	4.75	4.7	10.65	10.4
45°	13.4	13.9	17.1	17.6	6.2	6.3	14.6	14.9
30°	18.4	17.8	22.2	21.4	7.6	--	18.4	--
0°	25.8	23.8	29.5	27.5	9.65	9.0	22.8	21.5
15°	25.3	23.8	27.5	26.1	8.5	8.6	20.5	20.85
30°	24.6	23.0	27.0	25.4	8.6	8.3	20.5	19.9
45°	21.7	19.9	24.2	22.7	7.9	7.3	18.9	17.6
60°	17.0	16.5	19.6	19.2	6.3	6.3	14.8	14.9

TABLE E-5: Spectroradiometer Readings from Mississippi Delta Alluvial Soil Taken with Photomultiplier Tube

$\theta = 15^{\circ}$

ε	Spectroradiometer Readings ~ Millivolts					
	λ = 0.55		λ = 0.60		λ = 0.65	
	Run 39	Run 40	Run 39	Run 40	Run 39	Run 40
60°	15.7	15.4	5.0	4.7	3.2	3.1
45°	20.8	21.0	6.85	6.9	4.4	4.4
30°	25.0	--	8.6	--	5.7	5.2
0°	30.7	28.9	11.0	10.1	7.3	6.5
15°	27.5	27.5	9.7	9.4	6.8	6.2
30°	27.5	26.5	9.85	9.0	6.4	5.9
45°	25.2	23.4	8.75	7.7	5.7	5.2
60°	20.6	20.45	6.65	6.6	4.4	4.2

TABLE E-5 (Con't): Spectroradiometer Readings from Mississippi Delta Alluvial Soil Taken with Photomultiplier Tube

$\theta = 15^{\circ}$

ζ	Spectroradiometer Readings ~ Millivolts					
	λ = 0.40	λ = 0.45	λ = 0.50	λ = 0.55	λ = 0.60	λ = 0.65
60.0°	1.55	2.6	7.5	7.6	0.8	0.6
52.5°	2.0	3.3	9.6	9.5	1.05	0.7
45.0°	2.2	4.0	11.5	11.3	1.2	0.7
37.5°	2.6	4.7	13.4	13.2	1.5	0.9
30.0°	2.9	5.9	19.2	19.5	2.2	0.8
00.0°	2.8	5.1	14.7	14.7	1.5	0.95
7.5°	2.5	4.8	14.1	14.0	1.5	0.9
15.0°	2.5	4.7	13.5	13.4	1.4	0.9
22.5°	2.2	4.1	12.3	12.4	1.4	0.8
30.0°	2.2	3.9	11.5	11.4	1.2	0.7
37.5°	1.9	3.6	10.8	10.8	1.2	0.7
45.0°	1.9	3.3	9.7	9.7	1.0	0.6
52.5°	1.8	3.0	8.7	8.9	0.9	0.6
60.0°	1.7	2.8	8.0	9.6	0.9	0.7

TABLE E-6: Spectroradiometer Readings from Bermuda Grass Taken with Photomultiplier Tube

θ = 15°

ζ	Spectroradiometer Readings ~ Millivolts				
	λ = 0.70	λ = 0.75	λ = 0.85	λ = 1.00	λ = 1.25
60.0°	2.2	4.2	22.0	27.4	21.8
52.5°	2.4	5.4	31.4	37.5	33.3
45.0°	3.8	7.8	40.4	47.1	43.6
37.5°	4.0	8.6	44.8	52.8	50.1
30.0°	3.7	8.0	40.0	48.1	47.1
00.0°	4.5	9.5	46.7	55.0	52.2
7.5°	4.3	9.1	45.4	53.3	49.7
15.0°	3.6	8.0	42.9	51.1	47.5
22.5°	3.9	8.3	43.3	51.0	46.6
30.0°	3.5	7.4	40.4	47.9	44.3
37.5°	3.4	7.5	40.3	46.7	42.5
45.0°	3.0	6.3	36.4	43.8	39.2
52.5°	3.1	6.1	34.2	40.2	35.5
60.0°	2.5	4.9	28.9	35.7	30.7

TABLE E-7: Spectroradiometer Readings From Bermuda Grass Taken with Lead Sulfide Detector

θ = 15°

ζ	Spectroradiometer Readings ~ Millivolts				
	λ = 1.50	λ = 1.75	λ = 2.00	λ = 2.25	λ = 2.50
60.0°	14.1	4.4	4.3	3.6	0.9
52.5°	21.0	7.4	7.6	5.3	1.2
45.0°	27.4	10.5	10.8	7.5	1.9
37.5°	33.9	13.9	14.1	8.9	2.1
30.0°	28.4	12.6	12.5	7.6	1.9
00.0°	36.6	14.4	14.7	9.6	2.0
7.5°	33.2	12.4	12.2	8.3	1.9
15.0°	32.2	12.2	12.0	7.7	1.8
22.5°	31.0	11.3	11.3	7.3	1.7
30.0°	29.4	10.7	10.8	7.2	1.9
37.5°	27.2	9.9	10.1	6.6	1.3
45.0°	24.7	8.5	9.0	5.9	1.2
52.5°	22.5	7.5	7.5	4.9	1.3
60.0°	18.4	6.2	6.5	4.5	1.1

TABLE E-7 (Con't): Spectroradiometer Readings From Bermuda Grass Taken with Lead Sulfide Detector

θ = 15°

APPENDIX F

CALCULATION OF SOLAR ELEVATIONS AND AZIMUTH

One of the aims of this investigation was the determination of the effect of the relative azimuth and zenith angles on the reflectance measurements. In order to know what these angles were when reflectance readings were made in the field the azimuth and elevation of the sun at the time of observation had to be known. Although these angles could have been measured with a sextant at the time of observation, it would have been difficult. Also it was necessary to know the angles beforehand in order to facilitate set-up of the experiment.

Algorithm

The coordinate system transformation algorithm as well as formal definitions of the coordinate systems involved are given in Escobel [62]. The algorithm developed requires as input the latitude, longitude, and elevation of the place of observation as well as the right ascension and declination of the sun for a particular time. The output is the azimuth and the elevation of the sun for that time. The algorithm was adapted and expressed in FORTRAN for use on the computer. The operation of the algorithm for a single time value is illustrated below. Definitions of the symbols are given in the nomenclature at the end of this Appendix.

Example - 1:00 pm CDT September 1, 1974

A. Preliminary Calculations and Operations

1. $\varphi = 30.410^{o}$

   $\lambda = 268.810^{o}$

   $H = 0.0047$ miles

2. Interpolate α, δ, R from Ephemeris [63]

   Cubic interpolation using forward divided differences

Date	α	Δ_d^1	Δ_d^2	Δ_d^3
8/31	158.9289			
		0.9079		
9/1	159.8368		-0.7×10^{-4}	
		0.9065		3.333×10^{-6}
9/2	160.7433		-0.6×10^{-4}	
		0.9053		
9/3	161.6486			

	δ			
8/31	8.860972			
		-0.360002		
9/1	8.500970		-1.1375×10^{-3}	
		-0.362277		8.6667×10^{-6}
9/2	8.138693		-1.1115×10^{-3}	
		-0.3645		
9/3	7.774193			

	r			
8/31	93,836,016			
		-21984		
9/1	93,814,032		-136	
		-22256		45.333
9/2	93,791,776		0	
		-22256		
9/3	93,769,520			

1:00 pm CDT = 13:00 CDT = 18:00 U.T.

9/1, 18:00 U.T. = 9/1.75

$$\alpha_c = 158.9289 + 1.75(0.9079 + 0.75(-0.7\times10^{-4} - 0.25(3.333\times10^{-6})))$$

$$\alpha_c = 160.5176$$

$$\delta_c = 8.860972 + 1.75(-0.360002 + 0.75(-1.1375\times10^{-3} - 0.25(8.6667\times10^{-6})))$$

$$\delta_c = 8.229473$$

$$R_c = 93,836,016 + 1.75(-21,984 + 0.75(-136 - 0.25(45.333)))$$

$$R_c = 93,797,351$$

B. Determination of Sidereal Time

1. Determine JD

JD of Jan 0, 1974 = 2,442,048

Day of year, Sept. 1 = 244

JD September 1, 1974 2,442,292

$$T_u = \frac{JD - 2{,}415{,}020}{36525} = \frac{2{,}442{,}292 - 2{,}415{,}020}{36525}$$

$T_u = 0.746667$

2. Determine θ_{g_o} from T_u

$$\theta_{g_o} = 99.6909833^\circ + 36000.7689^\circ T_u + 0.00038708^\circ T_u^2$$

$$\theta_{g_o} = 26980.2653^\circ = 340.2653^\circ$$

$$\theta_o = \theta_{g_o} + \lambda = 340.2653^\circ + 268.810^\circ = 609.0753^\circ$$

$$\theta_o = 249.0753^\circ$$

$$\theta = \theta_o + 0.25068447(t)$$

$t = 18^{hr}$ UT = 1080 min

$$\theta = 249.0753^\circ + 0.25068447\ (1080) = 519.8145^\circ$$

$$\theta = 159.8145^\circ$$

C. Flattening, geodetic latitude and altitude factors

$f = 0.0033529$ $\qquad e = (2f - f^2) = 0.0066946$

$a_e = 3963.205$ miles

$$G_1 = \frac{a_e}{\sqrt{(1 - e \cdot \sin^2\varphi)}} + H$$

$G_1 = 3966.613$ miles

$$G_2 = \frac{a_e(1 - f)^2}{\sqrt{(1 - e \cdot \sin^2\varphi)}} + h$$

$G_2 = 3940.058$ miles

D. Coordinate Transformation

$x = -G_1 \cos\varphi \cos\theta = 3210.797$

$y = -G_1 \cos\varphi \sin\theta = -1180.421$

$z = -G_2 \sin\varphi = -1994.395$

$U_x = \cos\delta_c \cos\alpha_c = -0.9330363$

$U_y = \cos\delta_c \sin\alpha_c = 0.3300830$

$U_z = \sin\delta_c = 0.1431381$

$\rho_x = r_c U_x + x = -87513120.0$

$\rho_y = r_c U_y + y = 30959730.0$

$\rho_z = r_c U_z + z = 13423980.0$

$$\rho_h = \sqrt{\rho_x^2 + \rho_y^2 + \rho_z^2} = 93,793,680$$

$L_x = \rho_x/\rho_h = -0.9330386$

$L_y = \rho_y/\rho_h = 0.3300833$

$L_z = \rho_z/\rho_h = 0.1431224$

$S_x = \sin\varphi \cos\theta = -0.4750946$

$S_y = \sin\varphi \sin\theta = 0.1746643$

$S_z = -\cos\varphi = -0.8624253$

$E_x = -\sin\theta = -0.3450607$

$E_y = \cos\theta = -0.9385804$

$E_z = 0.0 = 0.0$

$Z_x = \cos\theta \cos\varphi = -0.8094555$

$Z_y = \sin\theta \cos\varphi = 0.2975891$

$Z_z = \sin\varphi = 0.5061843$

$$\begin{matrix} L_{x_h} & S_x & S_y & S_z & L_x \\ L_{y_h} & E_x & E_y & E_z & L_y \\ L_{z_h} & Z_x & Z_y & Z_z & L_z \end{matrix}$$

$L_{x_h} = 0.3775030$

$L_{y_h} = 0.01214524$

$L_{z_h} = 0.9259787$

$\sin h = L_2 h = 0.9259287$

$\cos h = \sqrt{1 - \sin^2 h} = 0.3776983$

$h = \sin^{-1}(\sin h) = \underline{67.809^\circ}$

$\sin A = \dfrac{L_y h}{\cos h} = 0.03215593$

$\cos A = \dfrac{-L_x h}{\cos h} = -0.9994829$

$A = 180^\circ - \sin^{-1}(\sin A) = \underline{178.157^\circ}$

Program Adaptation

It was desired to calculate the solar angles for several consecutive times of day over several days. Therefore the program was written to accept as time information an initial and final date, an initial and final time of day, and a time increment in minutes between successive determinations.

The output is presented in the form of a separate table for each day from the initial to the final day, listing the solar angles at each increment from the initial to the final time of day. Each of these listings is in the form of local time, azimuth, and elevation.

The data in the Ephemeris [63] is presented as right ascension in hours, minutes, and seconds, and r (distance from earth to celestial body) in astronomical units. The angles were to be converted to radians and r to miles. Since the Ephemeris data is read in each time the program is run, it would have been necessary to convert the data every time it was used. Instead, an auxilliary program was written to convert the data and punch a new deck to be read in each time the main program was executed. Thus, a deck was manually prepared by punching the information as it appears in the Ephemeris. This allowed for ease of preparation of the data for input. In order to preserve accuracy, the output deck is written in hexadecimal format and, of course, is read in by the main program in hexadecimal format. In this manner the bit patterns of the internal floating-point representations of the data values are transmitted to the main program. There they are exactly reconstructed in the new memory domain. This makes the output deck somewhat unintelligiable but simplifies input of the Ephemeris data to the main program.

Listings of both the auxillary program and the main program used to calculate the solar zenith and azimuth angles are given on the following pages.

```
IV G1  RELEASE 2.0              MAIN                DATE = 74211          15/03/47
      C THIS PROGRAM READS THE EPHEMERIS DATA (ALPHA,DELTA,R) FROM CARDS
      C THE DATA IS CONVERTED AS FOLLOWS...
      C RIGHT ASCENSION (ALPHA) FROM HOURS, MINUTES, AND SECONDS TO RADIANS
      C DECLINATION (DELTA) FROM DEGREES, MINUTES, AND SECONDS TO RADIANS
      C R FROM ASTRONIMCAL UNITS TO MILES
      C THE CONVERTED DATA IS PUNCHED ON CARDS IN HEXADECIMAL
      C
            INTEGER*4 DATE(20)
            COMMON RAHRS(100),RAMIN(100),RASEC(100),DECDE(100),DECMI(100),
           DECSE(100),R(100)
            DIMENSION ACCESS(100,7),RARAD(100),DERAD(100)
            EQUIVALENCE (ACCESS(1,1),RARAD(1),RAHRS(1)),(DERAD(1),DECDE(1))
      C
      C READ THE STARTING DATE, THEN THE EPHEMERIS DATA
      C
            READ(5,4)DATE
            J=0
      1     J=J+1
            READ(5,5,END=2)(ACCESS(J,K),K=1,7)
            GO TO 1
      2     N=J-1
      C
      C THIS LOOP TAKES CARE OF THE CONVERSIONS
      C
            DO 3 I=1,N
            RARAD(I)=15.0*((RASEC(I)/60.0+RAMIN(I))/60.0+RAHRS(I))/57.29578
            DERAD(I)=((DECSE(I)/60.0+DECMI(I))/60.0+DECDE(I))/57.29578
            R(I)=R(I)*92957130.4
      3     CONTINUE
      C
      C PUNCH THE CONVERTED DATA
      C
            WRITE(7,6)DATE,((ACCESS(J,K),K=1,7,3),J=1,N)
            STOP
      4     FORMAT(20A4)
      5     FORMAT(T1,3(F6.0),T30,3(F6.0),T60,F10.0)
      6     FORMAT(20A4/(T1,Z8,T30,Z8,T60,Z8))
            END
```

```
G1  RELEASE 2.0                MAIN                DATE = 74214          13/14/35

      REAL LAMBDA,INVAR(3),INOUT(2,144),LX,LY,LZ,LXH,LYH,LZH
      DOUBLE PRECISION TU,RHOX,RHOY,RHOZ,RHOH,THETGO,THETAO,DTHETA
      INTEGER YD(12),GEO,GCLT,IDATE(3),FDATE(3),EDATE(3),INIX(3),
     &FINAX(2),INCX(2),Z,EPHMRS,TI,TF,TINC,TM,PRESX(3,144),PDATE(3)
      COMMON ALPHA(100),DELTA(100),R(100),ALPHAC,DELTAC,RC
      DIMENSION ACCESS(100,3),DD(3,3,2)
      EQUIVALENCE (ACCESS(1,1),ALPHA(1)),(INVAR(1),ALPHAC),(PDATE(1),
     &IDATE(1))
      DATA YD/0,31,59,90,120,151,181,212,243,273,304,334/,GCLT/***    */,
     &EF/0.0033529/,F/0.0066946/,AE/3963.205/
      READ(5,10100)PHI,GEO,LAMBDA,H,IDATE,FDATE,INIX,FINAX,INCX,Z,EDATE
      MU=0
10    MU=MU+1
      READ(5,10101,END=15)ALPHA(MU),DELTA(MU),R(MU)
      GO TO 10
15    EPHMRS=MU-1
      TI=60*INIX(1)+INIX(2)
      TF=60*FINAX(1)+FINAX(2)
      TINC=60*INCX(1)+INCX(2)
      TERAC=FLOAT(INIX(3))/60.0
      IF(TINC.LT.10)TINC=10
      JDI=YD(IDATE(1))+IDATE(2)+2442048
      JDF=YD(FDATE(1))+FDATE(2)+2442048
      JDEI=YD(EDATE(1))+EDATE(2)+2442048
      JDEF=JDEI+EPHMRS-1
      IF(JDI.GE.JDEI)GO TO 20
      JDI=JDEI
      WRITE(6,11000)
20    IF(JDF.LE.JDEF)GO TO 24
      JDF=JDEF
      WRITE(6,11001)
24    PHI=PHI/57.29578
      IF(GEO.NE.GCLT)GO TO 30
      PHI=ATAN2(SIN(PHI),COS(PHI)*(1.0-F)**2)
30    G1=AE/SQRT(1.0-F*SIN(PHI)**2)
      G2=G1*(1.0-F)**2+H
      G1=G1+H
      DO 1000 JD=JDI,JDF
      PDATE(2)=JD-2442048
40    IF(PDATE(2).LE.YD(IDATE(1)+1))GO TO 45
      IDATE(1)=IDATE(1)+1
      GO TO 40
45    PDATE(2)=PDATE(2)-YD(IDATE(1))
      WRITE(6,11002)PDATE
      IL=JD-JDEI
      IF(IL.EQ.0)IL=1
      IF(IL.GT.EPHMRS-3)IL=EPHMRS-3
      DO 1001 I=1,3
      DD(I,1,1)=ACCESS(IL+1,I)-ACCESS(IL,I)
      DD(I,1,2)=ACCESS(IL+2,I)-ACCESS(IL+1,I)
      DD(I,3,2)=ACCESS(IL+3,I)-ACCESS(IL+2,I)
      DD(I,2,1)=(DD(I,1,2)-DD(I,1,1))/2.0
      DD(I,2,2)=(DD(I,3,2)-DD(I,1,2))/2.0
      DD(I,3,1)=(DD(I,2,2)-DD(I,2,1))/3.0
1001  CONTINUE
      TU=(DFLOAT(JD)-2415020.0)/36525.000
      THETGO=99.690983300+TU*(36000.7689D0+TU*0.0003870800)
      THETAO=THETGO+DBLE(LAMBDA)
```

```
V G1  RELEASE 2.0                MAIN                    DATE = 74214          13/14/35

      DO 1002 TM=TI,TF,TINC
      T=FLOAT(TM)+TFRAC+60.0*FLOAT(Z)
      DTHETA=THETA0+0.2506944447*DBLE(T)+360.0D0
   35 DTHETA=DTHETA-360.0D0
      IF(DTHETA.GE.360.0D0)GO TO 35
      THETA=DTHETA/57.2957795
      DELTAX=T/1440.0
      IF(JD-JDEI.EQ.0)DELTAX=DELTAX-1.0
      IF(IL.EQ.EPHMRS-2)DELTAX=DELTAX+1.0
      IF(IL.EQ.EPHMRS-1)DELTAX=DELTAX+2.0
      DO 1003 I=1,3
      INVAR(I)=ACCESS(IL,I)+(DELTAX+1.0)*(DD(I,1,1)+DELTAX*(DD(I,2,1)
     &+(DELTAX-1.0)*DD(I,3,1)))
 1003 CONTINUE
      TRIPHC=COS(PHI)
      TRIPHS=SIN(PHI)
      TRITHC=COS(THETA)
      TRITHS=SIN(THETA)
      TRIALC=COS(ALPHAC)
      TRIALS=SIN(ALPHAC)
      TRIDEC=COS(DELTAC)
      TRIDES=SIN(DELTAC)
      XV=-G1*TRIPHC*TRITHC
      YV=-G1*TRIPHC*TRITHS
      ZV=-G2*TRIPHS
      UX=TRIDEC*TRIALC
      UY=TRIDEC*TRIALS
      UZ=TRIDES
      RHOX=RC*UX+XV
      RHOY=RC*UY+YV
      RHOZ=RC*UZ+ZV
      RHOH=DSQRT(RHOX**2+RHOY**2+RHOZ**2)
      LX=RHOX/RHOH
      LY=RHOY/RHOH
      LZ=RHOZ/RHOH
      SX=TRIPHS*TRITHC
      SY=TRIPHS*TRITHS
      SZ=-TRIPHC
      EX=-TRITHS
      EY=TRITHC
      EZ=0.0
      ZX=TRITHC*TRIPHC
      ZY=TRITHS*TRIPHC
      ZZ=TRIPHS
      LXH=SX*LX+SY*LY+SZ*LZ
      LYH=EX*LX+EY*LY+EZ*LZ
      LZH=ZX*LX+ZY*LY+ZZ*LZ
      TRIELC=SQRT(1.0-LZH**2)
      TRIAZC=-LXH/TRIELC
      TRIAZS=LYH/TRIELC
      ELVTN=57.29578*ARSIN(LZH)
      AZMTH=57.29578*ARSIN(TRIAZS)
      IF(TRIAZC.LT.0.0)AZMTH=180.0-AZMTH
      IF(AZMTH.LT.0.0)AZMTH=AZMTH+360.0
      INDEX=1+(TM-TI)/TINC
      PRESX(1,INDEX)=TM/60
      PRESX(2,INDEX)=MOD(TM,60)
      PRESX(3,INDEX)=INIX(3)
```

```
V G1  RELEASE 2.0          MAIN          DATE = 74214          13/14/35
      INOUT(1,INDEX)=AZMTH
      INOUT(2,INDEX)=ELVTN
1002  CONTINUE
      COLUM=FLOAT(INDEX)/4.0
      LEN=COLUM
      IF(AMOD(COLUM,1.0).GT.0.0)LEN=LEN+1
      DO 1004 K=1,LEN
      WRITE(6,11003)((PRESX(I,L),I=1,3),(INOUT(J,L),J=1,2),
     &L=K,INDEX,LEN)
1004  CONTINUE
1000  CONTINUE
      STOP
10100 FORMAT(T1,F11.0,T12,A1,T20,F20.0,T40,F10.0/T1,2(I2,1X),I4,T15,
     &2(I2,1X),I4,T30,2(I2,1X),I2,T40,I2,1X,I2,T50,I2,1X,I2,T60,I2/
     &T1,2(I2,1X),I4)
10101 FORMAT(T1,Z8,T30,Z8,T60,Z8)
11000 FORMAT('0',' INITIAL DATE SPECIFIED IS EARLIER THAN AVAILABLE EPHEM
     &ERIS DATA.  INITIAL EPHEMERIS DATE WILL BE USED.')
11001 FORMAT('0',' FINAL DATE SPECIFIED IS LATER THAN AVAILABLE EPHEMERIS
     & DATA.  FINAL EPHEMERIS DATE WILL BE USED.')
11002 FORMAT('0',T48,'EPHEMERIS FOR GREGORIAN DATE ',I2,'/',I2,'/',I4/
     &'0',T5,3('LOCAL TIME  AZIMUTH  ELEVATION  '),T104,'LOCAL TIME  AZ
     &IMUTH ELEVATION'/)
11003 FORMAT(4(5X,I2,':',I2,':',I2,2X,F8.3,3X,F7.3))
      END
```

Results

During the time that data was obtained, the elevation of the sun was never greater than about 76^{o} ($\zeta_{o} = 14^{o}$). The azimuth was due South shortly after 13:00 CDT which was the time when the solar elevation was at its maximum.

Data was taken in two ways. One set of data was taken with the viewing plane in the same plane as the solar plane, that is $\Psi = 0^{o}$ or $\Psi = 180^{o}$. Another set of data was taken with the viewing azimuth kept constant ($\varphi = 270^{o}$) while the solar plane φ_{o} varied as calculated by the program.

In order to interpolate the solar angles for times not listed by the program, graphs of azimuth and elevation against time of day were prepared. Samples of these are shown in Figures F-1 and F-2.

Angles were measured in the field with a magnetic compass. A correction of 6.5 degrees had to be made to the compass readings to correct for the difference between true north and magnetic north [64].

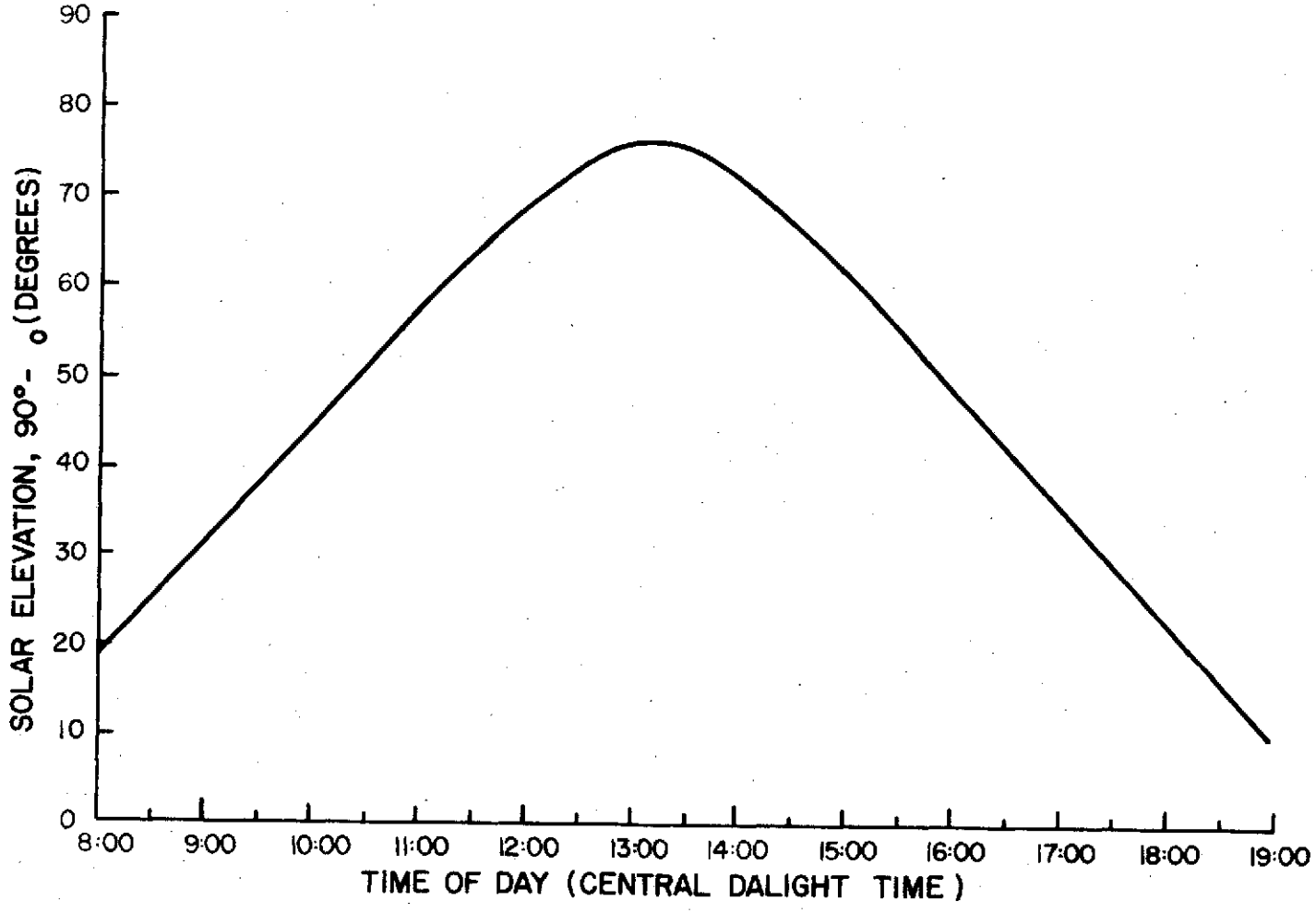

FIGURE F-1. SOLAR ELEVATION VERSUS TIME OF DAY FOR AUGUST 6, 1974

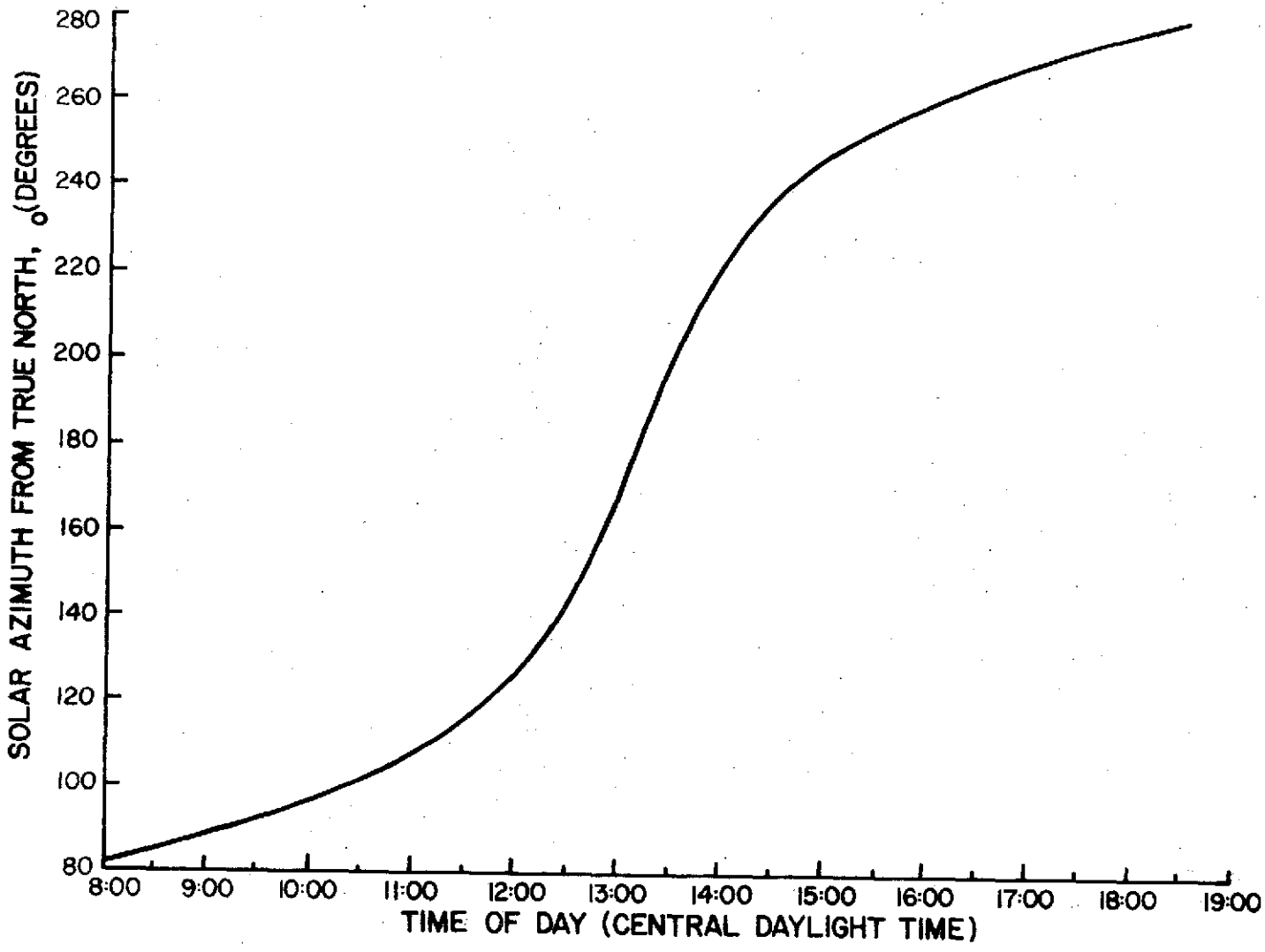

FIGURE F-2. SOLAR AZIMUTH VERSUS TIME OF DAY FOR AUGUST 6, 1974

NOMENCLATURE

α	Right ascension
δ	Declination
r	Distance from earth to celestial body
φ	Goedetic latitude of observation station
λ	Longitude of station
H	Altitude of station
t	Time, minutes
A	Azimuth
h	Elevation
ρ_h	Slant range, the distance from earth to celestial body
θ	Sidereal time
a_e	Equatorial radius of earth
f	Flattening factor
e	$2f-f^2$, the eccentricity of earth
G_1, G_2	Factors to account for earth's eccentricity
U.T.	Universial time, same as Greenwich mean time
JD	Julian date
Tu	Intermediate variable in calculation of sidereal time
$\Delta_\delta^k = k^{+h}$	Divided difference
c	Subscript for interpolated values
g	Subscript for Greenwich meridian
o	Subscript for 0 hour universal time

APPENDIX G

REFLECTANCE DATA FROM FIELD TESTS

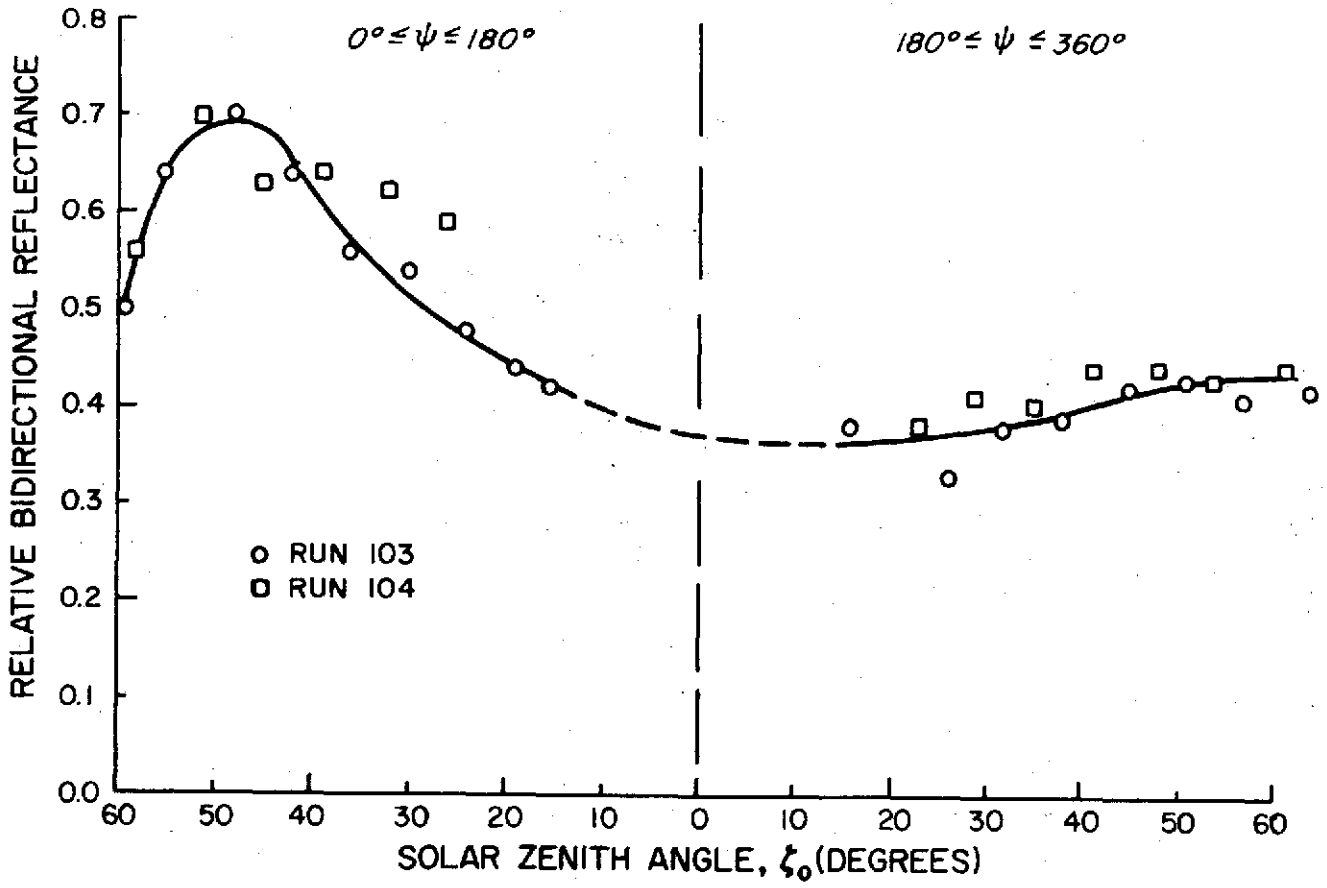

FIGURE G-I. RELATIVE BIDIRECTIONAL REFLECTANCE OF BERMUDA GRASS AT λ=.35 MICRONS TAKEN IN FIELD WITH PLATFORM MOUNTED MIRROR

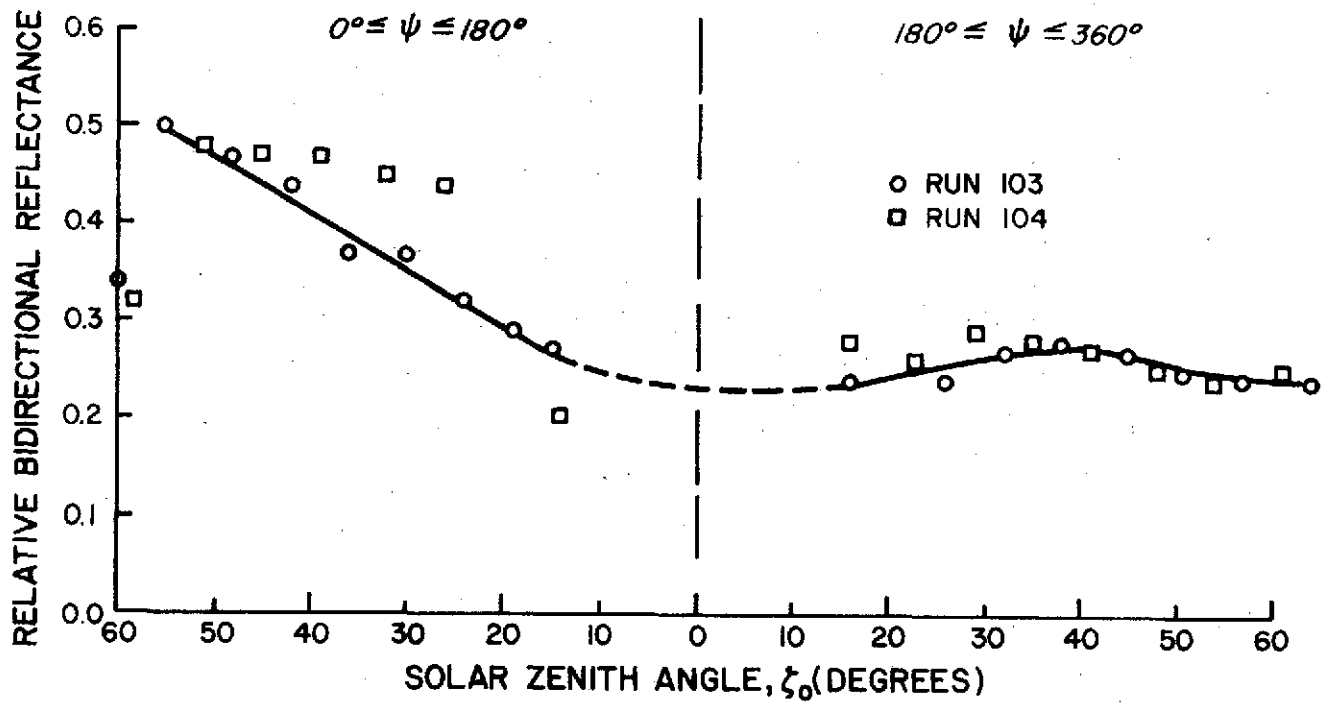

FIGURE G-2. RELATIVE BIDIRECTIONAL REFLECTANCE OF BERMUDA GRASS AT $\lambda = .40$ MICRONS TAKEN IN FIELD WITH PLATFORM MOUNTED MIRROR

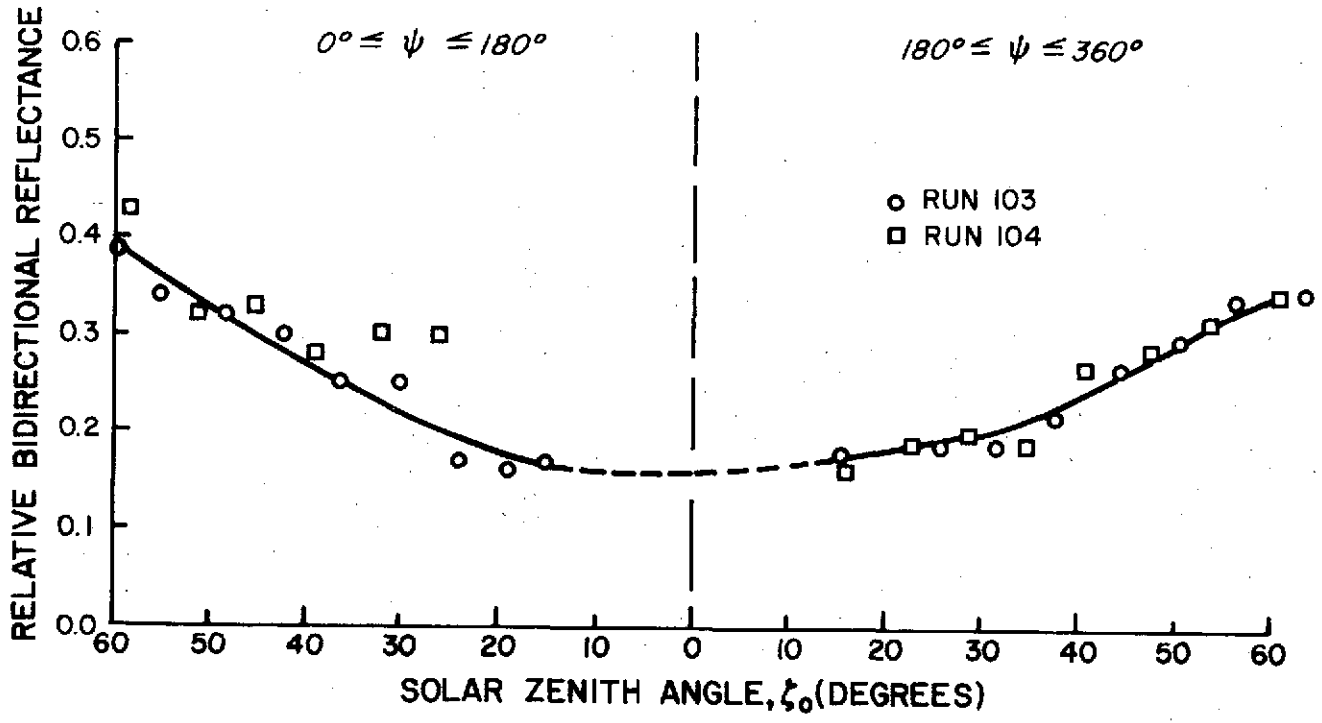

FIGURE G-3. RELATIVE BIDIRECTIONAL REFLECTANCE OF BERMUDA GRASS AT λ=.45 MICRONS TAKEN IN FIELD WITH PLATFORM MOUNTED MIRROR

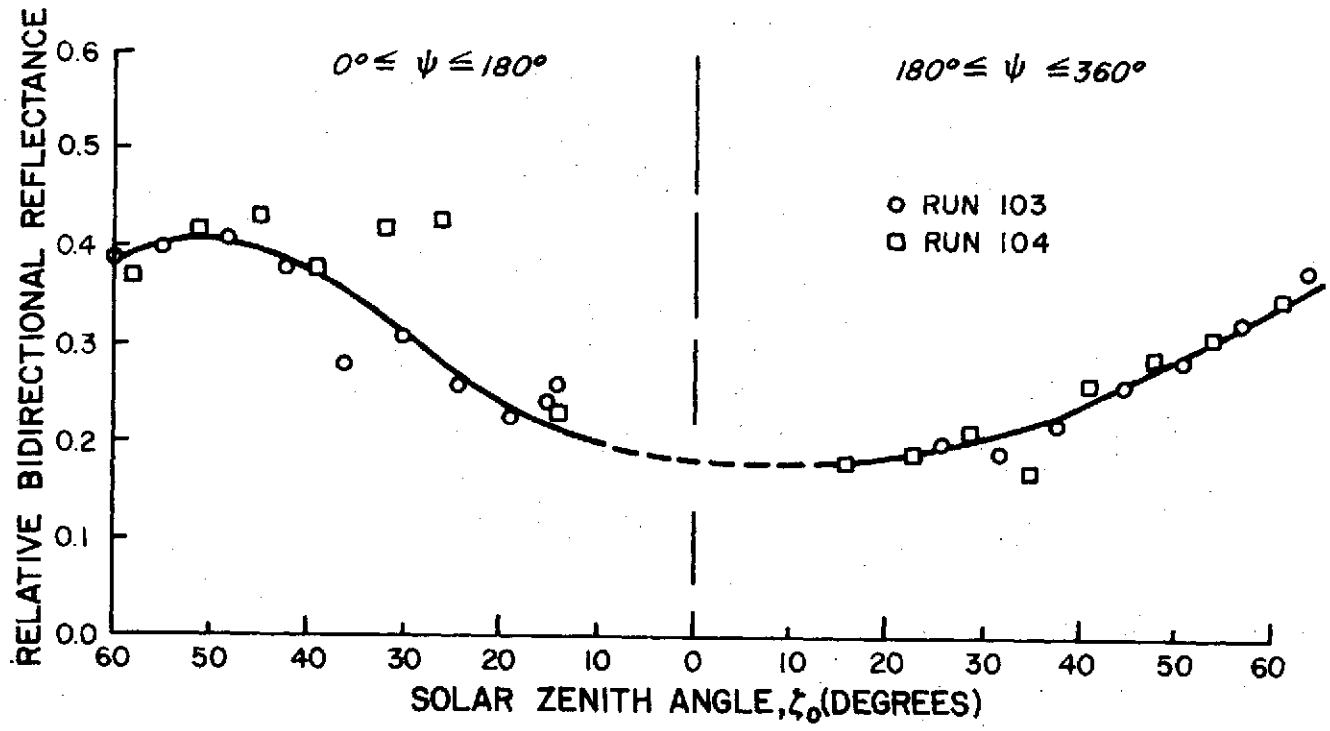

FIGURE G-4. RELATIVE BIDIRECTIONAL REFLECTANCE OF BERMUDA GRASS AT λ=.50 MICRONS TAKEN IN FIELD WITH PLATFORM MOUNTED MIRROR

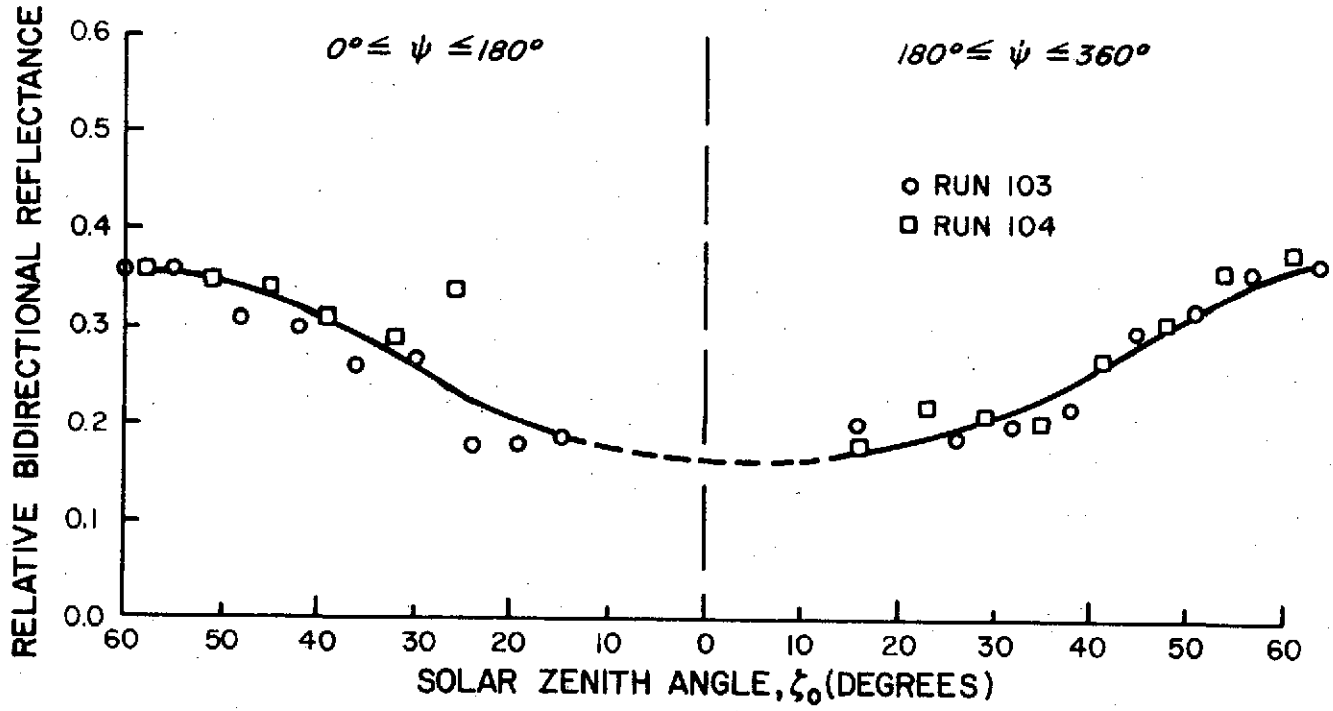

FIGURE G-5. RELATIVE BIDIRECTIONAL REFLECTANCE OF BERMUDA GRASS AT λ=.55 MICRONS TAKEN IN FIELD WITH PLATFORM MOUNTED MIRROR

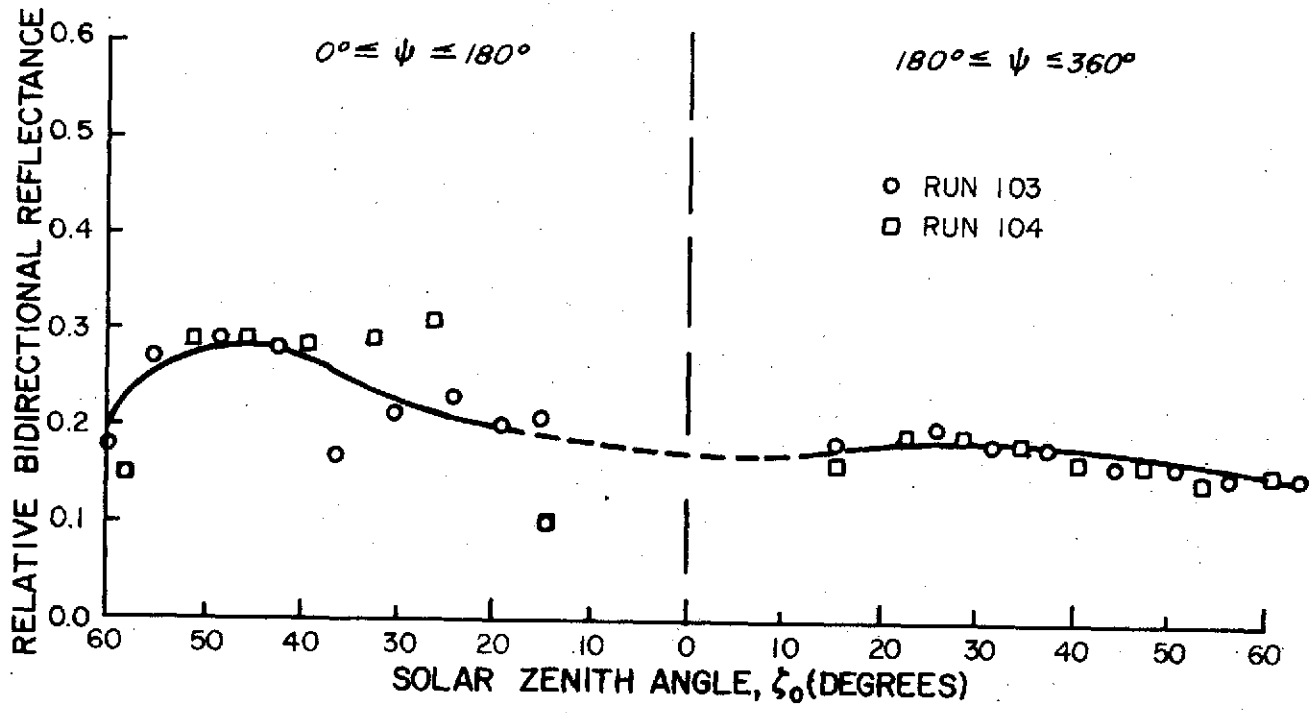

FIGURE G-6. RELATIVE BIDIRECTIONAL REFLECTANCE OF BERMUDA GRASS AT $\lambda = .60$ MICRONS TAKEN IN FIELD WITH PLATFORM MOUNTED MIRROR

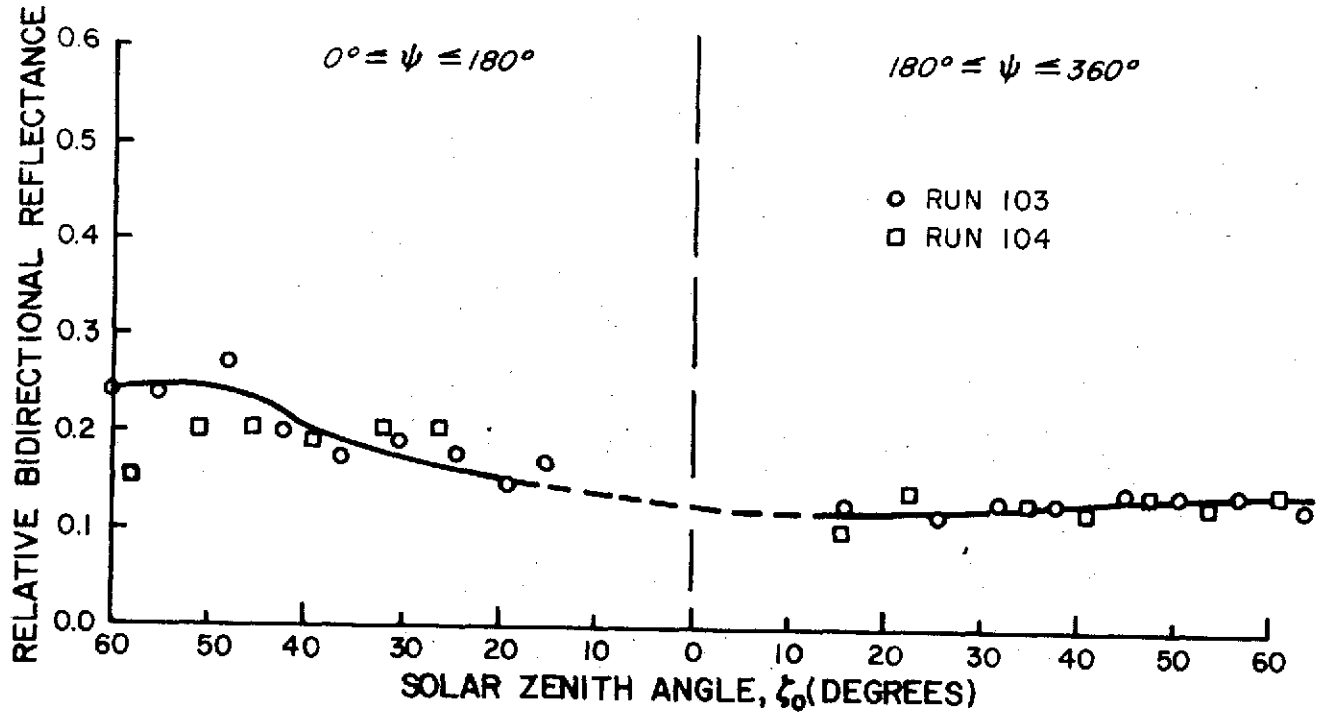

FIGURE G-7. RELATIVE BIDIRECTIONAL REFLECTANCE OF BERMUDA GRASS AT $\lambda = .65$ MICRONS TAKEN IN FIELD WITH PLATFORM MOUNTED MIRROR

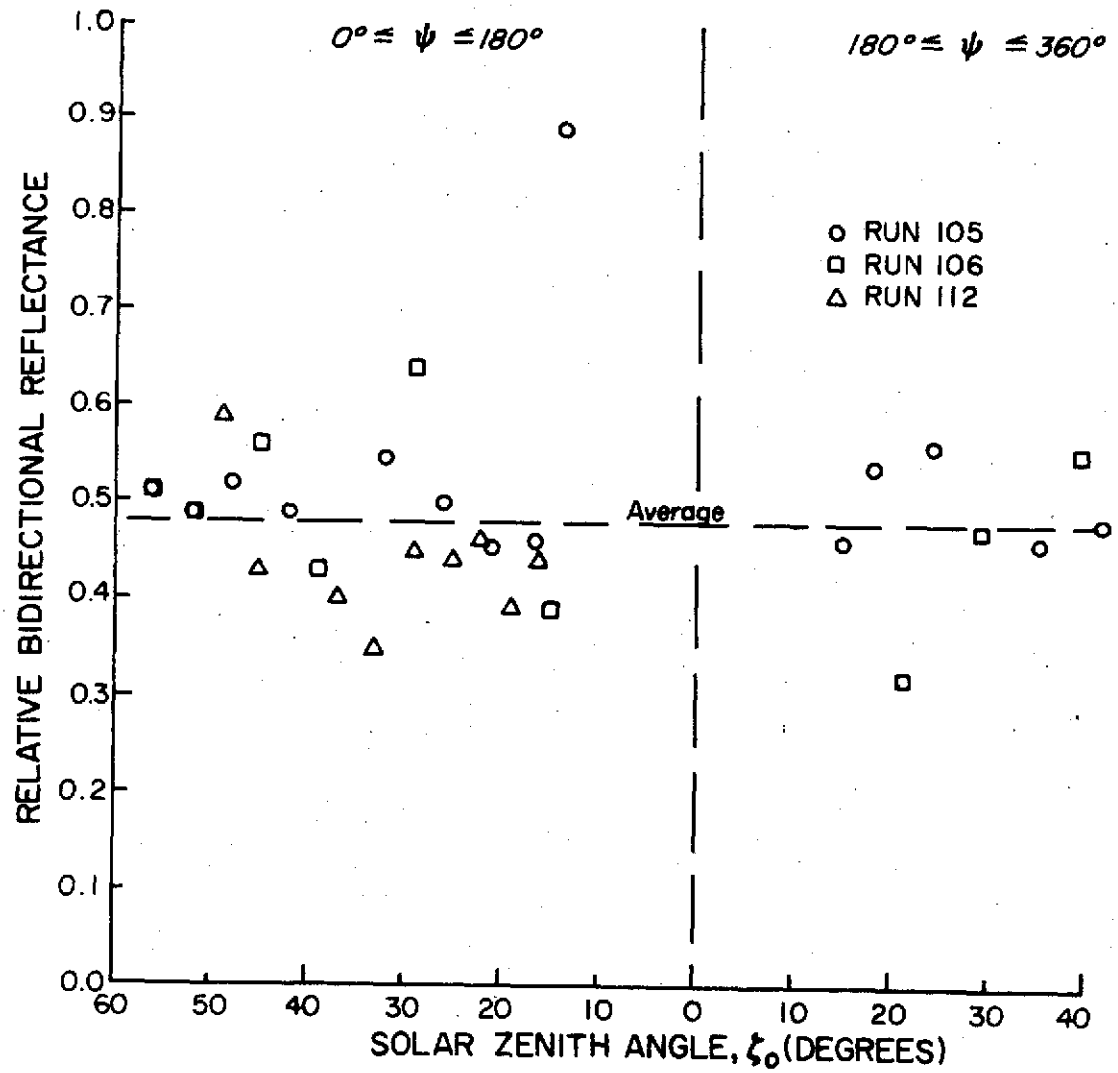

FIGURE G-8. RELATIVE BIDIRECTIONAL REFLECTANCE OF BERMUDA GRASS PLOT AT λ=0.70 MICRONS TAKEN IN FIELD

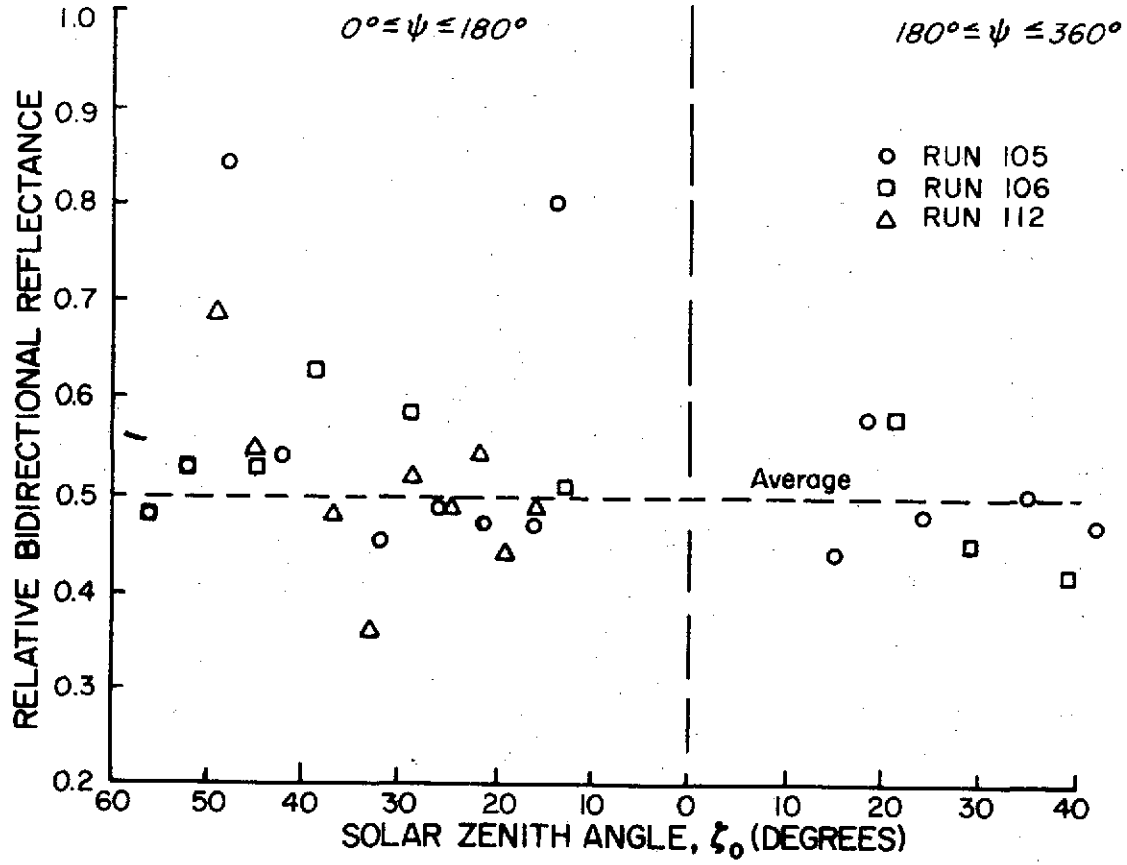

FIGURE G-9. RELATIVE BIDIRECTIONAL REFLECTANCE OF BERMUDA GRASS PLOT AT λ=0.75 MICRONS TAKEN IN FIELD

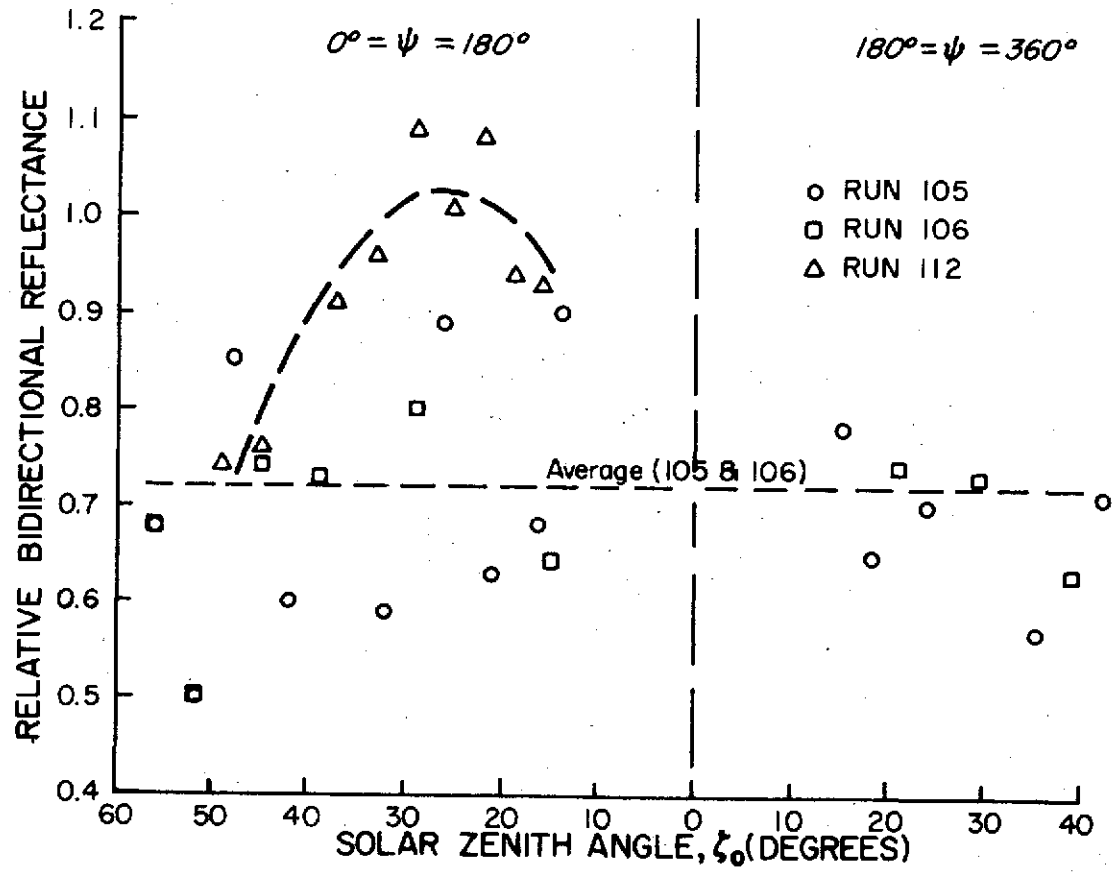

FIGURE G-10. RELATIVE BIDIRECTIONAL REFLECTANCE OF BERMUDA GRASS PLOT AT λ=0.85 MICRONS TAKEN IN FIELD

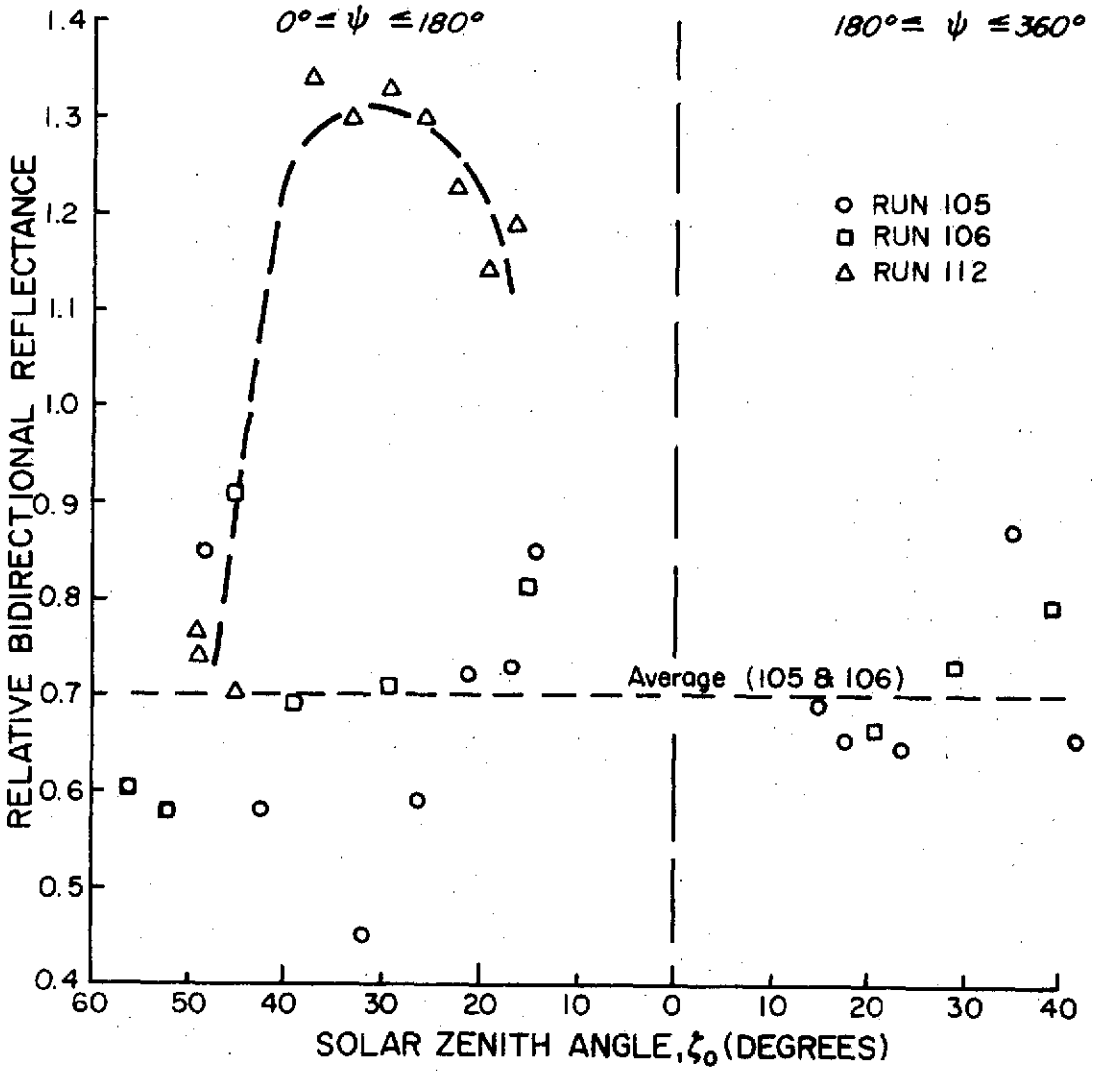

FIGURE G-11. RELATIVE BIDIRECTIONAL REFLECTANCE OF BERMUDA GRASS PLOT AT λ≒1.00 MICRONS TAKEN IN FIELD

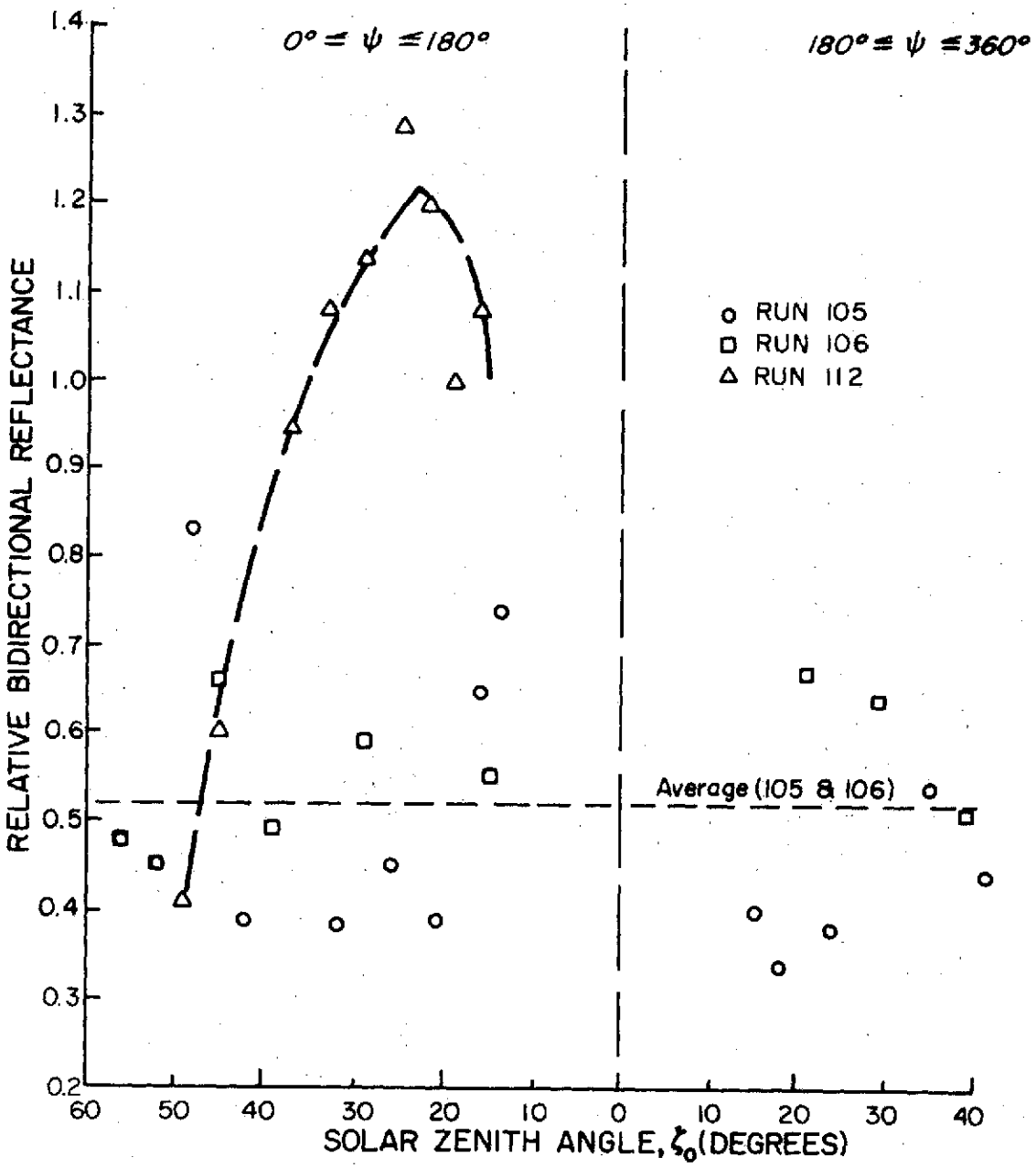

FIGURE G-12. RELATIVE BIDIRECTIONAL REFLECTANCE OF BERMUDA GRASS PLOT AT λ=1.25 MICRONS TAKEN IN FIELD

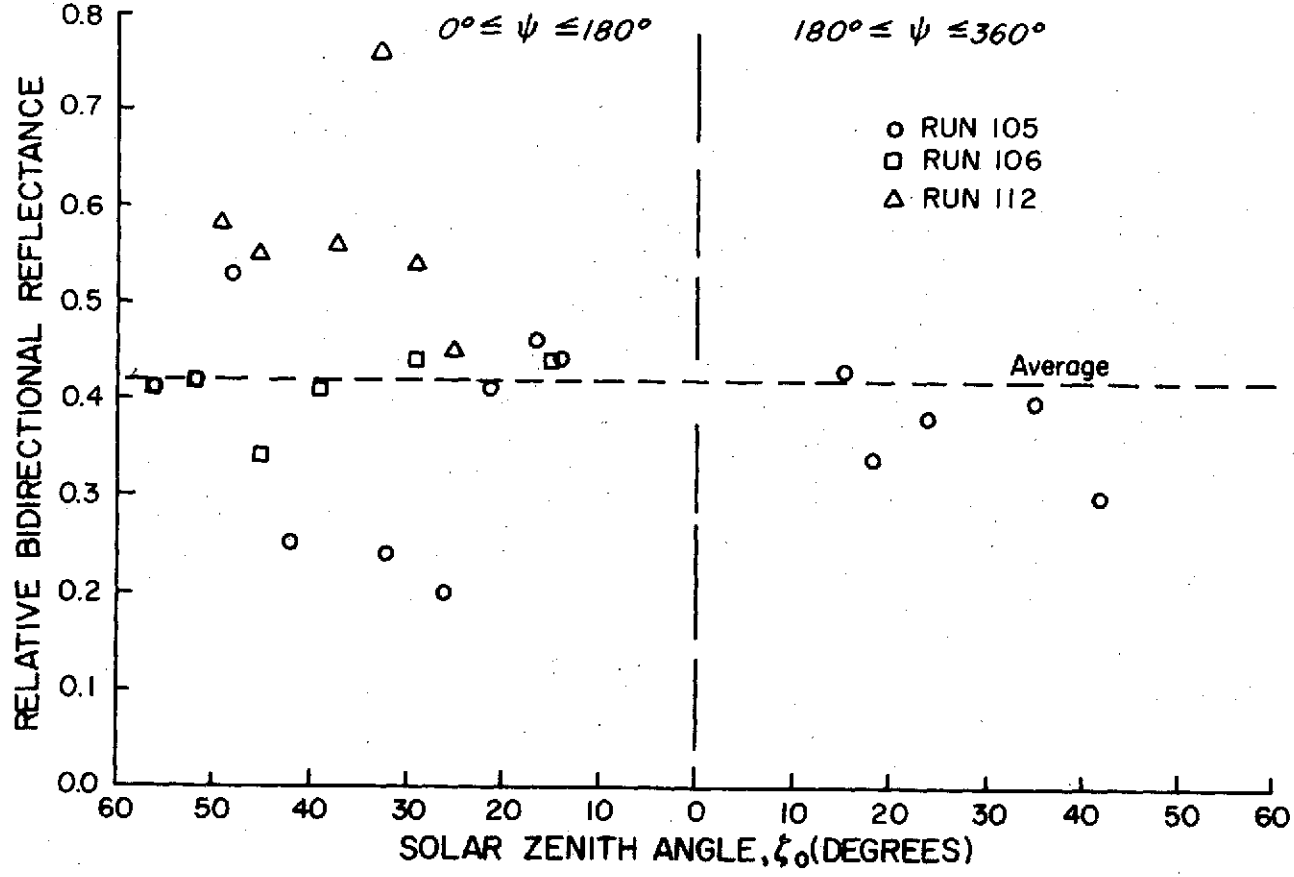

FIGURE G-13. RELATIVE BIDIRECTIONAL REFLECTANCE OF BERMUDA GRASS PLOT AT λ=1.50 MICRONS TAKEN IN FIELD

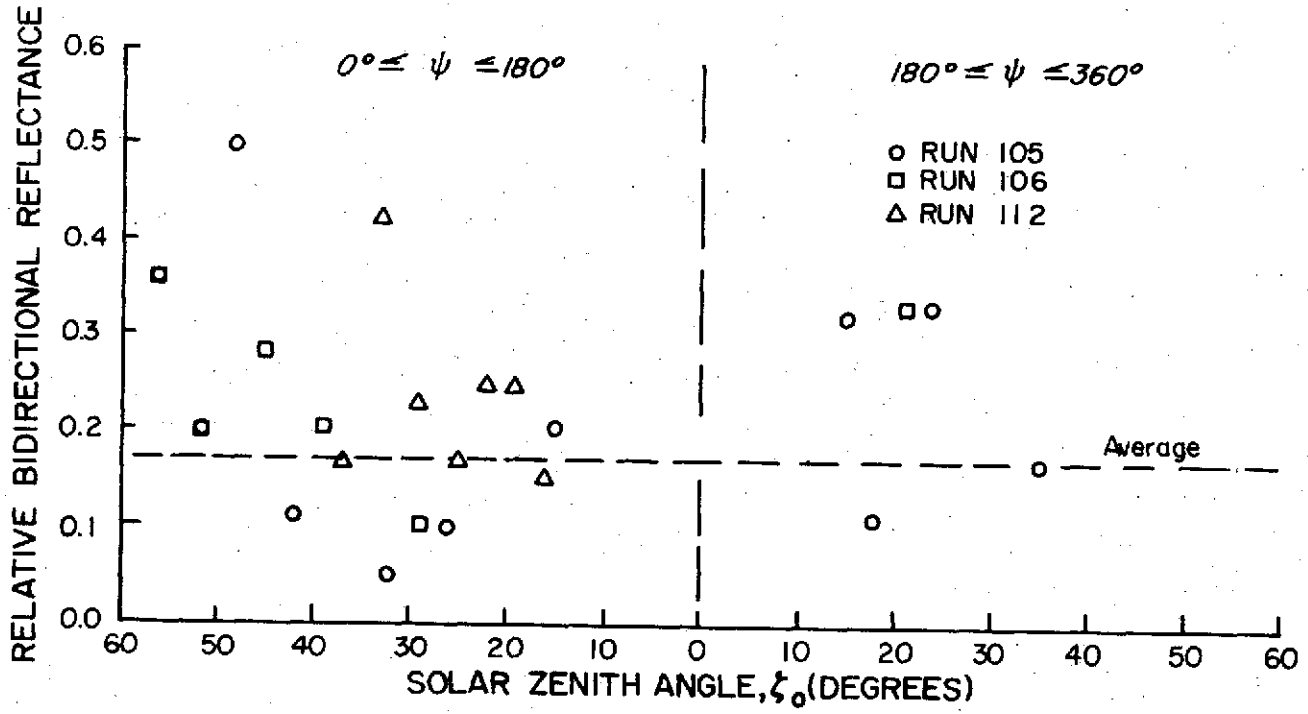

FIGURE G-14. RELATIVE BIDIRECTIONAL REFLECTANCE OF BERMUDA GRASS PLOT AT $\lambda = 1.75$ MICRONS TAKEN IN FIELD

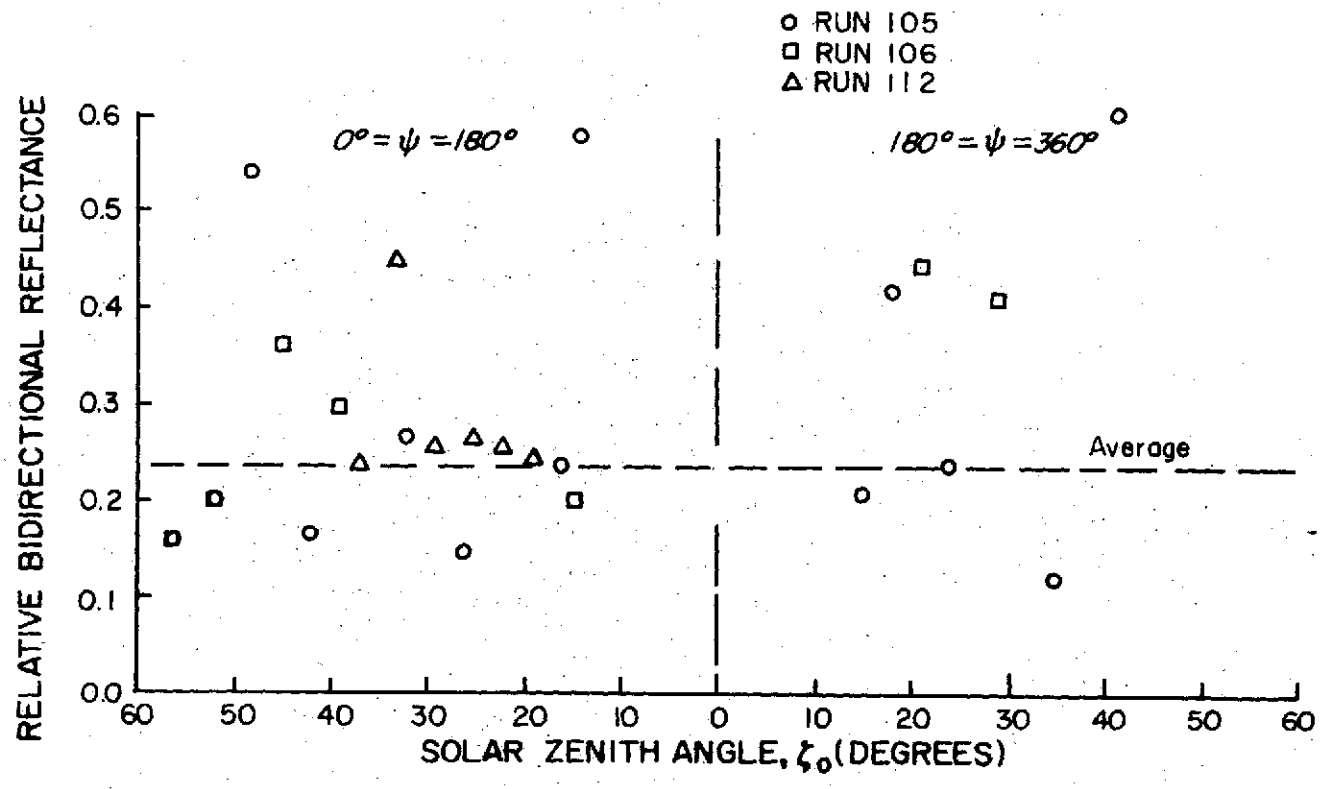

FIGURE G-15. RELATIVE BIDIRECTIONAL REFLECTANCE OF BERMUDA GRASS PLOT AT $\lambda = 2.00$ MICRONS TAKEN IN FIELD

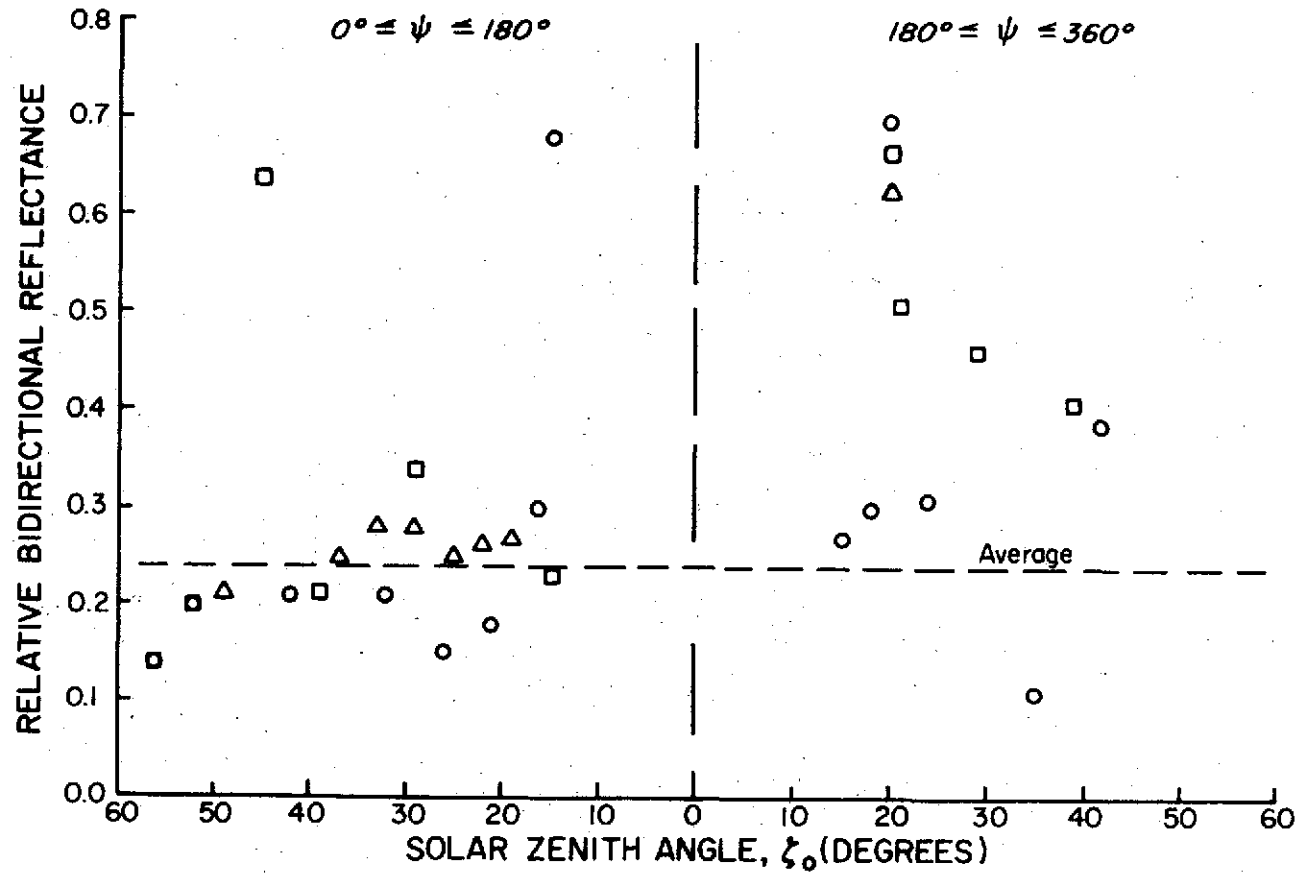

FIGURE G-16. RELATIVE BIDIRECTIONAL REFLECTANCE OF BERMUDA GRASS PLOT AT λ=2.25 MICRONS TAKEN IN FIELD